Spring 1-1-2014

Design and Synthesis of Pyrimidine Fused Heterocycles as Single Agents with Combination Chemotherapy Potential

Roheeth Pavana

DESIGN AND SYNTHESIS OF PYRIMIDINE FUSED HETEROCYCLES AS SINGLE AGENTS WITH COMBINATION CHEMOTHERAPY POTENTIAL

A Dissertation

Submitted to the Graduate School of Pharmaceutical Sciences

Duquesne University

In partial fulfillment of the requirements for

the degree of Doctor of Philosophy

By

Roheeth Kumar Pavana

May 2014

Name:	Roheeth Kumar Pavana
Dissertation:	DESIGN AND SYNTHESIS OF PYRIMIDINE FUSED HETEROCYCLES AS SINGLE AGENTS WITH COMBINATION CHEMOTHERAPY POTENTIAL
Degree:	Doctor of Philosophy
Date:	March 5, 2014

APPROVED & ACCEPTED

Aleem Gangjee, Ph. D. (Committee Chair)
Professor of Medicinal Chemistry
Graduate School of Pharmaceutical Sciences
Duquesne University, Pittsburgh, PA

APPROVED

Marc W. Harrold, Ph. D. (Committee member)
Professor of Medicinal Chemistry
Graduate School of Pharmaceutical Sciences
Duquesne University, Pittsburgh, PA

APPROVED

David J. Lapinsky, Ph. D. (Committee member)
Associate Professor of Medicinal Chemistry
Graduate School of Pharmaceutical Sciences
Duquesne University, Pittsburgh, PA

APPROVED

Patrick T. Flaherty, Ph. D. (Committee member)
Associate Professor of Medicinal Chemistry
Graduate School of Pharmaceutical Sciences
Duquesne University, Pittsburgh, PA

APPROVED

Lawrence H. Block, Ph. D. (Committee member)
Professor of Pharmaceutics, Emeritus
Graduate School of Pharmaceutical Sciences
Duquesne University, Pittsburgh, PA

APPROVED

James K. Drennen, Ph.D.
Associate Dean, Research and Graduate Programs
Graduate School of Pharmaceutical Sciences
Duquesne University, Pittsburgh, PA

APPROVED

J. Douglas Bricker, Ph. D.
Dean of Mylan School of Pharmacy and the Graduate School of Pharmaceutical Sciences, Duquesne University, Pittsburgh, PA

ABSTRACT

DESIGN AND SYNTHESIS OF PYRIMIDINE FUSED HETEROCYCLES AS SINGLE AGENTS WITH COMBINATION CHEMOTHERAPY POTENTIAL

By

Roheeth Kumar Pavana

May 2014

Dissertation supervised by Professor Aleem Gangjee

This dissertation describes the design, synthesis and biological evaluation of pyrimidine fused heterocycles as single agents with combination chemotherapy potential. Major limitations of cancer chemotherapy include dose limiting toxicities of clinically used agents and the development of multidrug resistance by the tumor. Agents that interfere with microtubules are important antitumor agents. Tumor angiogenic mechanisms that are vital for tumor growth and metastasis are targeted by antiangiogenic agents. Antiangiogenic agents are usually not tumoricidal but are mainly cytostatic. Combination chemotherapy with antiangiogenic and cytotoxic agents have shown significant promise and several studies with such combinations are in progress in the clinic. Single agents with both antiangiogenic activities as well as cytotoxicity would afford single agents that circumvent pharmacokinetic problems of multiple agents, avoid

drug-drug interactions, could be used at lower doses to alleviate toxicity, be devoid of overlapping toxicities, and delay or prevent tumor cell resistance. The work in this dissertation is centered on the design and synthesis of single entities that have both antiangiogenic effects and cytotoxic effects.

These efforts led to the identification of structural features that are necessary for inhibition of tubulin polymerization. Structural modifications also led to the identification of novel antiangiogenic agents which inhibit one or more of the receptor tyrosine kinases (RTKs)- vascular endothelial growth factor receptor-2 (VEGFR2), platelet derived growth factor receptor-β (PDGFRβ) and epidermal growth factor receptor (EGFR). The complexity of the angiogenic pathways in tumors implies that disrupting a single mechanism of angiogenesis may not result in significant clinical success. Multiple RTKs are co-activated in tumors and redundant inputs drive and maintain downstream signaling, thereby limiting the efficacy of therapies targeting single RTKs.

This work reviews the role of RTKs in angiogenesis, microtubules as antitumor targets, the vascular normalization theory and multitargeted agents. This work also reviews the synthesis of substituted pyrrolo[3,2-*d*]pyrimidines, furo[3,2-*d*]pyrimidines, pyrimido[5,4-*b*]indoles and benzofuro[3,2-*d*]pyrimidines. A discussion of methods employed in the synthesis of pyrimidine fused heterocycles as single agents with combination chemotherapy potential is provided.

Dedicated to My Family, Friends and Teachers

ACKNOWLEDGEMENTS

I would like to express my sincere gratitude to everyone who contributed to this work. In particular I am most grateful to my supervisor, Professor Dr. Aleem Gangjee, for his guidance and support which made the research presented in this dissertation possible. I am indebted to him for his scientific guidance and training and also for his constant encouragement and financial support.

I would like to thank the members of my dissertation committee: Drs. Marc W. Harrold, David J. Lapinsky, Patrick T. Flaherty, Lawrence H. Block and Aleem Gangjee for their advice and support. I would like to thank Drs. Fraser Fleming and Bruce Beaver for their valuable courses in Organic Chemistry. I wish to express my sincere appreciation to Nancy Hosni, Mary Caruso, Jackie Farrer and Deborah Willson for all their help and assistance. I would like to give thanks to all my colleagues in the Graduate School of Pharmaceutical Sciences for their insights and encouragement. I would like to thank the Graduate School of Pharmaceutical Sciences for financial support.

Finally and most importantly, I would like to express my love and gratitude to my beloved family for their endless love and support.

TABLE OF CONTENTS

	Page
ABSTRACT	iv
DEDICATION	vi
ACKNOWLEDGEMENTS	vii
LIST OF ABBREVIATIONS	ix
LIST OF TABLES	x
LIST OF FIGURES	xi
LIST OF SCHEMES	xiii
I. BIOLOGICAL REVIEW	1
II. CHEMICAL REVIEW	29
III. STATEMENT OF THE PROBLEM	56
IV. CHEMICAL DISCUSSION	80
V. EXPERIMENTAL	104
VI. SUMMARY	153
VII. BIBLIOGRAPHY	158

LIST OF ABBREVIATIONS

ABC	ATP binding cassette
ATP	adenosine triphosphate
BP	back pocket
CA4	combretastatin A4
CA4P	combretastatin A4 phosphate
CAM	Chorioallantoic membrane
DFG	aspartate-phenylalanine-glycine
DHFR	dihydrofolate reductase
EGF	endothelial growth factor
EGFR	endothelial growth factor receptor
GDP	guanosine diphosphate
GTP	guanosine triphosphate
MAP	microtubule associated proteins
MDR	multidrug resistance
PDGF	platelet derived growth factor
PDGFR	platelet derived growth factor receptor
Pgp	P-glycoprotein
PLGF	placenta growth factor
RTK	receptor tyrosine kinase
TS	thymidylate synthase
VDA	vascular disrupting agents
VEGF	vascular endothelial growth factor
VEGFR	vascular endothelial growth factor receptor

LIST OF TABLES

Page

Table 1 Effects on tubulin and VEGFR2 in cellular assays 61

Table 2 Effects of **181**·HCl on tubulin and EGFR in cellular assays 71

Table 3 Inhibition of kinases in cellular assays 76

LIST OF FIGURES

		Page
Figure 1	The angiogenic process	1
Figure 2	General structure and role of RTKs	3
Figure 3	Representative RTK inhibitors approved for clinical use in USA	4
Figure 4	ATP-binding site of RTKs	8
Figure 5	Microtubule growth and shrinkage	13
Figure 6	Microtubule treadmilling	13
Figure 7	Microtubules during the cell cycle	14
Figure 8	Vinca binding site and representative vinca alkaloids	16
Figure 9	Taxane binding site and representative taxanes	17
Figure 10	Colchicine binding site and combretastatins	18
Figure 11	Antiangiogenic therapy and vessel normalization	23
Figure 12	Single agents with RTK and DHFR inhibitory activity	26
Figure 13	Single agents with RTK and TS inhibitory activity	26
Figure 14	Single agents with RTK inhibitory activity and cytotoxicity	27
Figure 15	Disconnection strategies towards pyrrolo[3,2-*d*]pyrimidines	29
Figure 16	Disconnection strategies towards precursor pyrroles	36
Figure 17	Indole precursors to pyrimido[5,4-*b*]indoles	45
Figure 18	Furan precursors to furo[3,2-*d*]pyrimidines	47
Figure 19	Benzofuran precursors to benzofuro[3,2-*d*]pyrimidines	52
Figure 20	Steps involved in cascade reaction	54
Figure 21	Lead compounds	60
Figure 22	Series I	62
Figure 23	Series II	62
Figure 24	Tricyclic VEGFR2 inhibitors	63
Figure 25	Series III	63
Figure 26	Series IV	64

Figure 27 Pyrimido[5,4-*b*] indoles as RTK inhibitors 64
Figure 28 Series V 65
Figure 29 Series VI 65
Figure 30 Series VII 66
Figure 31 Predicted binding modes of **187** in VEGFR2 67
Figure 32 Series VIII 70
Figure 33 Series IX 71
Figure 34 Series X 72
Figure 35 Benzofuro[3,2-*d*]pyrimidines as RTK inhibitors 72
Figure 36 Series XI 73
Figure 37 Series XII 73
Figure 38 Series XIII 74
Figure 39 Series XIV 74
Figure 40 Series XV 75
Figure 41 Series XVI 76
Figure 42 VEGFR2 and PDGFRβ dual inhibitor 76
Figure 43 Series XVII 77
Figure 44 Reported RTK inhibitors used in the design of Series XIX 78
Figure 45 Series XVIII 79
Figure 46 Retrosynthesis of target compounds 80
Figure 47 Comparison of ^{1}H NMRs 97

LIST OF SCHEMES

		Page
Scheme 1	Enamines in the synthesis of pyrrolo[3,2-*d*]pyrimidines	30
Scheme 2	Copper (I) catalyzed cyclization towards pyrrolo[3,2-*d*]pyrimidines	31
Scheme 3	One-pot protocol for the synthesis of pyrrolo[3,2-*d*]pyrimidines	32
Scheme 4	Furneaux method for synthesis of 2-amino 4-oxo pyrrolo[3,2-*d*] pyrimidines	32
Scheme 5	Taylor strategy for synthesis of 2-amino 4-oxo pyrrolo[3,2-*d*] pyrimidines	33
Scheme 6	Taylor modified strategy for the synthesis of 2-amino 4-oxo pyrrolo[3,2-*d*] pyrimidines	34
Scheme 7	Madelung cyclization strategy for synthesis of pyrrolo[3,2-*d*] pyrimidines	35
Scheme 8	Pyrimidine ring construction	36
Scheme 9	Pyrrole ring construction from cyanoacetylenes	37
Scheme 10	Pyrrole ring construction from α-cyano ketones	37
Scheme 11	Pyrrole ring construction from α-cyano aldehydes	38
Scheme 12	Synthesis of 2-alkyl-4-oxo-pyrrolo[3,2-*d*]pyrimidines	38
Scheme 13	Synthesis of 2-H-4-oxo-pyrrolo[3,2-*d*]pyrimidines	39
Scheme 14	Synthesis of 2-amino-4-oxo-pyrrolo[3,2-*d*]pyrimidines	39
Scheme 15	Synthesis of 2-carbamate-4-oxo-pyrrolo[3,2-*d*]pyrimidines	40
Scheme 16	Synthesis of 2-sulfanyl-4-oxo-pyrrolo[3,2-*d*]pyrimidines	40
Scheme 17	Synthesis of pyrrolo[3,2-*d*]pyrimidine 2,4-dione	41
Scheme 18	Synthesis of 2-amino-4-oxo-pyrrolo[3,2-*d*]pyrimidines from pyrimidines	42
Scheme 19	Synthesis of 2-amino-4-oxo-pyrrolo[3,2-*d*]pyrimidines from pyrroles	43
Scheme 20	Alkylation/acylation of 2-amino-4-oxo-pyrrolo[3,2-*d*]pyrimidines	44
Scheme 21	Synthesis of indole precursors	45

Scheme 22 Copper catalyzed cascade reaction 46
Scheme 23 Palladium catalyzed pyrimidine formation 46
Scheme 24 Synthesis of 2-amino-4-oxo-pyrrolo[3,2-*d*]pyrimidines 47
Scheme 25 Synthesis of key furan precursors 48
Scheme 26 Synthesis of 3-amino 2-carboxy furans 48
Scheme 27 Synthesis of 3-amino 2-cyanao furans 49
Scheme 28 Synthesis of 3-amino 2-carboxy furans 50
Scheme 29 Synthesis of 2-H-4-oxo-furo[3,2-*d*]pyrimidines 50
Scheme 30 Synthesis of furo[3,2-*d*]pyrimidine 2,4-dione 51
Scheme 31 Synthesis of furo[3,2-*d*]pyrimidine 2,4-dione 51
Scheme 32 Synthesis of 2-amino-4-oxo-furo[3,2-*d*]pyrimidines 52
Scheme 33 Synthesis of benzofuran precursors 53
Scheme 34 Copper(I)-mediated cascade reactions 53
Scheme 35 Synthesis of benzofuro[3,2-*d*]pyrimidines 54
Scheme 36 Synthesis of 2-amino- benzofuro[3,2-*d*]pyrimidines 55
Scheme 37 Synthesis of **161** 81
Scheme 38 Synthesis of **162** 82
Scheme 39 Synthesis of **163**-**167** 83
Scheme 40 Synthesis of **170**-**173** 84
Scheme 41 Synthesis of **174**-**176** 85
Scheme 42 Synthesis of **178**-**180** 87
Scheme 43 Synthesis of **181**-**185** 88
Scheme 44 Synthesis of **187**-**190** 89
Scheme 45 Synthesis of **191**-**195** 90
Scheme 46 Synthesis of **196**-**197** 91
Scheme 47 Synthesis of **198**-**200** 92
Scheme 48 Synthesis of **202**-**204** 93
Scheme 49 Synthesis of **205**-**206** 95

Scheme 50 Synthesis of **207-210** 96
Scheme 51 Synthesis of **211-214** 97
Scheme 52 Synthesis of **215-216** 98
Scheme 53 Synthesis of **217-220** 99
Scheme 54 Synthesis of **222-224** 101
Scheme 55 Synthesis of **225-232** 102

I. BIOLOGICAL REVIEW

A. Angiogenesis

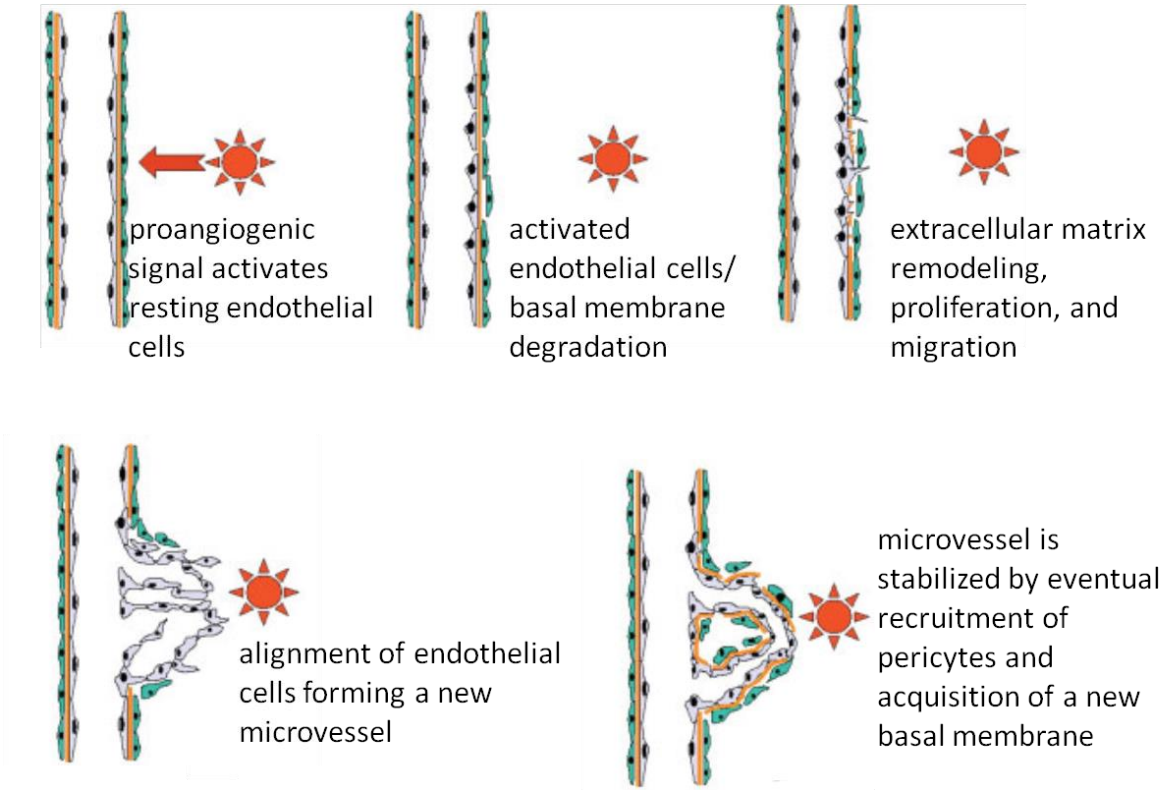

Figure 1. The angiogenic process (modified from ref. 1)

Angiogenesis is a complex physiological process of sprouting of new blood vessels from existing blood vessels.[2] It involves a complex cascade of cellular events that are tightly regulated by proangiogenic factors including several growth factors and antiangiogenic factors.[3] Rapidly proliferating tumor cells inherently require metabolic substrates for nourishment and removal of metabolic end products. During the early stages of development of a tumor, blood supply to the tumor tissue comes from the vasculature supplying the surrounding normal healthy cells. As the tumor exceeds a critical mass of about 2 mm in diameter, it requires its own blood supply to support its

growth. The fast tumor growth rate also induces hypoxia, which in turn causes an angiogenic switch within the tumor microenvironment and initiates other pathways involved in over expression of proangiogenic factors. These include vascular endothelial growth factor (VEGF), platelet derived endothelial growth factor (PDGF) and epidermal growth factor (EGF), which promote endothelial cell proliferation/migration thereby leading to angiogenesis (Figure 1).[2, 4, 5] The new blood vessels grow and infiltrate into the tumor, thereby providing nutrients and oxygen to sustain tumor expansion and a route for cancer cell dissemination. This results in tumor progression and metastases.[6] The sustained growth of solid tumors is highly dependent on angiogenesis. Thus antiangiogenic agents have been widely used in the treatment of cancer.[7, 8]

The growth of tumor tissue vasculature is chaotic and leaky. Therefore, tumor vasculature differs from normal tissue vasculature in several aspects including the hierarchy of organization and nature of endothelium .[9]

A.1 Receptor Tyrosine Kinases in Angiogenesis

Proangiogenic growth factors such as VEGF, PDGF and EGF bind to their corresponding receptors and initiate signal transduction. These receptor tyrosine kinases (RTKs), namely vascular endothelial growth factor receptor (VEGFR), platelet-derived growth factor receptor (PDGFR), and epidermal growth factor receptor (EGFR), possess an extracellular domain, a transmembrane domain and an intracellular kinase catalytic domain (Figure 2).[10] Growth factor binding to the extracellular domain of RTKs results in receptor dimerization (homodimerzation or heterodimerization) and autophosphorylation of the tyrosine residues within the cytoplasmic domain. Autophosphorylation then

triggers a cascade of downstream cell signalling pathways. These pathways are tightly monitored and regulated under normal physiological conditions. Disregulation of these signalling pathways has been linked to malignancy and significantly contributes to the hallmarks of cancer:[11] self sufficiency in growth signals, insensitivity to antigrowth signals, evasion of apoptosis, unlimited replicative potential, sustained angiogenesis, tumor invasion and metastases. Thus, inhibition of these RTKs offers a key therapeutic strategy for cancer therapy.[12]

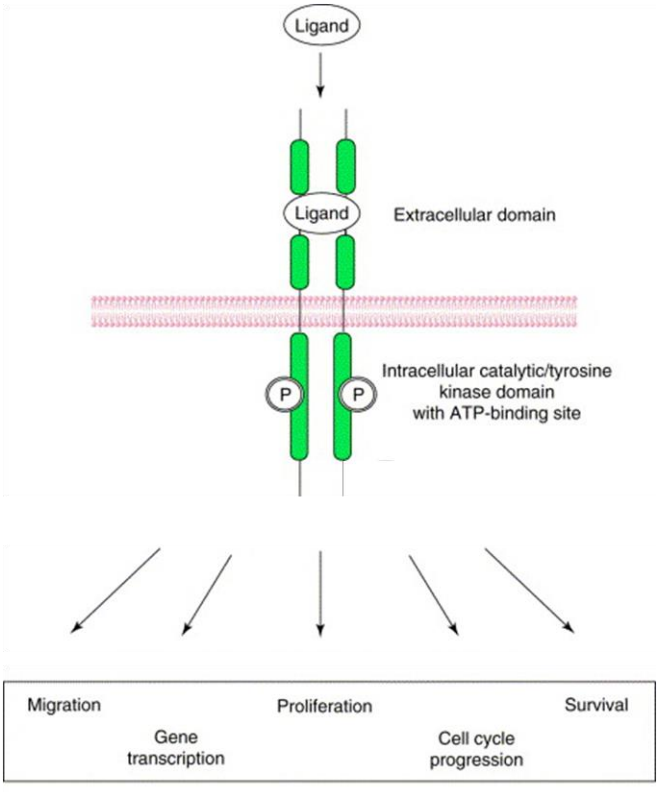

Figure 2. General structure and role of RTKs (modified from ref. 10)

Several RTK targeting small molecular inhibitors (representative compounds shown in Figure 3) including crizotinib, dasatinib, erlotinib, imatinib, gefitinib, lapatinib, nilotinib, pazopanib, ruxolitinib, sorafenib, sunitinib, vandetanib, and vemurafenib have

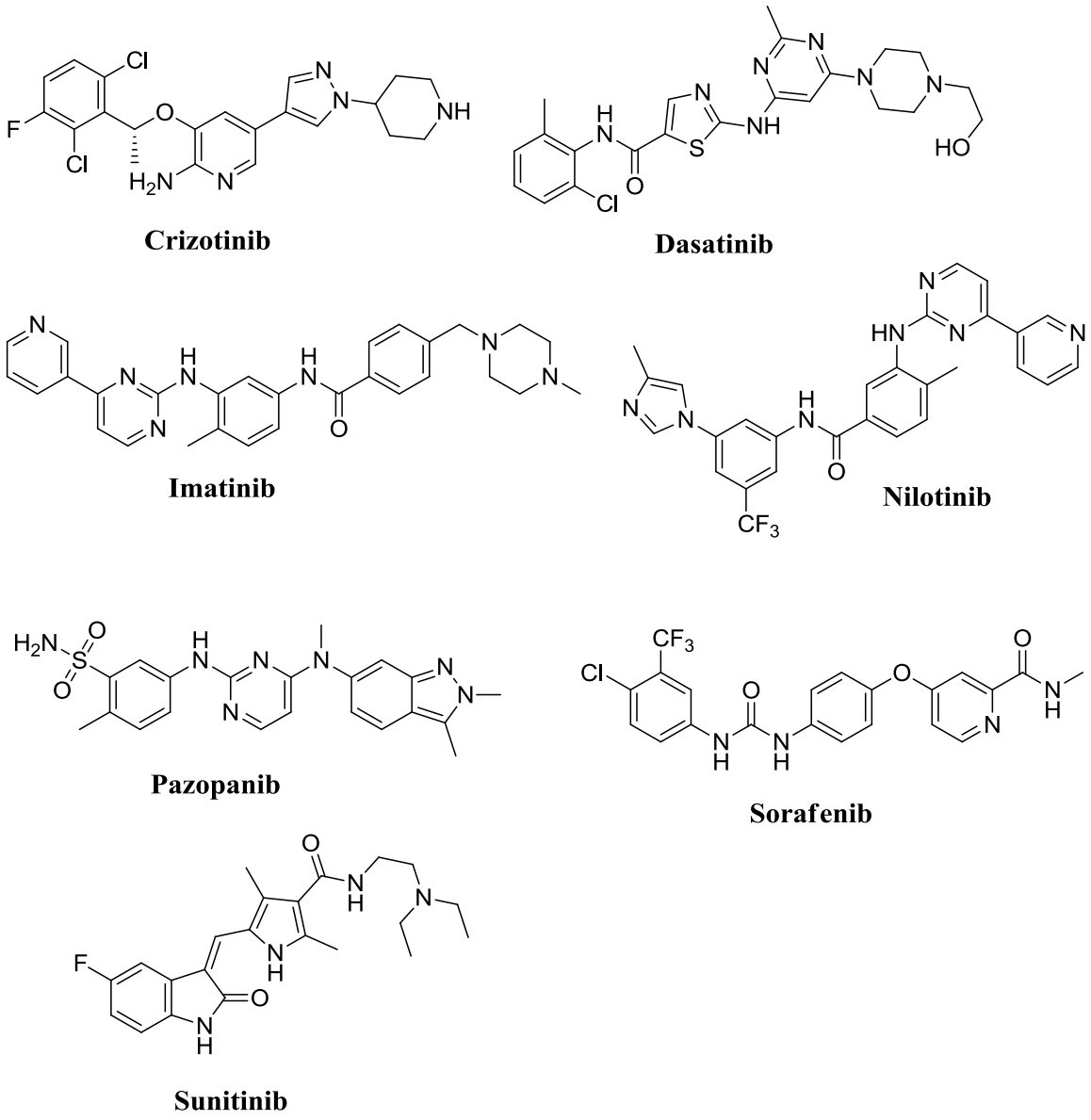

Figure 3. Representative RTK inhibitors approved for clinical use in USA.

been approved as "targeted agents" for the clinical treatment of various types of cancer.[12,13]

VEGFR

VEGF is an important growth factor that is involved in angiogenesis and vasculogenesis (i.e., the formation of the embryonic circulatory system).[14] The VEGF family consists of five members, VEGF-A, VEGF-B, VEGF-C, VEGF-D, and placenta growth factor (PLGF). Three types of VEGFRs have been identified, VEGFR1, VEGFR2 and VEGFR3. VEGFRs are almost exclusively expressed on endothelial cells. In addition, VEGFRs are overexpressed on several tumor types with different expression patterns, ligand specificity and cellular/physiological effects of these receptors. VEGFR2 has been recognized as the kingpin in angiogenesis.[15] Targeted inhibition or disruption of VEGFR2 produces an abrogation of angiogenesis, decreased endothelial cell survival and decreased tumor growth.[14, 16] Several inhibitors of VEGFR2 including sunitinib and semaxanib have displayed antiangiogenic activity.[7, 17]

PDGFR

This family of growth factors is comprised of four structurally related, soluble polypeptides that exist as five different homodimers and heterodimer ligands: -AA, -BB, -CC, -DD, and -AB.[18] PDGF can bind to and activate two of its receptors PDGFRα and PDGFRβ.[19] These receptors are expressed on pericytes, smooth muscle cells that provide mechanical support to vasculature. PDGFR pays an important role in angiogenesis by stimulating the formation of microvascular pericytes, thereby stabilizing the newly formed blood vessels. They are also involved in the induction of VEGF secretion and consequently, angiogenesis.

EGFR

The EGF family is comprised of eleven known members that bind to one of four EGFR family receptors.[20] EGFR is one of the four members of the EGFR family of RTKs. Overexpression of EGFR, its growth factors, and aberrant EGFR tyrosine kinase activity lead to increased tumor cell proliferation, survival and invasiveness.[19] Inhibition of EGFR signaling has been shown to promote selective apoptosis in tumor endothelial cells.[21] As a result, EGFR has been extensively studied and targeted by small molecule inhibitors and monoclonal antibodies. [20]

A.2 ATP Binding Site of RTKs

Several crystal structures of RTKs areavailable in the protein data bank. All kinases share a catalytic domain that contains the adenosine triphosphate (ATP) binding site. The ATP binding site of RTKs has been indicated as a promising target for rational drug design. Structural homology and diversity among the ATP-binding sites of kinases has allowed the building of pharmacophore models for rational drug design.[22, 23] The overall three-dimensional structure of the kinase domain is conserved throughout the protein kinase family. A twisted β-sheet of five antiparallel β-strands and one α-helix make up the N-terminal lobe. The C-terminal lobe is made up of four β-strands and eight α-helices. Advances in ATP-bound or inhibitor-bound RTK crystal structures has enabled a detailed analysis of the catalytic site, its binding pockets in both active and inactive states as well as the mode of binding of RTK inhibitors. [23]

RTK Catalytic Cleft:

The catalytic cleft usually consists of two regions commonly referred to as the front cleft and the back cleft.[24] The ATP-binding site occupies the front cleft of the catalytic domain, while the back cleft comprises elements responsible for the regulation of phosphorylation of peptide substrates. These two regions share a border that includes the aspartate-phenylalanine-glycine (DFG) motif and the β3 segment. A gatekeeper residue and a β3-lysine residue form a gate between the front and back cleft. Access to the back cleft is controlled by kinase gatekeeper residues. Small amino acid residues such as threonine and alanine or bulky gatekeeper residues such as phenylalanine, leucine or methionine control entry to the back pocket and selectivity for inhibitors. The β3-lysine which is conserved in all kinase enzymes can adopt varied conformations in different protein kinases and helps to anchor the α and β- phosphates of ATP in the active state.

In a fully active state, protein kinases adopts a DFG-in conformation where the side chain of the DFG aspartate is directed into the ATP binding site and the aromatic ring of the phenylalanine is positioned in the back cleft.[24] The aspartate is required to chelate Mg^{2+} and helps to orient the γ-phosphate of ATP for its transfer in the active DFG-in conformation.[23, 24] The aromatic side chain of phenylalanine in the active DFG-in motif is in contact with αC. This contact in many active kinases facilitates the formation of a Lys-Glu ion pair for kinase catalysis. [23]

In the inactive state, the DFG motif is in either a DFG-in or DFG-out conformation.[24] In the DFG-out conformation, the phenylalanine aromatic ring is positioned in the ATP pocket and the aspartate residue of the DFG motif is in the back cleft.[23]

The Front Cleft:

The front cleft includes the ATP binding site and small, non-ATP contact regions. The ATP site is broadly divided into the following subregions depending on the binding mode (Figure 4). [23]

1. Adenine region: This pocket is predominantly hydrophobic and is involved in binding various inhibitor scaffolds. This region is bordered by the hinge region and the

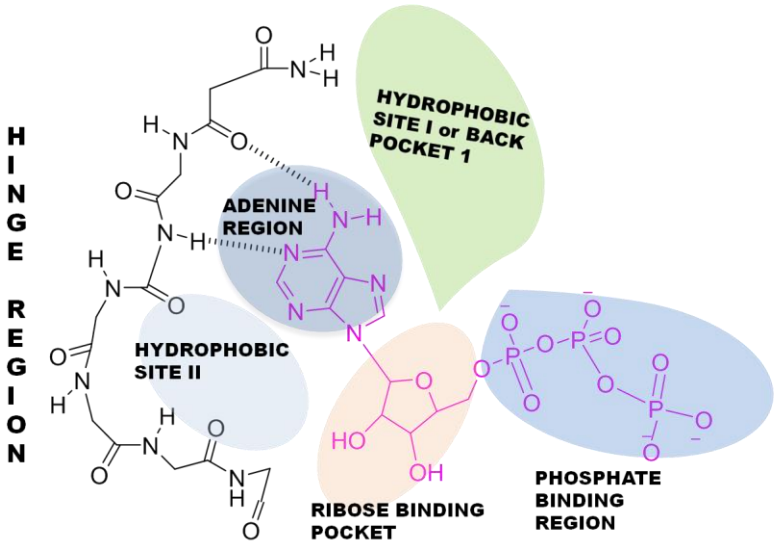

Figure 4. ATP-binding site of RTKs [ATP is in pink] (modified from ref. 25)

gatekeeper. Two key hydrogen bonds are formed by the interaction of the N1 and N6 amino nitrogens of the adenine ring with the NH and carbonyl groups of the peptide backbone of the hinge region residues of the RTKs. Several RTK inhibitors use at least one of these key hydrogen bonds. Other backbone amide groups in the hinge region can serve as hydrogen bond donors or acceptors for inhibitor binding.

2. Ribose binding region: The ribose pocket accommodates the sugar moiety of ATP and is adjacent to a hydrophilic, solvent exposed region. This pocket includes includes three

hydrophobic and hydrophilic residues. These hydrophobic residues (Ile, Val and Leu) have traditionally been exploited in developing EGFR inhibitors.[25]

3. Phosphate binding region: This region is covered by Asp, Lys and Asn residues and the DFG motif. This region is highly flexible, hydrophilic and solvent exposed, and is therefore considered less important in improving inhibitor affinity and potency. However, this region has been explored to improve physicochemical properties of inhibitors.

4. Hydrophobic region II: This pocket is not used by ATP and serves as an entrance for ligand binding. Variation in the residues and conformation of this pocket have been reported for various kinase targets. Thus, this region has been used to gain selectivity in the design of kinase inhibitors.

The Back Cleft:

In addition to the ATP-binding site, the back cleft provides important binding regions. ATP does not bind in the pockets in the back cleft.[24, 25]

1. Hydrophobic region I: The hydrophobic pocket in the back cleft adjacent to the adenine pocket is called Hydrophobic region I or Back pocket I (BP-I). This pocket has been explored in the design of inhibitors to gain selectivity for kinase targets with small gatekeeper residues. [24]

2. In addition to BP-I, additional binding pockets BP-II, BP-III, and BP-IV become available to inhibitors depending on the binding state of the RTKs.[23]

Major progress has been made with small molecule inhibitors targeting the ATP-binding site of RTKs. The front catalytic cleft of all kinase enzymes is accessible to ligand binding. Small molecule inhibitors that target the front cleft use a core scaffold to recognize the adenine pocket. The core scaffold is then substituted to extend into the

different pockets of the ATP-binding site resulting in improved binding affinity and selectivity for RTKs.[12]

B. Microtubules

Cytoskeletal protein polymers which include actin filaments, intermediate filaments and microtubules (MTs) are crucial for cytoskeletal function. Actin filaments and intermediate filaments provide mechanical support and resistance against physical stress. Microtubules are essential for intracellular transport, maintenance of cell shape and cell division during mitosis. The proper functioning of the microtubules, particularly during mitosis, depends on exquisite dynamics and these dynamics are highly sensitive to chemical intervention.[26] For this reason, microtubule-binding agents that interfere with these dynamics possess potent inhibitory activities against a wide variety of tumors.[27] Drugs targeting microtubules have been highly successful in clinic and have been integrated into therapeutic regimens against both solid tumors (e.g., breast, ovarian, non-small-cell lung cancer, and Kaposi's sarcoma) and hematological malignancies (non-Hodgkin's lymphomas).[26, 28]

B.1 Structures of Microtubules

Microtubules are tube-like protein filamentous fibers made of individual tubulin dimers. The tubulin heterodimer, present in the cytoplasm in soluble form, consists of one α- and one β-tubulin subunit each with a molecular weight of about 50 kDa. [26] Tubulin dimers polymerize "head-to-tail" between the α- and β-tubulin to form protofilaments. Protofilaments further arrange in parallel to form the wall of the tube like hollow

cylindrical microtubule structure. The resulting microtubule consists of nine to sixteen protofilaments laterally, and has an outer diameter of 24 nm, a wall thickness of 5 nm, and a length extendable to about 25 μm.

Guanosine triphosphate (GTP) is also an essential component of microtubule structure. Each α- and β-tubulin heterodimer structure includes two GTP molecules, one of which is tightly bound and cannot be removed without denaturing the heterodimer. The other bound GTP molecule is freely exchangeable with unbound GTP. The non-exchangeable GTP is bound to α-tubulin, whereas GTP and guanosine diphosphate (GDP) are exchangeable on β-tubulin. This exchangeable GTP is highly involved in the regulation of different tubulin functions. GTP binding is required for microtubule polymerization whereas GTP hydrolysis is required for microtubule depolymerization.

Several proteins associated with microtubules, commonly referred to as microtubule associated proteins (MAP), are important for the formation and stability of microtubules. The two nonequivalent ends of microtubules are structurally well organized. The slow growing minus end is generally anchored at the centrosome or microtubule organizing center, and the fast growing plus end probes the cytoplasm in a search-and capture process to reach different targets. [27]

B.2 Microtubule Dynamics

Microtubule dynamics, which are tightly regulated processes, are responsible for the functional role of microtubules in cells.[27] Nucleotides, MAPs, kinases, phosphatases, and coordinated interactions with other cytoskeletal components regulate these dynamics. Disturbing microtubule dynamics has critical consequences on cellfate. Thus, disrupting

microtubule dynamics has traditionally represented an important therapeutic strategy to develop antitumor agents.

The polymerization of tubulin occurs by a nucleation-elongation mechanism.[28] This process involves slow formation of a short microtubule nucleus followed by rapid microtubule elongation through reversible, non-covalent addition of soluble αβ-tubulin heterodimers. GTP binding to β-tubulin causes straightening of the dimer to a conformation that promotes polymerization.[29] The polymerization is driven by the hydrolysis of GTP upon the attachment of the GTP-bound tubulin dimer to the ends of the microtubule, thereby forming tubulin–GDP and P_i, providing energy for the addition of a tubulin dimer. Following hydrolysis of GTP, the loss of the phosphate is not immediate and this delayed hydrolysis of GTP results in the formation of a "GTP-cap", which contains GTP or GDP with unreleased phosphate (GDP-P_i). The presence of a GTP cap at the end of the microtubule stabilizes the open-sheet conformation of the growing microtubule plus end, increases its affinity for tubulin dimers with bound GTP, thus leading to lengthening of the microtubule. The cap is usually a single layer of tubulin, although its size depends on the polymerization rate.[28, 30] As the GTP cap prevents microtubule shrinkage, the microtubule end shortens rapidly after loss of the GTP cap. At the final stage of the polymerization process, the cap dissociates and leaves a microtubule core of β-tubulin bound with GDP.[31]

Microtubules display two major forms of non-equilibrium dynamics *in vitro* and in cells, namely dynamic instability and treadmilling.[28] Dynamic instability (Figure 5) or the switching of microtubules between phases of lengthening and shortening is defined by four main factors:[29, 33] 1) the rate of growth; 2) the rate of shrinkage; 3) the frequency of

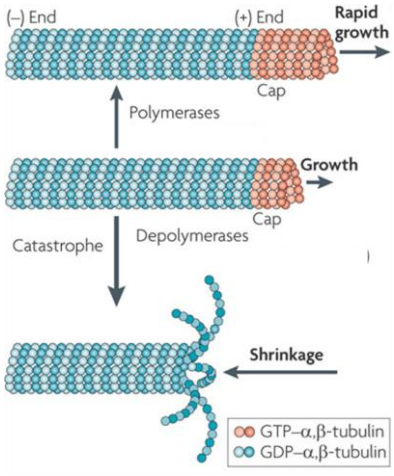

Figure 5. Microtubule growth and shrinkage (modified from ref. 32)microtubule catastrophe (i.e., switching from the growing or paused state to shrinking) and 4) the frequency of microtubule rescue (i.e., switching from shrinking to growing or pause). The assembly of microtubules occurs more rapidly at the plus end, where the β-tubulin is exposed, than at the minus end, where the α-tubulin is exposed. Treadmilling (Figure 6) is a process in which tubulin subunits continuously flux from the minus end to the plus end. Furthermore, this process is characterized by net growth at one end and balanced equivalent shortening at the opposite end.

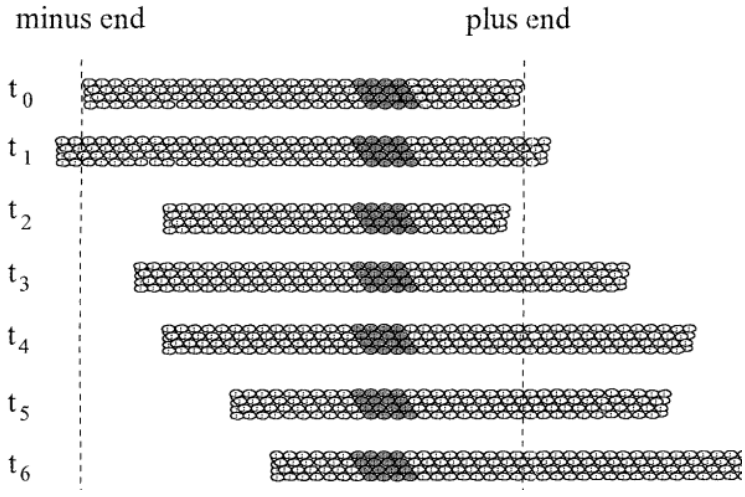

Figure 6. Microtubule treadmilling (modified from ref. 34)

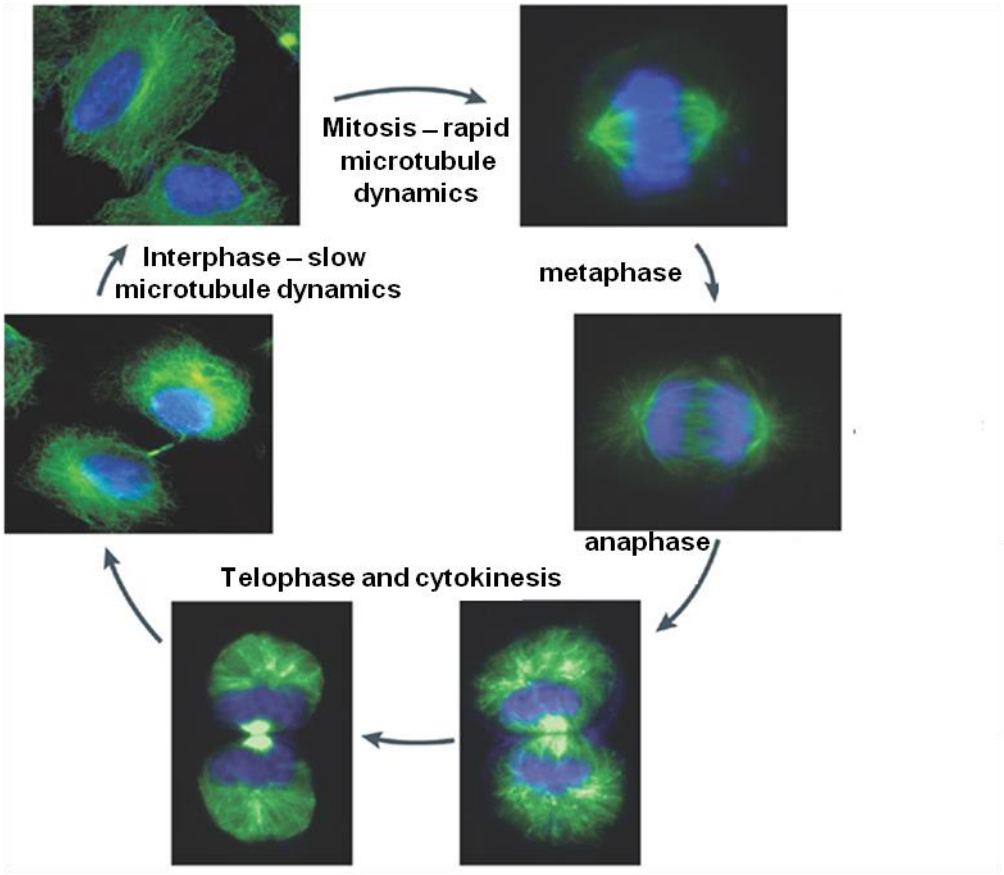

Figure 7. Microtubules (shown in green) during the cell cycle (modified from ref. 35)

The rate of microtubule dynamics changes rapidly throughout the cell cycle wherein the slowest dynamics occur during interphase.[35] During the prophase of mitosis, microtubules become more dynamic and a bipolar spindle-shaped array of microtubules is assembled outwards from the centrosome. In prometaphase, these microtubules attach to the kinetochore center of chromosomes. When cells enter metaphase, microtubule dynamics increase by 4- to 100-fold, whereas in anaphase microtubules start shortening in length (the rate accelerates). As different stages of mitosis are dependant on these delicate microtubule dynamics (Figure 7), tubulin-binding agents, which inhibit microtubule function during mitosis, result in cell cycle arrest, eventually causing cell death.[35]

B.3 Microtubule Binding Agents

Microtubule inhibitors, also known as antimitotic agents, have been classified on the basis of their mechanism of action and effects on polymerization dynamics, and binding site on tubulin.[36] Based on their effects on microtubule stability they are classified as follows. [36]

1) *Microtubule-destabilizing agents*: These agents inhibit microtubule polymerization and promote microtubule disassembly. These included natural products such as the Vinca alkaloids, cryptophycins, halichondrins, estramustine, colchicine and its analogs and combretastatin.

2) *Microtubule-stabilizing agents*: These agents induce microtubule polymerization and include paclitaxel, docetaxel, epothilones and discodermolide. Thes agents promote microtubule assembly and prevent depolymerization.

Distinct classes of microtubule binding agents classified by their binding sites on tubulin are as follows. [36]

1) *The Vinca alkaloids*

The Vinca alkaloids, including vinblastine, vincristine, vindesine, and vinorelbine have a broad spectrum of activity and have been widely used in cancer chemotherapy for leukemia, lymphomas and non-small-cell lung cancer.[36] At low concentrations, vinblastine inhibits microtubule assembly and depolymerization of microtubules. At higher concentrations, vinblastine causes paracrystal formation by tubulin assembly. The Vinca alkaloids bind to the β-subunit of soluble tubulin heterodimers at a region commonly referred to as the Vinca-binding domain.[37] The rapid and reversible binding of

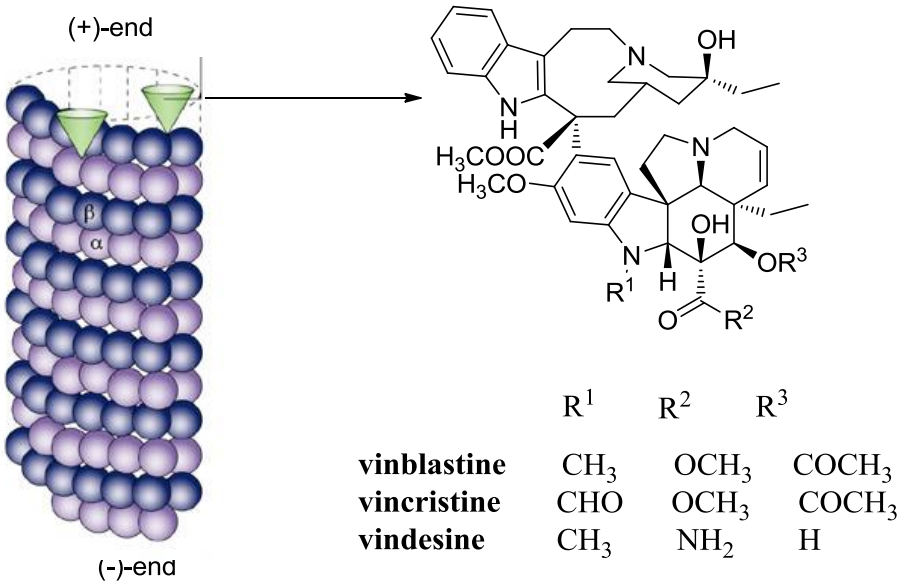

	R^1	R^2	R^3
vinblastine	CH_3	OCH_3	$COCH_3$
vincristine	CHO	OCH_3	$COCH_3$
vindesine	CH_3	NH_2	H

Figure 8.Vinca binding site and representative vinca alkaloids (modified from ref. 36)

vinblastine to soluble tubulin has been suggested to induce a conformational change that preventsintegration of the dimer into the microtubule.[37] Vinblastine binds with high affinity to the end of the microtubules but binds poorly to tubulin that is buried in the tubulin lattice (Figure 8). The Vinca alkaloids depolymerize microtubules and destroy mitotic spindles at high concentrations of 10–100 nM in HeLa cells, At low but clinically relevant concentrations(i.e., IC_{50} = 0.8 nM in HeLa cells) vinblastine does not depolymerize microtubules, yet it powerfully blocks mitosis by suppression of microtubule dynamics. The binding of one or two molecules of vinblastine per microtubule is sufficient to reduce tubulin dynamics by about 50% without causing appreciable microtubule depolymeriza-tion. Other antitubulin agents suchas the cryptophycins, halichondrins and dolastatins also bind at the Vinca binding site.

2) *Taxanes and Epothilones*

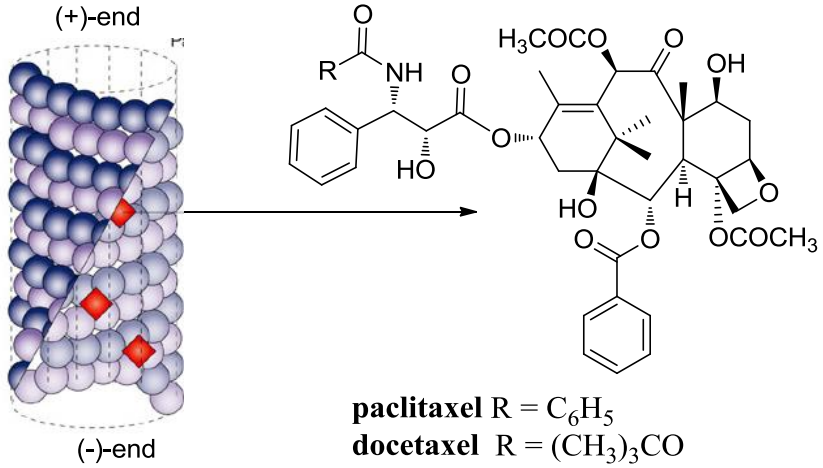

Figure 9. Taxane binding site and representative taxanes (modified from ref. 36)

Paclitaxel and its derivatives bind poorly to soluble tubulin, but bind strongly to tubulin along the length of the microtubule.[38] The binding site for paclitaxel is in the β-subunit on the internal surface of the microtubule (Figure 9).[37, 39] Paclitaxel is suggested to bind by diffusing through nano-size pores in the microtubule lattice. Binding of paclitaxel stabilizes the microtubule by inducing a conformational change in β-tubulin that increases its affinity for adjacent tubulin molecules. Low concentrations of Taxol are sufficient to cause cell cycle arrest and induce apoptosis without changing microtubule mass. The IC_{50} for an antimitotic effect of paclitaxel in HeLa cells is 8 nM while the IC_{50} for an increase in microtubule polymerization is 80 nM.

Most antimitotic agents that increase microtubule polymerization, such as the epothilones, discodermolide, eleutherobin, and sarcodictyins, bind to the Taxol-binding site.[39] The taxanes are widely used for breast cancer, ovarian cancer, non small cell lung cancer, and Kaposi`s sarcoma. Ixabepilone, which belongs to the Epothilone class of paclitaxel-site binders, was approved for the treatment of drug-refractory metastatic

breast cancer in 2007.[39]

3) *Colchicine binding site agents*

Colchicine binding site agents include podophyllotoxin, combretastatin and flavonols. Colchicine is not used clinically in cancer treatment due to its toxicity at doses that produce antimitotic effects.[40] Colchicine binds to soluble tubulin at a distinct site referred to as the colchicine binding site. The colchicine binding site is on β-tubulin at the interface between α- and β- tubulins (Figure 10).[37] With tubulin, colchicine forms a poorly reversible tubulin–colchicine complex, which copolymerizes into the microtubule ends along with free tubulin molecules. The ends continue to grow with the complex, but their dynamics are suppressed. These effects lead to cell cycle arrest and apoptotic cell death.

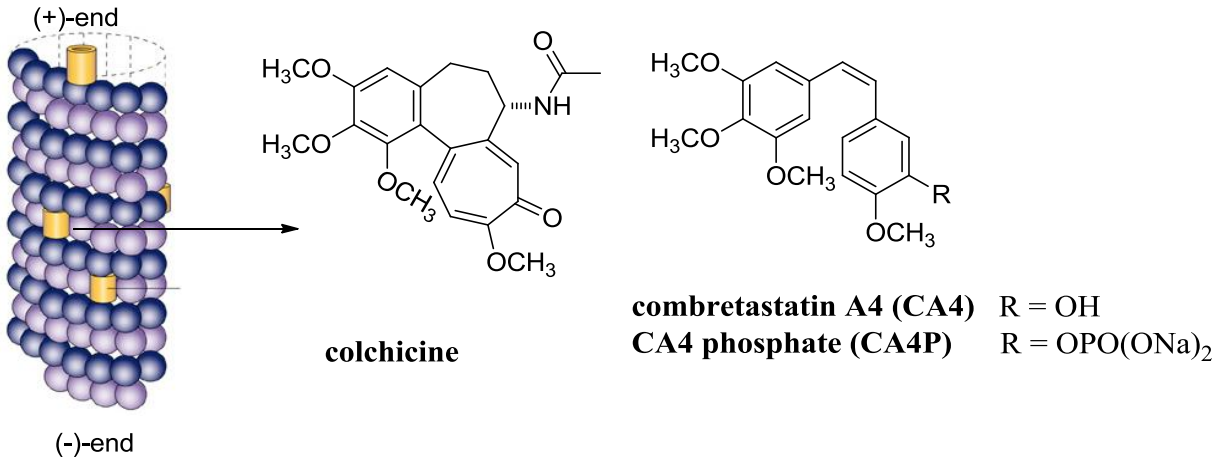

Figure 10. Colchicine binding site and combreatastatins (modified from ref. 36)

Combretastatins are also potent vascular-disrupting agents (VDA) in addition to creating antimitotic effect.[41, 42] Combretastatin A4 phosphate (CA4P) rapidly

depolymerizes the microtubules of endothelial cells, reduces blood flow to the tumor within one hour by 95%, increases vascular permeability and hemorrhage of peripheral vessels.[43] Based on this property of some colchicine binding site agents, both combretastatin A4 (CA4) and CA4P have been developed as antivascular agents for clinical trials.[44, 45] It is believed that selectivity for tumor vasculature over normal blood vessels was suggested to lie in the differences between the mature vasculature of normal tissues and the immature or forming vasculature of tumors.[43, 46] The actin cytoskeleton in endothelial cells of immature tumor vasculature is underdeveloped, which is likely to make the cells more susceptible to antitubulin intervention.[47] In addition, the differences in the endothelial cell proliferation rate may also be a causative factor to the observed tumor selectivity.[43]

4. *Additional binding sites:* Several antimitotic agents such as welwistatin, noscapine, laulimalide, the taccalonolides, and estramustine show potent microtubule inhibitory effects but do not bind to the above mentioned three sites on tubulin.[37, 39] Owing to the important roles of GTP on the regulation of microtubule dynamics, nucleoside analogs have also been studied as antimitotic agents. Two GTP analogs were reported to weakly bind to the GTP binding site of β-tubulin.[48] It has been suggested that tubercidin binds weakly to the nucleotide binding site on α-tubulin.[49]

B.4 Resistances to microtubule-binding agents

Multiple-drug resistance (MDR) is a common cause of cancer chemotherapy failure, which includes microtubule-binding agents.[26, 38, 50] Among different resistance mechanis-

sms for this category of drugs, the most clinically significant are drug efflux by ATP binding cassette (ABC) proteins and structural alteration of the microtubules.[35, 51]

Membrane efflux by ABC proteins (e.g., P-glycoprotein (Pgp)) was identified as the chief mechanism of resistance to vinca alkaloids and taxanes *in vitro*.[52] For example, in Pgp-overexpressing SK-OV-3 MDR-1-6/6 cell lines the potency of paclitaxel was reduced 800-fold versus parental cell lines.[53] Lower responses to microtubule-binding agents is frequently correlated with the expression of the ABC pumps. Interestingly the combination of Pgp inhibitors with microtubule-binding agents failed to reverse resistance in clinical trials.[54] The clinical consequence of this resistance mechanism is still under question due to inadequate data on the ABC pumps in cancer patients.[35, 51, 55]

Structural alterations of microtubules promote changes in microtubule-associated proteins (MAP) or the expression of certain isotypes of tubulin in cells. MAP binding stabilizes the microtubules, and depending on the type of the microtubule-binding agent, changeable levels in the expression of the MAPs such as tau, MAP2, and MAP4 could lead to resistance or increased activity.[50] For example, the down-regulation of MAP4 lead to resistance against paclitaxel, yet augmented response to vinblastine.[35, 51, 56, 57]

More than 13 diverse isotypes of tubulins are known to be implicated in the assembly of microtubules. Among them, increased levels of class III β-tubulin (βIII-tubulin) is of highest concern since it is strongly associated with clinical resistance against taxanes in lung, breast and ovarian cancers.[58, 59] In HeLa cell lines, the activity of paclitaxel decreased five-fold times when the cells were adapted to express βIII-tubulin.[60] It was hypothesized that resistance to taxanes was due to loss of a key Ser275 on βIII-

tubulin. This key ineraction facilitates the diffusion of paclitaxel across the pores.[61] However, this theory failed to explain the βIII-tubulin-mediated resistance of vinca alkaloids.[59] In addition, βIII-tubulin was shown to cause resistance against a wide range of drugs with different mechanisms of action.[62] Several studies confirmed the vital role played by βIII-tubulin in protecting cells from drug-induced genotoxic stresses.[63-65] It is likely that the role of βIII-tubulin in cancer may extend further than drug resistance and will continue be an active area of future research.[27]

C. Combination Chemotherapy

The concept of using a combination of drugs each with activity against a different biological target has been used in the treatment of several diseases.[66] Modulating a single biological target associated with a disease will not be effective unless that target is of critical importance, which often is not the case because living systems are complex interconnected networks of molecular components.[66, 67] In order to bypass inhibition of a single biological target, these systems often find alternative compensatory signalling routes. These findings provide the rationale for the use of drugs able to target multiple unrelated proteins. It is not surprising that this strategy has found utility in complex disease states such as cancer with remarkable clinical success.[66] As a result, the central idea of combination chemotherapy is that by modulating multiple pathways simultaneously, the utilization of alternate survival pathways that allow tumor cells to evade the therapy can be prevented.[67]

In general, antiangiogenic RTK inhibitors are cytostatic agents that prevent further growth of the tumor and are required to be used in combination with cytotoxic agents for

complete abrogation of tumors.[67, 68] Of significant interest is the remarkable clinical success of combinations of antiangiogenic agents and cytotoxic agents.[69-72] Metronomic chemotherapy, the delivery of low doses over a long term so as to avoid toxic side effects, along with antiangiogenic agents also results in significant success in the clinic.

D. Vascular Normalization Theory

According to the central idea of combination therapy combined administration of antiangiogenic and cytotoxic therapies is expected to yield maximal antitumor response because such combinations would attack independant pathways. Antiangiogenic agents would target endothelial cell-mediated angiogenesis and indirectly stop growth of tumor cells by depriving them of nutrients, while cytotoxic agents would kill cancer cells directly. However, destroying the tissue vasculature is expected to severely compromise the delivery of the cytotoxic agent to the solid tumor and render these compounds inactive. Surprisingly, synergistic antitumor effects *via* the use of antiangiogenic and cytotoxic drug combinations lead to the proposal of the "vascular normalization" theory.[73, 74]

Tumor vasculature differs significantly from normal tissue vasculature.[9] Under healthy physiological conditions, a balance between endogenous proangiogenic and antiangiogenic factors maintains normal vessels. These vessels are arranged in a hierarchical manner (i.e., arteries, capillaries, and veins) forming an orderly distributed compact network, whereas tumor vasculature is disorganized and morphologically abnormal with a leaky endothelium. Although the factors controlling tumor vascular growth are the same as those involved in healthy tissue growth, the growth of tumor vasculature is poorly regulated. In tumor environments, an abundance of proangiogenic

growth factors results in vascular growth being vigorous and random in all possible directions at all junctures. Consequently, the difference in pressure between the arterioles and venules is reduced, resistance to blood flow is increased, and blood supply to the tumor is impaired.[75] The vascular network appears haphazard with high vascular density in certain regions of the tumor and lack of vasculature in others.[76] The border of tumor-normal tissue is usually highly vascularized, while the interior core of the tumor could be avascular. Inefficient tumor blood flow due to abnormal vasculature can negatively affect the delivery of cytotoxic drugs and also cause systemic toxicities. Inefficient blood flow also affects the delivery of antiangiogenic drugs. However, as the targets of antiangiogenic agents are located in contact with the bloodstream, these drugs are considered to suffer less from delivery obstacles than drugs targeting tumor cells in the extravascular space.

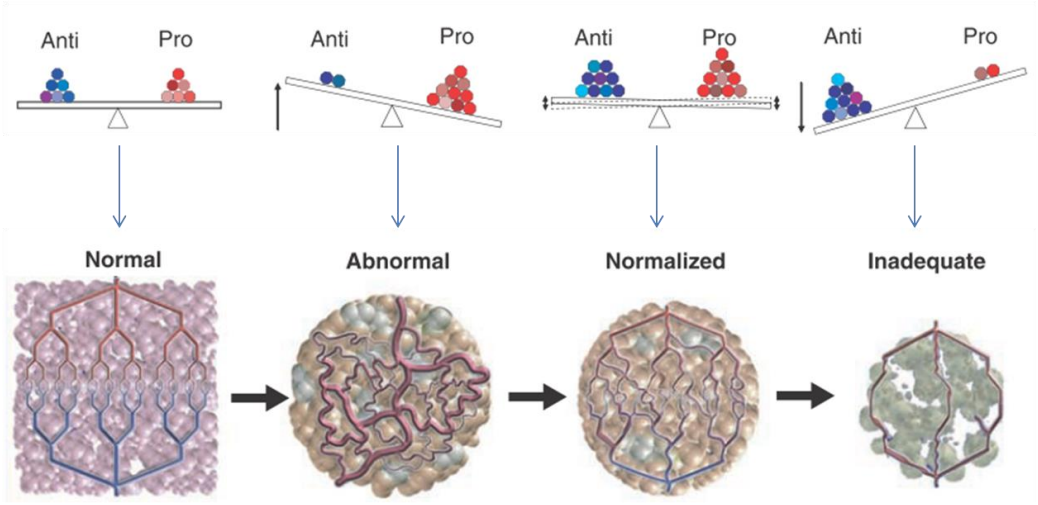

Figure 11. Antiangiogenic therapy and vessel normalization (modified from ref. 73)

The vascular normalization theory[73, 74] proposes that the effect of antiangiogenic agents is twofold: first, they can prune some of the abnormal vessels and second, due to

their antiangiogenic nature these agents can balance the effect of proangiogenic factors and result in a normalized vasculature (Figure 11). This normalization is both structural and functional. The normalized vasculature is central for blood flow with the least obstruction and blood supply to the tumor. As a result, there is improved delivery of the cytotoxic agent to the tumor thereby explaining the synergy observed in the use of antiangiogenic and cytotoxic drug combinations.

Several studies have shown that anti-VEGF treatment induces a normalization process that leads to pruning of immature vessels, and improvement of the integrity and function of the remaining vasculature by enhancing perivascular cell and basement membrane coverage.[77, 78] Normalization of tumor vasculature increases uptake and delivery of cytotoxic antitumor drugs.[79, 80] However, enhancement in the delivery of cytotoxic agents to the tumor is both dose- and time-dependent. The cytotoxic agent should be delivered to the tumor during the "window of normalization" in order to maximise the intratumoral cytotoxic drug levels. Excessive pruning of vessels can lead to inadequate vasculature and shorten the window of normalization. As a result, optimal scheduling of antiangiogenic therapy with chemotherapy and/or radiation therapy requires knowledge of the timing window during which the vessels initially become normalized, and an understanding of the duration of the normalized vasculature. In order to utilize the normalization window for appropriate scheduling of the cytotoxic agent, it is proposed that combination treatment of antiangiogenic agents with cytotoxic agents will require imaging and/or circulating biomarkers based on an in-depth understanding of the dynamics of the vascular response to the antiangiogenic agent, particularly the balance between vascular pruning and normalizing effects. If these cautions are not exercised the

chemotherapeutic agent could miss the therapeutic window and suboptimal effects of combination chemotherapy would result.

E. Multiple target inhibition with single agents

Multitargeted drugs or designed multiple ligands are defined as rationally designed single chemical entities capable of selectively target two or more biological targets or processes.[81] The most commonly used strategy in the design of multitargeted agents is that of "designing in" or combining structural elements from different compounds that bind to their respective targets. If the pharmacophores for the respective targets overlap, the common structural features of the lead compounds can be "merged" resulting in a designed multiple ligand.

As with combination chemotherapy, targeting different pathways in tumor cells using multitargeted agents can increase therapeutic effectiveness, as this strategy may prevent cancer cells from developing resistance.[82] Other advantages include a lower risk of drug-drug interactions *in vivo* and improved patient compliance resulting from reduction in the number of medications required. A challenging factor in the design of multitargeted agents is optimizing the pharmacokinetics of the lead compound while retaining a balanced target profile (i.e, optimizing the ratio of activities at the different targets and the effects of metabolism to ensure a therapeutic, but non-toxic, effect at each of these targets).[81]

Several anticancer multitarget strategies have been studied in cancer therapy.[83, 84] A clinical strategy that has been successful is the combination of antiangiogenic and cytotoxic agents.[66, 85-90] Multitarget agents that combine antiangiogenic effects by RTK inhibition and cytotoxic effects, are reviewed in the following section.

E.1 Dual DHFR and RTK inhibition

Almost a decade ago, Gangjee *et al.*[91] reported the design and synthesis of 5-substituted, 2,4-diaminofuro[2,3-*d*]pyrimidines **1** and **2** (Figure 12) as inhibitors of multireceptor tyrosine kinases and dihydrofolate reductase (DHFR) with antiangiogenic and antitumor activity. A 2:1 *E/Z* mixture of **1** and the *E*-isomer of **2** demonstrated dual VEGFR2 and PDGFRβ inhibitory activity comparable to semaxanib and

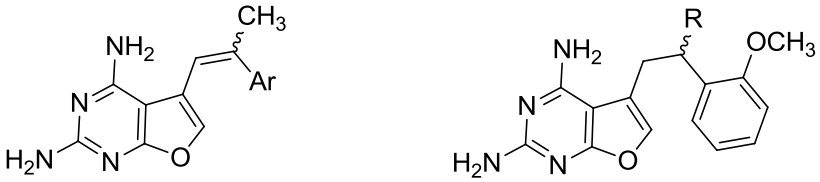

1 Ar = 2-naphthyl
2 Ar = 2-OCH_3-Phenyl

3 R = isopropyl
4 R = cyclopropyl

Figure 12. Single agents with dual RTK and DHFR inhibitory activity

AG1295 as standard compounds respectively. These compounds also showed potent antiangiogenic activity in the chicken embryo chorioallantoic membrane (CAM) assay. *In vivo*, these compounds are as active as the standard antitumor agent methotrexate, both against primary tumors and metastases, in a B16 melanoma model. Further attempts to increase DHFR inhibitory activity of these compounds lead to the identification of saturated derivatives **3** and **4** possessing dual EGFR and PDGFRβ inhibitory activity along with DHFR inhibition.[92]

E.2 Dual TS and RTK inhibition

Gangjee *et al.*[93] have reported the design and synthesis of substituted pyrimido[4,5-*b*]indoles as single agents with antiangiogenic and cytotoxic activities. Pyrimido[4,5-

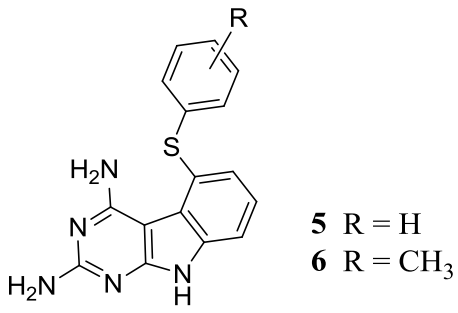

5 R = H
6 R = CH_3

Figure 13. Single agents with dual RTK and TS inhibitory activity

b]indoles **5** and **6** (Figure 13) inhibit VEGFR2 and PDGFRβ for antiangiogenic effects and human thymidylate synthase (hTS) for cytotoxic effects with inhibitory potencies comparable or better than semaxanib (VEGFR2 inhibitor), DMBI (PDGFRβ inhibitor) and raltitrexed (hTS inhibitor) as standard compounds. In a COLO-205metastatic colon cancer xenograft mouse model, thioether **5** significantly decreased tumor growth as measured by tumor growth inhibition (i.e., TGI = 76% at 35 mg/kg). Remarkably without any toxicity, compound **5** significantly decreased liver metastases, and also displayed significant antiangiogenic effects when compared with untreated control and DMBI.

E.3 Unknown cytotoxic mechanism and RTK inhibition

More recently, a series of 4-anilino substituted tricyclic indeno[2,1-*d*]pyrimidines (**7**–**19** , Figure 14) were reported as single entities with dual antiangiogenic and cytotoxic activities.[94] Most of the analogs demonstrated potent inhibitory activity against PDGFRβ compared to SU4312 as a standard compound. The 4-chloro analog **13** was about 4.5-fold more potent against PDGFRβ than **19**. The 4-isopropyl analog **9** was equipotent with semaxanib as a standard against VEGFR2. Compound **9** was also a dual inhibitor of

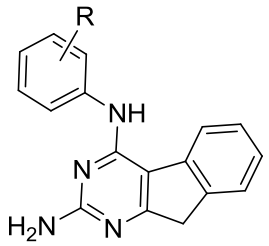

R		R	
7	H	**14**	3-Br
8	2-$C(CH_3)_2$	**15**	4-Br
9	4-$C(CH_3)_2$	**16**	4- CF_3
10	3-F	**17**	3-OCH_3
11	4-F	**18**	4-F, 3-Cl
12	3-Cl	**19**	2-F, 4-Cl
13	4-Cl		

Figure 14. Single agents with dual RTK inhibitory activity and cytotoxicity

VEGFR2 and PDGFRβ. Analogs **7**, **10**, **13**, **17**, and **19** exhibited potent cytotoxicity comparable to cisplatin as a standard in A431 cells. Unsubstituted aniline **7** also inhibited most of the NCI 60 tumor cell lines with GI_{50}s at nanomolar to micromolar levels. Inhibition of hTS or DHFR or dihydroorotate dehydrogenase are not the mechanisms of cytotoxic effects of these compounds. The cytotoxic mechanism(s) of action of **13** is currently under investigation. In a B16-F10 syngeneic mouse melanoma model, 4-chloro derivative **13** decreased tumor growth rate and inhibited angiogenesis similar to SU6668 and much more than in the untreated control animals. These studies[91-94] attest to the potential of designing compounds with antiangiogenic and cytotoxic activities as combination chemotherapy *via* a single chemical entity.

II. CHEMICAL REVIEW

The chemistry related to the work described in this dissertation is reviewed in this section and includes synthetic approaches to the following hetrocyclic ring systems.

A. Pyrrolo[3,2-*d*]pyrimidines

B. Pyrimido[5,4-*b*]indoles

C. Furo[3,2-*d*]pyrimidines

D. Benzofuro[3,2-*d*]pyrimidines

A. Synthesis of pyrrolo[3,2-*d*]pyrimidines

Synthetic strategies that were used in the synthesis of pyrrolo[3,2-*d*]pyrimidines can be broadly classified into two strategies:

1. Strategy A: From pyrimidine precursors

2. Strategy B: From pyrrole precursors

A.1. Pyrrolo[3,2-*d*]pyrimidines from pyrimidine precursors

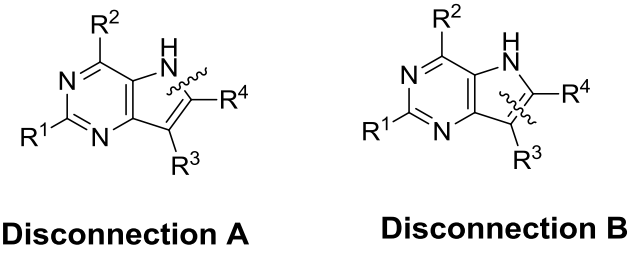

Figure 15. Disconnection strategies towards pyrrolo[3,2-*d*]pyrimidines

Different methods used in the synthesis of pyrrolo[3,2-*d*]pyrimidines from pyrimidine precursors utilize disconnections A or B (Figure 15). For disconnection A, the

precursors to cyclization are generally enamines[95] or alkynes.[96]

Scheme 1. Enamines in the synthesis of pyrrolo[3,2-*d*]pyrimidines

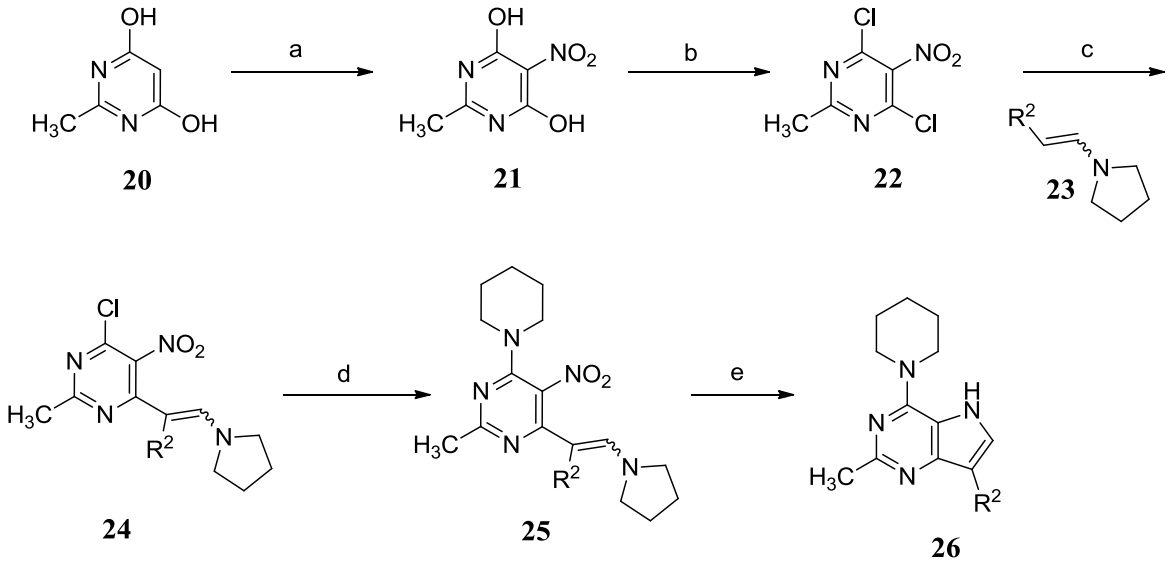

Reagents: (a) TFA, HNO_3; (b) $POCl_3$, DIPEA, toluene; (c) DIPEA, toluene; (d) piperidine, triethylamine, toluene:dioxane; (1:2); (e) $SnCl_2$, DMF

Nitration of appropriately substituted pyrimidine **20** (Scheme 1) using nitric acid provides 2-methyl-4,6-dihydroxy-5-nitropyrimidine (**21)** and subsequent chlorination using phosphorous oxychloride affords key intermediate **22**.[95] Enamines with general structure **23** are treated with dichloro intermediate **22** to provide intermediate **24**. Appropriately substituted enamines are obtained by tin tetrachloride-mediated condensation of corresponding methyl ketones with pyrrolidine. Nucleophilic aromatic substitution of **24** with piperidine affords **25** which can then be subjected to reductive cyclization using tin(II) chloride to afford pyrrolo[3,2-*d*]pyrimidine **26**.

Alternative to reductive cyclization of enamines, metal catalyzed cyclization of acetylenes can be utilized as a key strategy in the construction of pyrrolo[3,2-*d*]pyrimidines from pyrimidine precursors (Scheme 2).[96]

Scheme 2. Copper (I)-catalyzed cyclization towards pyrrolo[3,2-*d*]pyrimidines

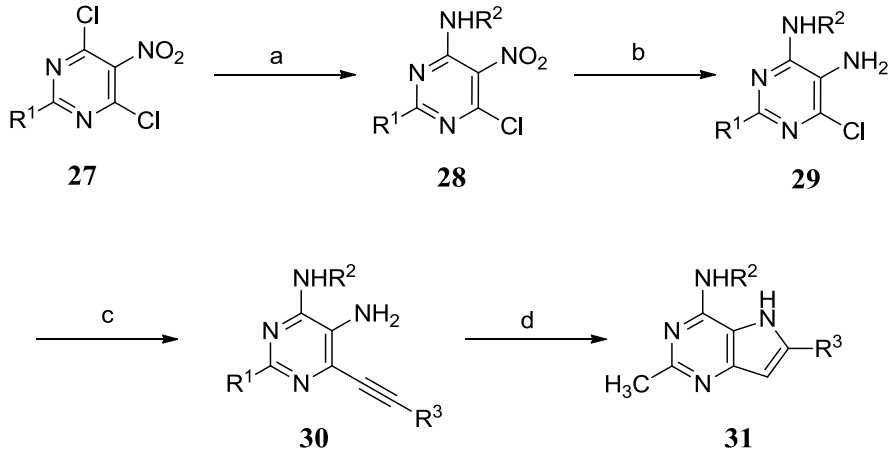

Reagents: (a) H_2NR_2, triethylamine, THF; (b) $SnCl_2.H_2O$, $(C_2H_5)_2O$, HCl (conc); (c) $HC{\equiv}CR_2$, $Pd(PPh_3)_2Cl_2$, CuI, triethylamine; (d) CuI, DMF

Nucleophilic aromatic substitution of dichloropyrimidine **27** (Scheme 2) with amines is used to provide appropriately substituted pyrimidines (**28)**.[96] Reduction of the nitro group in these polysubstituted pyrimidines affords the corresponding anilines (**29)**. Palladium catalyzed treatment with terminal acetylenes the affords key intermediate **30**. Copper (I) iodide mediated intramolecular cyclization of **30** subsequently provides pyrrolo[3,2-*d*]pyrimidines with general structure **31**.

Zhao *et al*. have reported a one-pot protocol for the syntheses of 2-chloro-pyrrolo[3,2-*d*]pyrimidines.[97] As a part of this work 2,4-Dichloro-5-nitropyrimidine (**32**,

Scheme 3) was subjected to nucleophilic aromatic substitution with ethyl benzoylacetate **33** to afford intermediate **34** which was converted into the 2-chloro-pyrrolo[3,2-*d*]pyrimidine **36** through a reductive cyclization process .

Scheme 3. One-pot protocol for the syntheses of pyrrolo[3,2-*d*]pyrimidines

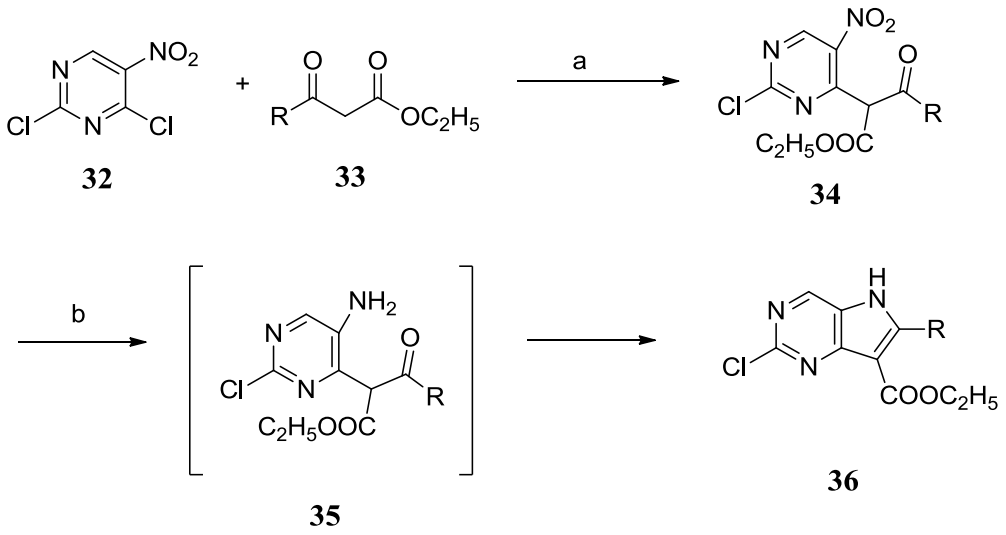

Reagents: (a) NaH, THF; (b) Fe, CH_3COOH

Scheme 4. Furneaux method[98] for synthesis of 2-amino 4-oxo pyrrolo[3,2-*d*]pyrimidines

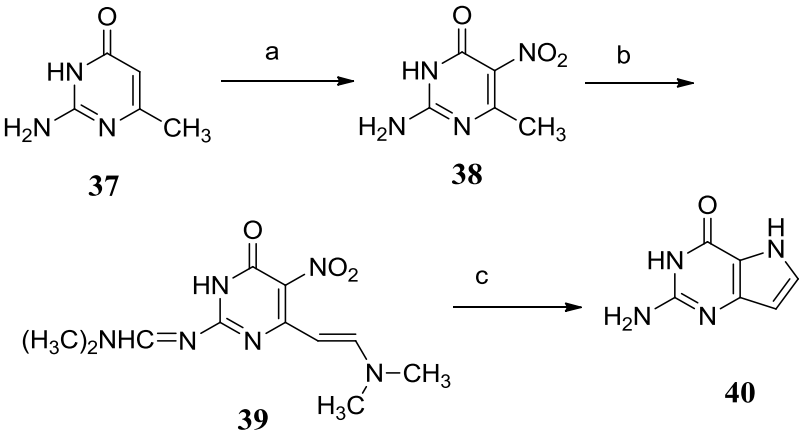

Reagents: (a) H_2SO_4, HNO_3; (b) DMF dimethylacetal, DMF; (c) $Na_2S_2O_4$, H_2O

Furneaux *et al*. reported the synthesis of 2-amino-3*H*,5*H*-pyrrolo[3,2-*d*]pyrimidin-4-one **40** (Scheme 4).[98] Nitration of 2-amino-6-methylpyrimidin-4(3*H*)-one **37** affords compound **38**. On treatment of nitro derivative **38** with 6 equiv of DMF dimethyl acetal in DMF at 100 °C, compound **39** is obtained which upon subsequent dithionite reduction and cyclization affords pyrrolo[3,2-*d*]pyrimidine **40** in 36% overall yield.

Scheme 5. Taylor strategy for synthesis of 2-amino 4-oxo pyrrolo[3,2-*d*]pyrimidines

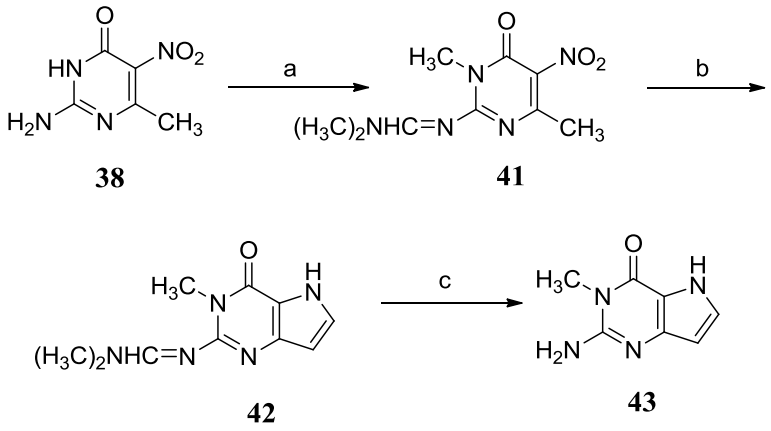

Reagents: (a) DMF dimethylacetal, DMF; (b) $Na_2S_2O_4$, THF/H_2O; (c) 1 N NaOH

However, Taylor *et al*.[99] obtained pyrimidinone lactam N-alkylated product **41** (Scheme 5) upon reaction of compound **38** with DMF dimethyl acetal in DMF. Subsequent treatment with sodium dithionite provides annulated product **42**, which is then subjected to base hydrolysis to provide N-methylated pyrrolo[3,2-*d*]pyrimidine **43**. The synthetic sequence was modified (Scheme 6) to include protection of the pyrimidine lactam nitrogen to prevent methylation.

Scheme 6. Taylor modified strategy for synthesis of pyrrolo[3,2-*d*]pyrimidines

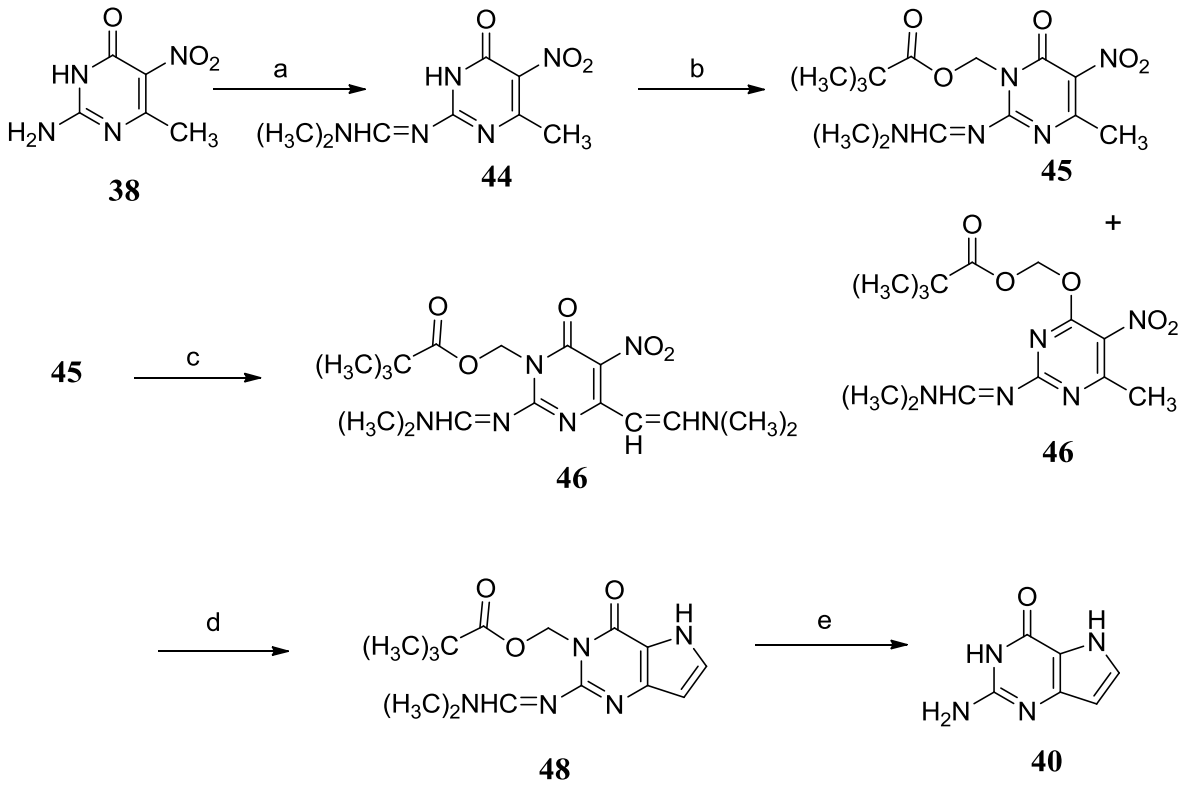

Reagents: (a) DMF dimethylacetal, CH_2Cl_2; (b) NaH. chloromethyl pivalate; (c) DMF dimethylacetal, DMF; (d) $Na_2S_2O_4$; (e) 1 N NaOH.

Treatment of nitropyrimidine **38** with DMF dimethylacetal in CH_2C1_2 generates compound **44** (Scheme 6).[99] Reaction of pyrimidine **44** with sodium hydride followed by addition of excess chloromethyl pivalate provides a 4:l mixture of N-alkylated **45** and its O-alkylated isomer **46**. Pyrimidine **45** can then be converted to **47** upon treatment with DMF dimethylacetal at room temperature. Subsequent reductive annulation affords bicyclic **48** which can bedeprotected using aqueous sodium hydroxide to afford 2-amino-3*H*,5*H*-pyrrolo[3,2-*d*]pyrimidin-4-one **40** in 25% overall yield.

Scheme 7. Madelung cyclization strategy for synthesis of pyrrolo[3,2-*d*]pyrimidines

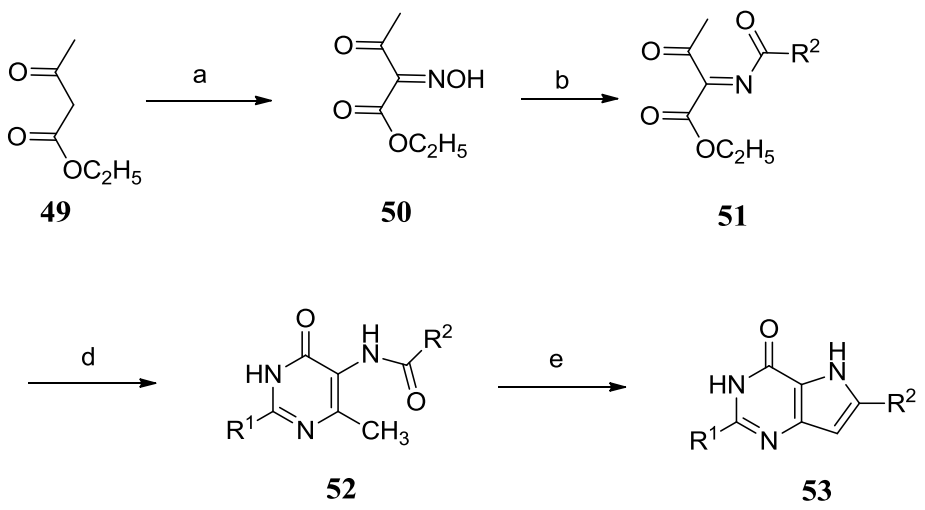

Reagents: (a) $NaNO_2$, AcOH, H_2O; (b) Zn, H_2SO_4, H_2O; (c) $R_2(C=O)Cl$, NaOAc; (d) $R_1(C=NH)NH_2$. HCl, $NaOC_2H_5$, C_2H_5OH; (e) $NaOC_2H_5$, 360 °C.

Madelung cyclization (Disconnection B, Figure 1) can be utilized in the synthesis of several pyrrolo[3,2-*d*]pyrimidines (Scheme 7).[100] Treatment of ethyl acetoacetate **49** with sodium nitrite and acetic acid affords ethyl 2-hydroxyimino-3-butyrate **50**. Zinc and sulfuric acid mediated reduction of **50** provides the corresponding 2-aminoacetoacetate. which upon isolation and acylation with an appropriate acid chloride affords **51**. However, in situ acylation of the intermediate without isolation affords higher yields. Base catalyzed condensation of the ethyl *N*-acylated-2-aminoacetoacetates **51** with acetamidine hydrochloride provides acylpyrimidine intermediates **52**. Madelung cyclization of pyrimidines **52** at elevated temperatures affords pyrrolo[3,2-*d*]pyrimidines **53**.

A.2. Pyrrolo[3,2-*d*]pyrimidines from pyrrole precursors

Scheme 8. Pyrimidine ring construction

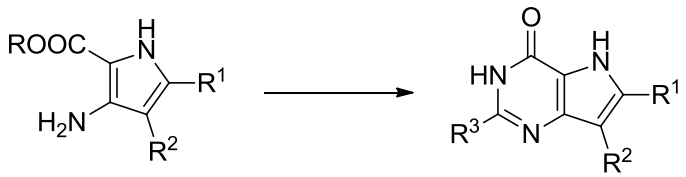

54 **55**

Several pyrrolo[3,2-*d*]pyrimidine analogs with varying substitution patterns have been successfully synthesised using they key pyrroles with general structure **54** (Scheme 8). Synthetic strategies towards the synthesis of pyrrole **54** utilize key disconnection strategy shown in Figure 16. Preparation of appropriately substituted pyrroles can be accomplished using cyanoacetylenes[101] or α-cyano ketones[102] or α-cyano aldehydes[103] in 20 to 63% yields.

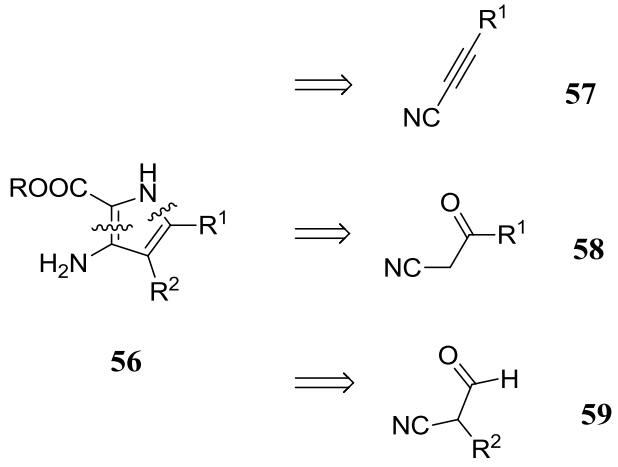

Figure 16. Disconnection strategies towards precursor pyrroles

Scheme 9. Pyrrole ring construction from cyanoacetylenes

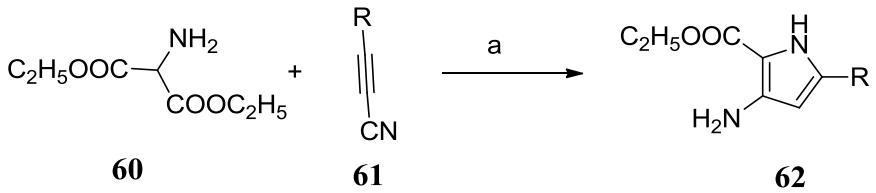

60 **61** **62**

Reagents: (a) $NaOC_2H_5$, C_2H_5OH

Treatment of cyanoacetylenes **61** (Scheme 9) with diethylaminomalonate **60** followed by a base catalysed intramolecular cyclization affords pyrroles **62**.[101] This methodology can provide pyrroles with R_2 = H [**56**, Figure 16].

Scheme 10. Pyrrole ring construction from α-cyano ketones

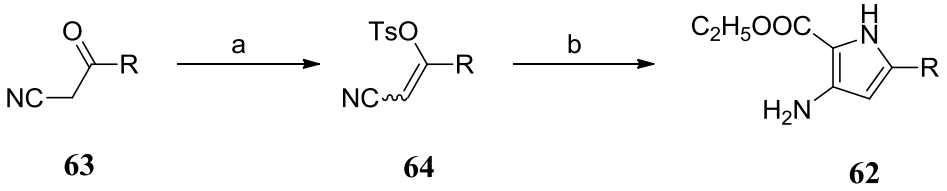

63 **64** **62**

Reagents: (a) Ts_2O, triethylamine, CH_2Cl_2; (b) $NaOC_2H_5$, C_2H_5OH

Treatment of α-cyano ketones **63** (Scheme 10) with p-toluenesulfonic anhydride provides the corresponding p-toluenesulfonyl enol esters **64**.[102] The crude enol esters **64** are immediately condensed with diethyl aminomalonate **60** using sodium ethoxide to provide substituted pyrroles **62**.

Scheme 11. Pyrrole ring construction from α-cyano aldehydes

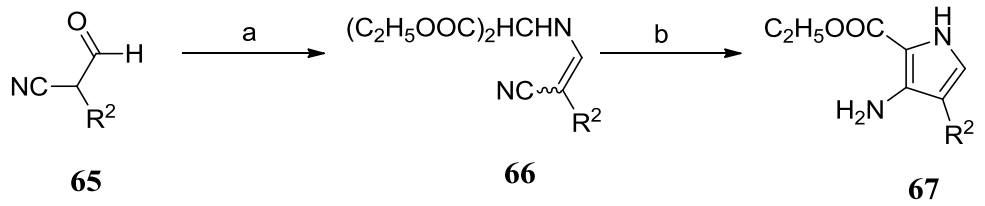

65 **66** **67**

Reagents: (a) diethyl aminomalonate, $NaOCH_3$; (b) $NaOCH_3$, CH_3OH

Treatment of appropriately substituted α-cyano aldehydes **65** (Scheme 11) with diethyl aminomalonate provides the enamine **66**.[103] Base catalysed intramolecular cyclization using sodium methoxide affords pyrroles **67**.

With a variety of pyrroles with appropriate 4- or 5-substituents, several pyrrolo[3,2-*d*]pyrimidines with desired substituents on the 2-position of the pyrimidine ring can be prepared (48 to 85% yields) as shown in Schemes 12-18. Some examples of pyrrolo[3,2-*d*]pyrimidine analogs synthesized by this strategy are 2-alkyl-4-oxo-pyrrolo[3,2-*d*]pyrimidines,[104] 2-amino-4-oxo-pyrrolo[3,2-*d*]pyrimidines,[104-106] 6-phenyl-2-sulfanyl-4-oxo-pyrrolo[3,2-*d*]pyrimidines[107] and 6-phenylpyrrolo[3,2-*d*]pyrimidine-2,4-diol.[106]

Scheme 12. Synthesis of 2-alkyl-4-oxo-pyrrolo[3,2-*d*]pyrimidines

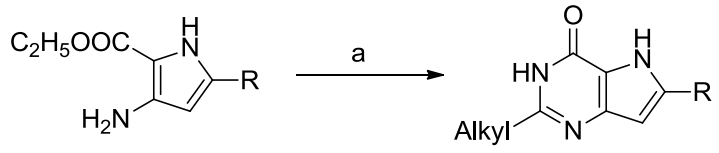

68 **69**

Reagents: (a) Alkylnitrile, HCl; (b) NaOH, C_2H_5OH

Pyrrolo[3,2-*d*]pyrimidines with 2-alkyl substituents are obtained by treatment of pyrroles **68** (Scheme 12) with an alkyl nitriles in anhydrous hydrochloric acid at room temperature followed by heating with sodium hydroxide.[104]

Scheme 13. Synthesis of 3*H*-pyrrolo[3,2-*d*]pyrimidin-4(5*H*)-ones

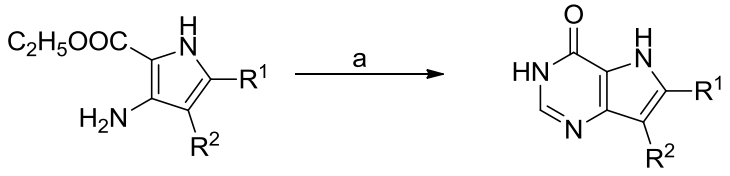

70 **71**

Reagents: (a) formamidine acetate, C_2H_5OH

Similarly pyrrolo[3,2-*d*]pyrimidines with 2-H are obtained by cyclocondensation of pyrroles **70** (Scheme 13) with formamidine in refluxing ethanol.[98, 108]

Scheme 14. Synthesis of 2-amino-4-oxo-pyrrolo[3,2-*d*]pyrimidines

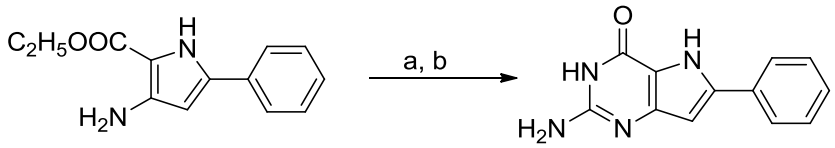

72 **73**

Reagents: (a) Cyanamide, HCl; (b) aq. NaOH

Pyrrolo[3,2-*d*]pyrimidines with 2-amino substituents are obtained by treatment of pyrroles **72** (Scheme 14) with cyanamide and hydrochloric acid in dioxane at reflux followed by heating with aqueous sodium hydroxide.[104]

Scheme 15. Synthesis of 2-carbamate-4-oxo-pyrrolo[3,2-*d*]pyrimidines

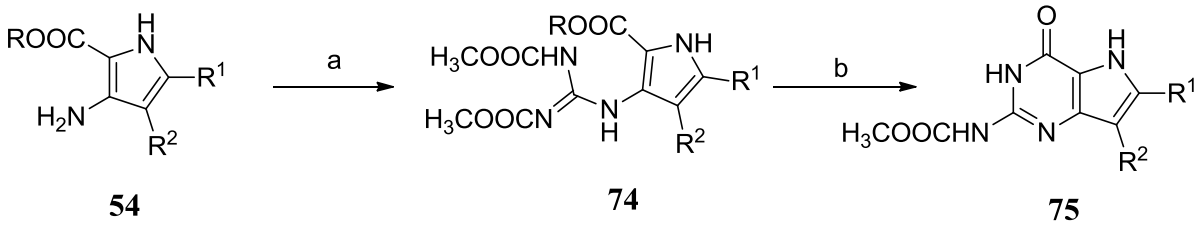

54 **74** **75**

Reagents: (a) 1,3-dicarbomethoxy-2-methyl-2-thiopseudourea, CH_3COOH; (b) $NaOCH_3$, CH_3OH

Another approach that has been utilized in the synthesis of pyrrolo[3,2-*d*]pyrimidines with 2-carbamate or 2-amino is shown in Scheme 15. This method involves the use of 1,3-dicarbomethoxy-2-methyl-2-thiopseudourea as the guanylating agent to afford intermediate **74** which upon base catalysed cyclization affords pyrrolo[3,2-*d*]pyrimidines **75**. [105]

Scheme 16. Synthesis of 2-sulfanyl-4-oxo-pyrrolo[3,2-*d*]pyrimidines

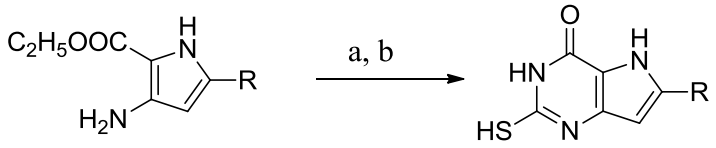

76 **77**

Reagents: (a) $S=C=NCOOC_2H_5$, HCl; (b) aq. NaOH

Similarly pyrrolo[3,2-*d*]pyrimidines with 2-sulfanyl substituent can be obtained by treatment of pyrroles **76** (Scheme 16) with an ethyl isothiocyanatoformate and hydrochloric acid in benzene at reflux followed by heating with aqueous sodium hydroxide.[107]

Scheme 17. Synthesis of pyrrolo[3,2-*d*]pyrimidine 2,4-dione

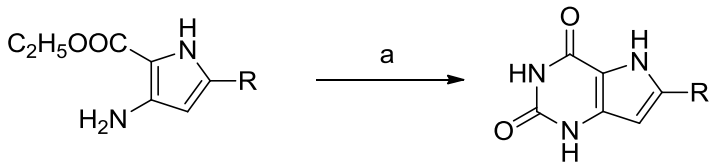

76 **79**

Reagents: (a) KNCO, CH_3COOH; (b) aq. NaOH

Similarly pyrrolo[3,2-*d*]pyrimidines with 2,4-dioxo substituent are obtained by cyclocondensation of pyrroles **76** with potassium cyanate under acidic conditions at room temperature followed by heating with aqueous sodium hydroxide.[106]

Schemes 18-20 outline different synthetic strategies used in the synthesis of 7-benzyl pyrrolo[3,2-*d*]pyrimidines. Nitration of 2-amino-4-oxo 6-chloro pyrimidine **80** (Scheme 18) using a mixture of nitric and sulphuric acid provides nitro pyrimidine **81**.[109, 110]

Nucleophilic displacement of benzyl bromide **82** with the carbanion of ethyl cyanoacetate **83** affods intermediate **84** which can be used in a nucleophilic aromatic substitution of the 6-chloro group of **81** to afford **85**. Compound **85** can be subjected to a ester hydrolysis and decarboxylation to afford **86**. Nitro pyrimidine **86** can be subjected to a catalytic hydrogenation reaction to afford an intermediate amine **87** which undergoes a reductive cyclodeamination under acidic conditions to form **89**.[109-111]

Scheme 18. Synthesis of 2-amino-4-oxo-pyrrolo[3,2-*d*]pyrimidines from pyrimidines

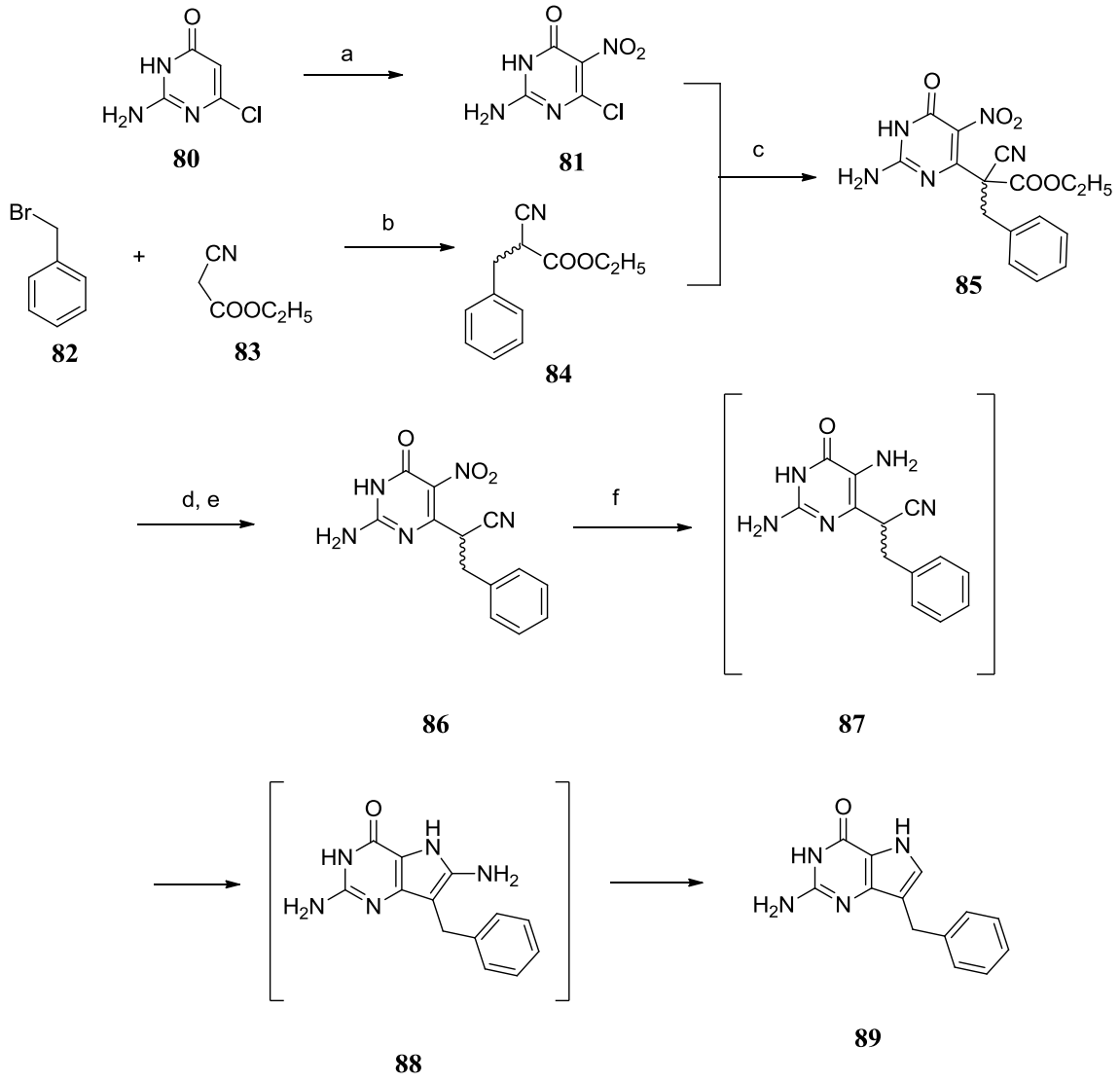

Conditions: [a] (a) H_2SO_4, HNO_3; (b) K_2CO_3, DMF; (c) K_2CO_3, DMSO; (d) NaOH, H_2O; (e) HCl, H_2O; (f) Pd/C, H_2, 6N HCl

Arylpropenenitrile **90** (Scheme 19) can be prepared by the condensation of the appropriate aldehyde with cyanoacetic acid and subsequent catalytic (Pd/C) hydrogenation affords the corresponding propanenitrile **91**. Sodium hydride in THF is

Scheme 19. Synthesis of 2-amino-4-oxo-pyrrolo[3,2-*d*]pyrimidines from pyrroles

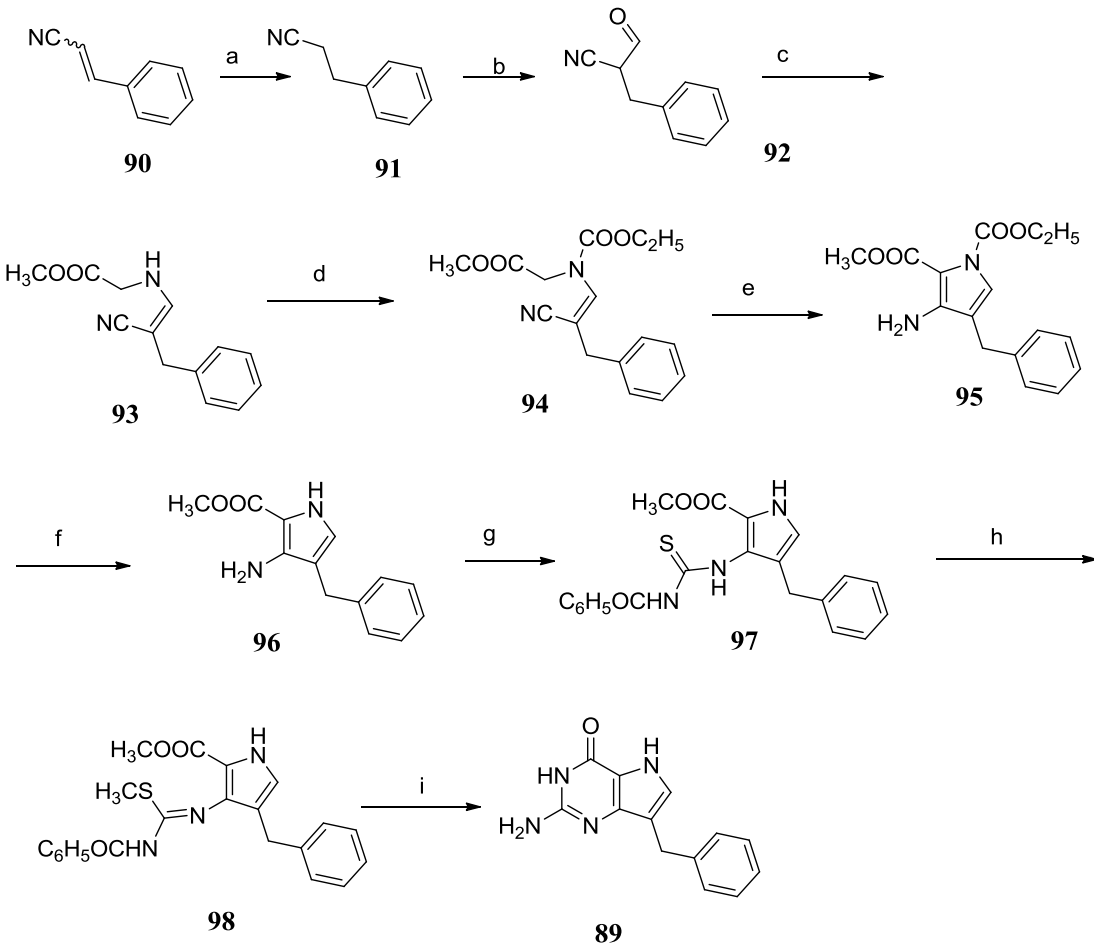

Reagents: (a) Pd/C, H_2; (b) NaH, THF, $HCOOC_2H_5$; (c) methyl glycinate hydrochloride, CH_3COONa, CH_3OH, H_2O; (d) $ClCOOC_2H_5$, DBN, 0 °C; (e) rt; (f) Na_2CO_3, CH_3OH; (g) benzoyl isothiocyanate, CH_2Cl_2; (h) DBN, CH_3I; (i) NH_3, CH_3OH

used to deprotonate α to the cyano group and the resulting anion can be treated with ethyl formate to provide the desired 2-formyl-propanenitrile **92**. The reaction of 2-formylpropanenitrile **92** with methyl glycinate hydrochloride in aqueous methanol at room temperature in the presence of sodium acetate readily affords the enaminonitriles **93**. Compound **93** can be treated with ethyl chloroformate and DBN first at 0 °C for 1 h (to afford intermediate **94**) and then 16 h at room temperature to provide the cyclized pyrrole **95**. Compound **95** can then be decarbethoxylated to **96** by treatment with sodium

carbonate in methanol. Treatment of **96** with benzoyl isothiocyanate in dichloromethane at room temperature affords the desired 2-(carbomethoxy)-3-[*N*-benzoyl(thiocarbamoyl) aminol]-1*H*-pyrrole **97**. *S*-methylation of **97** by treatment with methyl iodide in the presence of DBN in dichloromethane affords compound **98**. Treatment of **98** with methanolic ammonia provides 2-amino 4-oxo pyrrolo[3,2-*d*]pyrimidine **89.**

Pyrrolo[3,2-*d*]pyrimidine **99** (Scheme 20) can be subjected to Friedel–Crafts acylation or alkylation, using triflic acid as catalyst to afford the corresponding 7-substituted pyrrolo[3,2-*d*]pyrimidine **100** or **89** respectively in 20% yields.[112] The benzoylated compound **100** can be transformed into the corresponding benzyl **89** analog by a Wolff–Kishner reduction.

Scheme 20. Alkylation/acylation of 2-amino-4-oxo-pyrrolo[3,2-*d*]pyrimidines

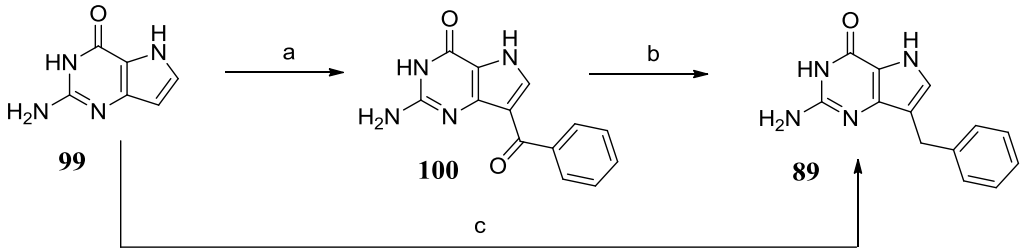

Reagents: (a) Benzoyl chloride, triflic acid (b) hydrazine, KOH (c) Benzyl bromide, triflic acid

B. Synthesis of pyrimido[5,4-*b*]indoles

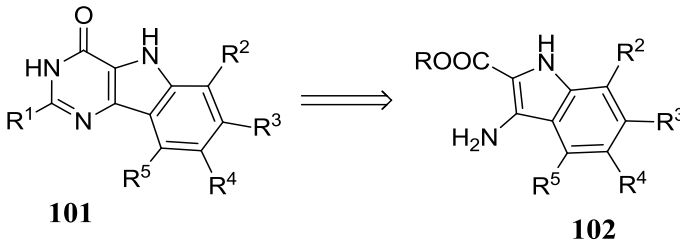

Figure 17. Indole precursors to pyrimido[5,4-*b*]indoles

Several pyrimido[5,4-*b*]indole analogs with varying substitution patterns have been successfully synthesized using they key indoles **102** (Figure 17).[113-115]

Scheme 21. Synthesis of indole precursors

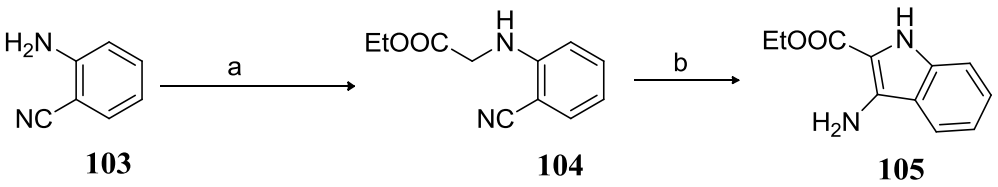

Reagents: (a) ethyl bromoacetate, $NaHCO_3$; (b) t-BuOK

Anthranilonitrile **103** (Scheme 21) can be alkylated under basic conditions with ethyl bromoacetate to afford intermediate **104**.[113, 115] On treatment with a base, compound **104** cyclizes to form the indole **105** which is the key precursor to pyrimido[5,4-*b*]indoles.

An efficient one-step synthesis of 2-amino-5*H*-pyrimido[5,4-*b*]indoles through a copper-catalyzed cascade reaction between 3-haloindole-2-carbaldehydes **106** (Scheme 22) and guanidine hydrochloride was reported by Biswas *et al*.[116] However these reaction

Scheme 22. Copper catalyzed cascade reaction

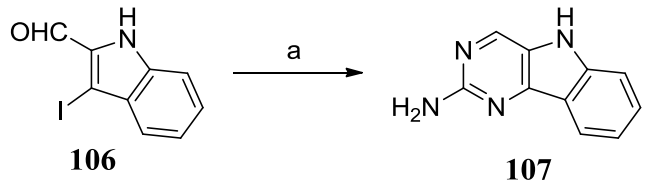

106 **107**

(a) Guanidine hydrochloride, CuI, *L*-proline, Cs_2CO_3, DMSO

conditions did not provide the 2-methyl pyrimidoindole when guanidine was replaced with acetamidine.

Scheme 23. Palladium catalyzed pyrimidine formation

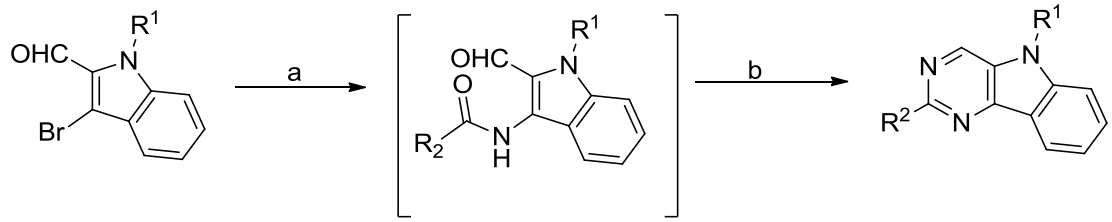

108 **109** **110**

Reagents: (a) R_2CONH_2, $Pd_2(dba)_3$, BINAP, Cs_2CO_3, Toluene; (b) $HCOONH_4$, *t*-BuOH

Kumar *et al*.[117] have published a palladium catalyzed amidation method which converts 3-bromoindole **108** (Scheme 23) to intermediate **109** which on treatment with ammonium acetate cyclizes to form pyrimido[5,4-*b*]indole **110**.

An aldol condensation at room temperature between ketone derivatives **111** (Scheme 24) with aldehyde **112** in the presence of a catalytic amount of sodium hydroxide provides the benzylidene adduct, which upon heating to reflux in ethanol with a solution of guanidine under basic condition affords **113**.[118]

Scheme 24. Synthesis of 2-amino-4-oxo-pyrrolo[3,2-*d*]pyrimidines

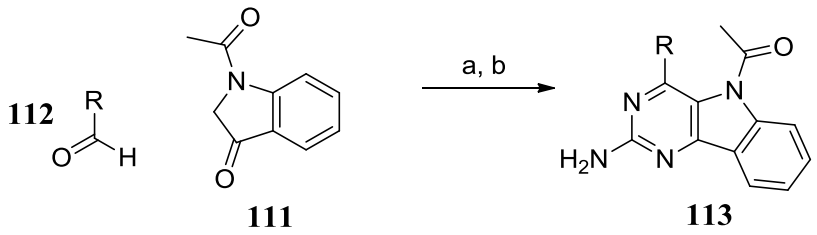

Reagents: (a) NaOH, C_2H_5OH; (b) guanidine, C_2H_5OH

C. Synthesis of furo[3,2-*d*]pyrimidines

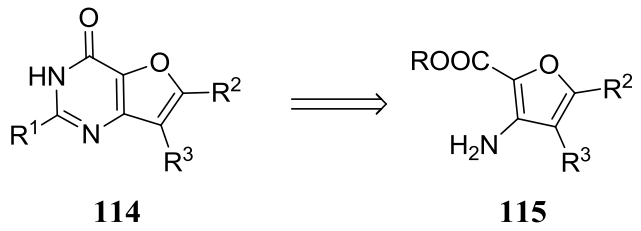

Figure 18. Furan precursors to furo[3,2-*d*]pyrimidines

Several furo[3,2-*d*]pyrimidine analogs with varying substitution patterns have been successfully synthesised using substituted furans with general structure **115** (Figure 18).[119-123]

Carbanions of appropriately substituted alkylnitriles **116** (Scheme 25) are treated with ethyl formate **117** to form the sodium enolate **118**.[119, 121, 123-125] This reaction can be accomplished using strong base sodium hydride and weak base sodium methoxide. The enolate **118** can be O-alkylated with diethyl chloromalonate to afford intermediate **119**. Subsequent treatment of **119** with a base promotes cyclization and decarboxylation to

Scheme 25. Synthesis of key furan precursors

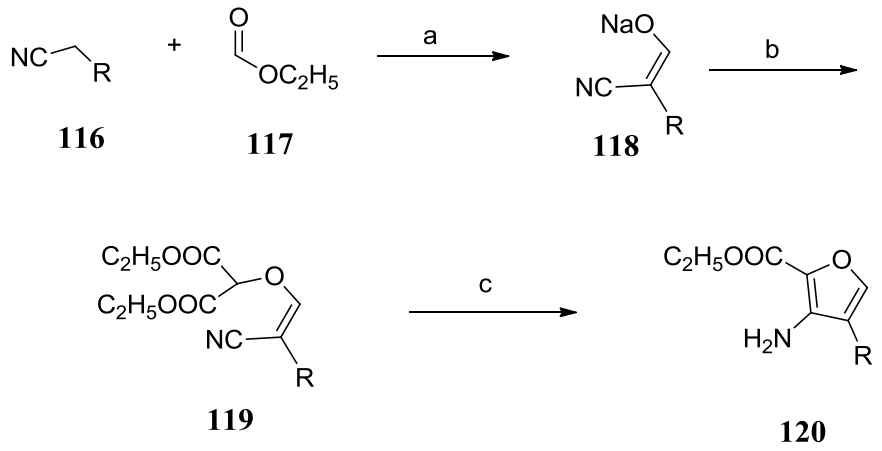

116 **117** **118** **119** **120**

Reagents: (a) CH_3ONa, CH_3OH (or) NaH, THF; (b) $ClCH(COOC_2H_5)_2$; (c) DBN C_2H_5OH

provide key furan **120**. This synthetic methodology has been reported for R = H,[121] R = aryl, [124, 125] R= alkyl[123] and R = benzyl[119, 126, 127]

Scheme 26. Synthesis of 3-amino-2-carboxy furans

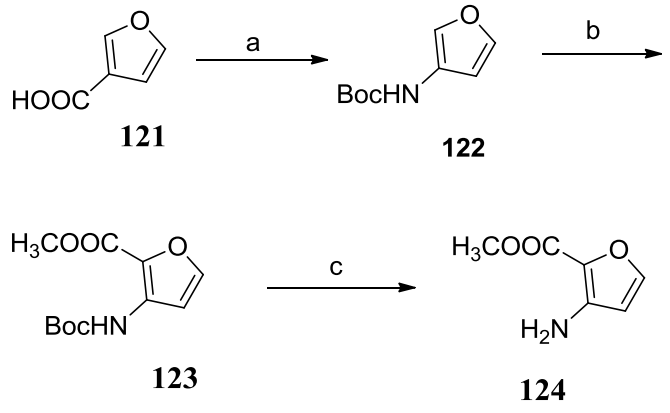

121 **122** **123** **124**

Reagents: (a) DPPA, triethylamine, *t*-BuOH; (b) *n*-BuLi, TMEDA, $CO(OCH_3)_2$; (c) TFA, CH_2Cl_2

Alternatively, furan-3-carboxylic acid **121** (Scheme 26) can be converted to the requisite amino group by a Curtius rearrangement to give the Boc-protected furanamine **122**.[120, 122] Lithiation of **122** followed by quenching of the reaction with dimethyl carbonate followed by amine deprotection provides **124** with methyl ester introduced at the 2-position.

Scheme 27. Synthesis of 3-amino 2-cyanao furans

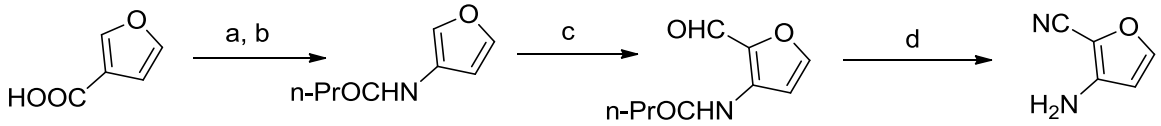

121 **125** **126** **127**

Reagents: (a) DPPA, triethylamine, toluene; (b) propyl magnesium chloride; (c) $POCl_3$, DMF; (d) NH_2OH, 4-methylbenzenesulfonic acid

Similarly, furan-3-carboxylic acid **121** can be reacted under Curtius conditions to generate N-furan-3-ylbutanamide **125** (Scheme 27).[128] Vilsmeier Haack reaction of **125** provides furaldehyde **126** which upon amination provides the cyano analog **127**.

Another approach utilized in the synthesis of furan precursors for furo[3,2-*d*]pyrimidines was developed by Redman *et al.*[127] Mitsunobu reaction of 3-(4-chloro-phenyl)-3-oxo-propanenitrile **128** (Scheme 28) with ethyl glycolate affords intermediate **129** which on treatment with sodium hydride leads to ring closure to provide aminofuran **130**. This synthetic sequence is limited to the synthesis of 5-alkyl-, 5-aryl-, and 4,5-fused bicyclic furans.

Scheme 28. Synthesis of 3-amino-2-carboxy furans

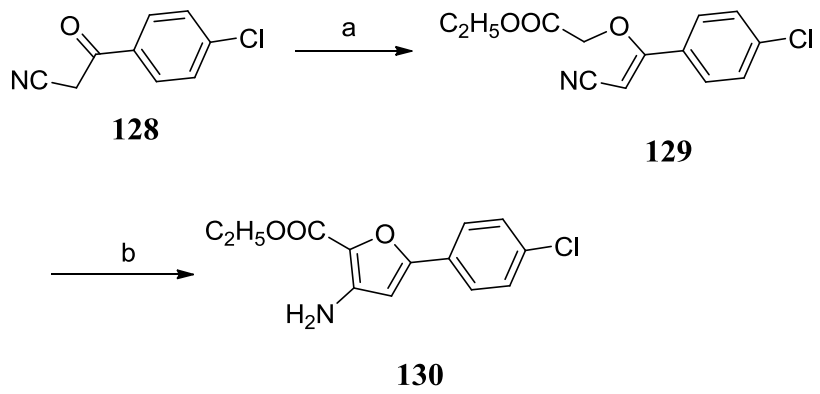

128 **129** **130**

Reagents: (a) PPh_3, DIAD, THF, ethyl glycolate; (b) NaH, THF

Furo[3,2-*d*]pyrimidines **132** (Scheme 29) with 2-H can be obtained by cyclocondensation of furan **131** with formamidine in ethanol at reflux. [127]

Scheme 29. Synthesis of 4-oxo-furo[3,2-*d*]pyrimidines

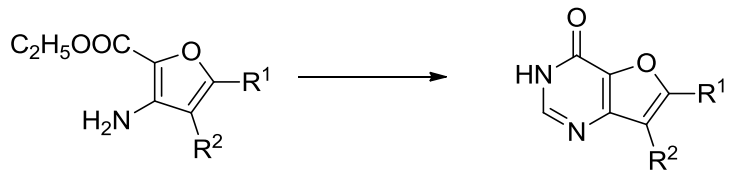

131 **132**

Reagents: (a) formamidine acetate, C_2H_5OH

Similarly, furo[3,2-*d*]pyrimidines with 2-oxo substituent are obtained by treating furan **133** (Scheme 30) with chlorosulfonyl isocyanate for converting the amine to a urea **134** which then undergoes cyclization in basic methanol to afford the furo[3,2-*d*]pyrimidine 2,4-dione **135**.[120]

Scheme 30. Synthesis of furo[3,2-*d*]pyrimidine 2,4-dione

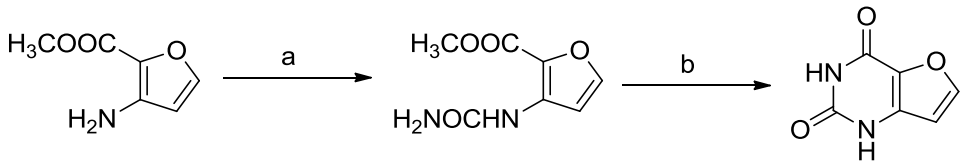

133 **134** **135**

Reagents: (a) ClO_2SNCO, CH_2Cl_2; (b) NaOH, CH_3OH

Scheme 31. Synthesis of 2-alkyl-4-oxo-furo[3,2-*d*]pyrimidine

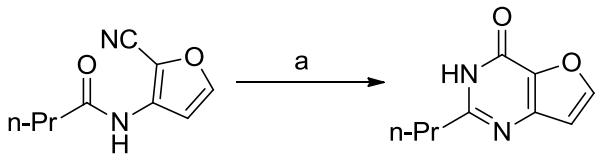

136 **137**

Reagents: (a) KOH, *t*-BuOH

Similarly furo[3,2-*d*]pyrimidine **137** (Scheme 31) with 2-alkyl substituent can be obtained by treating 3-amido furan **136** with a hydroxide base to form cyclized furo[3,2-*d*]pyrimidine.[128]

Furo[3,2-*d*]pyrimidines with 2-carbamate or 2-amino substituent involves the use of 1,3-dicarbomethoxy-2-methyl-2-thiopseudourea as the guanylating agent to provide the guanidine adduct **139** (Scheme 32).[119, 121] Treatment of **139** with sodium methoxide leads to cyclization with loss if a carbamate group to afford 2-carbamido-furo[3,2-*d*]pyrimidine **140** which upon reacting with sodium hydroxide provides 2-amino-furo[3,2-*d*]pyrimidine **141**.

Scheme 32. Synthesis of 2-amino-4-oxo-furo[3,2-*d*]pyrimidines

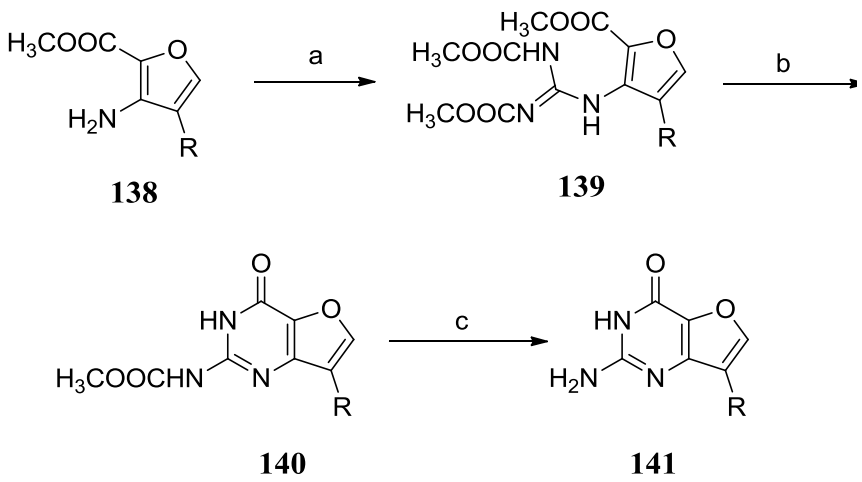

Reagents: (a) 1,3-dicarbomethoxy-2-methyl-2-thiopseudourea, CH_3COOH; (b) $NaOCH_3$, CH_3OH; (c) aq. NaOH

D. Synthesis of benzofuro[3,2-*d*]pyrimidines

Several benzofuro[3,2-*d*]pyrimidine analogs **142** (Figure 19) with varying substitution patterns have been successfully synthesised using the key benzofurans with general structure **143**.[115]

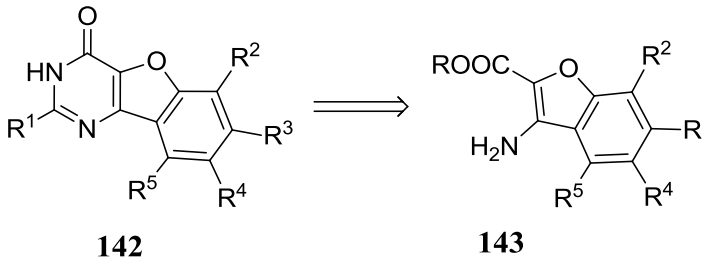

Figure 19. Benzofuran precursors to benzofuro[3,2-*d*]pyrimidines

Scheme 33. Synthesis of benzofuran precursors

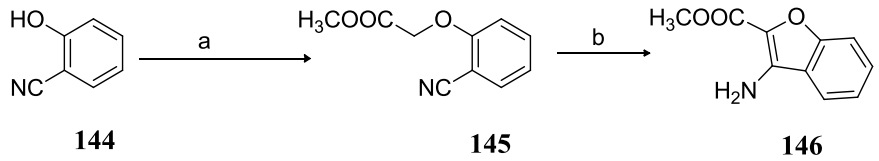

144 **145** **146**

Reagents: (a) methyl bromoacetate, K_2CO_3, acetone; (b) NaH, DMSO

2-Hydroxy benzonitrile **144** (Scheme 33) can be alkylated under basic conditions with methyl bromoacetate to afford intermediate **145**.[115] On treatmentwith a base, compound **145** cyclizes to form the benzofuran **146** which is the key precursor to benzofuro[3,2-*d*]pyrimidines.

Scheme 34. Copper(I)-mediated cascade reactions

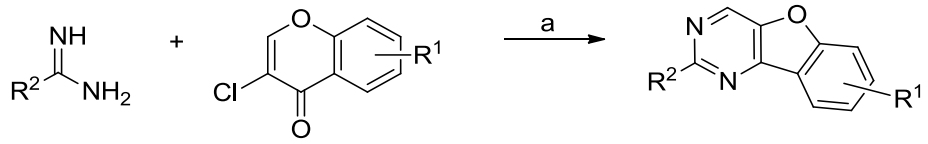

147 **148** **149**

Reagents: (a) CuBr, DBU, DMF

Recently Chao *et al.*[129] have reported an efficient approach to the synthesis of functionalized benzofuro[3,2-*d*]pyrimidines **149** (Scheme 34) which involves copper(I)-mediated cascade reactions. This reaction utilizes 3-chlorochromenones **148** and various amidines **147** and their analogs as starting materials. The process is promoted by copper(I) bromide and takes place *via* a chemoselective Michael addition-elimination double intramolecular cyclization sequence as shown in Figure 20.

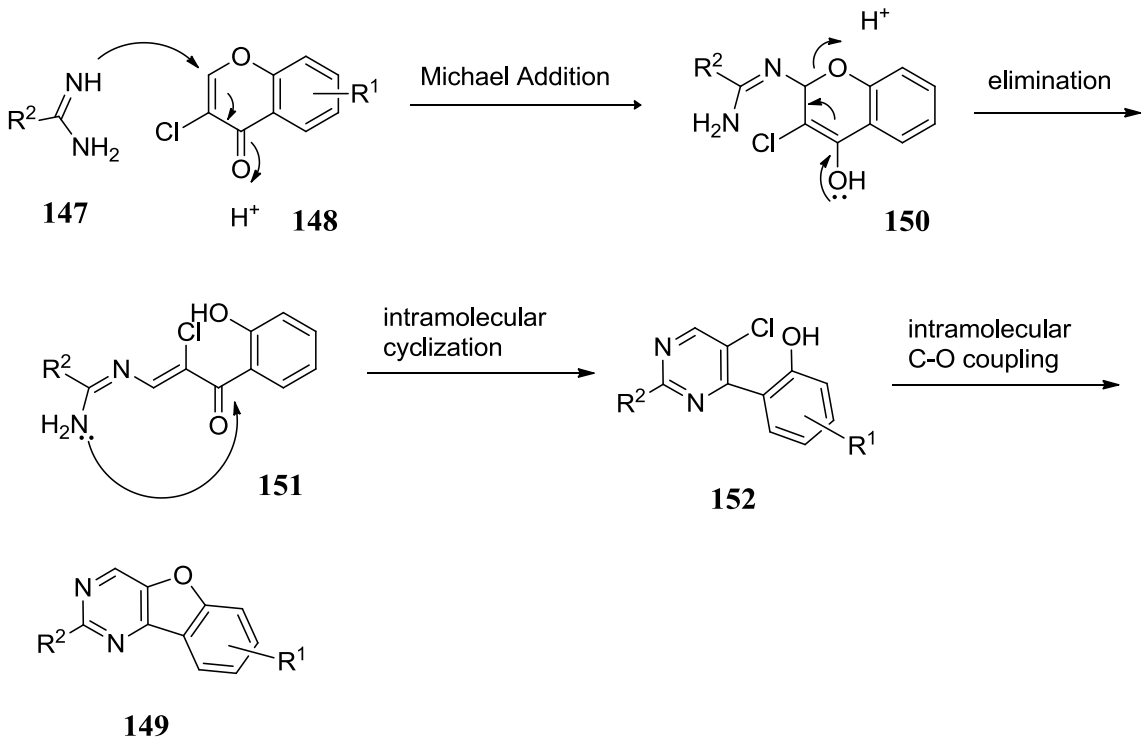

Figure 20. Steps involved in cascade reaction

Scheme 35. Synthesis of benzofuro[3,2-*d*]pyrimidines

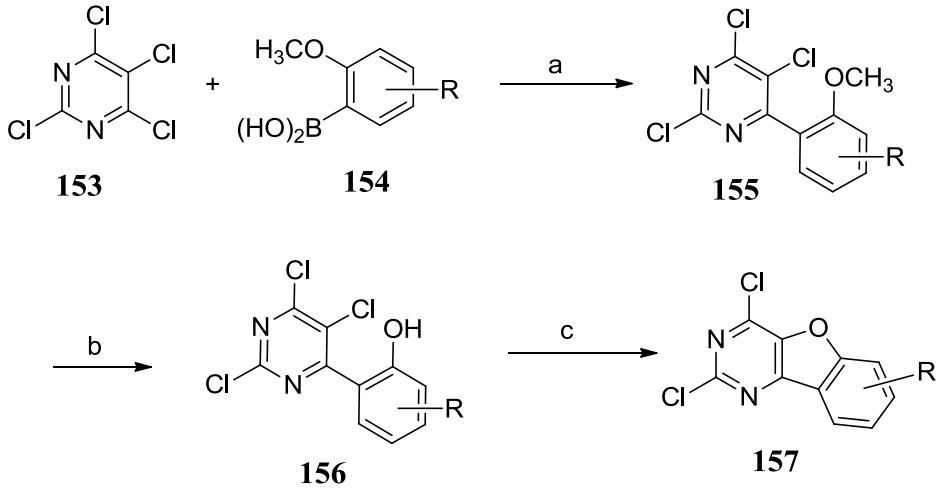

Reagents: (a) $Pd(OOCCH_3)_2$, PPh_3, K_3PO_4; (b) BBr_3, CH_2Cl_2; (c) copper(I) thiophene-2-carboxylate, NMP

Liu *et al.*[130] have reported a concise synthesis for the facile assembly of fused benzofuropyrimidine **157** (Scheme 35). Chemo/regioselective Suzuki coupling between 1,2-dihaloarene **153** and α -methoxyphenylboronic acid **154** gives biaryl phenoxy ether **155**, followed by demethylation to form the biaryl phenol **156**, which then undergoes copper(I) thiophene-2-carboxylate mediated intramolecular cyclization to afford **157**.[130, 131]

Scheme 36. Synthesis of 2-amino- benzofuro[3,2-*d*]pyrimidines

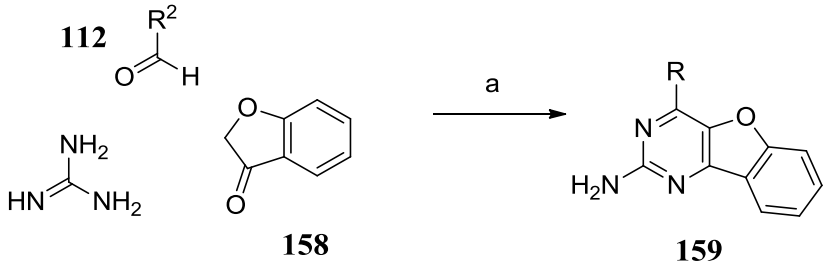

Reagents: (a) NaOH, C_2H_5OH

An aldol condensation at room temperature between ketone derivatives **158** (Scheme 36) with aldehyde **112** in the presence of a catalytic amount of sodium hydroxide provides the benzylidene adduct, which when heated to reflux in ethanol with a solution of guanidine under basic condition affords benzofuro[3,2-*d*]pyrimidines **159**.[118]

III. STATEMENT OF THE PROBLEM

When a tumor grows beyond 2 mm^3 it requires nutrients and oxygen for maintenance and growth and initiates the process of having a blood supply system.[3] Under hypoxic conditions it secretes several proangiogenic factors of which VEGF is the key mediator of angiogenesis.[132] VEGF binds to its receptor VEGFR2 and stimulates the process of angiogenesis which supports rapid tumor growth and metastases.[14] One of the key strategies to obtain antiangiogenic effects is to develop VEGFR2 kinase inhibitors.[15] These inhibitors were found to arrest tumor growth and cause tumor shrinkage.[133] However resistance to VEGFR2 inhibitors results in increased invasion and metastases.[134] At the onset of VEGFR2 inhibition there are two possible effects: regression of tumor vessels and normalization of surviving vessels.[73, 74] This process of vessel normalization was found to transiently improve blood flow. Investigations into the combined use of VEGFR2 with cytotoxic therapies have yielded more promising results than VEGF-targeting monotherapy.[74, 135] Combinations of cytotoxic agents and VEGFR2 inhibitors have shown synergistic effects suggesting that there is improved delivery of the cytotoxic agent during this transient phase of vessel normalization.[135]

Yoshizawa *et al.*[79] have reported enhanced tumor penetration and in vivo antitumor activity of cytotoxic paclitaxel in combination with the VEGFR2 inhibitor semaxanib in Colon-26 solid tumor-bearing mice. Tumors treated with semaxanib contained significantly smaller hypoxic regions compared with the nontreated control group, suggesting that structural normalization of the tumor vasculature resulted in an improvement in tumor vessel functions, including oxygen supply. Immunostaining for

endothelial cells and pericytes showed that the treatment with semaxanib enhanced the pericyte coverage of the tumor vasculature. Treatment with semaxanib increased the distribution of paclitaxel in the core region of the tumor, hence decreasing the ratio of their peripheral distribution. These results suggest that the structural and functional normalization of the tumor vasculature by the treatment with semaxanib to reach the deeper regions within tumor tissues lead to more potent antitumor activity of paclitaxel. This strategy of utilizing the VEGFR2 inhibition based vascular normalization phase to enhance blood supply and the delivery of cytotoxic agent may also address the problem of dose limiting toxicities as there is decreased peripheral distribution.[79]

The outcome of combination treatment is likely to be affected by the effects of the antiangiogenic agent on the tumor (cells/vasculature) and the intratumoral levels of the cytotoxic agent. [136] In order to maximise the intratumoral levels of the cytotoxic agent, it is necessary to appropriately schedule administering the cytotoxic agent to ensure that it is used during the period of vessel normalization.[137] Tumor targeted drug delivery has the potential to improve cancer care by reducing off-target toxicities and increasing the efficacy of the cytotoxic agent.[138] Judicious scheduling is an influential and critical factor because of the impact on intratumoral cytotoxic drug level.[133, 137, 139] The effect of the VEGFR2 inhibitor depends on factors such as the type of tumor, levels of VEGFR production and VEGFR2 overexpression.[140] Hence, if not appropriately scheduled the cytotoxic agent may miss the timing window of normalization.[141] Also, administering separate antiangiogenic and cytotoxic agents may not alleviate the issues of dose limiting toxicities of cytotoxic agents. Therefore compounds with antiangiogenic and cytotoxic activities in single entities allow the cytotoxicity to be mainfested as soon as the

antiangiogenic effects are operable. Such multitargeted agents could exert their cytotoxic action as soon as or even during transient tumor vasculature normalization due to the antiangiogenic effects. Thus such agents might not need to be as potent as conventional cytotoxic agents. Dosing of such an antiangiogenic RTK inhibitor with an incorporated cytotoxic mechanism would be equivalent to providing a combination of antiangiogenic agents along with a metronomic dosing of a cytotoxic agents. Several literature reports indicate the success of using antiangiogenic agents with metronomic doses of cytotoxic agents.[69-72, 101] Moreover these multitargeted single agents would circumvent the pharmacokinetic problems of multiple agents, would avoid drug - drug interactions, could be used at lower doses to alleviate toxicity, could be devoid of overlapping toxicities, and could delay or prevent tumor cell resistance. Other advantages of such single agents are in the reduced cost and increased patient compliance, which are sometimes as significant contributors to chemotherapy failure as resistance, toxicity, and lack of efficacy.

The antiangiogenic component is usually targeted to tumor cells and under most circumstances it is not targeted to normal cells. However, the cytotoxic component is targeted to the tumor cells but not exclusively. Thus the challenge in designing single agents with a cytotoxic component is that the cytotoxic component should be potent enough to kill tumor cells that have been compromised *via* the antiangiogenic effect but not potent enough to cause serious toxicity to normal cells not affected by the antiangiogenic effect.[93] Undoubtedly one of the problems with conventional cytotoxic chemotherapeutic agents is dose-limiting toxicities. These single agents should avoid these toxicities since they do not need to be as potent as conventional chemotherapeutic agents.

Gangjee *et al.*[91-94] have reported the discovery of single agents with dual antiangiogenic and cytotoxic activities. The antiangiogenic effets of these compounds were due to inhibition of RTKs and the cytotoxic effects were due to inhibition of dihydrofolate reductase[91] or thymidylate synthase[93] or an unknown target.[94] In this study VEGFR2 was chosen as the target for the antiangiogenic component as it is the principal mediator of angiogenesis. Tubulin was chosen as the target for cytotoxic effects as several clinical and preclinical combinations of tubulin inhibitors and VEGFR2 inhibitors have been successful.[87, 142, 143] Several clinical trials are ongoing for a variety of cancers including colorectal, breast, lung among others that involve FDA approved antiangiogenic agents as well as those in development, and cytotoxic chemotherapeutic agents and include CA4P, paclitaxel, docetaxal, vineristine, vinblastine with antiangiogenic agents bevacizumab, axitinib, sorafenib, sunitinib, cediranib, pazopanib, vandetanib and vatalanib.[146] Additionally, half of all human tumors have mutations in the p53 gene, and p53 status effects vulnerability of tumour cells to have its cell cycle arrested. The most effective drugs in cell lines with p53 gene mutations are tubulin binding agents.[144, 145] Our approach can be looked at as a combination of two strategies: rational target combinations designed to attack several key mechanisms contributing to cancer growth and survival simultaneously such as angiogenesis and proliferation; another involves the development of compounds that cover multiple mechanisms within a single agent.

Several highly potent antitubulin agents have failed in the early stages of clinical trials due to toxicities. Discodermolides and cryptophycin 52 (LY355703) are recent examples of such agents.[147, 148] All microtubule-binding agents share a neurological

toxicity as the most prominent dose-limiting side effect.[26] This potentially rigorous and dose-accumulative side effect usually manifests as painful peripheral axonal neuropathy.[149] The impact of this can persist for several years after the end of treatment. The reasons for this nervous-system-preferred toxicity are uncertain. However, the relative abundance and sensitivity of the neuronal microtubules could be a cause.[26] Other common toxicities of microtubule-binding agents include myelosuppression and neutropenia. The myeloid toxicity, which is usually reversible, is seen in vinca alkaloids and taxanes.[150, 151] Neutropenia was observed in several combination chemotherapy clinical trials with other drugs and was mostly manageable.[152-154]

Design of single agents with dual tubulin and RTK inhibitory potential

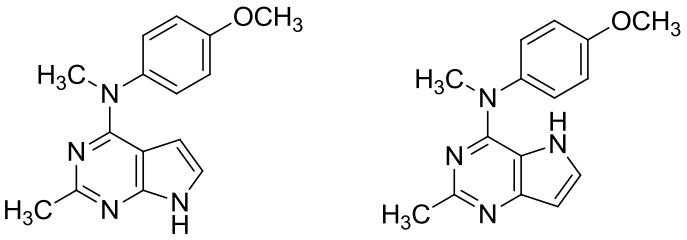

160 **161**

Figure 21. Lead compounds

Efforts to elucidate the plausible binding modes of multiple RTK-inhibitors led Gangjee *et al.*[155] to the discovery of a highly potent water-soluble antimitotic antitumor pyrrolo[2,3-*d*]pyrimidine: **160** (Figure 21). [156, 157] It was discovered to be a colchicine site binding, microtubule depolymerizing agent that inhibited the growth of cancer cells with GI_{50} in the nanomolar range. Compound **160** also overcomes the two most clinically relevant tumor resistance mechanisms that limit activity of microtubule targeting agents:

overexpression of Pgp[158, 159] and βIII-tubulin.[160-164] Additionally, compound **160** was readily convertible to the water-soluble hydrochloride salt. These attributes encouraged the choice of **160** as the lead molecule for the design of dual acting VEGFR2 and tubulin inhibitors. Pyrrolo[3,2-*d*]pyrimidine derivatives have been reported to possess inhibitory activity against several RTKs such as VEGFR2,[165-167] PDGFRβ,[167] EGFR.[168] Hence, the design of pyrrolo[3,2-*d*]pyrimidine analogs of compound **160** may provide compounds with dual RTK inhibitory activity and tubulin inhibitory activity. Compound **161** was designed as a regioisomer of the pyrrolo[2,3-*d*]pyrimidine **160**.

Table 1. Effects on tubulin and VEGFR2 in cellular assays

	EC_{50} Microtubule Depolymerization (μM)	**MDA-MB-435 IC_{50} ± SD** (nM)	**VEGFR2 kinase inhibition IC_{50} ± SD**
160	5.8	183 ± 3.4	
161·HCl	1.2	96.6 ± 5.3	183 ± 3.4 nM
CSA4	0.0131	3.47 ± 0.6	
Sunitinib			18.9 ± 2.7 nM

It was determined that **161** is about 5-times more potent than **160** against tubulin polymerization and it was not a potent VEGFR2 inhibitor (Table 1). Before designing compounds to structurally engineer VEGFR2 inhibitory potential, it was of interest to identify the structural features that are crucial for antitubulin activity. Hence **Series I** (Figure 22) was designed as antitubulin agents. Compounds **162**, **163** and **164** were designed to evaluate the importance of the 2-CH_3, 4′-OCH_3 and 4-NCH_3 moieties

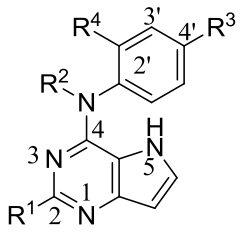

	R_1	R_2	R_3	R_4
162	H	CH_3	OCH_3	H
163	CH_3	CH_3	H	H
164	CH_3	H	OCH_3	H
165	CH_3	H	OCH_3	OCH_3

Figure 22. Series I

respectively to antitubulin activity. Compound **165** was designed by incorporating a 2′-OCH_3 group to explore the effect of substituents in this position to antitubulin activity.

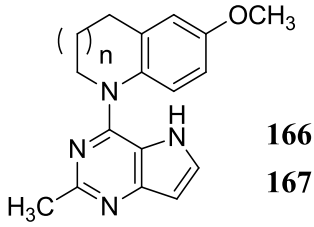

166 n = 0
167 n = 1

Figure 23. Series II

Series II (Figure 23) focuses on conformationally restricted analogs of **161**. Compounds **166** and **167** were designed by incorporating the bicyclic 6-methoxy-tertrahydroquinoline or the bicyclic 5-methoxy-dihydroindole respectively onto the 4-position of the 2-methyl pyrrolo[3,2-*d*]pyrimidine. Compared to the *N*-methylaniline, these bicyclics incorporated on the 4-position restrict the conformation of the phenyl ring thereby eliminating the rotation around the N-phenyl bond, thus affording a much more rigid structure than **161** but still maintaining the phenyl and alkyl substitutions on the *N*4 as in **161**.

Toward the goal of identifying single agents with VEGFR2 and tubulin inhibitory activities in the same entity, several compounds were designed and synthesized.

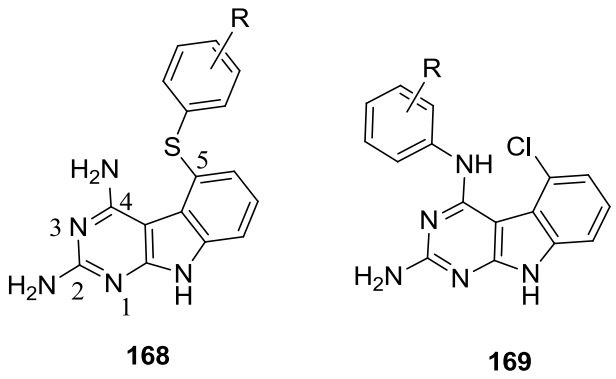

Figure 24. Tricyclic VEGFR2 inhibitors

Tricyclic pyrimido[4,5-*b*]indoles with general structures **168** and **169** (Figure 24) have been reported by Gangjee *et al.* [88, 163] to be inhibitors of VEGFR2.[93, 169] Hence it was hypothesized that small hydrophobic methyl groups at positions 5 or 6 of the pyrrolo[3,2-*d*]pyrimidine scaffold could afford additional VEGFR2 inhibitory activity. **Series III** (compounds **170**-**173**, Figure 25) was designed to ascertain whether a 5-methyl group is conducive to tubulin and VEGFR2 inhibitory activities. The 5-methyl group could have two effects: allow additional hydrophobic interactions with the targets and restrict the rotation around the N-phenyl bond, thus providing conformational rigidity which could increase potency.

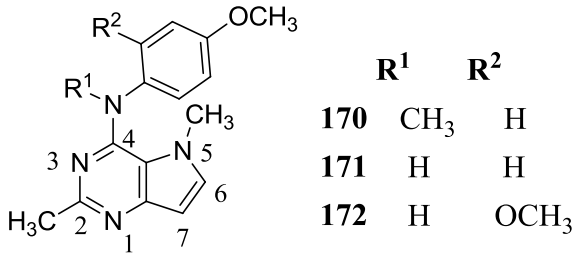

	R^1	R^2
170	CH_3	H
171	H	H
172	H	OCH_3

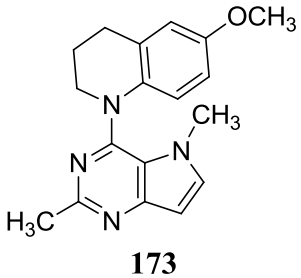

173

Figure 25. Series III

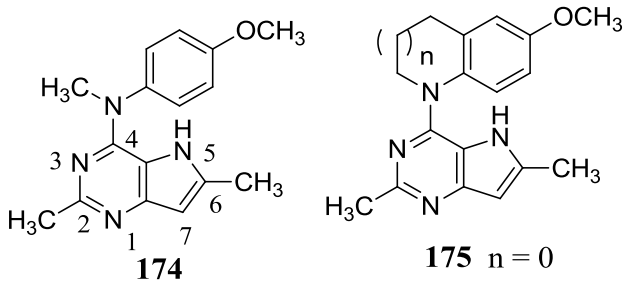

174

175 n = 0

176 n = 1

Figure 26. Series IV

Series IV (compounds **174-176**, Figure 26) was designed to check whether a 6-methyl group is conducive to tubulin and VEGFR2 inhibitory activities. The 6-methyl group could allow additional hydrophobic interactions with the targets.

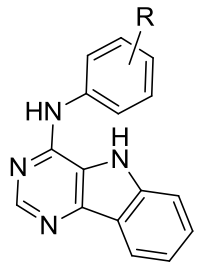

177

Figure 27. Pyrimido[5,4-*b*]indoles as RTK inhibitors

Showalter *et al.*[115] have reported the RTK inhibitory activities of tricyclic pyrimido[5,4-*b*]indoles with general structure **177** (Figure 27). It was hypothesized that fusion of a third aromatic ring at the appropriate positions of pyrrolo[3,2-*d*]pyrimidine **161** will allow additional hydrophobic interactions with VEGFR2 and improve VEGFR2 inhibitory potency without loss of tubulin inhibition. **Series V** (compounds **178-180**, Figure 28) was designed to study the effect of the tricyclic pyrimido[5,4-*b*]indole scaffold on tubulin and VEGFR2 inhibitory activities.

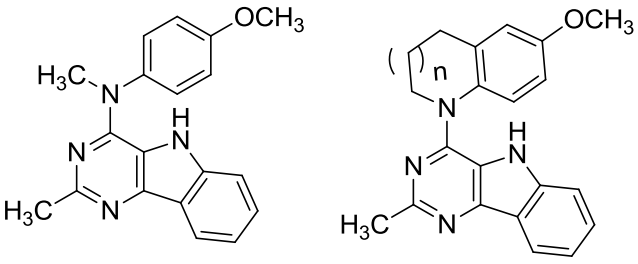

178

179 n = 0
180 n = 1

Figure 28. Series V

Series VI (Figure 29) was designed by an isosteric replacement of the N5 in **161** with an oxygen which would not only change the electronics of the bicyclic ring but would also have different hydrogen bonding capabilities compared to Series I. Compounds **181**-**185** will evaluate the effect of replacing the pyrrolo[3,2-*d*]pyrimidine scaffold in **161** with a furo[3,2-*d*]pyrimidine scaffold and the importance of hydrogen bond donor vs acceptor at the 5-position.

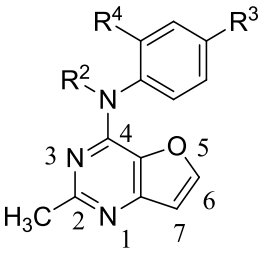

	R^2	R^3	R^4
181	CH_3	OCH_3	H
182	H	OCH_3	H
183	H	OCH_3	OCH_3

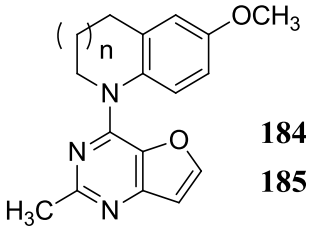

184 n = 0
185 n = 1

Figure 29. Series VI

Substituted 7-benzyl pyrrolo[2,3-*d*]pyrimidines with general structure **186** (Figure 30) were reported as antiangiogenic, antimetastatic and antitumor agents.[170] Substituents on the benzyl group and the location of the benzyl group dictate RTK inhibitory activity in pyrrolo[2,3-*d*]pyrimidines. Hence, having determined the antitubulin effects of **161**, it

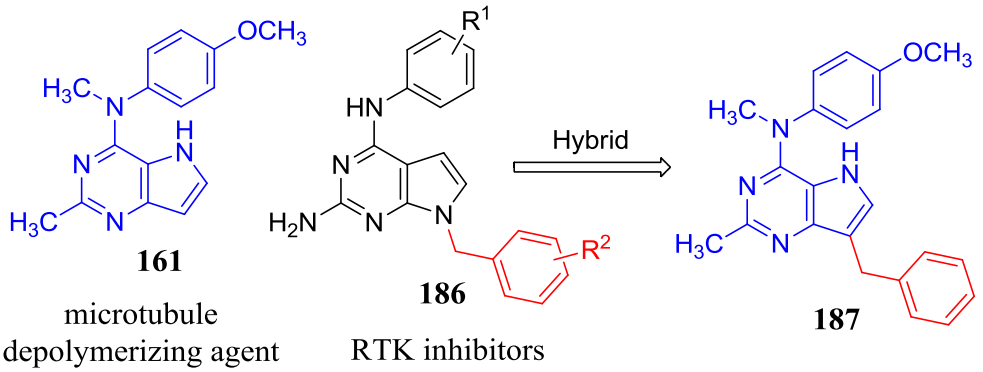

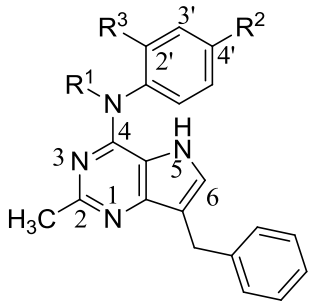

	R^1	R^2	R^3
188	CH_3	H	H
189	H	OCH_3	H
190	H	OCH_3	OCH_3

Figure 30. Series VII

was of interest to engineer RTK inhibitory activity without loss of antitubulin activity by incorporating the 7-benzyl group onto the pyrrolo[3,2-*d*]pyrimidine scaffold in **161**. The results of this hybrid design afforded compound **187**. Compounds **188** and **189** were designed to evaluate the importance of the 4'-OCH_3 and the 4-NCH_3 moieties, respectively. Compound **190** was designed by incorporating a 2'-OCH_3 group to explore the effect of substituents at this position.

The general RTK pharmacophore model consists of an Adenine region, a Sugar binding pocket and a Phosphate binding region which binds the adenine ring, the sugar moiety and the triphosphate moiety of ATP respectively. Additionally, there are two hydrophobic regions I and II, neither of which are used by ATP for binding. The pyrrolo[3,2-*d*]pyrimidine ring of the designed compounds could bind to the Adenine

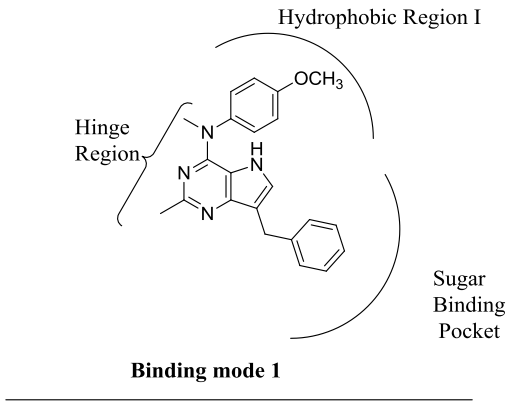

Binding mode 1

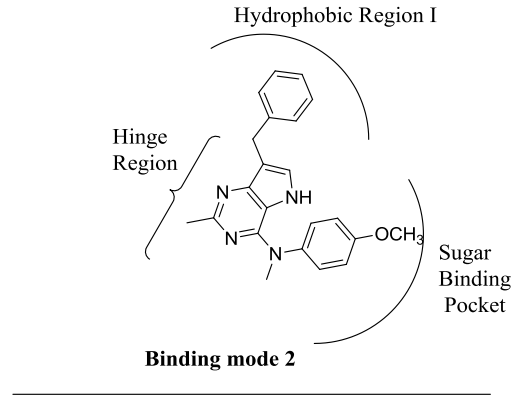

Binding mode 2

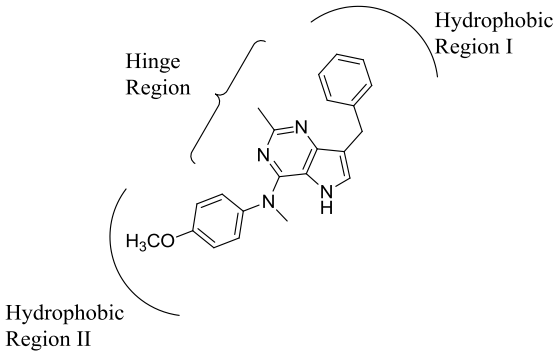

Binding mode 3

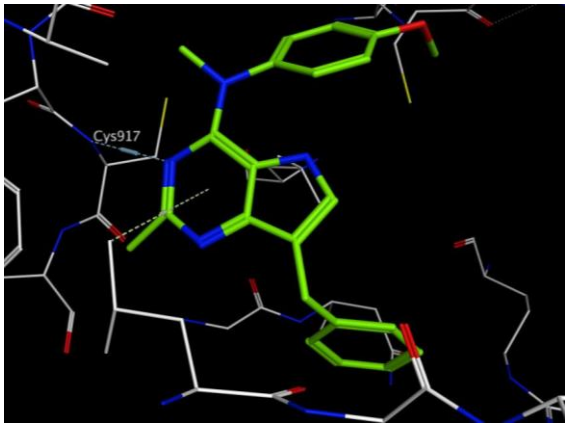

Binding mode 1

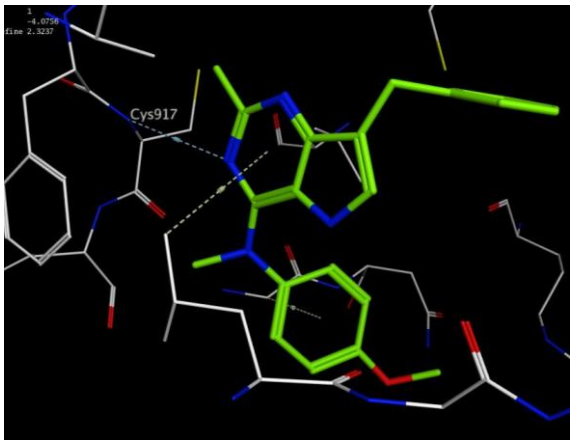

Binding mode 2

In both binding modes **187** makes a hydrogen bond interaction with the backbone of Cysteine in the hinge region.

Figure 31. Predicted binding modes of **187** in VEGFR2

region similar to heterocyclic scaffold inhibitors such as pyrimidines, quinazolines and pyrrolo[2,3-*d*]pyrimidines.[171] The 7-benzyl group was could access the Sugar binding

pocket as shown in mode 1 [Figure 31]. Alternatively, the pyrrolo[3,2-*d*]pyrimidine compounds could adopt mode 2 in which the compounds are rotated around the 2-CH_3-C2 bond. In this mode the 7-benzyl group and the 4-anilino groups could occupy Hydrophobic region I and Sugar binding pockets respectively. These compounds could also adopt binding mode 3 in which the molecule is rotated by 60^o (from mode 2). In this mode, the 7-benzyl group could orient towards the Phosphate binding pocket and the 4-anilino groups could occupy Hydrophobic region II. Docking studies performed on the X-ray crystal structure of VEGFR2 [pdb: IYWN][172] suggested the possibility of several binding modes. Representative low energy binding modes are shown in Figure 31.

Biological evaluation indicated that a single agent **187** that was designed to have both cytotoxic and antiangiogenic effects did indeed display these activities. Compound **187** has an inhibitory potency comparable with the clinically used sunitinib and clinically evaluated semaxinib against VEGFR2. The antiangiogenic effect was probably mediated *via* VEGFR2 inhibition. The cytotoxic effect was mediated by tubulin inhibition and was independent of overexpression of Pgp and βIII-tubulin. The compound caused cellular microtubule depolymerization, arrested cells in the G_2/M phase and triggered apoptotic cell death.

Compound **187**, showed a 3-digit nanomolar GI_{50} in all the NCI 60 tumor cell lines, showing moderate cytotoxic activity (as desired) against tumor cells. The antiangiogenic component of **187** is not active in these cell culture assays. This perhaps is an indication of low toxicity to normal cells.

In vivo, compound **187** reduced tumor size and vascularity in two flank xenograft models [the BLBC MDA-MB-435 and U251 glioma models] and in a 4T1 triple negative

breast orthotopic allograft model. In these *in vivo* models, the activity of **187** was superior to those of clinically used agents temozolomide (U251), docetaxel and sunitinib (MDA-MB-435 and 4T1) without overt toxicity to the animals.

Design of single agents with combination chemotherapy and multiple RTK inhibitory potential

The complexity of the angiogenic pathways implies that disrupting only a single aspect of angiogenesis may not result in significant clinical success. Multiple RTKs are co-activated in tumors and redundant inputs drive and maintain downstream signaling, thereby limiting the efficacy of therapies targeting single RTKs.[19, 173] Resistance to anti-VEGF treatment is associated with increased PDGFR expression within the tumor, increased recruitment of pericytes to tumor vasculature, and increases in other proangiogenic factors.[174] Preclinical models suggest that PDGF-mediated recruitment of pericytes may contribute to resistance to VEGF blockade. EGFR inhibition can lead to VEGFR2 up-regulation which subsequently promotes tumor growth signaling independent of EGFR and thus contributes to the resistance of EGFR inhibitors.[175, 176] The effect of EGFR inhibition can also be partially overcome by activation of PDGFR signaling and the subsequent transactivation of HER-3 signaling to promote alternate tumor growth signaling.[20, 175] Hence, targeting multiple RTKs maximizes the proportion of angiogenic signalling that is effectively targeted.[173, 175] Moreover, high intratumoral heterogeneity has been reported with different subpopulations producing distinct growth factors. [177-179] Targeting a single RTK could be ineffective due to subpopulations of cells that are either not affected by the drug mechanism and possess or acquire a greater drug

resistance.[180] Hence it was of interest to explore the effect of different structural changes on activity against the RTKs VEGFR2, PDGFRβ and EGFR in addition to having cytotoxic antitubulin effects with the goal of identifying single agents with antitubulin and multiple RTK inhibitory potential.

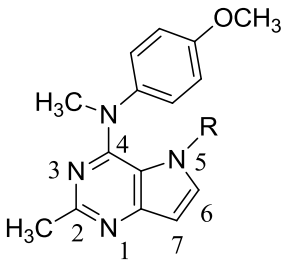

	R
191	Et
192	*i*Pr
193	*n*Pr
194	*i*Bu
195	*n*Bu

Figure 32. Series VIII

Series VIII (compounds **191-195**, Figure 32) was designed to study the biological effects of sterically induced conformational restriction of the molecule, on tubulin and multiple RTK inhibition. Introduction of alkyl substituents at the N5-position of the pyrrolo[3,2-*d*]pyrimidine scaffold was expected to restrict rotation around the N-phenyl bond, thus affording a much more rigid structure than **161**. Conformational restriction of the 4-anilino moiety could lock the compound in a conformation which could be conducive to multiple RTKs and tubulin inhibition.

Attempts to structurally modify the tubulin inhibitor **161** to achieve dual tubulin and VEGFR2 inhibition led to the identification of **181** (Series VI, Figure 9) as a novel compound with dual tubulin and EGFR inhibitory activities in a single agent. This result was of significant interest as it combines two different mechanisms of antitumor activity in the same compound (Table 2).[181] Several clinical and preclinical combinations of EGFR inhibitors and antitubulin agents have been successful.[146, 182-185] It was of interest

Table 2. Effects of **181**·HCl on tubulin and EGFR in cellular assays

	Bovine tubulin Assembly IC_{50} ± SD (μM)	**OVCAR-8 IC_{50} ± SD (nM)**	**EGFR kinase IC_{50} ± SD (nM)**
181·HCl	1.1 ± 0.04	11 ± 0.1	5 ± 0.8
CSA4	1.1 ± 0.1	1.3 ± 0.6	
Erlotinib			1.2 ± 0.2

to design structural modifications that could potentially incorporate VEGFR2 inhibitory activity without the loss of EGFR and tubulin inhibitory activities. Towards this goal several compounds were designed and synthesized.

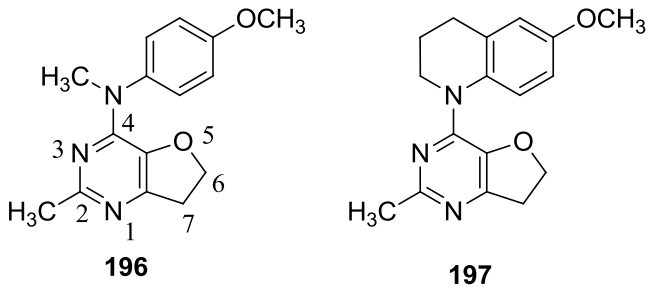

Figure 33. Series IX

Series IX (Figure 33) was designed by replacing the furo[3,2-*d*]pyrimidine in **181** with a 6,7-dihydro-furo[3,2-*d*]pyrimidine. Structurally, 6,7-dihydro-pyrrolo[2,3-*d*]pyrimidines **196** and **197** are akin to the cyclopenta[*d*]pyrimidine analogs, which are highly potent colchicine-site binding antimitotic antitumor agents.[156, 157] Reduction of the 6,7-bond allows less delocalization of the furo O5-lone pair thus changing the ring electronics and also provides some flexibility in the dihydrofuro ring.

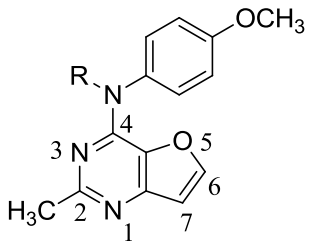

	R
198	Et
199	*i*Pr
200	*n*Pr

Figure 34. Series X

Series X (compounds **198-200**, Figure 34) was designed as conformationally restricted analogs of **181**. Introduction of a 4-N alkyl substituent restricts rotation around the N-phenyl bond, thus affording a more rigid structure than **181**. Conformational restriction of the 4-anilino moiety could lock the compound in a conformation that is conducive to multiple RTK inhibition without loss of tubulin and EGFR inhibitory activities.

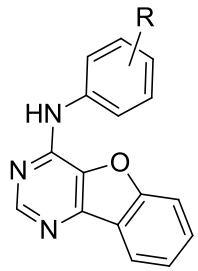

201

Figure 35. Benzofuro[3,2-*d*]pyrimidines as RTK inhibitors

Tricyclic benzofuro[3,2-*d*]pyrimidines with general structure **201** (Figure 35) have been reported to be inhibitors of RTKs.[115] It was hypothesized that fusion of a third aromatic ring at the appropriate positions of the furo[3,2-*d*]pyrimidine **181** would allow additional hydrophobic interactions with RTKs and perhaps improve RTK inhibitory potency without loss of tubulin inhibition. Hence we designed compounds **202-204** (**Series XI**, Figure 36) with the tricyclic benzofuro[3,2-*d*]pyrimidine scaffold.

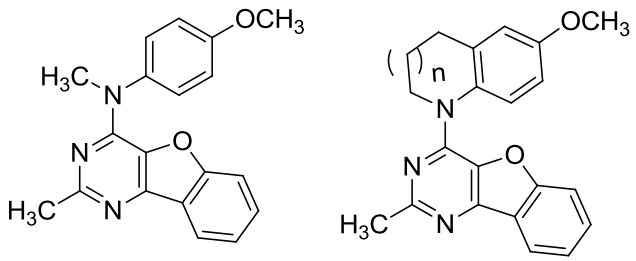

202 **203** n = 0
204 n = 1

Figure 36. Series XI

Another approach that was chosen for the design of multiple RTK and tubulin inhibitors is that of hybrid design. **Series XII** (Figure 37) was designed as hybrids of the tubulin and EGFR dual inhibitors **181**, and the tubulin and VEGFR2 dual inhibitor **187**. Incorporating the 7-benzyl group onto the furo[3,2-*d*]pyrimidine scaffold in **181** afforded **205** and **206** with potential for multiple RTK and tubulin inhibition.

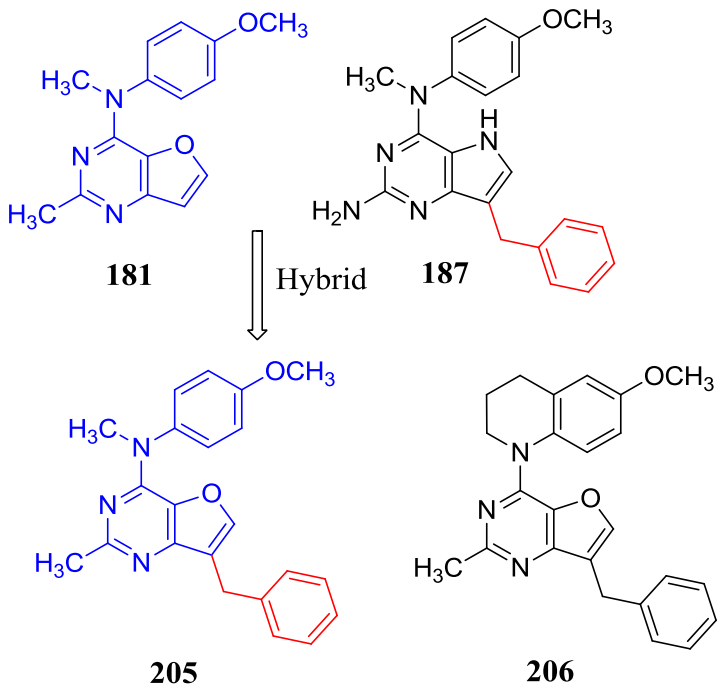

181 **187**

205 **206**

Figure 37. Series XII

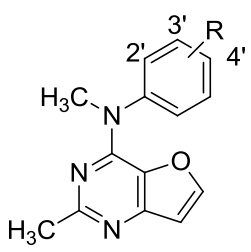

	R
207	H
208	4'-CH_3
209	4'-Cl
210	3',4'-diCl

Figure 38. Series XIII

Furo[3,2-*d*]pyrimidines are a relatively unexplored scaffold as EGFR inhibitors. Hence **Series XIII** (Figure 38) was designed by substitutions on the 4-anilino moiety using a Topliss approach.[186] The biological activities of compounds **182** (**Series VI**, Figure 29) and **207**-**210** will allow a determination of the effect of hydrophobicity and/or electronics on EGFR, VEGFR2 and PDGFRβ inhibition and guide the choice of substituents for inhibition of tubulin and multiple RTKs.

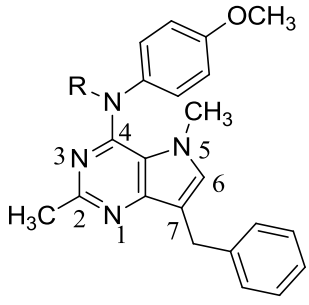

	R
211	H
212	CH_3

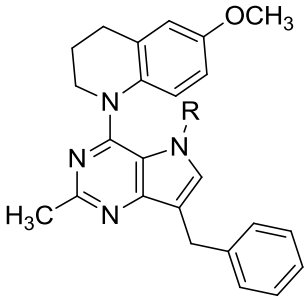

	R
213	H
214	CH_3

Figure 39. Series XIV

Series XIV (Figure 39) was designed as analogs of dual acting agent **187** with restricted rotation around the 4-N-phenyl bond. This was accomplished by placing a methyl on the N4 (**211**, **212**) and incorporating the known active quinazoline moiety at the 4-position with (**214**) and without (**213**) an N5-methyl group. Compounds **211**-**214**

could potentially favour a conformation which inhibits multiple RTKs without loss of tubulin and VEGFR2 inhibitory activities.

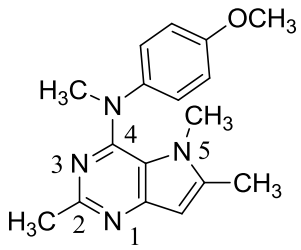

215

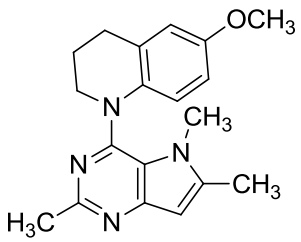

216

Figure 40. Series XV

Similarly **Series XV** (Figure 40) was designed as conformationally restricted analogs of dual VEGFR2 and tubulin inhibitors **174** and **176** (**Series IV**, Figure 6). The 5-methyl group in **215** and **216** could have two effects: allow additional hydrophobic interactions with the targets and restrict the rotation around the N-phenyl bond, thus providing conformational rigidity and better potency.

Series XVI (Figure 41) was designed to study the effect of a 2-amino group on multiple RTK inhibition. Gangjee *et al.*[187] have reported that a 2-amino group on fused pyrimidine ring systems improves hinge region binding and provides multiple-RTK inhibition. Compounds **217** and **218** were designed by replacing the 2-CH_3 group in the dual acting VEGFR2 and tubulin inhibitors **187** and **213** with a 2-amino group which could potentially increase binding to the hinge region of EGFR or PDGFRβ *via* hydrogen bonds, without loss of tubulin and VEGFR2 inhibitory activities. Similarly, compounds **219** and **220** were designed by replacing the 2-CH_3 group in the dual acting VEGFR2 and tubulin inhibitors **174** and **176** (**Series IV**, Figure 26) with a 2-amino group.

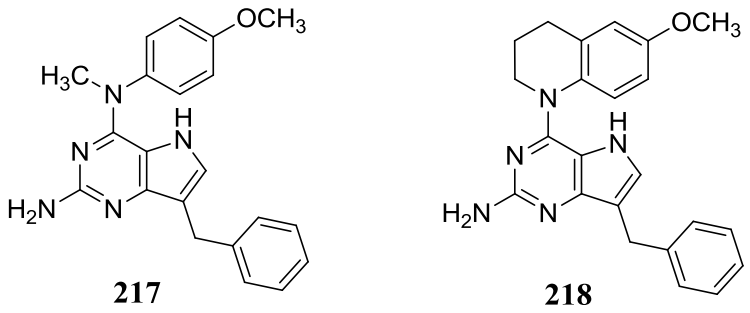

217

218

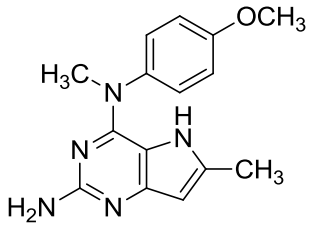

219

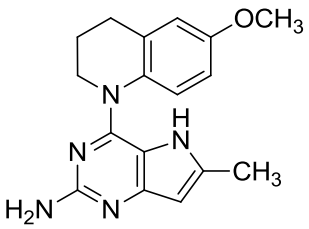

220

Figure 41. Series XVI

Series XVII was designed based on previous reports by Gangjee *et al.*[188] Compound **221** (Figure 42) was reported to have potent VEGFR2 and PDGFRβ inhibitory activities (Table 3). Substituents on the benzyl group and the location of the benzyl group on

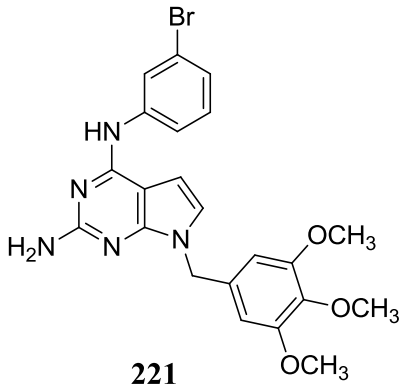

221

Figure 42. VEGFR2 and PDGFRβ dual inhibitor

Table 3. Inhibition of kinases in cellular assays

Compound	VEGFR2 **IC_{50}** ± SD (μM)	PDGFRβ **IC_{50}** ± SD (μM)
221	25.7	1.8
Semaxanib	12.9	
DMBI		3.75

the pyrrolo[2,3-*d*]pyrimidine scaffold were found to dictate RTK inhibitory activity. Compounds **222**-**224** (**Series XVII**, Figure 43) were designed by incorporating the 7-(3′,4′,5′-trimethoxybenzyl) group as such a motif has demonstrated potential for multiple RTK inhibition.[188]

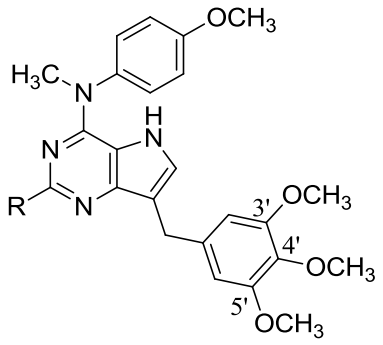

	R
222	CH_3
223	NH_2
224	H

Figure 43. Series XVII

While the pyrrolo[2,3-*d*]pyrimidine scaffold has been used in the design of RTK inhibitors there is a dearth in the literature of the regioisomeric pyrrolo[3,2-*d*]pyrimidine scaffold as RTK inhibitors. Thus it was of interest to design appropriately substituted pyrrolo[3,2-*d*]pyrimidines as multitargeted RTK inhibitors. However, multiple or promiscuous RTK inhibitors are in some instances more prone to yield side effects, in the clinic, compared to selective RTK inhibitors.[19, 24] Selectivity has proven to be a significant challenge due to the large number of important protein kinases in human cells, the conserved structure of the kinase ATP binding domain and the high cellular concentrations (micromolar) required for these compounds to compete with millimolar cellular ATP concentrations.[189] The optimal selectivity profile of a promising inhibitor, must exclude off-target kinases such as insulin signaling kinases,[190] cAMP-dependent protein kinase[191] and several others[192] critical for normal cell function. Thus, there

remains considerable interest in the development of RTKs with optimal targeted RTK inhibitory effects and minimal off target inhibitions and side-effects.

In order to rule out off target toxicity, compound **187** was evaluated with the assistance of a kinase profiling service (Luceome Biotechnologies) against 50 other kinases and found no significant activity at 10 µM. This data supported the design of 2-methyl 7-benzyl pyrrolo[3,2-*d*]pyrimidine as a scaffold with potential for "selectively non-selective" kinase inhibitor design. A variety of specific substituents on the phenyl ring were incorporated in the target compounds based on reported[7, 18, 193] potent RTK inhibitors (Figure 44).

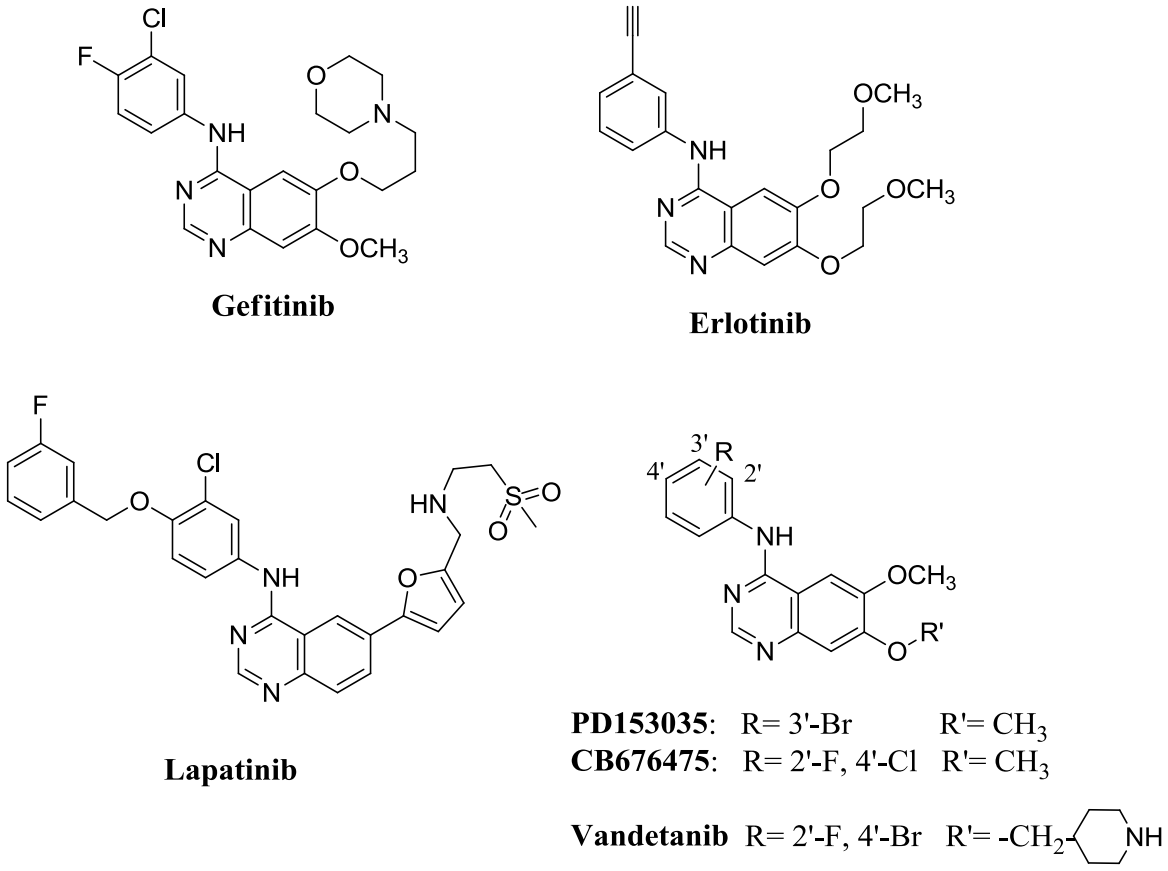

Figure 44. Reported RTK inhibitors used in the design of Series XVIII

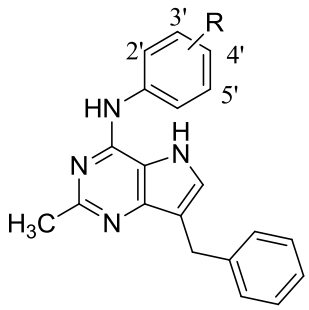

R

225 2'-F, 4'-Br
226 2'-F, 4'-Cl
227 3'-ethynyl
228 3'-Br
229 3'-Cl, 4'-F
230 3'-Cl, 4'-OCH_3
231 3',4',5'-triOCH_3
232 H

Figure 45. Series XVIII

Substituents from vandetanib, CB676475, erlotinib, PD153035, gefitinib and lapatinib were incorporated in the design of compounds **225-230** (Figure 45) respectively. As the 4-anilino substituents in **225-229** are electron-withdrawing, compound **231** was designed to evaluate the effect of electron-donating substituents that have previously[194] shown multi-RTK inhibitory potential in the pyrrolo[3,2-*d*]pyrimidine class of inhibitors.

IV. CHEMICAL DISCUSSION

The synthesis of target compounds was envisioned to be accomplished *via* nucleophilic substitution reactions[169] of 4-chloro-fused-pyrimidines with general structure **B** (Figure 46) which could be prepared by condensation of appropriately substituted precursors **C** with acetamidine type reagents.[115]

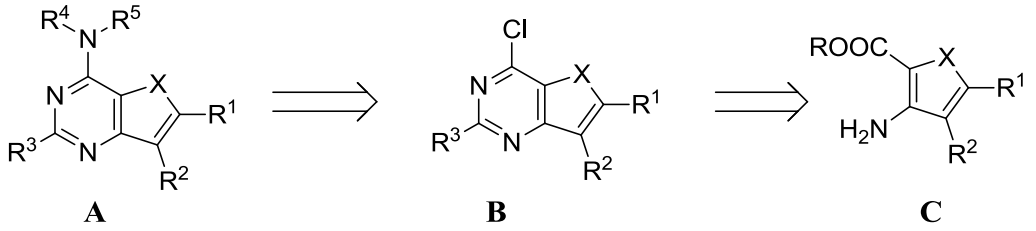

Figure 46. Retrosynthesis of target compounds

Synthesis of 161

With the above synthetic strategy for the synthesis of pyrrolo[3,2-*d*]pyrimidine **161** in mind, the key intermediate pyrrole **236** (Scheme 37) was synthesized by modifications of reported[98] procedures. Isoxazole **233** was treated with a base to afford aldehyde **234** which on treatment with diethylaminomalonate provided imine **235**. Imine **235** was subject to a base catalysed cyclization and decarboxylation using sodium ethoxide to give ethyl 3-amino-1*H*-pyrrole-2-carboxylate **236**. Furneaux *et al.*[98] suggest reaction times of two days for the preparation of enamine **235** from the aldehyde **234** and three days for the preparation of pyrrole **236** from the enamine **235**. However, it was found that these long reaction times afforded several side products [monitored by thin layer chromatography (TLC)] and significantly reduced the yield. The reactions were carefully monitored by

Scheme 37. Synthesis of **161**

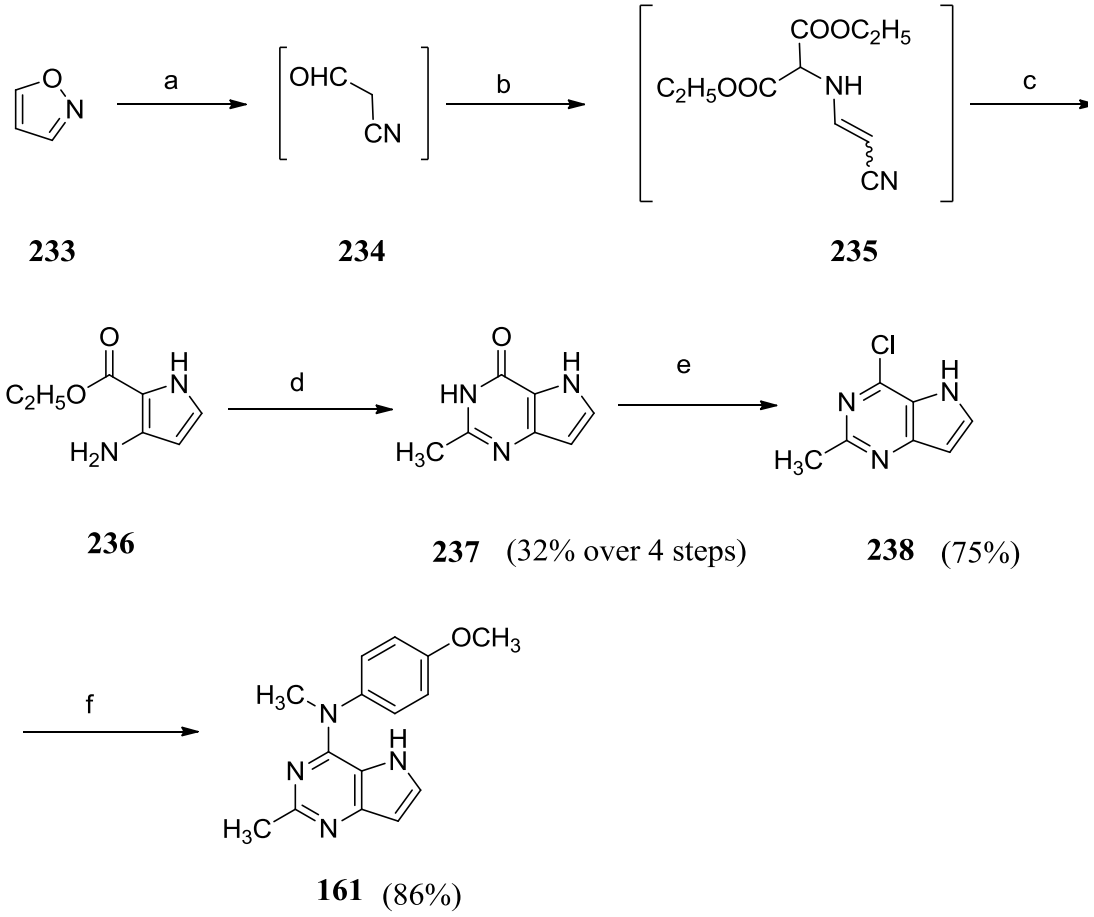

Reagents and conditions: (a) $NaOC_2H_5$, C_2H_5OH, 0 °C, 1 h; (b) diethylaminomalonate, CH_3COONa, C_2H_5OH, rt, 24 h; (c) $NaOC_2H_5$, C_2H_5OH, rt, 24 h; (d) CH_3CN, HCl, rt, 2 h; (e) $POCl_3$, 110 °C, 4 h; (f) 4-methoxy *N*-methylaniline, $(CH_3)_2CHOH$, reflux, 4 h

TLC and the reaction times were optimized to significantly decrease formation of side products and to afford crude pyrrole **236** which could be used without futher purification by column chromatography. Reported condensation of guanidine/cyanamide[104] and formamidine with similar pyrroles[98, 108] encouraged us to attempt condensation of pyrrole **236** with acetamidine. This condensation reaction requires heating the pyrrole with acetamidine hydrochloride in ethanol at reflux.[98] These reaction conditions resulted in

degradation of the pyrrole **236** without the formation of **237**. Condensation was also attempted under basic conditions[195] using sodium ethoxide, but similar degradation was observed. The synthesis of bicyclic pyrrolo[3,2-*d*]pyrimidine **237** was accomplished by treatment of pyrrole **236** with acetonitrile under acidic conditions[104] (32% yield over 4 steps from **233)**. The 2-methyl-4-oxo-pyrrolo[3,2-*d*]pyrimidine **237** was chlorinated[188] with phosphorus oxychloride to generate 2-methyl-4-chloro-pyrrolo[3,2-*d*] pyrimidine **238** which was subjected to a nucleophilic aromatic substitution reaction[169] using 4-methoxy *N*-methylaniline to afford **161**.

Synthesis of 162

Scheme 38. Synthesis of **162**

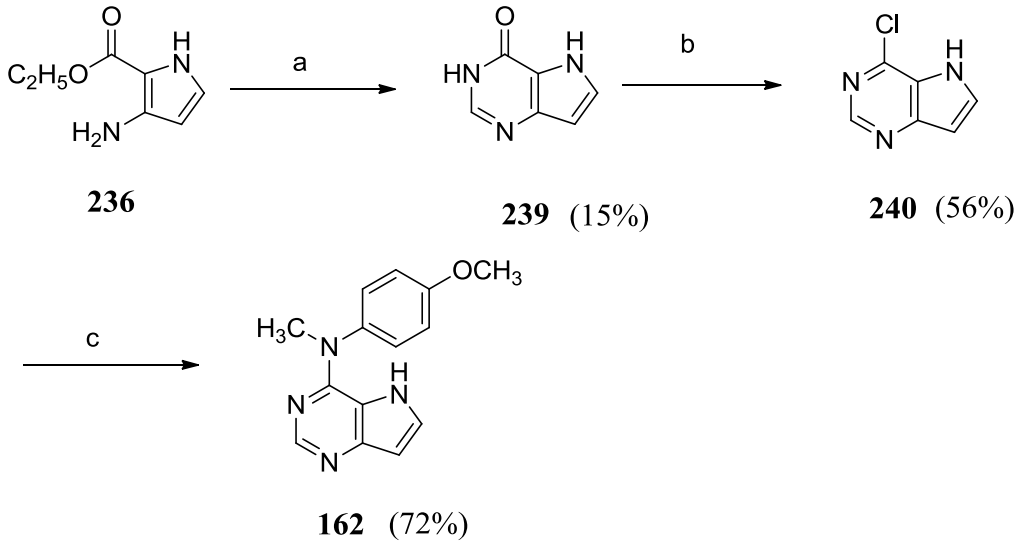

Reagents and conditions: (a) fomamidine acetate, C_2H_5OH, reflux, 18 h (b) $POCl_3$, 110 °C, 6 h; (c) 4-methoxy *N*-methylaniline, $(CH_3)_2CHOH$, reflux, 6 h

Ethyl 3-amino-1*H*-pyrrole-2-carboxylate **236** (Scheme 38) was subjected to a condensation with formamidine to afford bicyclic pyrrolo[3,2-*d*]pyrimidine **239**.[98] In contrast to the condensation with acetamidine, this reaction afforded the bicyclic pyrrolo[3,2-*d*]pyrimidine. Although side products (possibly due to pyrrole degradation in ethanol at reflux) were observed, the reaction sequence afforded **239** in 15% yield over 4 steps from **233**. Purification of **239** required extensive column chromatography. The 2-*H*-4-oxo pyrrolo[3,2-*d*]pyrimidine **239** was chlorinated with phosphorus oxychloride to generate 2-*H*-4-chloro-pyrrolo[3,2-*d*]pyrimidine **240** which was subjected to a nucleophilic aromatic substitution reaction using 4-methoxy *N*-methylaniline in isopropanol at reflux to afford **162**.

Synthesis of 163-167

Scheme 39. Synthesis of **163-167**

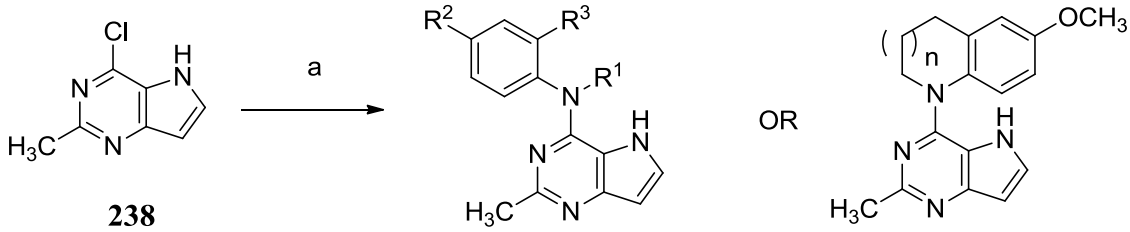

238

	R^1	R^2	R^3				
163	CH_3	H	H	(78%)	**166**	n = 0	(72%)
164	H	OCH_3	H	(81%)	**167**	n = 1	(79%)
165	H	OCH_3	OCH_3	(76%)			

Reagents and conditions: (a) appropriately substituted amine, $(CH_3)_2CHOH$, reflux, 4-24 h

Nucleophilic aromatic substitution reactions[169] of 2-methyl-4-chloro-pyrrolo[3,2-*d*] pyrimidine **238** (Scheme 37) with appropriately substituted amines in isopropanol at reflux afforded compounds **163-167** (Scheme 39). Displacement reactions with bulky nucleophiles 5-methoxyindoline and 6-methoxy-1,2,3,4-tetrahydroquinoline required longer reaction times compared to other amines for complete disappearance of starting material estimated from TLC.

Synthesis of 170-173

Scheme 40. Synthesis of **170-173**

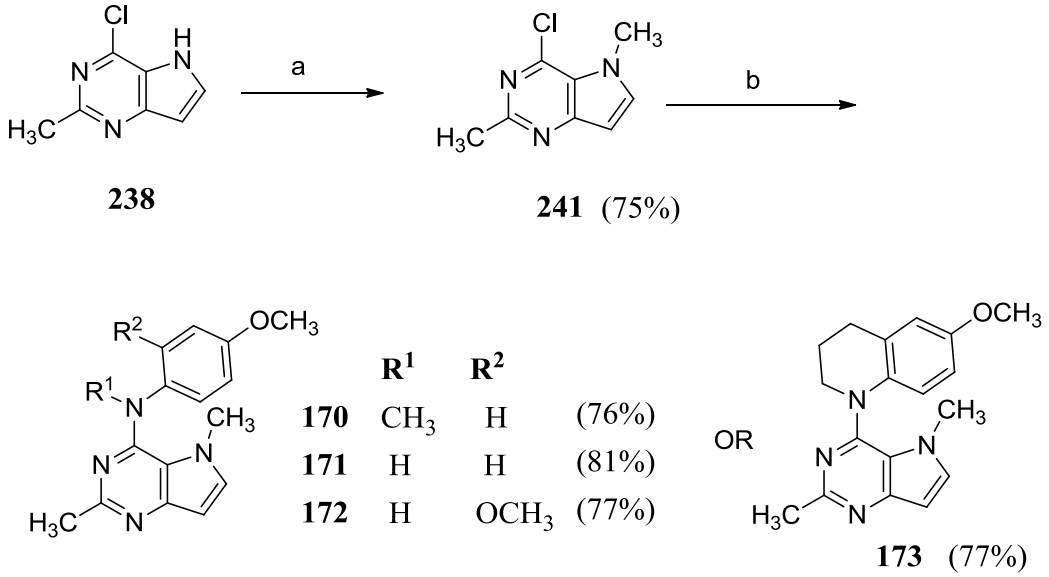

Reagents and conditions: (a) NaH, CH_3Br, $(CH_3)_2NCOH$ (b) appropriately substituted amine, $(CH_3)_2CHOH$, reflux, 4-24 h

4-Chloro-2-methyl-5*H*-pyrrolo[3,2-*d*]pyrimidine **238** (Scheme 37) was deprotonated with sodium hydride[188] and methylated with methyl bromide to afford **241** (Scheme 40)

which on treatment with appropriately substituted amines in isopropanol at reflux afforded compounds **170-173**.

Synthesis of 174-176

Scheme 41. Synthesis of **174-176**

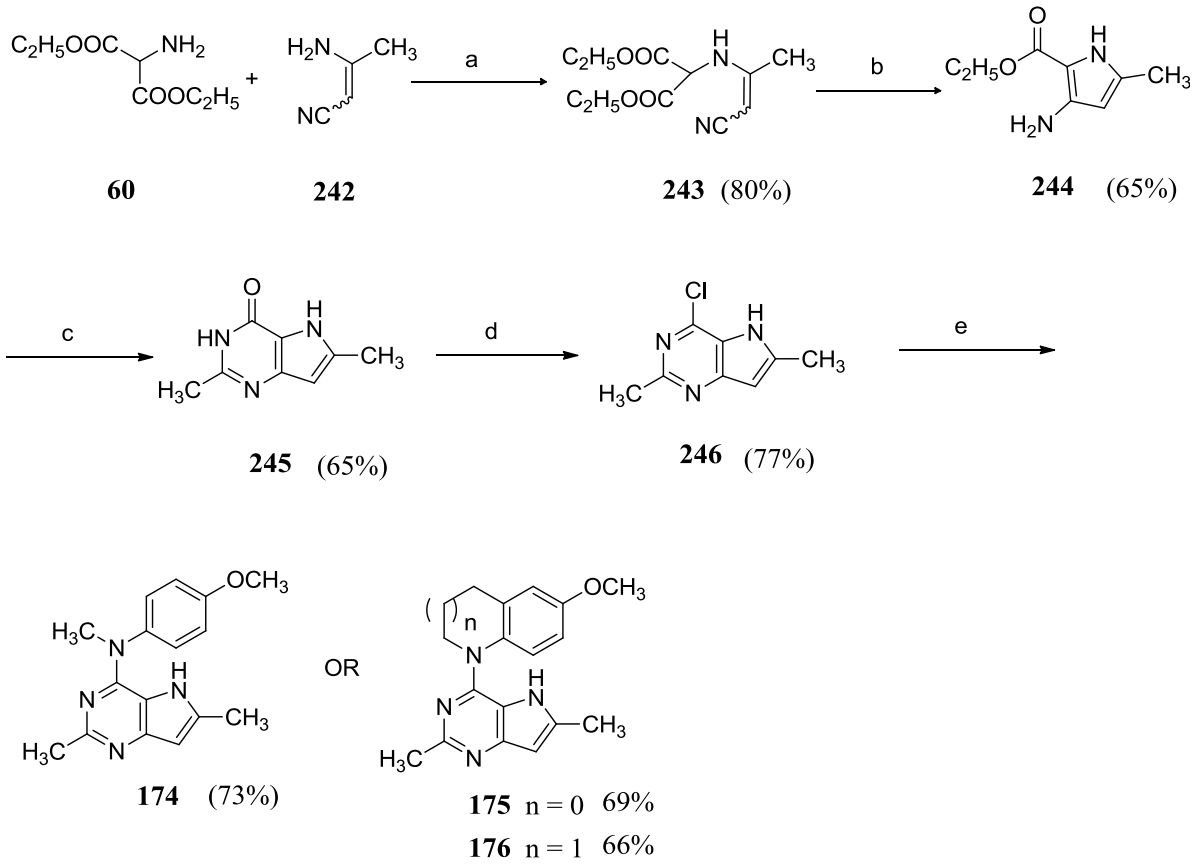

Reagents and conditions: (a) C_2H_5OH, rt, 6 h; (b) $NaOC_2H_5$, C_2H_5OH, 60 °C, 6 h; (c) CH_3CN, HCl, rt, 2 h; (d) $POCl_3$, 110 °C, 4 h; (e) appropriately substituted amine, $(CH_3)_2CHOH$, reflux, 4-24 h

A conjugate addition–elimination reaction[105] of 3-aminobut-2-enenitrile **242** (Scheme 41) using diethylaminomalonate in ethanol afforded enamino nitrile **243** which

was subjected to a base catalyzed cyclization and decarboxylation[103] using sodium ethoxide to afford ethyl 3-amino-5-methyl-1*H*-pyrrole-2-carboxylate **244**. Compared to the synthesis of enamine **235** and pyrrole **236**, reactions for the synthesis of **243** and **244** were clean and the products could be isolated by column chromatography. Condensation of pyrrole **244** with acetamidine was attempted but was unsuccessful. Although the pyrrole was stable under the reaction conditions of heating with acetamidine hydrochloride in ethanol, formation of new products were not observed. Pyrrole **244** was treated with acetonitrile under acidic conditions[104] to afford bicyclic pyrrolo[3,2-*d*]pyrimidine **245**. The 2-methyl- 4-oxo-pyrrolo[3,2-*d*]pyrimidine **245** was chlorinated[169] with phosphorus oxychloride to generate 2-methyl-4-chloro-pyrrolo[3,2-*d*]pyrimidine **246** which was subjected to nucleophilic aromatic substitution reactions[188] using the appropriately substituted amine to afford **174** - **176**.

Synthesis of 178-180

A nucleophilic displacement of ethyl bromoacetate **247** (Scheme 42) using anthranilonitrile **103** afforded **104** which was subjected to a base catalyzed cyclization using potassium *tert*-butoxide to afford ethyl 3-amino-1*H*-indole-2-carboxylate **103**.[113] Condensation of substituted indoles, analogous to **105**, with chlorformamidine have been successful and have afforded 2-amino-pyrimido[5,4-*b*]indoles.[196] Hence it was expected that the indole could be condensed with acetamidine. However, similar to reactions with previously discussed pyrroles, it was unsuccessful. Indole **103** was treated with acetonitrile under acidic conditions to afford tricyclic pyrimido[5,4-*b*]indole **248**.[104] The 2-methyl-4-oxo-pyrimido[5,4-*b*]indole **248** was chlorinated with phosphorus oxychloride

Scheme 42. Synthesis of **178-180**

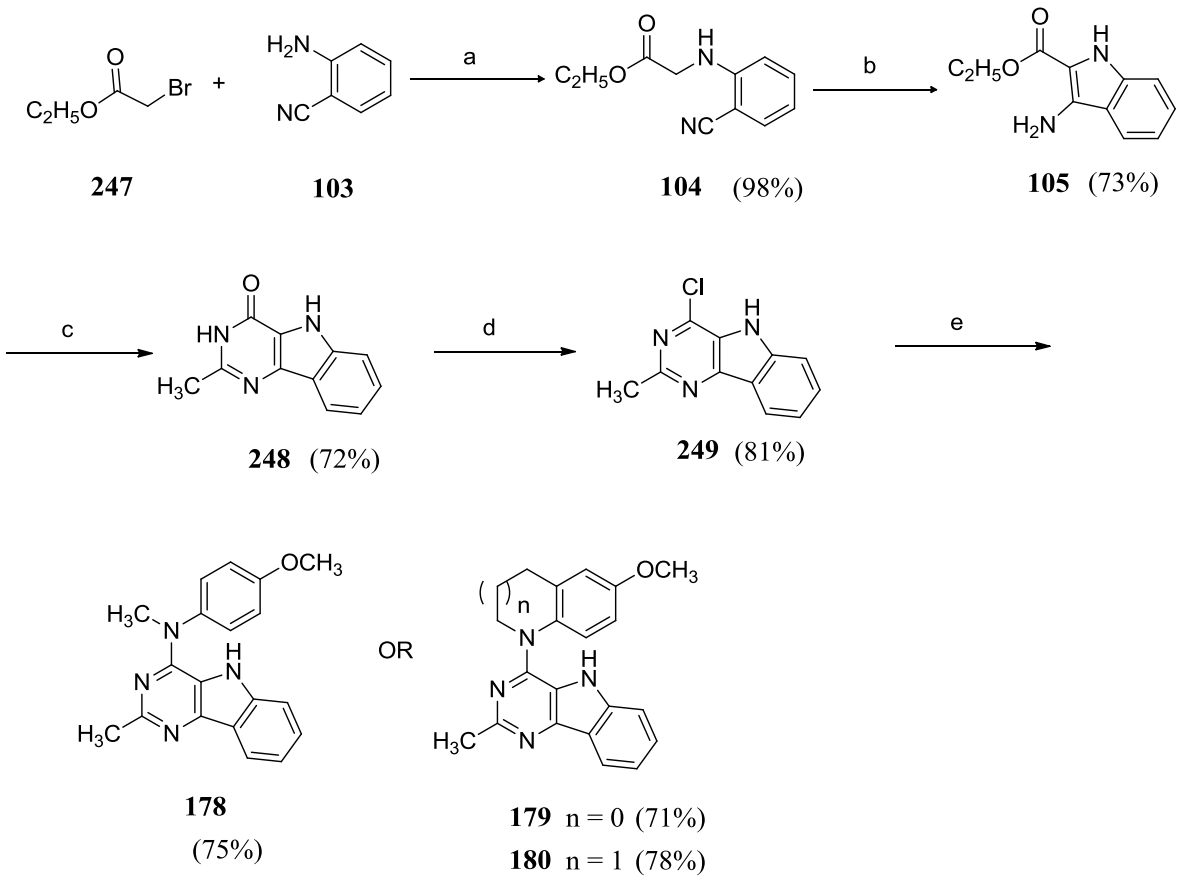

Reagents and conditions: (a) K_2CO_3, C_2H_5OH, reflux, 6 h; (b) *t*-BuOK, THF, rt, 6 h; (c) CH_3CN, HCl, rt, 2 h; (d) $POCl_3$, 110 °C, 4 h; (e) appropriately substituted amine, $(CH_3)_2CHOH$, reflux, 4-24 h

to generate 4-chloro-2-methyl-5*H*-pyrimido[5,4-*b*]indole **249** which was subjected to nucleophilic aromatic substitution reactions[156] as before to afford **178** - **180**. Compounds **248** and **249** had improved solubility in organic solvents compared to their pyrrolo[3,2-*d*]pyrimidine analogs hence allowing for shorter time for chromatographic purification.

Synthesis of 181-185

Scheme 43. Synthesis of **181**-**185**

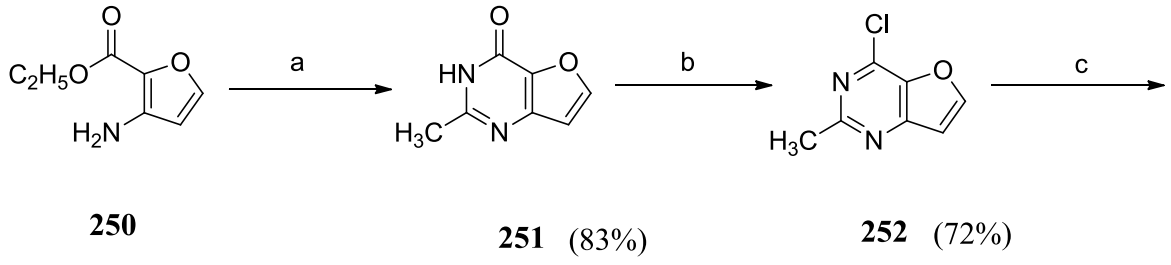

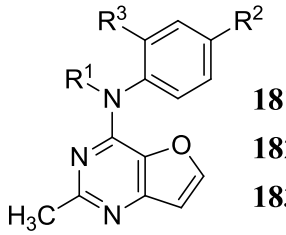

	R^1	R^2	R^3	
181	CH_3	OCH_3	H	(76%)
182	H	OCH_3	H	(80%)
183	H	OCH_3	OCH_3	(78%)

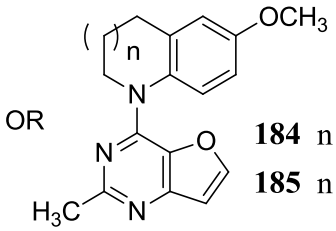

184 n = 0 (78%)
185 n = 1 (75%)

Reagents and conditions: (a) CH_3CN, HCl, rt, 8 h; (b) $POCl_3$, 110 °C, 4 h;

(c) appropriately substituted amine, $(CH_3)_2CHOH$, reflux, 4-24 h

Commercially available ethyl 3-aminofuran-2-carboxylate **250** was treated with acetonitrile under acidic conditions to afford bicyclic furo[3,2-*d*]pyrimidine **251**. The ^1H NMR of **250** obtained from the commercial source was identical to the reported[120] NMR confirming the substitution pattern on the furan ring. The 2-methylfuro[3,2-*d*]pyrimidin-4(3*H*)-one **251** was chlorinated[169] with phosphorus oxychloride to generate 2-methyl 4-chloro furo[3,2-*d*]pyrimidine **252** which was subjected to nucleophilic aromatic substitution reactions[188] using the appropriately substituted amines as before to afford **181** - **185**. Similar to pyrrolo[3,2-*d*]pyrimidine scaffold, displacement reactions with bulky nucleophiles 5-methoxyindoline and 6-methoxy-1,2,3,4-tetrahydroquinoline

required longer reaction times compared to other amines for complete disappearance of starting material as estimated from TLC.

Synthesis of 187-190

Scheme 44. Synthesis of **187-190**

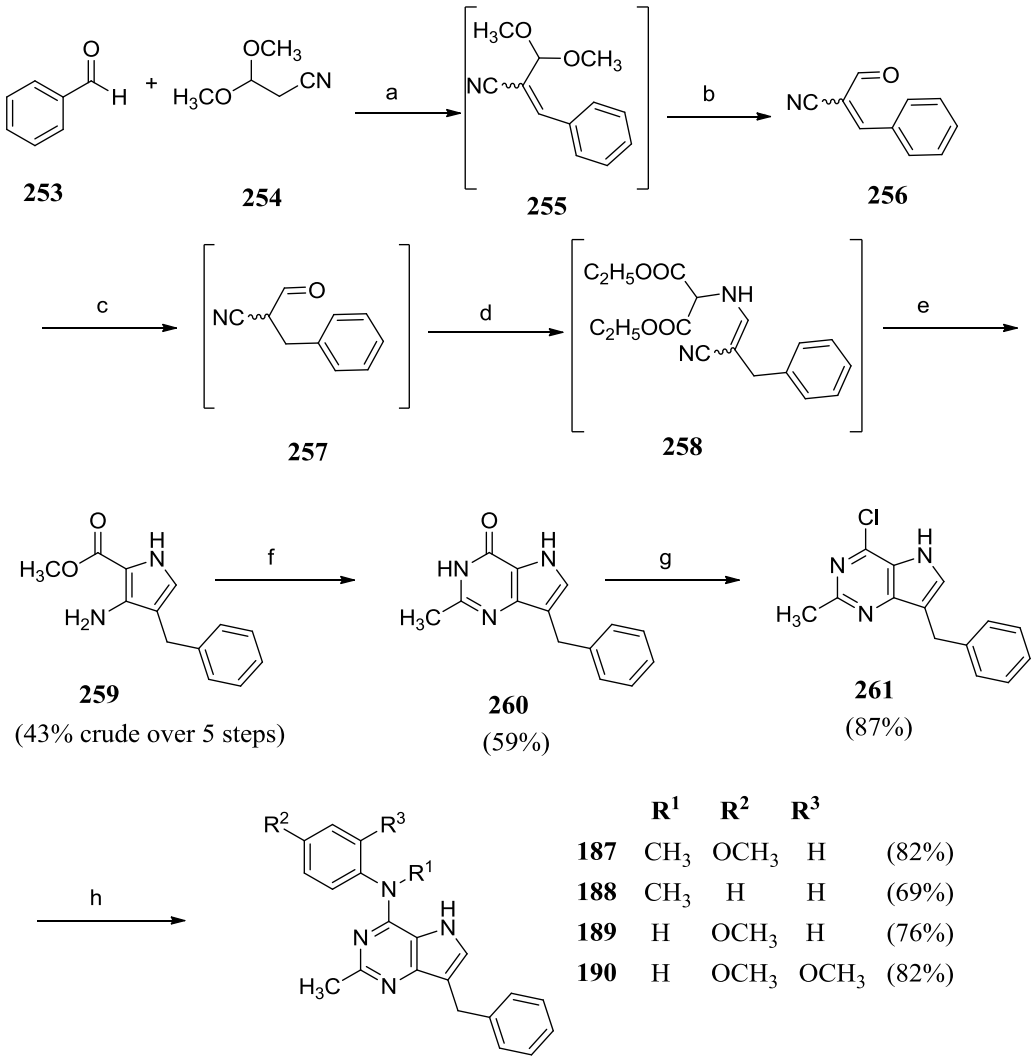

	R^1	R^2	R^3	
187	CH_3	OCH_3	H	(82%)
188	CH_3	H	H	(69%)
189	H	OCH_3	H	(76%)
190	H	OCH_3	OCH_3	(82%)

Reagents and conditions: (a) C_2H_5ONa, C_2H_5OH, rt, 6 h; (b) 6N HCl, rt, 2 h; (c) H_2, Pd/C, 55 psi, rt, 1 h (d) diethylaminomalonate, CH_3COONa, CH_3OH, rt, 16 h; (e) CH_3ONa, CH_3OH, rt, 12 h, reflux, 3 h; (f) CH_3CN, HCl, rt, 3 h; (g) $POCl_3$, 110 °C, 4 h;

(h) appropriately substituted amine, $(CH_3)_2CHOH$, reflux, 4-24 h

The key intermediate pyrrole **259** (Scheme 44) was synthesized by modifications in reported procedures.[103] Base catalysed condensation of benzaldehyde **253** and 3,3 dimethoxypropiononitrile **254** using sodium ethoxide in ethanol afforded **255** which was subjected to an acid catalyzed aldehyde deprotection to provide **256**. Catalytic hydrogenation of **256** using 10% Pd/C afforded aldehyde **257** which was treated with diethylaminomalonate in methanol to afford the enamino nitrile **258.** Compound **258** was treated to a base catalyzed cyclization and decarboxylation using sodium methoxide to afford methyl 3-amino-4-benzyl-1*H*-pyrrole-2-carboxylate **259**. Pyrrole **259** was treated with acetonitrile under acidic conditions[104] to afford bicyclic pyrrolo[3,2-*d*]pyrimidine **260**. The 2-methyl-4-oxo-pyrrolo[3,2-*d*]pyrimidine **260** was chlorinated[169] with phosphorus oxychloride to generate 2-methyl-4-chloro- pyrrolo[3,2-*d*]pyrimidine **261** which was subjected to nucleophilic aromatic substitution reactions[188] using the appropriately substituted amine to afford **187** - **190**. The 7-benzyl group of **260** and **261** significantly improved solubility compared to **237** and **238** in organic solvents.

Synthesis of 191-195

Scheme 45. Synthesis of **191**-**195**

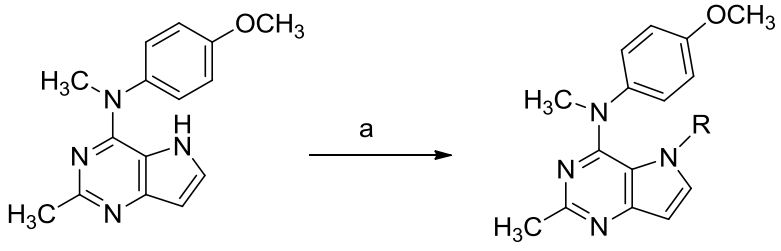

161

	R	
191	Et	(75%)
192	*i*Pr	(78%)
193	*n*Pr	(83%)
194	*i*Bu	(80%)
195	*n*Bu	(77%)

Reagents and conditions: (a) NaH, alkyl halide, DMF, 2-8 h

Pyrrolo[3,2-*d*]pyrimidine **161** (Scheme 37), which was synthesized from isoxazole in 6 steps as shown in Scheme 37, was deprotonated[188] with sodium hydride and treated with the the appropriate alkyl halide to afford the corresponding *N5*-alkylated pyrrolo[3,2-*d*]pyrimidine **191**-**195** (Scheme 45). Reactions involving combinations of cesium carbonate or potassium carbonate and dimethylformamide with microwave irradiation or conventional bench-top conditions did not show complete consumption of starting material. The mixture of **161** and the alkylated product could not be separated by column chromatography. The use of excess base or alkyl halide did not afford the alkylated product exclusively. Hence the deprotonation-alkylation sequence was chosen.

Synthesis of 196-197

Scheme 46. Synthesis of **196**-**197**

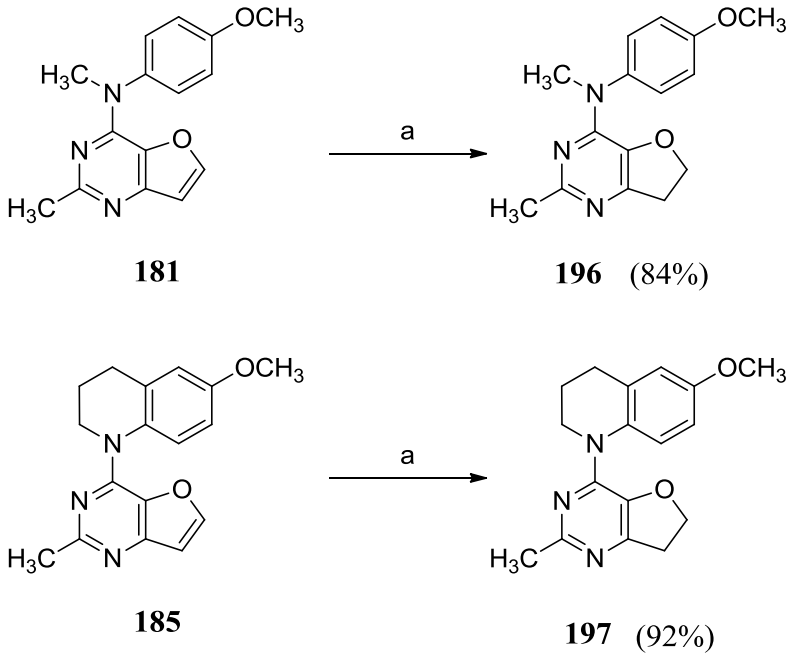

181 **196** (84%)

185 **197** (92%)

Reagents and conditions: (a) H_2, $Pd(OH)_2$, CH_3OH, rt, 24 h

The synthesis of 6,7-dihydrofuro[3,2-*d*]pyrimidine **196** (Scheme 46) was attempted by catalytic hydrogenation of furo[3,2-*d*]pyrimidines **181**(Scheme 43). The use of palladium on carbon as the catalytic bed for hydrogenation [upto 50 psi, 12 hours][196] afforded multiple spots which were significantly non-polar compared to the starting material. The isolated yield of **196** could not be improved beyond 36%. The synthesis of 6,7-dihydrofuro[3,2-*d*]pyrimidines **196** and **197** were accomplished by catalytic hydrogenation of furo[3,2-*d*]pyrimidines **181** and **185** respectively using palladium hydroxide. The use of palladium hydroxide resulted in clean reactions with no side products upto 24 hrs beyond which non-polar side products were observed.

Synthesis of 198-200

Scheme 47. Synthesis of **198**-**200**

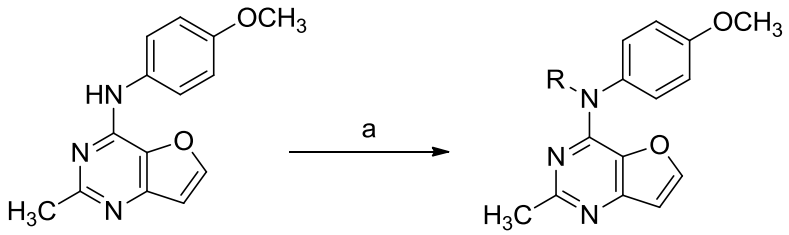

182

	R	
198	Et	(92%)
199	*i*Pr	(73%)
200	*n*Pr	(90%)

Reagents and conditions: (a) NaH, alkyl halide, DMF, 6-12 h

Furo[3,2-*d*]pyrimidine **182**, which was synthesized as shown in Scheme 43, was deprotonated[188] with sodium hydride and treated with the the appropriate alkyl halide to afford the corresponding pyrrole 4-*N*-alkylated furo[3,2-*d*]pyrimidines **198**-**200** (Scheme 47). Reactions involving combinations of cesium carbonate or potassium carbonate and dimethylformamide at conventional bench-top conditions did not show complete

consumption of starting material. Microwave irradiation afforded multiple spots. Hence sodium hydride was chosen as the reaction could be carried out at room temperature to afford good to excellent yields.

Synthesis of 202-204

Scheme 48. Synthesis of **202-204**

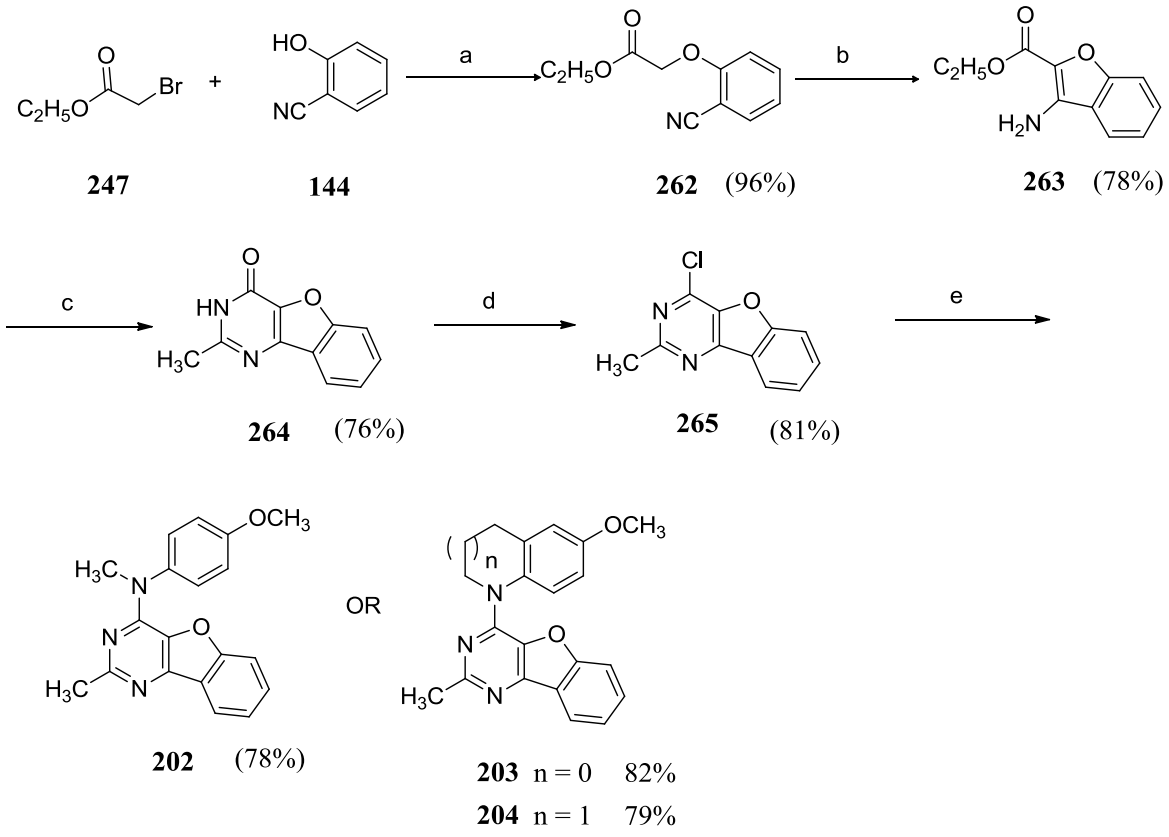

Reagents and conditions: (a) K_2CO_3, C_2H_5OH, reflux, 6 h; (b) *t*-BuOK, THF, rt, 6 h; (c) CH_3CN, HCl, rt, 2 h; (d) $POCl_3$, 110 °C, 4 h; (e) appropriately substituted amine, $(CH_3)_2CHOH$, reflux, 4-24 h

A nucleophilic displacement on ethyl bromoacetate **247** (Scheme 48) using 2-hydroxy benzonitrile **144** afforded **262** which was subjected to a base catalyzed

cyclization using potassium *tert*-butoxide to afford ethyl 3-aminobenzofuran-2-carboxylate **263**.[113, 115] Benzofuran **263** was treated with acetonitrile under acidic conditions[104] to afford tricyclic benzofuro[3,2-*d*]pyrimidine **264**. The 2-methylbenzofuro[3,2-*d*]pyrimidin-4(3*H*)-one **264** was chlorinated[197] with phosphorus oxychloride to generate 4-chloro-2-methylbenzo-furo[3,2-*d*]pyrimidine **265** which was subjected to nucleophilic aromatic substitution reactions[197] using the appropriately substituted amines to afford **202 - 204**. There was no significant change in reaction conditions for the synthesis of benzofuro[3,2-*d*]pyrimidines **202-204** compared with **178-180** (Scheme 42).

Synthesis of 205-206

Base catalysed condensation of 3-phenyl propionitrile **266** (Scheme 49) and ethyl formate using sodium ethoxide in ethanol afforded **267** which was alkylated with chloro diethylmalonate to provide **268**.[125] Compound **268** was subjected to a base catalyzed cyclization and decarboxylation using sodium ethoxide in ethanol to afford methyl 3-amino-4-benzylfuran-2-carboxylate **269**.[103] The cyclization-decarboxylation reaction was attempted with bases such as 1,5-diazabicyclo[4.3.0]non-5-ene and potassium bis(trimethylsilyl)amide. The yields of the reactions were comparable. Substituted furan **269** was treated with acetonitrile under acidic conditions[104] to afford bicyclic furo[3,2-*d*]pyrimidine **270**. The 7-benzyl-2-methylfuro[3,2-*d*]pyrimidin-4(3*H*)-one **270** was chlorinated[197] with phosphorus oxychloride to generate 7-benzyl-4-chloro-2-methylfuro[3,2-*d*]pyrimidine **271** which was subjected to nucleophilic aromatic substitution reactions[197] using the appropriately substituted amine to afford **205 - 206**.

Scheme 49. Synthesis of **205-206**

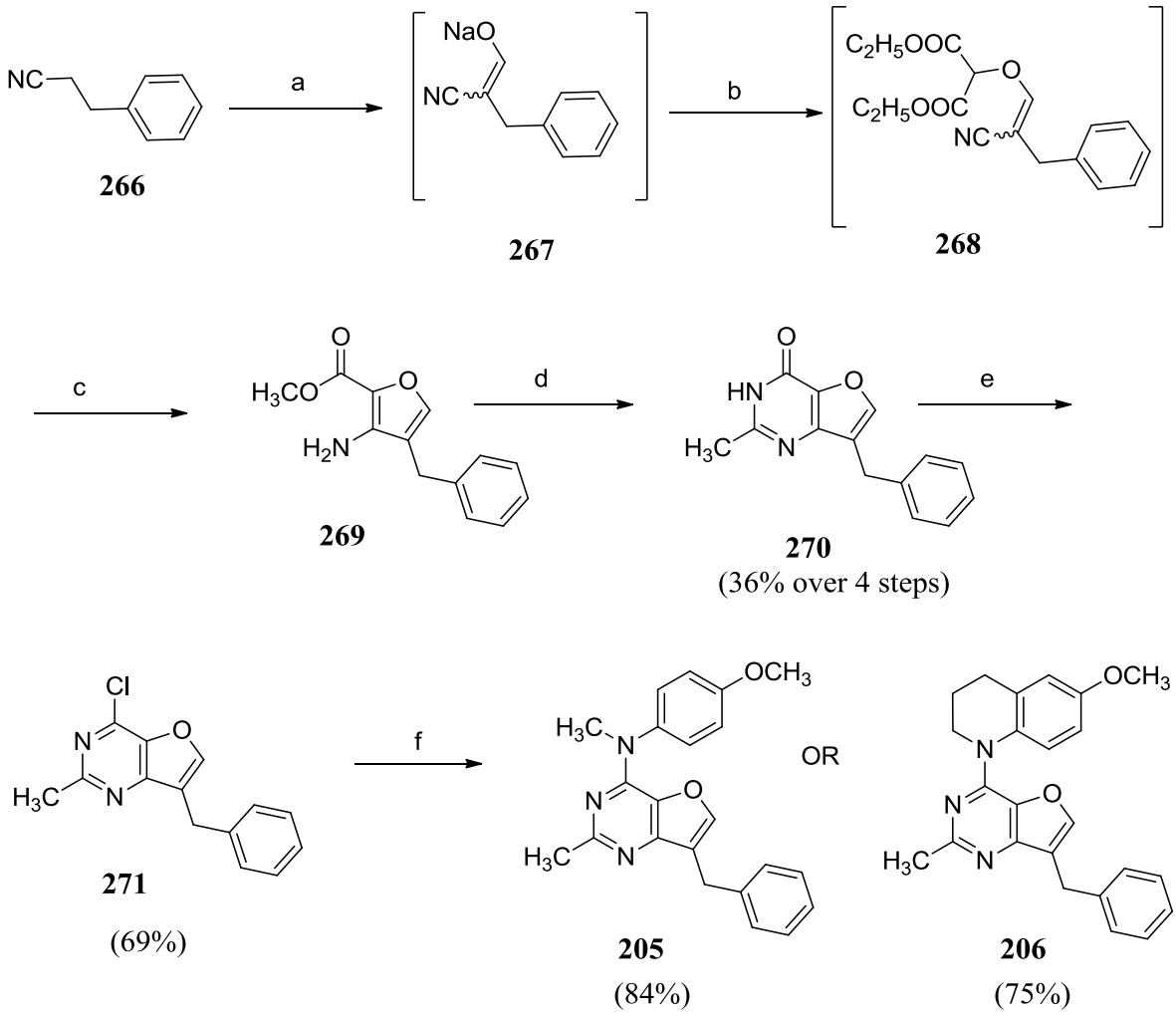

Reagents and conditions: (a) $HCOOC_2H_5$, C_2H_5ONa, C_2H_5OH, rt, 6 h (b) chloro diethylmalonate, CH_3COONa, CH_3OH, rt, 16 h; (c) C_2H_5ONa, C_2H_5OH, rt, 8 h, reflux, 30 min; (d) CH_3CN, HCl, rt, 2 h; (e) $POCl_3$, 110 °C, 4 h; (f) appropriately substituted amine, $(CH_3)_2CHOH$, reflux, 2-6 h

Synthesis of 207-210

Scheme 50. Synthesis of **207**-**210**

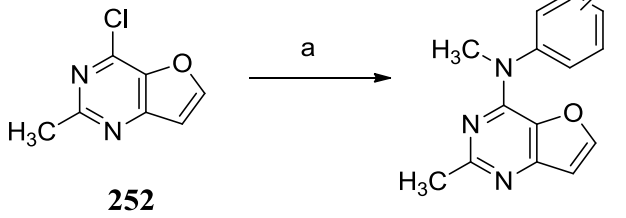

252

	R	
207	H	(78%)
208	4-CH_3	(72%)
209	4-Cl	(75%)
210	3,4-diCl	(81%)

Reagents and conditions: (a) appropriately substituted aromatic amines, $(CH_3)_2CHOH$, reflux, 4-12 h

Nucleophilic aromatic substitution reactions[197] of 4-chloro-2-methylfuro[3,2-*d*]pyrimidine **252** (Scheme 43) with appropriately substituted aromatic amines in isopropanol at reflux afforded compounds **207**-**210** (Scheme 50).

Synthesis of 211-214

7-Benzyl-4-chloro-2-methyl-5*H*-pyrrolo[3,2-*d*]pyrimidine **261** (Scheme 44) was deprotonated with sodium hydride and methylated with methyl bromide to afford **272** (Scheme 51) which on treatment with appropriately substituted amines in isopropanol at reflux afforded compounds **211**-**212**.[188] Treatment of pyrrolo[3,2-*d*]pyrimidines **261** and **272** with 6-methoxy tetrahydroquinoline afforded **213** and **214** respectively.

Comparison of ^{1}H NMRs of **187** and **212** with their synthetic precursors suggest a conformational preference of the 4-anilino moiety. As shown in Figure 47, the chemical shifts of the 5-H and 6-H in **187** compared with those in **261** indicate that these protons are in the shielding zone of the 4-methoxy-phenyl ring. Similarly, comparing the

Scheme 51. Synthesis of **211-214**

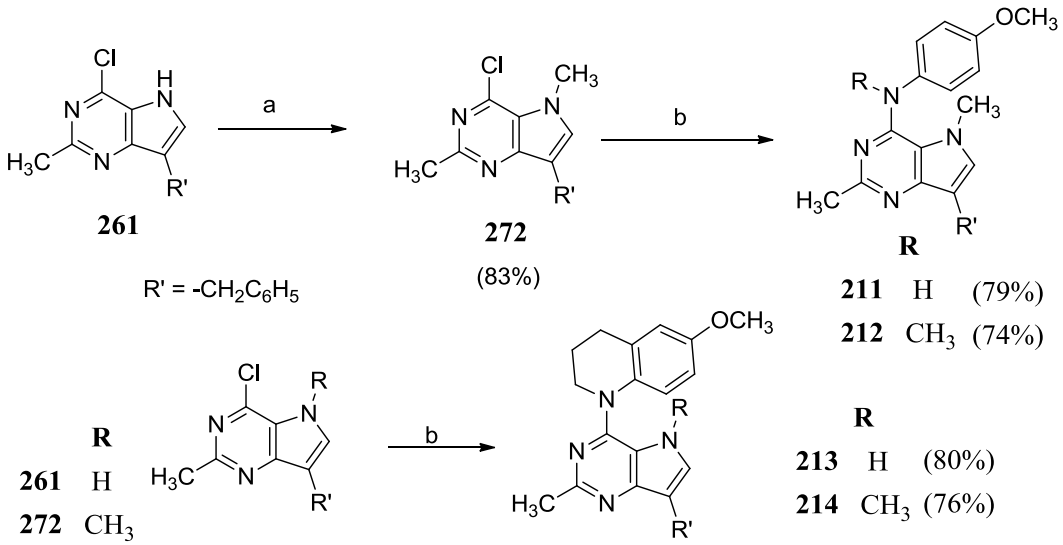

Reagents and conditions: (a) NaH, CH_3Br, $(CH_3)_2NCOH$ (b) appropriately substituted amine, $(CH_3)_2CHOH$, reflux, 4-24 h

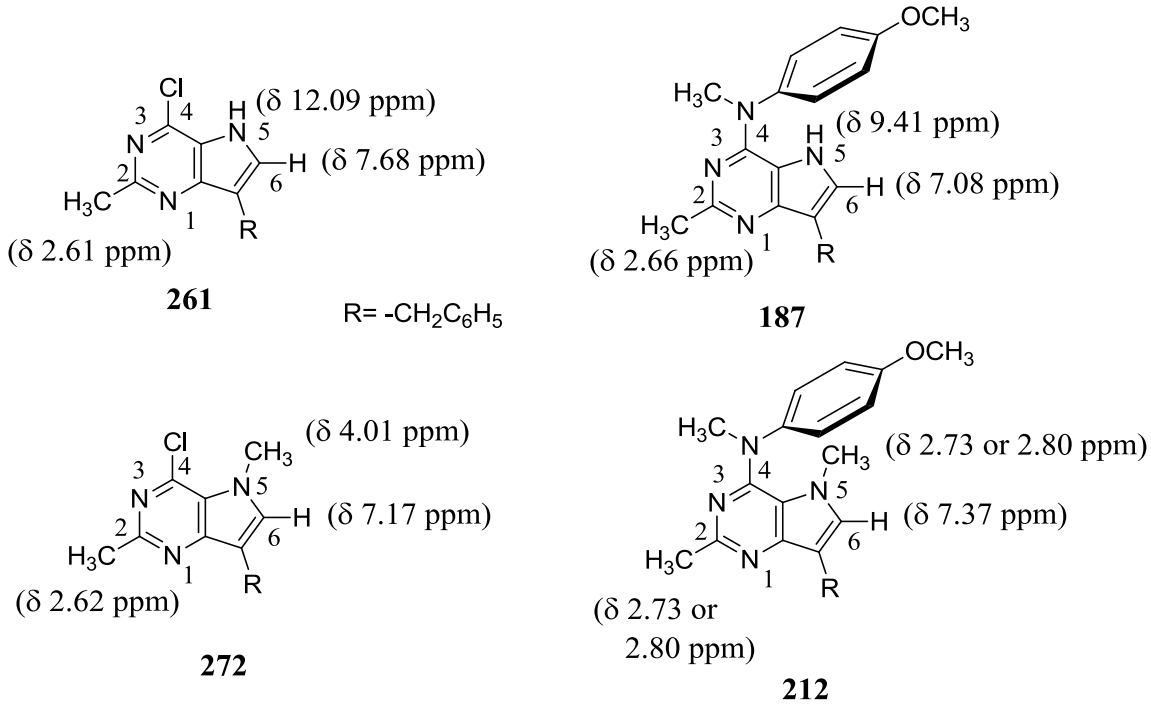

Figure 47. Comparison of ^1H NMRs

chemical shifts of the N5-CH_3 protons in **212** compared with those in **272** suggest similar conformational preference.

Synthesis of 215-216

Scheme 52. Synthesis of **215-216**

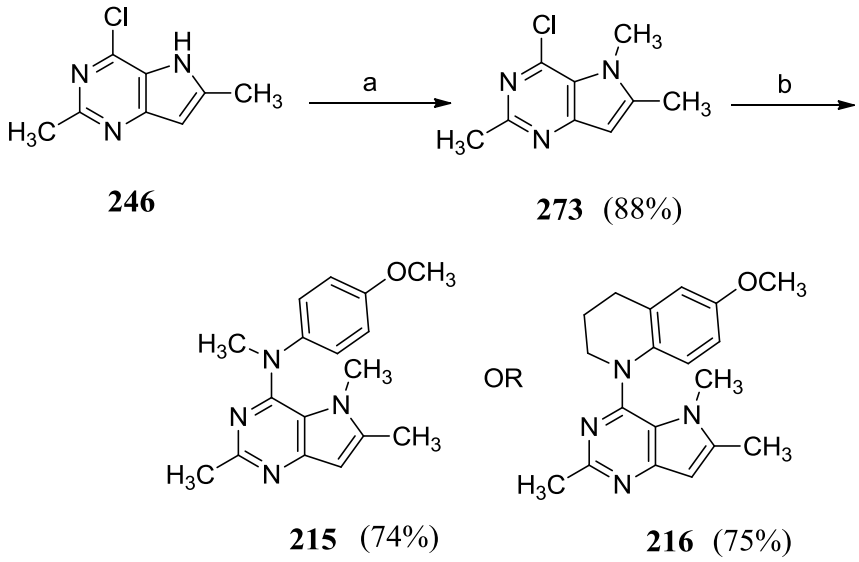

Reagents and conditions: (a) NaH, CH_3Br, $(CH_3)_2NCOH$ (b) appropriately substituted amine, $(CH_3)_2CHOH$, reflux, 4-24 h

4-Chloro-2,6-dimethyl-5*H*-pyrrolo[3,2-*d*]pyrimidine **246** (Scheme 41) was deprotonated[188] with sodium hydride and methylated with methyl bromide to afford **273** (Scheme 52) which on treatmentwith appropriately substituted amines in isopropanol at reflux afforded compounds **215-216**.

Synthesis of 217-220

3-Amino pyrroles **259** (Scheme 44) and **244** (Scheme 41) were treated with guanidine and chlorformamidine[93] and were found to be unreactive towards these

Scheme 53. Synthesis of **217-220**

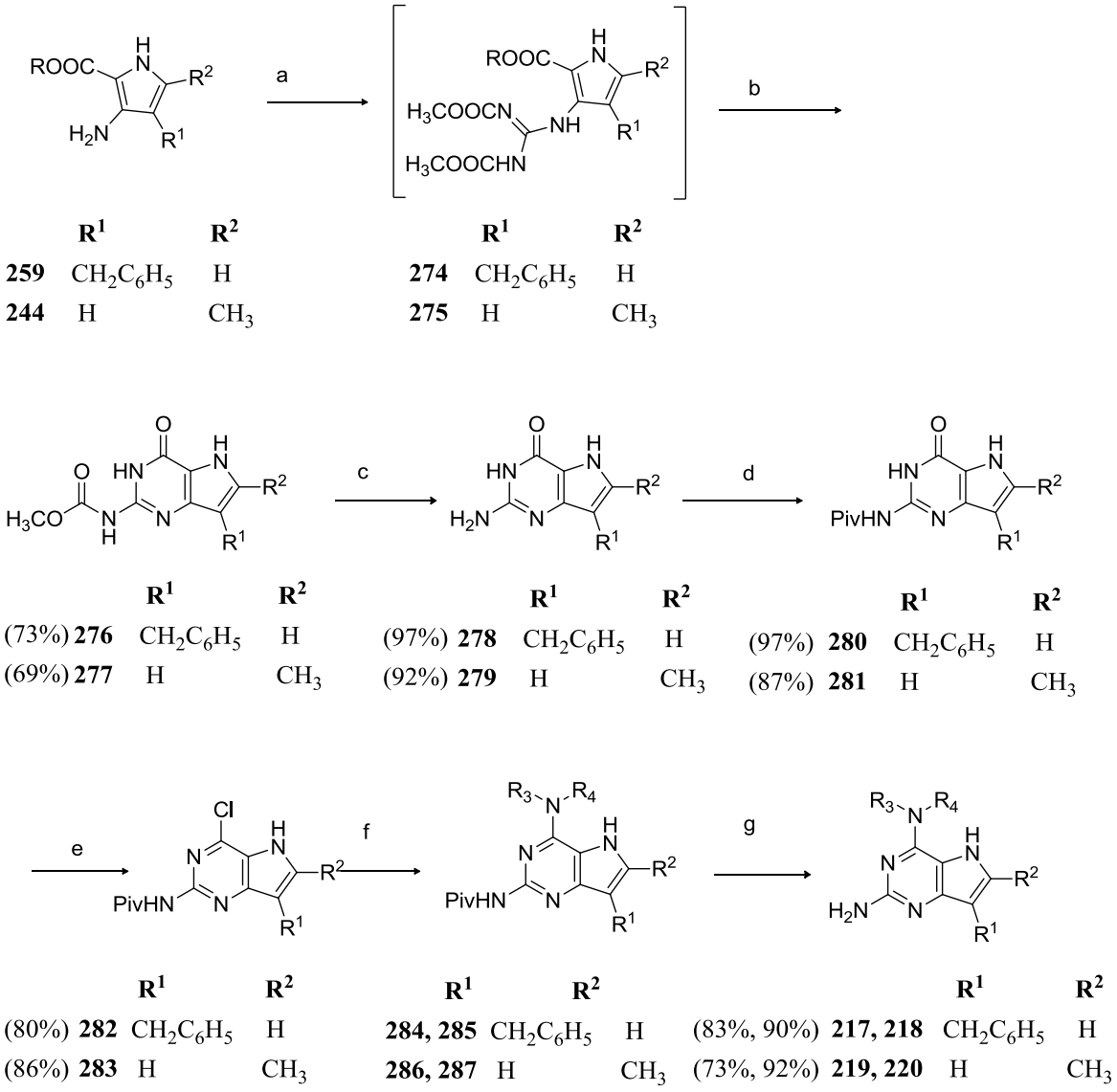

	R^1	R^2
259	$CH_2C_6H_5$	H
244	H	CH_3

	R^1	R^2
274	$CH_2C_6H_5$	H
275	H	CH_3

		R^1	R^2
(73%)	**276**	$CH_2C_6H_5$	H
(69%)	**277**	H	CH_3

		R^1	R^2
(97%)	**278**	$CH_2C_6H_5$	H
(92%)	**279**	H	CH_3

		R^1	R^2
(97%)	**280**	$CH_2C_6H_5$	H
(87%)	**281**	H	CH_3

		R^1	R^2
(80%)	**282**	$CH_2C_6H_5$	H
(86%)	**283**	H	CH_3

		R^1	R^2
	284, 285	$CH_2C_6H_5$	H
	286, 287	H	CH_3

		R^1	R^2
(83%, 90%)	**217, 218**	$CH_2C_6H_5$	H
(73%, 92%)	**219, 220**	H	CH_3

Reagents and conditions: (a) 1,3-dicarbomethoxy-2-methyl-2-thiopseudourea, CH_3COOH, rt, 24 h; (b) CH_3ONa, CH_3OH, rt, 12 h; (c) 1N NaOH, CH_3OH, reflux, 2 h; (d) trimethylacetic anhydride, 120 °C, 2 h; (e) $POCl_3$, 110 °C, 2 h; (f) substituted amine, $(CH_3)_2CHOH$, reflux, 4-24 h; (g) 1N NaOH, CH_3OH, reflux, 10 h

standard guanylating agents. Hence a three-step sequence was followed in the synthesis of **278 - 279**. 3-Amino pyrroles **259** and **244** were subjected to condensation with 1,3-bis(methoxy-carbonyl)-2-methylthiopseudourea to afford guanidine adducts **274** and **275** (Scheme 53) respectively.[103] Base-catalyzed cyclization in presence of sodium methoxide afforded bicyclic pyrrolo[3,2-*d*]pyrimidines **276** and **277**. Chlorination of the carbamate protected amines gave poor yields (<20%). Further the suqsequent aniline displacement reactions did not go to completion and separation of product from the starting materials required extensive column chromatography. Hence, the carbamate group in **276** and **277** was hydrolysed with aqueous sodium hydroxide to afford **278** and **279** which upon reaction with trimethylacetic anhydride provided amides **280** and **281** respectively. The 4-oxo pyrrolo[3,2-*d*] pyrimidines **280** and **281**, which had significantly improved solubility in organic solvents compared to **276 - 279**, were chlorinated with phosphorus oxychloride to generate 4-chloro-pyrrolo[3,2-*d*]pyrimidines **282** and **283** respectively which were subjected to nucleophilic aromatic substitution reactions using the appropriately substituted amines to afford **284 - 287**. Subsequent base catalyzed amide hydrolysis afforded **217 - 220**.

Synthesis of 222-224

Base catalysed condensation of 3,4,5-trimethoxy benzaldehyde **286** (Scheme 54) and 3,3 dimethoxypropiononitrile **254** using sodium ethoxide in ethanol followed by an acid catalyzed aldehyde deprotection provided **287**.[103] The use of sodium methoxide in methanol for the for the aldol-type condenstation required a longer reaction time (about

Scheme 54. Synthesis of **222-224**

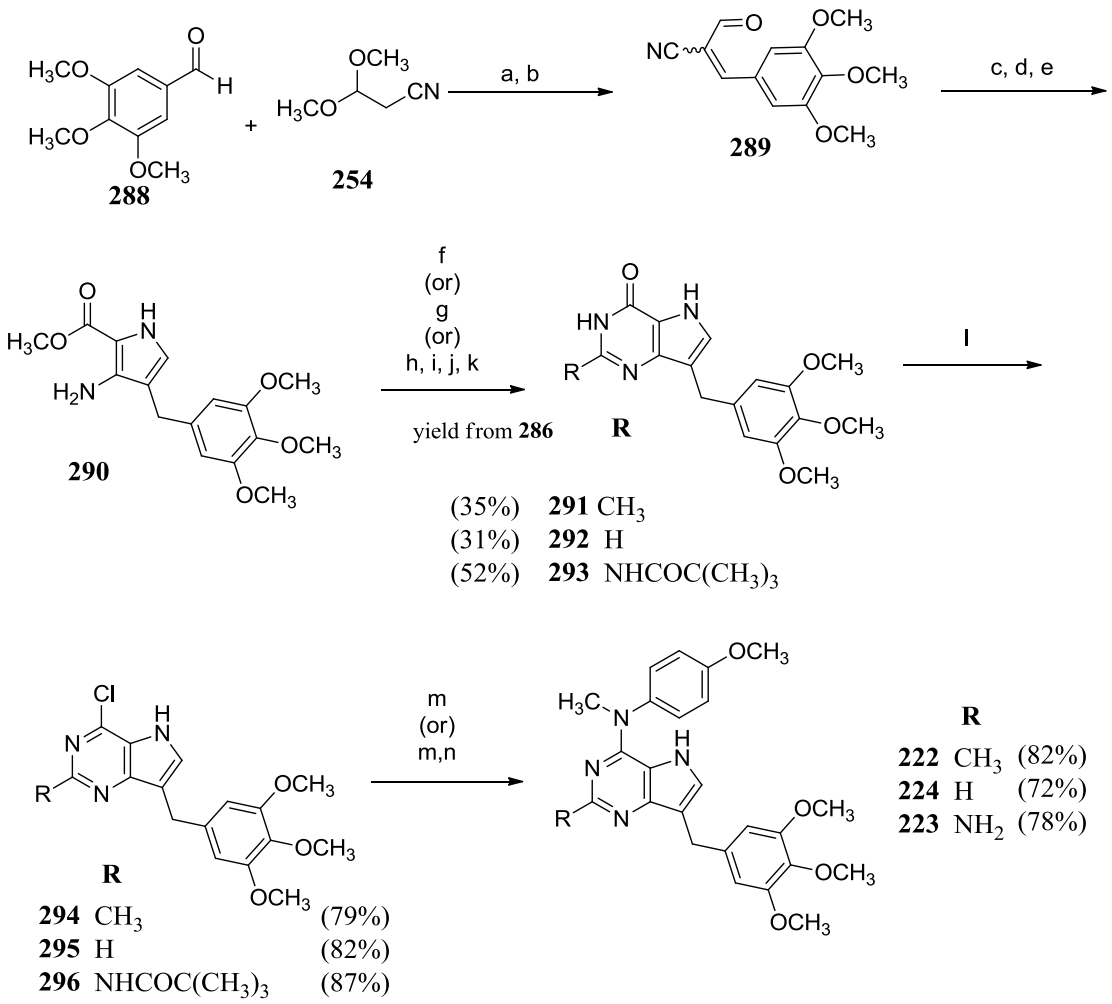

Reagents and conditions: (a) C_2H_5ONa, C_2H_5OH, rt, 6 h; (b) 6N HCl, rt, 2 h; (c) H_2, Pd/C, 55 psi, rt, 1 h (d) diethylaminomalonate, CH_3COONa, CH_3OH, rt, 16 h; (e) CH_3ONa, CH_3OH, rt, 12 h, reflux, 3 h; (f) CH_3CN, HCl, rt, 3 h; (g) fomamidine acetate, C_2H_5OH, reflux, 18 h; (h) 1,3-dicarbomethoxy-2-methyl-2-thiopseudourea, CH_3COOH, rt, 24 h; (i) CH_3ONa, CH_3OH, rt, 12 h; (j) 1N NaOH, CH_3OH, reflux, 2 h; trimethylacetic anhydride, 120 °C, 2 h; (k) trimethylacetic anhydride, 120 °C, 2 h; (l) $POCl_3$, 110 °C, 2-4 h; (m) 4-methoxy *N*-methyl aniline, $(CH_3)_2CHOH$, reflux, 4-12 h; (n) 1N NaOH, CH_3OH, reflux, 10 h

24 hours) compared to sodium ethoxide in ethanol (6 hours). Catalytic hydrogenation of alkenyl aldehyde **287** using 10% Pd/C afforded an intermediate alkyl aldehyde which was treated with diethylaminomalonate in methanol to afford an enamino nitrile. The enamino nitrile was subjected to a base catalyzed cyclization and decarboxylation using sodium methoxide to afford methyl-3-amino-4-(3,4,5-trimethoxybenzyl)-1*H*-pyrrole-2-carboxylate **288**. Pyrrole **288** was condensed with acetonitrile or fomamidine or 1,3-dicarbomethoxy-2-methyl-2-thiopseudourea under acidic conditions to afford bicyclic pyrrolo[3,2-*d*]pyrimidines **289-291**. The 4-oxo-pyrrolo[3,2-*d*]pyrimidines **289-291** were chlorinated with phosphorus oxychloride to generate the corresponding 4-chloro-pyrrolo[3,2-*d*]pyrimidines **292-294** which were subjected to nucleophilic aromatic substitution reactions using the appropriately substituted amine to afford **222-224**.

Synthesis of 225-232

Scheme 55. Synthesis of **225-232**

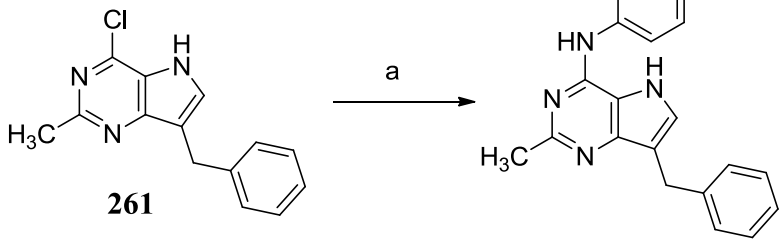

	R	
225	2-F, 4-Br	(76%)
226	2-F, 4-Cl	(67%)
227	3-ethynyl	(78%)
228	3-Br	(72%)
229	3-Cl, 4-F	(75%)
230	3-Cl, 4-OCH_3	(76%)
231	3,4,5-triOCH_3	(71%)
232	H	(75%)

Reagents and conditions: (a) appropriately substituted amine, $(CH_3)_2CHOH$, reflux, 4-12 h

Nucleophilic aromatic substitution reactions of 7-benzyl-4-chloro-2-methyl-5H-pyrrolo[3,2-*d*]pyrimidine **261** (Scheme 44) with appropriately substituted amines in isopropanol at reflux afforded compounds **225-232** (Scheme 55). It was interesting to note that there was no correlation between the electronics of the amines used and the reaction time or yields for the displacement reactions.

V. EXPERIMENTAL

All evaporations were carried out in vacuum with a rotary evaporator. Analytical samples were dried in vacuo in a CHEM-DRY drying apparatus over P_2O_5 at 50 °C. Melting points were determined either using a MEL-TEMP II melting point apparatus with FLUKE 51 K/J electronic thermometer or using an MPA100 OptiMelt automated melting point system and are uncorrected. Nuclear magnetic resonance spectra for proton (^{1}H NMR) were recorded on the Bruker Avance II 400 (400 MHz) or Bruker Avance II 500 (500 MHz) NMR systems with TopSpin processing software. The chemical shift values (δ)are expressed in ppm (parts per million) relative to tetramethylsilane as an internal standard: s, singlet; d, doublet; dd, doublet of doublet; t, triplet; q, quartet; m, multiplet; br, broad singlet; td, triplet of doublet; dt, doublet of triplet; quin, quintet. Thin-layer chromatography (TLC) was performed on Whatman® PE SIL G/UV254 flexible silica gel plates and the spots were visualized under 254 and 365 nm ultraviolet illumination. Proportions of solvents used for TLC are by volume. All analytical samples were homogeneous on TLC in at least two different solvent systems. Column chromatography was performed on the silica gel (70 to 230 meshes, Fisher Scientific) column. Flash chromatography was carried out on the CombiFlash® Rf systems, model COMBIFLASH RF. Pre-packed RediSep® Rf normal-phase flash columns (230 to 400 meshes) of various sizes were used. The amount (weight) of silica gel for column chromatography was in the range of 50-100 times the amount (weight) of the crude compounds being separated. Elemental analyses were performed by Atlantic Microlab, Inc., Norcross, GA. Element compositions are within ± 0.4% of the calculated values. Fractional moles of water or organic solvents frequently found in some analytical samples could not be

prevented despite 24 to 48 hours of drying in vacuo and were confirmed where possible by their presence in the ^{1}H NMR spectra.

2-Methyl-3*H*-pyrrolo[3,2-*d*]pyrimidin-4(5*H*)-one (237)

A solution of sodium ethoxide (5.17 g, 76 mmol) in ethanol (40 mL) was added dropwise to a stirred solution of isoxazole **233** (5g, 72.5 mmol) in ethanol (10 mL) in an ice bath. After an additional 1 h of stirring acetic acid (5.5 mL), diethylaminomalonate hydrochloride (15 g, 71 mmol), and sodium acetate (4.8, 58.51 mmol) were added, and the mixture was stirred at room temperature for 24 hours, after which most of the solvent removed under vacuum. The residue was partitioned between dichloromethane and water, and the organic phase was dried over sodium sulphate and filtered through a thick pad of silica. The filtrate was evaporated to afford a brown syrup of **235** which was dissolved in a solution of sodium ethoxide in ethanol (0.5 M, 100 mL), and the solution was stirred at room temperature for 24 hours. Acetic acid was added to adjust the pH to 7 and the solvent was removed under vacuum. The residue was partitioned between dichloromethane and water, and the organic phase was dried over sodium sulphate and filtered through a thick pad of silica. The filtrate was evaporated to afford crude syrupy **236** which was dissolved in acetonitrile (100 mL) and hydrogen chloride gas was bubbled through for 2 hours. The reaction mixture was neutralized with ammonium hydroxide and the solvent was evaporated and flash chromatographed ($CHCl_3$: CH_3OH; 100:1 to 50:3; v/v) to yield **237** as a light brown solid (4.1g, 32%). TLC R_f = 0.42 (CH_3OH: $CHCl_3$; 1:10); mp[198], 240-242 °C; ^{1}H NMR (400 MHz, DMSO-d_6) δ ppm 2.27 (s, 3 H, CH_3) 6.21

- 6.24 (m, 1 H, 7-CH) 7.27 - 7.31 (m, 1 H, 6-CH) 11.74 (br, 1 H, exch, NH) 11.89 (br, 1 H, exch, NH)

4-Chloro-2-methyl-5*H*-pyrrolo[3,2-*d*]pyrimidine (238)

2-Methyl-3*H*-pyrrolo[3,2-*d*]pyrimidin-4(5*H*)-one (**237**, 1 g, 6.54 mmol) was added to phosphorus oxychloride (20 mL) and heated at reflux for 4 h. The solvent was evaporated in vacuo, and the pH of the residue was adjusted to 8 with ammonia solution. The resulting precipitate was filtered and purified by column chromatography ($CHCl_3$: CH_3OH; 100:1 to 50:3; v/v) to give a light yellow solid (840 mg, 75%). TLC R_f = 0.32 (CH_3OH: $CHCl_3$; 1:10); mp, 138-139 °C; ^{1}H NMR, DMSO-d_6: δ 2.60 (s, 3 H, CH_3) 6.6 (m, 1 H, 7-CH) 7.9 (m, 1 H, 6-CH) 12.26 (s, 1 H, exch, NH).

***N*-(4-methoxyphenyl)-*N*,2-dimethyl-5*H*-pyrrolo[3,2-*d*]pyrimidin-4-amine (161)**

Compound **238** (0.1 g, 0.45 mmol) and 4-methoxy-N-methylaniline (0.12 g, 1.05 mmol) were dissolved in isopropanol (20 mL) and heated at reflux for 4 h. The solvent was evaporated in vacuo, and the residue was purified by column chromatography ($CHCl_3$: CH_3OH; 50:1; v/v) to give a brown solid (97.6 mg, 86%). TLC R_f = 0.42 (CH_3OH: $CHCl_3$; 1:10). The product obtained was dissolved in a minimum amount of ethyl acetate and diethyl ether (10 mL) was added to the solution. Hydrogen chloride gas was bubbled through for 2-3 mins. The precipitate obtained was collected by filtration. white solid; mp, 184-185 °C; ^{1}H NMR, DMSO-d_6: δ 2.63 (s, 3 H, 2-CH_3) 3.62 (s, 3 H, NCH_3) 3.84 (s, 3 H, OCH_3), 6.46 (s, 1 H, Ar) 7.1 (d, J = 8.9 Hz, 2 H, Ar) 7.42 (d, J = 8.86 Hz, 2 H, Ar) 9.661

(s, 1 H, exch, NH) 14.99 (s, 1 H, exch, NH). Anal. Calcd. for $C_{15}H_{16}N_4O \cdot HCl \cdot H_2O$: C, 55.81; H, 5.93; N, 17.36; Cl, 10.98. Found C, 55.94; H, 5.87; N, 17.17; Cl, 10.97.

3*H*-Pyrrolo[3,2-*d*]pyrimidin-4(5*H*)-one (239)

Crude **236** (prepared from **233** as described previously) was dissolved in ethanol (50 mL), formamidine acetate (2 equivalents) was added and heated to reflux for 18 hours. The reaction mixture was neutralized with ammonium hydroxide and the solvent was evaporated and flash chromatographed ($CHCl_3$: CH_3OH; 100:1 to 50:3; v/v) to yield **239** as a brown solid (15% over 4 steps from **233**). TLC R_f = 0.36 (CH_3OH: $CHCl_3$; 1:10); mp[199], 212-214 °C; ^{1}H NMR (400 MHz, DMSO-d_6) δ ppm 6.33 - 6.37 (m, 1 H, CH) 7.35 (t, J = 2.89 Hz, 1 H, CH) 7.77 (s, 1 H, CH) 11.83 (br, 1 H, exch, NH) 12.06 (br, 1 H, exch, NH)

4-Chloro-5*H*-pyrrolo[3,2-*d*]pyrimidine (240)

3*H*-Pyrrolo[3,2-*d*]pyrimidin-4(5*H*)-one (**239**, 500 mg, 3.7 mmol) was added to phosphorus oxychloride (20 mL) and heated at reflux for 6 h. The solvent was evaporated in vacuo, and the pH of the residue was adjusted to 8 with ammonia solution. The resulting precipitate was filtered and purified by column chromatography ($CHCl_3$: MeOH; 100:1 to 50:3; v/v) to give a light yellow solid (318 mg, 56%). TLC R_f = 0.36 (CH_3OH: $CHCl_3$; 1:10); mp[199], 161-162 °C; ^{1}H NMR, DMSO-d_6: δ 2.60 (s, 3 H, CH_3) 6.6 (m, 1 H, CH), 7.81 (s, 1 H, CH) 7.9 (m, 1 H, CH) 12.26 (s, 1 H, exch, NH).

***N*-(4-Methoxyphenyl)-*N*-methyl-5*H*-pyrrolo[3,2-*d*]pyrimidin-4-amine (162)**

Compound **162** (synthesized from **240** as described for **161**): yield 72%; TLC R_f = 0.33 (CH_3OH: $CHCl_3$; 1:5). ; white solid; mp, 150-151 °C; ^{1}H NMR, DMSO-d_6 δ 3.65 (s, 3 H, NCH_3) 3.84 (s, 3 H, OCH_3) 6.55 (s, 1 H, CH) 7.1 (d, J = 8.8 Hz, 2 H, C_6H_4) 7.4 (d, J = 8.7Hz, 2 H, C_6H_4) 7.56 (s, 1 H, CH) 8.71 (s, 1 H, CH) 9.96 (s, 1 H, exch, NH) 14.39 (s, 1 H, exch, HCl). Anal. Calcd. for $C_{14}H_{14}N_4O{\cdot}HCl{\cdot}H_2O$: C, 54.46; H, 5.55; N, 18.15; Cl, 11.48. Found C, 54.29; H, 5.46; N, 17.90; Cl, 11.26.

***N*,2-Dimethyl-*N*-phenyl-5*H*-pyrrolo[3,2-*d*]pyrimidin-4-amine (163)**

Compound **163** (synthesized from **238** and *N*-methyl aniline as described for **161**): yield 78%; TLC R_f = 0.42 (MeOH: $CHCl_3$; 1:5).; white solid; mp, 253-254 °C; ^{1}H NMR, DMSO-d_6: δ 2.62 (s, 3 H, 2-CH_3) 3.7 (s, 3 H, NCH_3) 6.49 (s, 1 H, Ar) 7.47-7.59 (m, 6 H, Ar) 10.07 (s, 1 H, exch, NH) 15.02 (s, 1 H, exch, HCl). Anal. Calcd. for $C_{15}H_{16}N_4O{\cdot}0.95$ $HCl{\cdot}0.25H_2O$: C, 60.61; H, 5.61; N, 20.1. Found C, 60.59; H, 5.6; N, 20.00.

***N*-(4-Methoxyphenyl)-2-methyl-5*H*-pyrrolo[3,2-*d*]pyrimidin-4-amine (164)**

Compound **164** (synthesized from **238** and *p*-anisidine as described for **161**): yield 81%; TLC R_f = 0.4 (CH_3OH: $CHCl_3$; 1:5); white solid; mp 260 °C (decomp); ^{1}H NMR, DMSO-d_6: δ 2.61 (s, 3 H, 2-CH_3) 3.77 (s, 3 H, OCH_3) 6.51 (s, 1 H, 7-CH) 7.0 (d, J = 9 Hz, 2 H, C_6H_5) 7.82 (d, J = 8.8 Hz, 2 H, C_6H_5) 7.89 (s, 1 H, 6-CH) 11.43 (s, 1 H, exch, NH) 12.94 (s, 1 H, exch, NH) 14.44 (s, 1 H, exch, HCl). Anal. Calcd. For $C_{14}H_{14}N4O{\cdot}HCl$: C, 57.83; H, 5.20; N, 19.27; Cl, 12.19. Found C, 57.73; H, 5.38; N, 19.05; Cl, 12.07.

_N_-(2,4-Dimethoxyphenyl)-2-methyl-5_H_-pyrrolo[3,2-_d_]pyrimidin-4-amine (165)

Compound **165** (synthesized from **238** and 2,4-dimethoxy aniline as described for **161**): yield 76%; TLC R_f = 0.6 (CH_3OH: $CHCl_3$; 1:10); white solid; mp, 262-264 °C; ^{1}H NMR, DMSO-d_6: δ 2.5 (s, 3 H, 2-CH_3) 3.8 (s, 6 H, OCH_3) 6.5 (m, 1 H, Ar) 6.59 (dd, J = 8.7, 2.6 Hz, 1 H, Ar) 6.7 (d, J = 2.6 Hz, 1 H, Ar) 7.48 (d, J = 8.7 Hz, 1 H, Ar) 7.85 (s, 1 H, Ar) 10.4 (s, 1 H, exch, NH) 12.65 (s, 1 H, exch, NH) 14.86 (s, 1H, exch, NH). Anal. Calcd. for $C_{15}H_{16}N_4O_2$·HCl·0.2H_2O: C, 55.54; H, 5.41; N, 17.27; Cl, 10.93. Found C, 55.74; H, 5.28; N, 17.21; Cl, 10.85.

4-(5-Methoxyindolin-1-yl)-2-methyl-5_H_-pyrrolo[3,2-_d_]pyrimidine (166)

Compound **166** (synthesized from **238** and 5-methoxyindoline as described for **161**): yield 72%; TLC R_f = 0.54 (CH_3OH: $CHCl_3$; 1:10); grey solid; mp, 310-312 °C; ^{1}H NMR, DMSO-d_6: δ 2.71 (s, 3 H, 2-CH_3) 3.34 (t, J = 8.16 Hz, 2 H, CH_2) 3.79 (s, 3 H, OCH_3) 4.73 (t, J = 8.16 Hz, 2 H, CH_2) 6.90 (dd, J = 8.91, 2.64 Hz, 1 H, Ar) 7.03 (d, J = 2.76 Hz, 1 H, Ar) 7.21 (d, J = 2.26 Hz, 1 H, Ar) 8.53 (d, J = 9.03 Hz, 1 H, Ar) 8.62 (d, J = 2.01 Hz, 1 H, Ar) 11.05 (s, 1 H, exch, NH) 14.85 (s, 1 H, exch, HCl). Anal. Calcd. for $C_{16}H_{16}N_4O$·HCl·H_2O: C, 57.40; H, 5.72; N, 16.73; Cl, 10.59. Found C, 57.21; H, 5.85; N, 16.43; Cl, 10.14.

6-Methoxy-1-(2-methyl-5_H_-pyrrolo[3,2-_d_]pyrimidin-4-yl)-1,2,3,4-tetrahydroquinoline (167)

Compound **167** (synthesized from **238** and 6-methoxy-1,2,3,4-tetrahydroquinoline as described for **161**): yield 79%; TLC R_f = 0.36 (CH_3OH: $CHCl_3$; 1:10); yellow solid; mp,

230-232 °C; ^{1}H NMR, DMSO-d_6: δ 2.01 (m, 2 H, CH_2) 2.63 (s, 3 H, 2-CH_3) 2.79 (t, 2 H, *J* = 6.5 Hz, CH_2) 3.8 (s, 3 H, OCH_3) 4.1 (t, *J* = 6.3 Hz, 2 H, CH_2) 6.53 (dd, *J* = 8.7, 2.6, 1H, CH) 6.8 (dd, *J* = 8.8, 2.9, 1 H, CH) 6.94 (d, *J* = 2.8 Hz, 1 H, CH) 7.15 (d, *J* = 8.8 Hz, H, CH) 7.65 (t, *J* = 2.7 Hz, 1 H, CH) 11.05 (s, 1 H, exch, NH) 14.85 (s, 1 H, exch, HCl). Anal. Calcd. for $C_{16}H_{18}N_4O{\cdot}HCl{\cdot}0.2H_2O$: C, 59.61; H, 6.06; N, 17.38; Cl, 11.00. Found C, 59.82; H, 6.05; N, 17.25; Cl, 10.85.

4-Chloro-2,5-dimethyl-5*H*-pyrrolo[3,2-*d*]pyrimidine (241)

4-Chloro-2-methyl-5*H*-pyrrolo[3,2-*d*]pyrimidine (**238**, 300 mg, 1.79 mmol) was dissolved in dimethylformamide (20mL) and sodium hydride (47 mg, 1.97 mmol) was added under nitrogen. The mixture was allowed to stir for 15 minutes after no further production of hydrogen gas was observed. Methyl bromide (0.3 mL) was added and the reaction was stirred for 3 hours. The reaction was quenched by addition of water and ethylacetate was added. The organic layer was collected, washed with brine and dried over sodium sulphate. A silica gel plug was made and purified by column chromatography ($CHCl_3$: MeOH; 100:1 v/v) to give an off-white solid (244 mg, 75%). TLC R_f = 0.45 (CH_3OH: $CHCl_3$; 1:10); mp, 156-158 °C; ^{1}H NMR (400 MHz, DMSO-d_6) δ ppm 2.62 (s, 3 H, CH_3) 4.01 (s, 3 H, CH_3) 6.6 (m, 1 H, 7-CH) 7.9 (m, 1 H, 6-CH)

***N*-(4-Methoxyphenyl)-*N*,2,5-trimethyl-5*H*-pyrrolo[3,2-*d*]pyrimidin-4-amine (170)**

Compound **170** (synthesized from **241** and 4-methoxy *N*-methyl aniline as described for **161**): yield 76%; TLC R_f = 0.55 (CH_3OH: $CHCl_3$; 1:10); white solid; mp, 218-220 °C; ^{1}H NMR (400 MHz, DMSO-d_6) δ ppm 2.69 (s, 3 H, CH_3) 2.84 (s, 3 H, CH_3) 3.63 (s, 3 H,

CH_3) 3.79 (s, 3 H, CH_3) 6.51 (d, *J* = 3.26 Hz, 1 H, Ar) 7.00 - 7.03 (m, 2 H, Ar) 7.27 - 7.31 (m, 2 H, Ar) 7.65 (d, *J* = 3.26 Hz, 1 H, Ar) 15.11 (s, 1 H, exch, HCl) Anal. Calcd. for $C_{16}H_{18}N_4O$·HCl: C, 60.28; H, 6.01; N, 17.57; Cl, 11.12. Found C, 60.52; H, 5.97; N, 17.53; Cl, 10.88.

***N*-(4-methoxyphenyl)-2,5-dimethyl-5*H*-pyrrolo[3,2-*d*]pyrimidin-4-amine (171)**

Compound **171** (synthesized from **241** and *p*-anisidine as described for **161**): yield 81%; TLC R_f 0.48 (CH_3OH: $CHCl_3$; 1:10); white solid; mp, 317-319 °C; ^{1}H NMR (400 MHz, DMSO-d_6) δ ppm 2.50 (s, 3 H, CH_3) 3.80 (s, 3 H, CH_3) 4.23 (s, 3 H, CH_3) 6.50 (d, *J* = 3.01 Hz, 1 H, Ar) 7.00 - 7.04 (m, 2 H, Ar) 7.47 - 7.51 (m, 2 H, Ar) 7.83 (d, *J* = 3.01 Hz, 1 H, Ar) 9.52 (s, 1 H, exch, NH) 14.70 (br, 1 H, exch, HCl) Anal. Calcd. for $C_{15}H_{16}N_4O$·HCl: C, 59.11; H, 5.62; N, 18.38; Cl, 11.63. Found C, 59.32; H, 5.68; N, 18.36; Cl, 11.37.

***N*-(2,4-dimethoxyphenyl)-2,5-dimethyl-5*H*-pyrrolo[3,2-*d*]pyrimidin-4-amine (172)**

Compound **172** (synthesized from **241** and 2,4-dimethoxy aniline as described for **161**): yield 77%; TLC R_f = 0.4 (CH_3OH: $CHCl_3$; 1:10); white solid; mp, 246-248 °C; ^{1}H NMR, DMSO-d_6: δ 2.5 (s, 3 H, 2-CH_3) 3.8 (s, 6 H, OCH_3) 4.23 (s, 3 H, CH_3) 6.5 (m, 1 H, Ar) 6.59 (dd, *J* = 8.7, 2.6 Hz, 1 H, Ar) 6.7 (d, *J* = 2.6 Hz, 1 H, Ar) 7.48 (d, *J* = 8.7 Hz, 1 H, Ar) 7.85 (s, 1 H, Ar) 10.4 (s, 1 H, exch, NH) 12.65 (s, 1 H, exch, NH) 14.86 (s, 1H, exch, NH). Anal. Calcd. for $C_{16}H_{18}N_4O_2$·HCl: C, 57.40; H, 5.72; N, 16.73; Cl, 10.59. Found C, 57.31; H, 5.80; N, 16.56; Cl, 10.37.

1-(2,5-dimethyl-5*H*-pyrrolo[3,2-*d*]pyrimidin-4-yl)-6-methoxy-1,2,3,4-tetrahydroquinoline (173)

Compound **173** (synthesized from **241** and 6-methoxy-1,2,3,4-tetrahydroquinoline as described for **161**): yield 77%; TLC R_f = 0.5 (CH_3OH: $CHCl_3$; 1:10); yellow solid; mp, 230-232 °C; ^{1}H NMR (400 MHz, DMSO-d_6) δ ppm 2.08 (quin, J = 6.59 Hz, 2 H, CH_2) 2.67 (s, 3 H, CH_3) 2.86 (t, J = 6.53 Hz, 2 H, CH_2) 3.00 (s, 3 H, CH_3) 3.76 (s, 3 H, CH_3) 4.03 (t, J = 6.02 Hz, 2 H, CH_2) 6.56 (d, J = 3.01 Hz, 1 H, Ar) 6.69 - 6.72 (m, 1 H, Ar) 6.76 - 6.79 (m, 1 H, Ar) 6.94 (d, J = 2.76 Hz, 1 H, Ar) 7.74 (d, J = 3.01 Hz, 1 H, Ar) 14.97 (b., 1 H, exch, HCl) Anal. Calcd. for $C_{18}H_{20}N_4O$·HCl: C, 62.69; H, 6.14; N, 16.25; Cl, 10.28. Found C, 62.62; H, 6.09; N, 6.10; Cl, 10.10.

Diethyl 2-((1-cyanoprop-1-en-2-yl)amino)malonate (243)

To a suspension of an *E*/*Z* mixture of 3-aminobut-2-enenitrile **242** (3 g, 35.1 mmol) in ethanol (60 mL) was added diethyl aminomalonate hydrochloride (7.9 g, 36.8 mmol). The resulting mixture was stirred at room temperature for 6 hours. Most of the solvent was removed under vacuum at room temperature and dichloromethane was added and washed with brine. The organic layer was separated and dried over sodium sulphate. A silica gel plug was made and flash-chromatographed (EtOAc in hexanes 0% to 15%). Fractions containing the desired product were pooled and evaporated to afford 6.74 g (80%) as an off-white solid. TLC R_f = 0.26 (EtOAc: Hexane; 1:2) mp[105], 50–52 °C; ^{1}H NMR (400 MHz, DMSO-d_6) δ ppm 1.16 - 1.24 (m, 6 H, CH_3) 2.05 (s, 3 H, CH_3) 3.95 (s, 1 H, CH) 4.13 - 4.25 (m, 4 H, CH_2) 4.95 (s, 1 H, CH) 7.51 - 7.55 (m, 1 H, exch, NH)

Ethyl 3-amino-5-methyl-1*H*-pyrrole-2-carboxylate (244)

To a stirred solution of diethyl 2-((1-cyanoprop-1-en-2-yl)amino)malonate (**244**, 1 g, 4 mmol) in 20 mL of ethanol, a 0.5 M solution of sodium ethoxide in ethanol (120 mL) was added slowly and the reaction mixture was stirred for 6 h at 60 °C. The reaction mixture was cooled to room temperature and the solvent was evaporated under reduced pressure. The crude product was purified by column chromatography on silica gel (EtOAc in Hexanes 10%) to afford 450 mg (65%) as an off-white solid. TLC R_f = 0.36 (EtOAc: Hexane; 1:1) mp[105], 85–87 °C; ^{1}H NMR (DMSO-d_6) δ 1.24 (t, J = 6.4 Hz, 3 H, CH_3), 2.03 (s, 3 H, CH_3), 4.12 (q, J = 6.4 Hz, 2 H, CH_2), 4.91 (s, 2 H, exch, NH_2), 5.26 (s, 1 H, CH), 10.21 (s, 1 H, exch, NH).

2,6-dimethyl-3H-pyrrolo[3,2-*d*]pyrimidin-4(5*H*)-one (245)

Dry hydrogen chloride gas was bubbled through a solution of ethyl 3-amino-5-methyl-1*H*-pyrrole-2-carboxylate (**244,** 500 mg, 7.81 mmol) in acetonitrile (15 mL) at room temperature for 15 min. A precipitate was formed, and it dissolved as the reaction progressed. Hydrogen chloride gas was bubbled through the solution for an additional hour, and the mixture was stirred at room temperature for 8 hours. Most of the solvent was evaporated in vacuo, water (40 mL) was added, and the aqueous mixture was neutralized with ammonia solution to afford a precipitate that was removed by filtration, washed with water and dried in vacuo to afford a white solid. Silica gel (4.5 g) and methanol (20 mL) were added; the solvent was evaporated to afford a plug. The silica gel plug obtained was loaded onto a silica gel column and eluted with 1% (v/v) CH_3OH in $CHCl_3$. Fractions containing the product (TLC) were pooled, and the solvent was

evaporated to afford 315 mg of **245** (65%). TLC $R_f = 0.42$ (CH_3OH: $CHCl_3$; 1:20); white solid; mp 254-256 °C; ^1H NMR (400 MHz, DMSO-d_6) δ ppm 2.26 (s, 3 H, CH_3) 2.29 (s, 3 H, CH_3) 5.98 (s, 1 H, 7-CH) 11.62 (br, 1 H, exch, NH) 11.66 (br, 1 H, exch, NH)

4-chloro-2,6-dimethyl-5*H*-pyrrolo[3,2-*d*]pyrimidine (246)

Compound **246** (synthesized from **245** as described for **238**): yield 77%; TLC R_f = 0.7 (CH_3OH: $CHCl_3$; 1:10); brown solid; mp, 230-232 °C; ^1H NMR, DMSO-d_6: δ 2.60 (s, 3 H, CH_3) 2.92 (s, 3 H, CH_3) 6.6 (m, 1 H, 7-CH) 12.26 (s, 1 H, exch, NH).

***N*-(4-methoxyphenyl)-*N*,2,6-trimethyl-5H-pyrrolo[3,2-*d*]pyrimidin-4-amine (174)**

Compound **174** (synthesized from **246** and 4-methoxy *N*-methyl aniline as described for **161**): yield 73%; TLC R_f = 0.52 (CH_3OH: $CHCl_3$; 1:20); light yellow solid; mp, 229-230 °C; ^1H NMR (400 MHz, DMSO-d_6) δ ppm 2.38 (s, 3 H, CH_3) 2.55 (s, 3 H, CH_3) 3.68 (s, 3 H, CH_3) 3.83 (s, 3 H, CH_3) 6.33 (d, J = 1.00 Hz, 1 H, Ar) 7.05 - 7.09 (m, 2 H, Ar) 7.34 - 7.38 (m, 2 H, Ar) 10.29 (br, 1 H, exch, NH) 14.59 (br, 1 H, exch, NH) Anal. Calcd. for $C_{16}H_{18}N_4O \cdot HCl \cdot 0.2H_2O$: C, 59.61; H, 6.06; N, 17.38; Cl, 11.00. Found C, 59.82; H, 6.05; N, 17.25; Cl, 10.85.

4-(5-methoxyindolin-1-yl)-2,6-dimethyl-5*H*-pyrrolo[3,2-*d*]pyrimidine (175)

Compound **175** (synthesized from **246** and 5-methoxyindoline as described for **161**): yield 69%; TLC R_f = 0.6 (CH_3OH: $CHCl_3$; 1:20); grey solid; mp 308-310 °C; ^1H NMR, DMSO-d_6: δ 2.71 (s, 3 H, 2-CH_3), 2.99 (s, 3 H, 2-CH_3), 3.34 (t, J = 8.16 Hz, 2 H, CH_2) 3.79 (s, 3 H, OCH_3) 4.73 (t, J = 8.16 Hz, 2 H, CH_2) 6.90 (dd, J = 8.91, 2.64 Hz, 1 H, Ar)

7.03 (d, *J* = 2.76 Hz, 1 H, Ar) 7.21 (d, *J* = 2.26 Hz, 1 H, Ar) 8.53 (d, *J* = 9.03 Hz, 1 H, Ar) 11.05 (s, 1 H, exch, NH) 14.85 (s, 1 H, exch, HCl). Anal. Calcd. for $C_{17}H_{18}N_4O{\cdot}HCl{\cdot}H_2O$: C, 58.53; H, 6.07; N, 16.06; Cl, 10.16. Found C, 58.76; H, 6.06; N, 16.00; Cl, 10.01.

1-(2,6-dimethyl-5*H*-pyrrolo[3,2-*d*]pyrimidin-4-yl)-6-methoxy-1,2,3,4-tetrahydroquinoline (176)

Compound **176** (synthesized from **246** and 6-methoxy-1,2,3,4-tetrahydroquinoline as described for **161**): yield 66%; TLC R_f = 0.6 (CH_3OH: $CHCl_3$; 1:20); yellow solid; mp, 141-143 °C; ^{1}H NMR (400 MHz, DMSO-d_6) δ ppm 1.97 - 2.06 (m, 2 H, CH_2) 2.42 (s, 3 H, CH_3) 2.58 (s, 3 H, CH_3) 2.81 (t, *J* = 6.40 Hz, 2 H, CH_2) 3.79 (s, 3 H, CH_3) 4.12 (t, *J* = 6.27 Hz, 2 H, CH_2) 6.36 (s, 1 H, Ar) 6.76 (dd, *J* = 8.78, 2.76 Hz, 1 H, Ar) 6.91 (d, *J* = 2.51 Hz, 1 H, Ar) 7.11 (d, *J* = 9.03 Hz, 1 H, Ar) 11.20 (br, 1 H, exch, NH) 14.60 (s, 1 H, exch, HCl) Anal. Calcd. for $C_{18}H_{20}N_4O{\cdot}HCl{\cdot}H_2O$: C, 59.58; H, 6.39; N, 15.44; Cl, 9.77. Found C, 59.89; H, 6.39; N, 15.14; Cl, 9.44.

Ethyl 2-((2-cyanophenyl)amino)acetate (104)

Ethyl bromoacetate (1.95 mL, 20 mmol) was added dropwise to a stirred solution of 2-anthranilonitrile (**103**, 2.38 g, 20 mmol) and potassium carbonate (2.78 g, 20.1 mmol) in ethanol (100 mL) at room temperature and heated to reflux for 6h. Most of the solvent was removed in vacuo and a silica gel plug was made. Flash chromatography with EtOAc: Hex 0% to 10 % afforded 3.82 g (98%) of brown solid. TLC R_f = 0.36 (EtOAc: Hexane; 1:1) mp[113], 105–107 °C; ^{1}H NMR (500 MHz, DMSO-d_6) δ ppm 1.21 (t, *J* = 7.07 Hz, 3 H, CH_3) 4.05 (d, *J* = 5.97 Hz, 2 H, CH_2) 4.14 (q, *J* = 6.92 Hz, 2 H, CH_2) 6.34 (t, *J* = 6.13 Hz,

1 H, exch, NH) 6.65 (d, *J* = 8.49 Hz, 1 H, CH) 6.68 - 6.73 (m, 1 H, CH) 7.39 - 7.44 (m, 1 H, CH) 7.50 (dd, *J* = 7.70, 1.41 Hz, 1 H, CH)

Ethyl 3-amino-1*H*-indole-2-carboxylate (105)

Ethyl 2-((2-cyanophenyl)amino)acetate (**104**, 3.8 g, 19 mmol) was added dropwise to a stirred solution of potassium *tert*-butoxide (2.78 g, 20.1 mmol) in tetrahydrofuran (100 mL) at room temperature and stirred for 6h. Most of the solvent was removed in vacuo and a silica gel plug was made. Flash chromatography with EtOAc: Hexanes 0% to 10 % afforded 3 g (73%) of brown semisolid. TLC R_f = 0.5 (EtOAc: Hexanes; 1:1) ^{1}H NMR (500 MHz, DMSO-d_6) δ ppm 1.34 (t, *J* = 7.07 Hz, 3 H, CH_3) 4.30 (q, *J* = 6.92 Hz, 2 H, CH_2) 5.67 (s, 2 H, exch, NH_2) 6.89 (dd, *J* = 8.10, 6.05 Hz, 1 H, CH) 7.18 - 7.23 (m, 2 H, CH) 7.74 (d, *J* = 8.17 Hz, 1 H, CH) 10.33 (s, 1 H, exch, NH)

2-Methyl-3*H*-pyrimido[5,4-*b*]indol-4(5*H*)-one (248)

Compound **248** (synthesized from **105** as described for **245**): yield 72%; TLC R_f = 0.6 (MeOH: $CHCl_3$; 1:20); white solid; mp, 200-202 °C; ^{1}H NMR (400 MHz, DMSO-d_6) δ ppm 2.43 (s, 3 H, CH_3) 7.16 - 7.22 (m, 1 H, CH) 7.40 - 7.45 (m, 1 H, CH) 7.47 - 7.52 (m, 1 H, CH) 7.96 (d, *J* = 8.03 Hz, 1 H, CH) 11.90 (s, 1 H, exch, NH) 12.27 (br, 1 H, exch, NH)

4-Chloro-2-methyl-5*H*-pyrimido[5,4-*b*]indole (249)

Compound **249** (synthesized from **248** as described for **238**): yield 81%; TLC R_f = 0.7 (CH_3OH: $CHCl_3$; 1:20); white solid; mp, 212-214 °C; ^{1}H NMR (400 MHz, DMSO-d_6) δ

ppm 2.68 (s, 3 H, CH_3) 7.28 - 7.41 (m, 1 H, CH) 7.48 - 7.50 (m, 1 H, CH) 7.52 - 7.57 (m, 1 H, CH) 8.11 (d, *J* = 8.03 Hz, 1 H, CH) 12.35 (br, 1 H, exch, NH)

_N_-(4-methoxyphenyl)-_N_,2-dimethyl-5_H_-pyrimido[5,4-_b_]indol-4-amine (178)

Compound **178** (synthesized from **249** and 4-methoxy *N*-methyl aniline as described for **161**): yield 75%; TLC R_f = 0.46 (CH_3OH: $CHCl_3$; 1:20); grey solid; mp, 283-285 °C; ^1H NMR (400 MHz, DMSO-d_6) δ ppm 2.79 (s, 3 H, CH_3) 3.74 (s, 3 H, CH_3) 3.87 (s, 3 H, CH_3) 7.12 (d, *J* = 8.78 Hz, 2 H, Ar) 7.34 (t, *J* = 6.90 Hz, 1 H, Ar) 7.46 (d, *J* = 8.53 Hz, 2 H, Ar) 7.55 - 7.62 (m, 1 H, Ar) 7.63 - 7.69 (m, 1 H, Ar) 8.40 (d, *J* = 8.28 Hz, 1 H, Ar) 9.76 - 10.11 (s, 1 H, exch, NH) 15.67 (br, 1 H, exch, HCl) Anal. Calcd. for $C_{15}H_{17}N_3O_2 \cdot HCl \cdot 0.5H_2O$: C, 61.27; H, 6.47; N, 16.81; Cl, 10.64. Found C, 60.89; H, 6.31; N, 16.58; Cl, 10.32.

4-(5-methoxyindolin-1-yl)-2-methyl-5_H_-pyrimido[5,4-_b_]indole (179)

Compound **179** (synthesized from **249** and 5-methoxyindoline as described for **161**): yield 71%; TLC R_f = 0.53 (CH_3OH: $CHCl_3$; 1:20); grey solid; mp, 328-330 °C; ^1H NMR (500 MHz, DMSO-d_6) δ ppm 2.74 (s, 3 H, CH_3) 3.72 (s, 3 H, CH_3) 3.86 (s, 3 H, CH_3) 7.07 - 7.11 (m, 2 H, Ar) 7.46 (d, *J* = 8.80 Hz, 2 H, Ar) 7.55 (t, *J* = 7.55 Hz, 2 H, Ar) 7.67 - 7.74 (m, 1 H, Ar) 8.33 (d, *J* = 7.86 Hz, 1 H, Ar) Anal. Calcd. for $C_{17}H_{17}N_3O_2 \cdot HCl \cdot 0.05H_2O$: C, 63.97; H, 5.11; N, 11.78; Cl, 9.94. Found C, 64.13; H, 5.12; N, 11.66; Cl, 9.81.

4-(6-methoxy-3,4-dihydroquinolin-1(2*H*)-yl)-2-methyl-5*H*-pyrimido[5,4-*b*]indole (180)

Compound **180** (synthesized from **249** and 6-methoxy-1,2,3,4-tetrahydroquinoline as described for **161**): yield 78%; TLC R_f = 0.56 (CH_3OH: $CHCl_3$; 1:20); yellow solid; mp, 275-276 °C; ^1H NMR (400 MHz, DMSO-d_6) δ ppm 2.08 (m, 2 H, CH_2) 2.72 - 2.95 (m, 5 H, CH_3, CH_2) 3.82 (s, 3 H, CH_3) 4.21 (m, 2 H, CH_2) 6.79 (m, 1 H, Ar) 6.99 (m, 1 H, Ar) 7.11 (d, *J* = 7.03 Hz, 1 H, Ar) 7.35 (m, 1 H, Ar) 7.63 (m, 2 H, Ar) 8.47 (m, 1 H, Ar) 10.85 (br, 1 H, exch, NH) 15.96 (br, 1 H, exch, HCl) Anal. Calcd. for $C_{21}H_{20}N_4O{\cdot}HCl{\cdot}0.3H_2O$: C, 65.30; H, 5.64; N, 14.50; Cl, 9.18. Found C, 65.37; H, 5.50; N, 14.48; Cl, 9.06.

2-methylfuro[3,2-*d*]pyrimidin-4(3*H*)-one (251)

Compound **251** (synthesized from **250** as described for **245**): yield 83%; TLC R_f = 0.55 (CH_3OH: $CHCl_3$; 1:20); white solid; mp, 180-182 °C; ^1H NMR (500 MHz, DMSO-d_6) δ ppm 2.34 (s, 3 H, CH_3) 6.88 (d, *J* = 2.20 Hz, 1 H, CH) 8.17 (d, *J* = 2.20 Hz, 1 H, CH) 12.42 (s, 1 H, exch, NH)

4-chloro-2-methylfuro[3,2-*d*]pyrimidine (252)

Compound **252** (synthesized from **251** as described for **238**): yield 72%; TLC R_f = 0.7 (MeOH: $CHCl_3$; 1:50); white solid; mp, 198-200 °C; ^1H NMR (400 MHz, DMSO-d_6) δ ppm 2.68 (s, 3 H, CH_3) 7.27 (d, *J* = 2.26 Hz, 1 H, CH) 8.60 - 8.61 (m, 1 H, CH)

***N*-(4-methoxyphenyl)-*N*,2-dimethylfuro[3,2-*d*]pyrimidin-4-amine (181)**

Compound **181** (synthesized from **252** and 4-methoxy *N*-methyl aniline as described for **161**): yield 76%; TLC R_f = 0.7 (MeOH: $CHCl_3$; 1:25); white solid; mp 241-243 °C; ^{1}H NMR (500 MHz, DMSO-d_6) δ ppm 2.65 (s, 3 H, CH_3) 3.66 (s, 3 H, CH_3) 3.82 (s, 3 H, CH_3) 7.05 - 7.09 (m, 3 H, Ar) 7.41 - 7.45 (m, 2 H, Ar) 8.24 (m, 1 H, Ar) Anal. Calcd. for $C_{15}H_{15}N_3O_2$·HCl: C, 58.92; H, 5.27; N, 13.74; Cl, 11.59. Found C, 58.93; H, 5.35; N, 13.73; Cl, 11.38.

***N*-(4-methoxyphenyl)-2-methylfuro[3,2-*d*]pyrimidin-4-amine (182)**

Compound **182** (synthesized from **252** and *p*-anisidine as described for **161**): yield 80%; TLC R_f = 0.7 (CH_3OH: $CHCl_3$; 1:25); white solid; mp, 265-267 °C; ^{1}H NMR (400 MHz, DMSO-d_6) δ ppm 2.62 (s, 3 H, CH_3) 3.79 (s, 3 H, OCH_3) 7.00 - 7.04 (m, 2 H, Ar) 7.20 (d, J = 2.26 Hz, 1 H, Ar) 7.64 (d, J = 7.78 Hz, 2 H, Ar) 8.57 (s, 1 H, Ar) 11.21 (br, 1 H, exch, NH) Anal. Calcd. for $C_{15}H_{15}N_3O_2$·HCl: C, 58.92; H, 5.27; N, 13.74; Cl, 11.59. Found C, 58.93; H, 5.35; N, 13.73; Cl, 11.38.

***N*-(2,4-dimethoxyphenyl)-2-methylfuro[3,2-*d*]pyrimidin-4-amine (183)**

Compound **183** (synthesized from **252** and 2,4-dimethoxy aniline as described for **161**): yield 78%; TLC R_f = 0.7 (CH_3OH: $CHCl_3$; 1:25); white solid; mp, 247-249 °C; ^{1}H NMR (400 MHz, DMSO-d_6) δ ppm 2.57 (s, 3 H, CH_3) 3.74 (s, 3 H, OCH_3) 3.82 (s, 3 H, OCH_3) 6.60 (dd, J = 8.53, 2.51 Hz, 1 H, Ar) 6.73 (d, J = 2.51 Hz, 1 H, Ar) 7.15 (s, 1 H, Ar) 7.31 (d, J = 8.78 Hz, 1 H, Ar) 8.47 (m, 1 H, Ar) 10.83 (br, 1 H, exch, NH) Anal. Calcd. for

$C_{15}H_{15}N_3O_3$·HCl: C, 55.99; H, 5.01; N, 13.06; Cl, 11.02. Found C, 56.14; H, 5.22; N, 12.85; Cl, 10.80.

4-(5-methoxyindolin-1-yl)-2-methylfuro[3,2-*d*]pyrimidine (184)

Compound **184** (synthesized from **252** and 5-methoxyindoline as described for **161**): yield 78%; TLC R_f = 0.7 (CH_3OH: $CHCl_3$; 1:25); grey solid; mp 297-299 °C; ^{1}H NMR (400 MHz, DMSO-d_6) δ ppm 2.71 (s, 3 H, CH_3) 3.34 (t, *J* = 8.16 Hz, 2 H, CH_2) 3.79 (s, 3 H, OCH_3) 4.73 (t, *J* = 8.16 Hz, 2 H, CH_2) 6.90 (dd, *J* = 8.91, 2.64 Hz, 1 H, Ar) 7.03 (d, *J* = 2.76 Hz, 1 H, Ar) 7.21 (d, *J* = 2.26 Hz, 1 H, Ar) 8.53 (d, *J* = 9.03 Hz, 1 H, Ar) 8.62 (d, *J* = 2.01 Hz, 1 H, Ar) Anal. Calcd. for $C_{16}H_{15}N_3O_2$.HCl: C, 60.48; H, 5.07; N, 13.22; Cl, 11.16. Found C, 60.47; H, 5.16; N, 13.17; Cl, 11.02.

4-(6-methoxy-3,4-dihydroquinolin-1(2*H*)-yl)-2-methylfuro[3,2-*d*]pyrimidine (185)

Compound **185** (synthesized from **252** and 6-methoxy-1,2,3,4-tetrahydroquinoline as described for **161**): yield 75%; TLC R_f = 0.66 (CH_3OH: $CHCl_3$; 1:25); yellow solid; mp 213-215 °C;

^{1}H NMR (400 MHz, DMSO-d_6) δ ppm 2.03 (quin, *J* = 6.40 Hz, 2 H, CH_2) 2.64 (s, 3 H, CH_3) 2.80 (t, *J* = 6.65 Hz, 2 H, CH_2) 3.79 (s, 3 H, CH_3) 4.20 (m, 2 H, CH_2) 6.82 (dd, *J* = 9.03, 2.76 Hz, 1 H, Ar) 6.88 - 6.92 (m, 1 H, Ar) 7.15 (d, *J* = 2.01 Hz, 1 H, Ar) 7.35 (d, *J* = 9.03 Hz, 1 H, Ar) 8.40 (m., 1 H, Ar) Anal. Calcd. for $C_{17}H_{17}N_3O_2$.HCl: C, 60.48; H, 5.07; N, 13.22; Cl, 11.16. Found C, 60.47; H, 5.16; N, 13.17; Cl, 11.02.

methyl 3-amino-4-benzyl-1*H*-pyrrole-2-carboxylate (259)

Benzaldehyde (**253**, 20 g, 0.25 mol) and 3,3-dimethoxypropionitrile (**254**, 35 g, 0.30 mol) were mixed together and added to a solution of sodium ethoxide in ethanol (0.5 M) during 15 min. The mixture was stirred at room temperature for 6 hours. Most of the solvent was removed in vacuo, and the residue was partitioned between EtOAc (500 mL) and water (450 mL). The organic layer was separated, washed with brine, dried with sodium sulphate and the solvent evaporated in vacuo. The residual oil (**255**) was treated cautiously with 6 N HCl (75 mL), and the mixture was stirred at room temperature for 2 hours. The solid was filtered off, washed well with water, and dried in vacuuo to give an off-white powder (**256**) which was shaken with methanol and 10% Pd/C under 50 psi H_2 in a hydrogenation bottle for 1 hour. The catalyst was removed by filtration, a mixture of diethyl aminomalonate, sodium acetate, and water was added, and the mixture was stirred at room temperature for 16 hours. Most of the solvent was removed in vacuo, and the residue was partitioned between EtOAc and water. The organic layer was separated and dried over sodium sulphate and evaporated in vacuo. The residual yellow oil (**258**) was dissolved in methanol containing sodium methoxide, stirred at room temperature for 12 hours and then heated to reflux for 3 hours. Most of the solvent was evaporated in vacuo, and the residue was treated with water (200 mL) to give **259** as a light yellow solid which was flash chromatographed with 1% (v/v) CH_3OH in $CHCl_3$. mp[103] 120-122 °C; ^{1}H NMR (400 MHz, DMSO-d_6) δ ppm 3.62 (s, 2 H, CH_2) 3.68 (s, 3 H, CH_3) 4.84 (br, 2 H, exch, NH_2) 6.46 (d, J = 3.51 Hz, 1 H, 6-H) 7.11 - 7.16 (m, 1 H, C_6H_5) 7.19 - 7.27 (m, 4 H, C_6H_5) 10.47 (br, 1 H, exch, NH)

7-Benzyl-2-methyl-3*H*-pyrrolo[3,2-*d*]pyrimidin-4(5*H*)-one [**260**]

To a 250 mL flask was added **259** (1.5g, 6.51 mmol) and acetonitrile (30 mL). Dry HCl gas was bubbled through the solution at room temperature for 15 min. A precipitate was formed, and it dissolved as the reaction progressed. HCl gas was bubbled through the solution for an additional hour, and the mixture was stirred for 3 h. Most of the solvent was evaporated *in vacuo*, water (20 mL) was added, and the aqueous mixture was neutralized with ammonia to afford a precipitate that was removed by filtration, washed with water and dried in vacuo to afford a light yellow solid. Silica gel and methanol were added; the solvent was evaporated to afford a plug. The silica gel plug obtained was loaded onto a silica gel column and eluted with 1% (v/v) MeOH/$CHCl_3$. Fractions containing the product (TLC) were pooled, and the solvent was evaporated to afford **259** (1.12 g, 59%). TLC R_f = 0.42 (CH_3OH: $CHCl_3$; 1:20); white solid; mp, 254-256 °C; ^{1}H NMR, DMSO-d_6: δ 2.29 (s, 3 H, 2-CH_3) 3.90 (s, 2 H, CH_2) 7.07(d, *J* = 2.90 Hz, 1 H, Ar) 7.10 – 7.15, (m, 1 H, Ar) 7.21 – 7.24, (m, 4 H, Ar) 12.086 (s, 1H, exch, NH) Anal. Calcd. for $C_{14}H_{13}N_3O$. 0.1 H_2O: C, 69.75; H, 5.52; N, 17.43. Found C, 69.81; H, 5.52; N, 17.44.

7-Benzyl-4-chloro-2-methyl-5*H*-pyrrolo[3,2-*d*]pyrimidine [**261**]

Compound **260** (1.5 g, 6.27 mmol) was added to $POCl_3$ (12 mL) and heated at reflux for 3 h. The solvent was evaporated in vacuo, and the residue was adjusted to pH 8 with an ammonia solution. The resulting precipitate was removed by filtration, washed with water and dried in vacuo over P_2O_5 to afford a light yellow solid. Silica gel (4.5 g) and methanol (20 mL) were added; the solvent was evaporated to afford a plug. The silica gel plug obtained was loaded onto a silica gel column and eluted with 1% (v/v) CH_3OH

/$CHCl_3$. Fractions containing the product (TLC) were pooled, and the solvent was evaporated to afford **260** (1.41 g, 87%). TLC R_f =0.56 (CH_3OH: $CHCl_3$; 1:20); white solid; mp 181-183 °C; ^{1}H NMR, DMSO-d_6: δ 2.61 (s, 3 H, 2-CH_3) 4.04 (s, 2 H, CH_2) 7.13 – 7.28 (m, 5 H, Ar) 7.68 (d, *J* = 2.72 Hz, 1 H, CH) 12.086 (s, 1H, exch, 5-NH) Anal. Calcd. for $C_{14}H_{12}N_3Cl$: C, 65.25; H, 4.69; N, 16.30. Found C, 65.23; H, 4.70; N, 16.31.

7-benzyl-*N*-(4-methoxyphenyl)-*N*,2-dimethyl-5*H*-pyrrolo[3,2-*d*]pyrimidin-4-amine (187)

Compound **261** (0.1 g, 0.39 mmol) and 4-methoxyphenylamine (64 mg, 0.47 mmol) were dissolved in isopropanol (15 mL) and heated at reflux for 3 h, after which the solvent was evaporated in vacuo. Silica gel (0.3 g) and methanol (7 mL) were added; the solvent was evaporated to afford a plug. The silica gel plug obtained was loaded onto a silica gel column and eluted with 1% (v/v) CH_3OH /$CHCl_3$. Fractions containing the product (TLC) were pooled, and the solvent was evaporated to afford **187** (114 mg, 82%). TLC R_f 0.48 (CH_3OH: $CHCl_3$; 1:10). The product obtained was dissolved in a minimum amount of ethyl acetate, and diethyl ether (10 mL) was added to the solution. Hydrogen chloride gas was bubbled through for 2-3 min. The precipitate obtained was collected by filtration and washed with diethyl ether to afford **187**·HCl.; white solid; mp, 223-225 °C; ^{1}H NMR (DMSO-d_6): δ 2.66 (s, 3 H, 2-CH_3) 3.6 (s, 3 H, NCH_3) 3.82 (s, 3 H, OCH_3) 4.08 (s, 2 H, CH_2) 7.08 (d, 2 H, *J* = 8.84 Hz, Ar) 7.17 – 7.26 (m, 6 H, Ar and 6-CH) 7.4 (d, 2 H, *J* = 8.73, Ar) 9.41 (br, 1H, exch, NH) 14.43 (s, 1H, exch, HCl). Anal. Calcd. for $C_{22}H_{22}N_4O$·HCl : C, 66.91; H, 5.87; N, 14.19; Cl, 8.98. Found C, 66.65; H, 5.90; N, 13.90; Cl, 9.02.

7-benzyl-*N*,2-dimethyl-*N*-phenyl-5*H*-pyrrolo[3,2-*d*]pyrimidin-4-amine (188)

Compound **188** (synthesized from **261** and *N*-methyl aniline as described for **187**): yield = 69%; TLC R_f = 0.5 (CH_3OH: $CHCl_3$; 1:10). white solid; mp, 225-227 °C; ^{1}H NMR (DMSO-d_6): δ 2.63 (s, 3 H, 2-CH_3) 3.64 (s, 3 H, NCH_3) 4.07 (s, 2 H, CH_2) 7.14 – 7.26 (m, 6 H, Ar and 6-CH) 7.41 – 7.54, (m, 5 H, Ar) 9.63 (s, 1H, exch, NH) 14.52 (s, 1H, exch, HCl). Anal. Calcd. for $C_{21}H_{20}N_4O$· 0.9HCl : C, 69.82; H, 5.83; N, 15.51; Cl, 8.83. Found C, 69.90; H, 5.76; N, 15.38; Cl, 8.68.

7-benzyl-*N*-(4-methoxyphenyl)-2-methyl-5*H*-pyrrolo[3,2-*d*]pyrimidin-4-amine (189)

Compound **189** (synthesized from **261** and *p*-anisidine as described for **187**): yield = 76% ; white solid; mp 296-298 °C; ^{1}H NMR (DMSO-d_6): δ 2.65 (s, 3 H, 2-CH_3) 3.77 (s, 3 H, OCH_3) 4.11 (s, 2 H, CH_2) 7.00 (d, 2 H, J = 9.02 Hz, Ar) 7.17 – 7.31, (m, 5 H, Ar) 7.67 (d, 1 H, J = 2.52 Hz, Ar) 7.79 (d, 2 H, J = 8.80 Hz, Ar) 11.31(s, 1 H, exch, 4-NH) 12.72 (br, 1 H, exch, NH) 14.34 (s, 1 H, exch, HCl). Anal. Calcd. for $C_{21}H_{20}N_4O$·HCl : C, 66.22; H, 5.56; N, 14.71; Cl, 9.31. Found C, 66.09; H, 5.52; N, 14.60; Cl, 9.24.

7-benzyl-*N*-(2,4-dimethoxyphenyl)-2-methyl-5*H*-pyrrolo[3,2-*d*]pyrimidin-4-amine (190)

Compound **190** (synthesized from **261** and 2,4-dimethoxy aniline as described for **187**): yield = 82%; yellow solid; mp, 191-193 °C; ^{1}H NMR (DMSO-d_6): δ 2.55 (s, 3 H, 2-CH_3) 3.80 (s, 6 H, OCH_3) 4.12 (s, 2 H, CH_2) 6.59 (d, 1 H, *J* = 8.58 Hz, Ar) 6.71 (d, 1 H, *J* = 2.52 Hz, Ar) 7.17 – 7.30, (m, 5 H, Ar) 7.50 (d, 1 H, *J* = 8.50 Hz, Ar) 7.62 (s, 1 H, Ar)

10.30(s, 1H, exch, NH) 12.46 (s, 1H, exch, NH). Anal. Calcd. for $C_{22}H_{22}N_4O_2 \cdot HCl \cdot H_2O$: C, 62.93; H, 5.76; N, 13.34; Cl, 8.44. Found C, 63.12; H, 5.69; N, 13.29; Cl, 8.45.

5-ethyl-*N*-(4-methoxyphenyl)-*N*,2-dimethyl-5*H*-pyrrolo[3,2-*d*]pyrimidin-4-amine (191)

N-(4-methoxyphenyl)-*N*,2-dimethyl-5*H*-pyrrolo[3,2-*d*]pyrimidin-4-amine (**161**, 100 mg, 0.373 mmol) was dissolved in dimethylformamide (6 mL) and sodium hydride (10.73 mg, 0.447 mmol) was added under nitrogen. The mixture was allowed to stir for 15 minutes after no further production of hydrogen gas was observed. Ethyl iodide (0.1 mL) was added and the reaction was stirred for 3 hours. The reaction was quenched by addition of water and ethylacetate was added. The organic layer was collected, washed with brine and dried over sodium sulphate. A silica gel plug was made and purified by column chromatography ($CHCl_3$: CH_3OH; 100:1 v/v) to give an off-white solid (726 mg, 75%). TLC R_f 0.42 (CH_3OH: $CHCl_3$; 1:20); mp, 145-147 °C; ^1H NMR (400 MHz, DMSO-d_6) δ ppm 1.30 - 1.42 (m, 3 H, CH_3) 2.69 (s, 3 H, CH_3) 2.87 (q, J = 7.15 Hz, 2 H, CH_2) 3.64 (s, 3 H, CH_3) 3.79 (s, 3 H, CH_3) 6.54 (d, J = 3.26 Hz, 1 H, Ar) 7.01 (d, J = 9.03 Hz, 2 H, Ar) 7.29 (d, J = 9.03 Hz, 2 H, Ar) 7.75 (d, J = 3.26 Hz, 1 H, Ar) 15.11 (br, 1 H, exch, NH) Anal. Calcd. for $C_{17}H_{20}N_4O$: C, 68.89; H, 6.80; N, 18.90. Found C, 68.78; H, 6.05; N, 18.59.

5-isopropyl-*N*-(4-methoxyphenyl)-*N*,2-dimethyl-5*H*-pyrrolo[3,2-*d*]pyrimidin-4-amine (192)

Compound **192** (synthesized from **161** and *iso*-propyl bromide as described for **191**): yield = 78%; TLC R_f 0.51 (CH_3OH: $CHCl_3$; 1:20); grey solid; mp, 244-246 °C; ^1H NMR (400 MHz, DMSO-d_6) δ ppm 0.99 (d, J = 7.28 Hz, 6 H, CH_3) 2.69 (s, 3 H, CH_3) 2.87 (m, 1 H, CH) 3.64 (s, 3 H, CH_3) 3.79 (s, 3 H, CH_3) 6.54 (d, J = 3.26 Hz, 1 H, Ar) 7.01 (d, J = 9.03 Hz, 2 H, Ar) 7.29 (d, J = 9.03 Hz, 2 H, Ar) 7.75 (d, J = 3.26 Hz, 1 H, Ar) 15.11 (br, 1 H, exch, NH) Anal. Calcd. for $C_{18}H_{22}N_4O$·HCl: C, 62.33; H, 6.68; N, 16.15; Cl, 10.22. Found C, 62.19; H, 6.69; N, 16.00; Cl, 10.13.

***N*-(4-methoxyphenyl)-*N*,2-dimethyl-5-propyl-5*H*-pyrrolo[3,2-*d*]pyrimidin-4-amine (193)**

Compound **193** (synthesized from **161** and *n*-propyl bromide as described for **191**): yield = 83%; TLC R_f = 0.5 (CH_3OH: $CHCl_3$; 1:20); light yellow solid; mp, 214-216 °C; ^1H NMR (400 MHz, DMSO-d_6) δ ppm 1.41 - 1.47 (m, 2 H, CH_3) 2.69 (s, 3 H, CH_3) 2.87 (t, J = 7.15 Hz, 2 H, CH_2) 3.64 (s, 3 H, CH_3) 3.79 (s, 3 H, CH_3) 6.54 (d, J = 3.26 Hz, 1 H, Ar) 7.01 (d, J = 9.03 Hz, 2 H, Ar) 7.29 (d, J = 9.03 Hz, 2 H, Ar) 7.75 (d, J = 3.26 Hz, 1 H, Ar) 15.11 (br, 1 H, exch, NH) Anal. Calcd. for $C_{18}H_{22}N_4O$·HCl: C, 62.33; H, 6.68; N, 16.15; Cl, 10.22. Found C, 62.17; H, 6.70; N, 15.98; Cl, 10.12.

5-isobutyl-*N*-(4-methoxyphenyl)-*N*,2-dimethyl-5*H*-pyrrolo[3,2-*d*]pyrimidin-4-amine (194)

Compound **194** (synthesized from **161** and *iso*-butyl bromide as described for **191**): yield = 80%; TLC R_f 0.55 (CH_3OH: $CHCl_3$; 1:20); white solid; mp, 260-261 °C; ^1H NMR (400 MHz, DMSO-d_6) δ ppm 0.47 (t, J = 7.28 Hz, 3 H, CH_3) 1.30 - 1.42 (m, 2 H, CH_2) 2.69 (s, 3 H, CH_3) 2.87 (t, J = 7.15 Hz, 2 H, CH_2) 3.64 (s, 3 H, CH_3) 3.79 (s, 3 H, CH_3) 6.54 (d, J = 3.26 Hz, 1 H, Ar) 7.01 (d, J = 9.03 Hz, 2 H, Ar) 7.29 (d, J = 9.03 Hz, 2 H, Ar) 7.75 (d, J = 3.26 Hz, 1 H, Ar) 15.11 (br, 1 H, exch, NH) Anal. Calcd. for $C_{19}H_{24}N_4O$·HCl: C, 63.23; H, 6.98; N, 15.52; Cl, 9.82. Found C, 63.20; H, 7.01; N, 15.39; Cl, 9.65.

5-butyl-*N*-(4-methoxyphenyl)-*N*,2-dimethyl-5*H*-pyrrolo[3,2-*d*]pyrimidin-4-amine (195)

Compound **195** (synthesized from **161** and *n*-butyl bromide as described for **191**): yield = 77%; TLC R_f =0.6 (CH_3OH: $CHCl_3$; 1:20); white solid; mp, 229-230 °C; ^1H NMR (400 MHz, DMSO-d_6) δ ppm 0.69 - 0.75 (m, 3 H, CH_3) 0.76 - 0.85 (m, 2 H, CH_2) 1.25 - 1.34 (m, 2 H, CH_2) 2.69 (s, 3 H, CH_3) 2.94 (t, J = 7.15 Hz, 2 H, CH_2) 3.65 (s, 3 H, CH_3) 3.79 (s, 3 H, CH_3) 6.54 (d, J = 3.01 Hz, 1 H, Ar) 7.01 (d, J = 9.03 Hz, 2 H, Ar) 7.28 (d, J = 9.03 Hz, 2 H, Ar) 7.76 (d, J = 3.26 Hz, 1 H, Ar) Anal. Calcd. for $C_{19}H_{24}N_4O$·HCl: C, 63.24; H, 6.98; N, 15.52; Cl, 9.82. Found C, 63.29; H, 6.91; N, 15.50; Cl, 9.66.

***N*-(4-methoxyphenyl)-*N*,2-dimethyl-6,7-dihydrofuro[3,2-*d*]pyrimidin-4-amine (196)**

To the solution of *N*-(4-methoxyphenyl)-*N*,2-dimethylfuro[3,2-*d*]pyrimidin-4-amine (**181**, 150 mg, 0.557 mmol) in methanol (10 mL) was added palladium hydroxide (45%) on

carbon (50 mg). The resulted suspension was hydrogenated (50 psi) in a Parr apparatus at room temperature for 24 hours after which the suspension was filtered through a layer of celite and washed with methanol (40 mL). The filtrate was evaporated in vacuo and a silica gel plug was made. Column chromatography with 10% EtOAc in hexane afforded 126 mg (84%) as a white solid. TLC R_f = 0.30 (EtOAc/hexane, 1:2); mp, 201-203 °C; ^{1}H NMR (400 MHz, DMSO-d_6) δ ppm 2.54 (s, 3 H, CH_3) 3.29 (t, J = 9.29 Hz, 2 H, CH_2) 3.53 (s, 3 H, CH_3) 3.79 (s, 3 H, CH_3) 4.43 (t, J = 9.03 Hz, 2 H, CH_2) 6.94 - 6.97 (m, 2 H, Ar) 7.24 - 7.27 (m, 2 H, Ar) Anal. Calcd. for $C_{15}H_{17}N_3O_2$·HCl·0.5H_2O: C, 56.87; H, 6.05; N, 13.26; Cl, 11.19. Found C, 56.94; H, 6.06; N, 13.14; Cl, 11.03.

4-(6-methoxy-3,4-dihydroquinolin-1(2*H*)-yl)-2-methyl-6,7-dihydrofuro[3,2-*d*]pyrimidine (197)

Compound **197** (synthesized from **185** as described for **196**): yield = 92%; TLC R_f = 0.35 (ethyl acetate/hexane, 1:2); white solid; mp 110-112 °C; ^{1}H NMR (400 MHz, DMSO-d_6) δ ppm 1.87 (quin, J = 6.34 Hz, 2 H, CH_2) 2.38 (s, 3 H, CH_3) 2.73 (t, J = 6.65 Hz, 2 H, CH_2) 3.13 (t, J = 9.03 Hz, 2 H, CH_2) 3.71 (s, 3 H, CH_3) 3.79 - 3.83 (m, 2 H, CH_2) 4.47 (t, J = 9.03 Hz, 2 H, CH_2) 6.62 - 6.66 (m, 1 H, Ar) 6.69 (d, J = 3.01 Hz, 1 H, Ar) 6.74 (d, J = 8.78 Hz, 1 H, Ar) Anal. Calcd. for $C_{17}H_{19}N_3O_2$: C, 68.67; H, 6.44; N, 14.13. Found C, 68.51; H, 6.50; N, 14.01.

***N*-ethyl-*N*-(4-methoxyphenyl)-2-methylfuro[3,2-*d*]pyrimidin-4-amine (198)**

Compound **198** (synthesized from **182** and ethyl iodide as described for **191**): yield = 92%; TLC R_f = 0.4 (EtOAc/hexane, 1:2); yellow solid; mp, 95-97 °C; ^{1}H NMR (400

MHz, DMSO-d_6) δ ppm 1.16 (t, J = 7.03 Hz, 3 H, CH_3) 2.49 (s, 3 H, CH_3) 3.81 (s, 3 H, CH_3) 4.02 (q, J = 7.03 Hz, 2 H, CH_2) 6.79 (d, J = 2.26 Hz, 1 H, Ar) 6.97 - 7.02 (m, 2 H, Ar) 7.24 - 7.30 (m, 2 H, Ar) 7.91 (d, J = 2.01 Hz, 1 H, Ar) Anal. Calcd. for $C_{16}H_{17}N_3O_2 \cdot 0.25H_2O$: C, 66.77; H, 6.13; N, 14.60. Found C, 66.91; H, 5.99; N, 14.47.

_N_-isopropyl-_N_-(4-methoxyphenyl)-2-methylfuro[3,2-_d_]pyrimidin-4-amine (199)

Compound **199** (synthesized from **182** and *iso*-propyl iodide as described for **191**): yield = 73%; TLC R_f = 0.5 (EtOAc/hexane, 1:2); white solid; mp, 154-156 °C; ^{1}H NMR (400 MHz, DMSO-d_6) δ ppm 1.12 (d, J = 6.78 Hz, 6 H, CH_3) 2.50 (s, 3 H, CH_3) 3.82 (s, 3 H, OCH_3) 5.37 (dt, J = 13.24, 6.56 Hz, 1 H, CH) 6.78 (d, J = 2.26 Hz, 1 H, Ar) 7.01 (d, J = 9.03 Hz, 2 H, Ar) 7.23 (d, J = 8.78 Hz, 2 H, Ar) 7.86 (d, J = 2.01 Hz, 1 H, Ar) Anal. Calcd. for $C_{17}H_{19}N_3O_2$: C, 68.67; H, 6.44; N, 14.13. Found C, 68.40; H, 6.50; N, 14.47.

_N_-(4-methoxyphenyl)-2-methyl-_N_-propylfuro[3,2-_d_]pyrimidin-4-amine (200)

Compound **200** (synthesized from **182** and *n*-propyl iodide as described for **191**): yield = 90%; TLC R_f = 0.55 (EtOAc/hexane, 1:2); white solid; mp, 110-112 °C; ^{1}H NMR (400 MHz, DMSO-d_6) δ ppm 0.89 (t, 3 H, CH_3) 1.56 - 1.63 (m, 2 H, CH_2) 2.46 (s, 3 H, CH_3) 3.80 (s, 3 H, CH_3) 3.92 - 3.97 (m, 2 H, CH_2) 6.77 (d, J = 2.26 Hz, 1 H, Ar) 6.99 (d, J = 8.78 Hz, 2 H, Ar) 7.27 (d, J = 9.03 Hz, 2 H, Ar) 7.89 - 7.90 (m, 1 H, Ar) Anal. Calcd. for $C_{17}H_{19}N_3O_2 \cdot 0.1C_6H_{14}$: 69.09; H, 6.72; N, 13.73. Found C, 69.09; H, 6.67; N, 13.66.

Ethyl 2-(2-cyanophenoxy)acetate (262)

Ethyl bromoacetate (1.95 mL, 20 mmol) was added dropwise to a stirred solution of 2-

hydroxy benzonitrile (**144**, 2.38 g, 20 mmol) and potassium carbonate (2.78 g, 20.1 mmol) in ethanol (100 mL) at room temperature and heated to reflux for 6h. Most of the solvent was removed in vacuo and a silica gel plug was made. Flash chromatography with EtOAc: Hex 0% to 10 % afforded 3.82 g (96%) of brown solid. TLC R_f = 0.36 (EtOAc: Hexane; 1:1) mp[115], 105–107 °C; ^{1}H NMR (500 MHz, DMSO-d_6) δ ppm 1.22 (t, J = 7.07 Hz, 3 H, CH_3) 4.18 (q, J = 7.02 Hz, 2 H, CH_2) 5.02 (s, 2 H, CH_2) 7.13 (t, J = 7.55 Hz, 1 H, CH) 7.18 (d, J = 8.49 Hz, 1 H, CH) 7.62 - 7.67 (m, 1 H, CH) 7.76 (dd, J = 7.70, 1.73 Hz, 1 H, CH)

Ethyl 3-aminobenzofuran-2-carboxylate (263)

Ethyl 2-(2-cyanophenoxy)acetate (**262**, 3.8 g, 19 mmol) was added dropwise to a stirred solution of potassium *tert*-butoxide (2.78 g, 20.1 mmol) in tetrahydrofuran (100 mL) at room temperature and stirred for 6h. Most of the solvent was removed in vacuo and a silica gel plug was made. Flash chromatography with EtOAc: Hex 0% to 10 % afforded 3 g (78%) of brown semisolid. TLC R_f = 0.5 (EtOAc: Hexane; 1:1) ^{1}H NMR (500 MHz, DMSO-d_6) δ ppm 1.32 (t, J = 7.07 Hz, 3 H, CH_3) 4.30 (q, J = 7.13 Hz, 2 H, CH_2) 6.34 (s, 2 H, exch, NH_2) 7.26 (dt, J = 7.94, 4.05 Hz, 1 H, CH) 7.49 (d, J = 3.46 Hz, 2 H, CH) 7.95 (d, J = 7.86 Hz, 1 H, CH)

2-methylbenzofuro[3,2-*d*]pyrimidin-4(3*H*)-one (264)

Compound **264** (synthesized from **263** as described for **245**): yield 76%; TLC R_f = 0.6 (MeOH: $CHCl_3$; 1:20); white solid; mp, 200-202 °C; ^{1}H NMR (400 MHz, DMSO-d_6) δ ppm 2.43 (s, 3 H, CH_3) 7.16 - 7.22 (m, 1 H, CH) 7.40 - 7.45 (m, 1 H, CH) 7.47 - 7.52 (m,

1 H, CH) 7.96 (d, *J* = 8.03 Hz, 1 H, CH) 12.27 (br, 1 H, exch, NH)

4-chloro-2-methylbenzofuro[3,2-*d*]pyrimidine (265)

Compound **265** (synthesized from **264** as described for **238**): yield 81%; TLC R_f = 0.7 (MeOH: $CHCl_3$; 1:20); off-white solid; mp 212-214 °C; ^{1}H NMR (400 MHz, DMSO-d_6) δ ppm 2.78 (d, *J* = 0.75 Hz, 3 H, CH_3) 7.58 - 7.64 (m, 1 H, CH) 7.84 - 7.89 (m, 1 H, CH) 7.97 (dd, *J* = 8.41, 0.63 Hz, 1 H, CH) 8.23 - 8.27 (m, 1 H, CH)

***N*-(4-methoxyphenyl)-*N*,2-dimethylbenzofuro[3,2-*d*]pyrimidin-4-amine (202)**

Compound **202** (synthesized from **265** and 4-methoxy N-methoxy aniline as described for **161**): TLC R_f = 0.6 (CH_3OH: $CHCl_3$; 1:20); white solid; mp, 238-240 °C; ^{1}H NMR (500 MHz, DMSO-d_6) δ ppm 2.74 (s, 3 H, CH_3) 3.72 (s, 3 H, CH_3) 3.86 (s, 3 H, CH_3) 7.07 - 7.11 (m, 2 H, Ar) 7.46 (d, *J* = 8.80 Hz, 2 H, Ar) 7.55 (t, *J* = 7.55 Hz, 2 H, Ar) 7.67 - 7.74 (m, 1 H, Ar) 8.33 (d, *J* = 7.86 Hz, 1 H, Ar) Anal. Calcd. for $C_{19}H_{17}N_3O_2 \cdot HCl \cdot 0.05H_2O$: C, 63.97; H, 5.11; N, 11.78; Cl, 9.94. Found C, 64.13; H, 5.12; N, 11.66; Cl, 9.81.

4-(5-methoxyindolin-1-yl)-2-methylbenzofuro[3,2-*d*]pyrimidine (203)

Compound **203** (synthesized from **265** and 5-methoxyindoline as described for **161**): TLC R_f = 0.6 (CH_3OH: $CHCl_3$; 1:20); yellow solid; mp, 284-286 °C; ^{1}H NMR (400 MHz, DMSO-d_6) δ ppm 2.71 (s, 3 H, CH_3) 2.84 (t, *J* = 6.53 Hz, 2 H, CH_2) 3.81 (s, 3 H, CH_3) 4.19 - 4.30 (m, 2 H, CH_2) 6.81 (dd, *J* = 8.91, 2.89 Hz, 1 H, Ar) 6.90 (d, *J* = 3.01 Hz, 1 H, Ar) 7.32 (d, *J* = 9.03 Hz, 1 H, Ar) 7.55 - 7.61 (m, 1 H, Ar) 7.69 - 7.80 (m, 2 H, Ar) 8.32

(d, *J* = 7.28 Hz, 1 H, Ar) Anal. Calcd. for $C_{20}H_{17}N_3O_2$·HCl: C, 65.31; H, 4.93; N, 11.42; Cl, 9.64. Found C, 65.25; H, 4.84; N, 11.39; Cl, 9.47.

4-(6-methoxy-3,4-dihydroquinolin-1(2*H*)-yl)-2-methylbenzofuro[3,2-*d*]pyrimidine (204)

Compound **204** (synthesized from **265** and 6-methoxy-1,2,3,4-tetrahydroquinoline as described for **161**): TLC R_f = 0.6 (CH_3OH: $CHCl_3$; 1:20); light yellow solid; mp 279-281 °C; ^{1}H NMR (400 MHz, DMSO-d_6) δ ppm 2.05 (t, *J* = 6.40 Hz, 2 H, CH_2) 2.71 (s, 3 H, CH_3) 2.84 (t, *J* = 6.53 Hz, 2 H, CH_2) 3.81 (s, 3 H, CH_3) 4.19 - 4.30 (m, 2 H, CH_2) 6.81 (dd, *J* = 8.91, 2.89 Hz, 1 H, Ar) 6.90 (d, *J* = 3.01 Hz, 1 H, Ar) 7.32 (d, *J* = 9.03 Hz, 1 H, Ar) 7.55 - 7.61 (m, 1 H, Ar) 7.69 - 7.80 (m, 2 H, Ar) 8.32 (d, *J* = 7.28 Hz, 1 H, Ar) Anal. Calcd. for $C_{21}H_{19}N_3O_2$·HCl: C, 66.05; H, 5.28; N, 11.00; Cl, 9.28. Found C, 65.90; H, 5.26; N, 10.85; Cl, 9.08.

7-benzyl-2-methylfuro[3,2-*d*]pyrimidin-4(3*H*)-one (270)

2-Phenyl propionitrile (**266**) was added to a solution of ethyl formate (1.1eq) and sodium ethoxide (1.1 eq) in ethanol (0.1M) and heated to reflux for 2 hours. The resulting precipitate was filtered and washed with ether to give crude **267**. Diethylchloromalonate (1.0 eq) was added to a stirred solution of the crude hydroxyacrylonitrile in DMF (0.1 M). After stirring for 5 hours at room temperature, the solvent was removed and the resulting oil of **268** was dissolved in ethanol. 1.5-diazabicyclo[4.3.0]non-5-ene (6.8 mL, 55 mmol) (1.0 eq) was added and the reaction mixture was heated to reflux and stirred overnight. After concentration, the crude product was dissolved in EtOAc and washed with water.

The solution was concentrated and an analytical sample was prepared by silica gel chromatography (EtOAc–hexane, 1:2). The organic phase was dried over sodium sulphate and filtered through a thick pad of silica. The filtrate was evaporated to afford crude syrupy **236** which was dissolved in acetonitrile and HCl gas was bubbled through for 2 hours. The reaction mixture was neutralized with ammonium hydroxide and the solvent was evaporated and flash chromatographed ($CHCl_3$: CH_3OH; 100:1 to 50:3; v/v) to yield **237** as a white solid (36%). TLC R_f 0.42 (CH_3OH: $CHCl_3$; 1:50); mp[198], 240-242 °C; ^{1}H NMR (400 MHz, DMSO-d_6) δ ppm 2.35 (s, 3 H, CH_3) 3.91 (s, 2 H, CH_2) 7.17 - 7.22 (m, 1 H, Ar) 7.29 (d, *J* = 4.52 Hz, 4 H, Ar) 7.96 (s, 1 H, Ar) 12.45 (br, 1 H, exch, NH)

7-benzyl-4-chloro-2-methylfuro[3,2-*d*]pyrimidine (271)

Compound **271** (synthesized from **270** as described for **261**): yield = 69%; TLC R_f 0.5 (CH_3OH: $CHCl_3$; 1:50). white solid; mp, 225-227 °C; ^{1}H NMR (400 MHz, DMSO-d_6) δ ppm 2.55 (s, 3 H, CH_3) 3.99(s, 2 H, CH_2) 7.24 - 7.29 (m, 1 H, Ar) 7.36 (d, *J* = 4.52 Hz, 4 H, Ar) 8.12 (s, 1 H, Ar)

7-benzyl-*N*-(4-methoxyphenyl)-*N*,2-dimethylfuro[3,2-*d*]pyrimidin-4-amine (205)

Compound **205** (synthesized from **271** and 4-methoxy *N*-methoxy aniline as described for **161**): TLC R_f = 0.6 (CH_3OH: $CHCl_3$; 1:50); white solid; mp, 210-212 °C; ^{1}H NMR (DMSO-d_6): δ 2.69 (s, 3 H, 2-CH_3) 3.7 (s, 3 H, NCH_3) 3.89 (s, 3 H, OCH_3) 4.11 (s, 2 H, CH_2) 7.18 (d, 2 H, J = 8.84 Hz, Ar) 7.27 – 7.32 (m, 6 H, Ar) 7.48 (d, 2 H, J = 8.73, Ar)

Anal. Calcd. for $C_{22}H_{21}N_3O_2 \cdot HCl \cdot H_2O$: C, 63.84; H, 5.84; N, 10.15; Cl, 8.57. Found C, 64.31; H, 5.76; N, 10.22; Cl, 8.48.

7-benzyl-4-(6-methoxy-3,4-dihydroquinolin-1(2*H*)-yl)-2-methylfuro[3,2-*d*]pyrimidine (206)

Compound **205** (synthesized from **271** and 6-methoxy-1,2,3,4-tetrahydroquinoline as described for **161**): TLC R_f = 0.54 (CH_3OH: $CHCl_3$; 1:50); yellow solid; mp, 230-232 °C; ^{1}H NMR (400 MHz, DMSO-d_6) δ ppm 1.97 - 2.05 (m, 2 H, CH_2) 2.67 (s, 3 H, CH_3) 2.76 - 2.82 (m, 2 H, CH_2) 3.79 (s, 3 H, CH_3) 4.11 (s, 4 H, CH_2) 6.77 - 6.82 (m, 1 H, Ar) 6.92 - 6.96 (m, 1 H, Ar) 7.12 - 7.24 (m, 2 H, Ar) 7.28 - 7.34 (m, 4 H, Ar) 7.44 - 7.48 (m, 1 H, Ar) Anal. Calcd. for $C_{24}H_{23}N_3O_2 \cdot HCl$: C, 68.32; H, 5.73; Cl, 8.40; N, 9.96. Found C, 68.19; H, 5.76; N, 10.04; Cl, 8.30.

***N*,2-dimethyl-*N*-phenylfuro[3,2-*d*]pyrimidin-4-amine (207)**

Compound **207** (synthesized from **252** and *N*-methyl aniline as described for **161**): TLC R_f = 0.5 (CH_3OH: $CHCl_3$; 1:25); white solid; mp, 199-200 °C; ^{1}H NMR (400 MHz, DMSO-d_6) δ ppm 1.97 - 2.05 (m, 2 H, CH_2) 2.67 (s, 3 H, CH_3) 2.76 - 2.82 (m, 2 H, CH_2) 3.79 (s, 3 H, CH_3) 4.11 (s, 4 H, CH_2) 6.77 - 6.82 (m, 1 H, Ar) 6.92 - 6.96 (m, 1 H, Ar) 7.12 - 7.24 (m, 2 H, Ar) 7.28 - 7.34 (m, 4 H, Ar) 7.44 - 7.48 (m, 1 H, Ar) Anal. Calcd. for $C_{24}H_{23}N_3O_2 \cdot HCl$: C, 68.32; H, 5.73; N, 9.96; Cl, 8.40. Found C, 68.19; H, 5.76; N, 10.04; Cl, 8.30.

***N*,2-dimethyl-*N*-(p-tolyl)furo[3,2-*d*]pyrimidin-4-amine (208)**

Compound **208** (synthesized from **252** and N-methyl p-toluidine as described for **161**): TLC R_f = 0.5 (CH_3OH: $CHCl_3$; 1:25); white solid; mp, 223-225 °C; ^1H NMR (400 MHz, DMSO-d_6) δ ppm 2.68 (s, 3 H, CH_3) 3.53 (s, 3 H, CH_3) 3.71 (s, 3 H, CH_3) 7.10 (d, J = 2.01 Hz, 1 H, Ar) 7.47 - 7.57 (m, 4 H, Ar) 8.26 (s, 1 H, Ar) Anal. Calcd. for $C_{14}H_{12}ClN_3O \cdot HCl$: C, 54.21; H, 4.22; N, 13.54; Cl, 22.86. Found C, 54.27; H, 4.33; N, 13.38; Cl, 22.71.

***N*-(4-chlorophenyl)-*N*,2-dimethylfuro[3,2-*d*]pyrimidin-4-amine (209)**

Compound **209** (synthesized from **252** and 4-chloro N-methylaniline as described for **161**): TLC R_f = 0.5 (CH_3OH: $CHCl_3$; 1:25); white solid; mp, 274-276 °C; ^1H NMR (400 MHz, DMSO-d_6) δ ppm 2.67 (s, 3 H, CH_3) 3.70 (s, 3 H, CH_3) 7.12 (d, J = 2.01 Hz, 1 H, Ar) 7.56 - 7.64 (m, 4 H, Ar) 8.32 (br, 1 H, Ar) Anal. Calcd. for $C_{14}H_{12}ClN_3O \cdot HCl$: C, 54.21; H, 4.22; N, 13.54; Cl, 22.86. Found C, 54.27; H, 4.33; N, 13.38; Cl, 22.71.

***N*-(3,4-dichlorophenyl)-*N*,2-dimethylfuro[3,2-*d*]pyrimidin-4-amine (210)**

Compound **210** (synthesized from **252** and 3,4 dichloro *N*-methylaniline as described for **161**): TLC R_f = 0.54 (CH_3OH: $CHCl_3$; 1:25); off-white solid; mp, 291-293 °C; ^1H NMR (400 MHz, DMSO-d_6) δ ppm 2.67 (s, 3 H, CH_3) 3.70 (s, 3 H, CH_3) 7.13 (d, J = 2.26 Hz, 1 H, Ar) 7.57 (dd, J = 8.78, 2.51 Hz, 1 H, Ar) 7.82 (d, J = 8.53 Hz, 1 H, Ar) 7.95 (d, J = 2.51 Hz, 1 H, Ar) 8.36 (s, 1 H, Ar) Anal. Calcd. for $C_{14}H_{11}Cl_2N_3O \cdot HCl$: C, 48.80; H, 3.51; N, 12.19; Cl, 30.86. Found C, 48.95; H, 3.59; N, 12.07; Cl, 30.77.

7-benzyl-4-chloro-2,5-dimethyl-5*H*-pyrrolo[3,2-*d*]pyrimidine (272)

Compound **272** (synthesized from **261** as described for **241**): yield = 83%; TLC R_f 0.5 (CH_3OH: $CHCl_3$; 1:25). white solid; mp, 145-147 °C ^1H NMR (400 MHz, DMSO-d_6) δ ppm 2.62 (s, 3 H, CH_3) 4.01 (s, 3 H, CH_3) 4.03 (s, 2 H, CH_2) 7.17 (td, *J* = 5.65, 2.76 Hz, 1 H, 6-CH) 7.26 - 7.30 (m, 4 H, C_6H_5) 7.64 (s, 1 H, C_6H_5)

7-benzyl-*N*-(4-methoxyphenyl)-2,5-dimethyl-5*H*-pyrrolo[3,2-*d*]pyrimidin-4-amine (211)

Compound **211** (synthesized from **272** and *p*-anisidine as described for **161**): yield = 79%; TLC R_f 0.5 (CH_3OH: $CHCl_3$; 1:20). white solid; mp, 291-292 °C; ^1H NMR (DMSO-d_6): δ 2.66 (s, 3 H, 2-CH_3) 3.6 (s, 3 H, NCH_3) 3.82 (s, 3 H, OCH_3) 4.08 (s, 2 H, CH_2) 7.08 (d, 2 H, J = 8.84 Hz, Ar) 7.17 – 7.26 (m, 6 H, Ar and 6-CH) 7.4 (d, 2 H, *J* = 8.73, Ar) 9.41 (br, 1H, exch, NH) 14.43 (s, 1H, exch, HCl). Anal. Calcd. for $C_{22}H_{22}N_4O$·HCl: C, 66.91; H, 5.87; N, 14.19; Cl, 8.98. Found C, 66.88; H, 5.86; N, 14.07; Cl, 8.84.

***7*-benzyl-*N*-(4-methoxyphenyl)-*N*,2,5-trimethyl-5*H*-pyrrolo[3,2-*d*]pyrimidin-4-amine (212)**

Compound **212** (synthesized from **272** and 4-methoxy *N*-methyl aniline as described for **161**): yield = 74%; TLC R_f = 0.5 (CH_3OH: $CHCl_3$; 1:20). grey solid; mp, 186-187 °C; ^1H NMR (400 MHz, DMSO-d_6) δ ppm 2.73 (s, 3 H, CH_3) 2.80 (s, 3 H, CH_3) 3.63 (s, 3 H, CH_3) 3.78 (s, 3 H, CH_3) 4.08 (s, 2 H, CH_2) 7.00 (d, *J* = 9.03 Hz, 2 H, Ar) 7.22 (d, *J* = 5.52 Hz, 1 H, Ar) 7.25 - 7.33 (m, 6 H, Ar) 7.37 (s, 1 H, Ar) 8.33 (s, 1 H, Ar) 14.63 (s, 1 H, exch, HCl) Anal. Calcd. for $C_{23}H_{24}N_4O$·HCl: C, 67.55; H, 6.16; N, 13.70; Cl, 8.67.

Found C, 67.41; H, 6.20; N, 13.59; Cl, 8.61.

1-(7-benzyl-2-methyl-5*H*-pyrrolo[3,2-*d*]pyrimidin-4-yl)-6-methoxy-1,2,3,4-tetrahydroquinoline (213)

Compound **213** (synthesized from **261** and 6-methoxy-1,2,3,4-tetrahydroquinoline as described for **161**): yield = 80%; TLC R_f = 0.6 (CH_3OH: $CHCl_3$; 1:25). pale yellow solid; mp 262-264 °C; ^{1}H NMR (400 MHz, DMSO-d_6) δ ppm 1.97 - 2.05 (m, 2 H, CH_2) 2.67 (s, 3 H, CH_3) 2.76 - 2.82 (m, 2 H, CH_2) 3.79 (s, 3 H, CH_3) 4.11 (s, 4 H, CH_2) 6.77 - 6.82 (m, 1 H, Ar) 6.92 - 6.96 (m, 1 H, Ar) 7.12 - 7.24 (m, 2 H, Ar) 7.28 - 7.34 (m, 4 H, Ar) 7.44 - 7.48 (m, 1 H, Ar) 10.88 (s, 1 H, exch, NH) 14.36 (s, 1 H, exch, HCl) Anal. Calcd. for $C_{24}H_{24}N_4O{\cdot}HCl{\cdot}0.25H_2O$: C, 67.75; H, 6.04; N, 13.17; Cl, 8.33. Found C, 67.84; H, 6.21; N, 12.95; Cl, 8.06.

1-(7-benzyl-2,5-dimethyl-5*H*-pyrrolo[3,2-*d*]pyrimidin-4-yl)-6-methoxy-1,2,3,4-tetrahydroquinoline (214)

Compound **214** (synthesized from **272** and 6-methoxy-1,2,3,4-tetrahydroquinoline as described for **161**): yield = 76%; TLC R_f 0.6 (CH_3OH: $CHCl_3$; 1:20) white solid; mp, 130-132 °C; ^{1}H NMR (400 MHz, DMSO-d_6) δ ppm 2.07 (t, J = 6.53 Hz, 2 H, CH_2) 2.72 (s, 3 H, CH_3) 2.79 - 2.88 (m, 2 H, CH_2) 2.97 (s, 3 H, CH_3) 3.72 - 3.78 (m, 3 H, CH_3) 3.96 - 4.06 (m, 2 H, CH_2) 4.13 (s, 2 H, CH_2) 6.68 - 6.72 (m, 1 H, Ar) 6.79 (d, J = 9.03 Hz, 1 H, Ar) 6.91 (d, J = 2.76 Hz, 1 H, Ar) 7.22 (td, J = 5.84, 2.64 Hz, 1 H, Ar) 7.30 - 7.35 (m, 4 H, Ar) 7.50 (s, 1 H, Ar) 14.71 (s, 1 H, exch, HCl)

4-Chloro-2,5,6-trimethyl-5*H*-pyrrolo[3,2-*d*]pyrimidine (273)

Compound **273** (synthesized from **246** as described for **241**): yield = 88%; TLC R_f = 0.5 (CH_3OH: $CHCl_3$; 1:10). off-white solid; mp, 159-161°C ^{1}H NMR (400 MHz, DMSO-d_6) δ ppm 2.62 (s, 3 H, CH_3) 3.65 (s, 3 H, CH_3) 4.01 (s, 3 H, CH_3) 6.6 (m, 1 H, 7-CH) 7.9 (m, 1 H, 6-CH)

***N*-(4-methoxyphenyl)-*N*,2,5,6-tetramethyl-5*H*-pyrrolo[3,2-*d*]pyrimidin-4-amine (215)**

Compound **215** (synthesized from **273** and 4-methoxy *N*-methyl aniline as described for **161**): yield = 74%; TLC R_f = 0.62 (CH_3OH: $CHCl_3$; 1:10). white solid; mp, 200-201 °C; ^{1}H NMR (400 MHz, DMSO-d_6) δ ppm 2.30 (s, 3 H, CH_3) 2.67 (s, 3 H, CH_3) 2.79 (s, 3 H, CH_3) 3.62 (s, 3 H, CH_3) 3.78 (s, 3 H, CH_3) 6.44 (s, 1 H, Ar) 6.98 (d, J = 8.78 Hz, 2 H, Ar) 7.22 (d, J = 9.03 Hz, 2 H, Ar) 15.09 (br, 1 H, exch, HCl) Anal. Calcd. for $C_{15}H_{17}N_3O_2 \cdot HCl \cdot 0.5H_2O$: C, 61.27; H, 6.47; N, 16.81; Cl, 10.64. Found C, 60.89; H, 6.31; N, 16.58; Cl, 10.32.

6-methoxy-1-(2,5,6-trimethyl-5*H*-pyrrolo[3,2-*d*]pyrimidin-4-yl)-1,2,3,4-tetrahydroquinoline (216)

Compound **216** (synthesized from **275** and 6-methoxy-1,2,3,4-tetrahydroquinoline as described for **161**): yield = 75%; TLC R_f 0.6 (CH_3OH: $CHCl_3$; 1:10). white solid; mp, 242-244 °C; ^{1}H NMR (400 MHz, DMSO-d_6) δ ppm 1.97 - 2.06 (m, 2 H, CH_2) 2.42 (s, 3 H, CH_3) 2.58 (s, 3 H, CH_3) 2.72 (s, 3 H, CH_3) 2.81 (t, J = 6.40 Hz, 2 H, CH_2) 3.79 (s, 3 H, CH_3) 4.12 (t, J = 6.27 Hz, 2 H, CH_2) 6.36 (s, 1 H, Ar) 6.76 (dd, J = 8.78, 2.76 Hz, 1 H, Ar) 6.91 (d, J = 2.51 Hz, 1 H, Ar) 7.11 (d, J = 9.03 Hz, 1 H, Ar) 14.60 (s, 1 H, exch, HCl)

Anal. Calcd. for $C_{19}H_{22}N_4O \cdot HCl$: C, 63.59; H, 6.46; N, 15.61; Cl, 9.88. Found C, 63.45; H, 6.58; N, 15.38; Cl, 9.59.

methyl (6-methyl-4-oxo-4,5-dihydro-3*H*-pyrrolo[3,2-*d*]pyrimidin-2-yl) carbamate (277)

Ethyl 3-amino-5-methyl-1*H*-pyrrole-2-carboxylate (**244**, 2.68 g, 16 mmol) was dissolved in methanol (40 mL), and 1,3-bis(methoxycarbonyl)-2-methyl-2-thiopseudourea (3.74 g, 18 mmol) was added followed by acetic acid (4.6 mL). The mixture was stirred at room temperature for 24 hours and became a thick paste of **275**. To the reaction mixture was added 45 mL of sodium methoxide in MeOH (25%), and stirring was continued at room temperature for 12 hours. The mixture was neutralized with acetic acid, and the solid was collected by filtration and washed well with water. After drying, **277** (2.44 g, 69%) was obtained as an off-white powder: mp[105] 234–236 °C; TLC R_f = 0.22 (CH_3OH /$CHCl_3$, 1:5); ^{1}H NMR (DMSO-d_6) δ 2.28 (s, 3 H, CH_3), 3.73 (s, 3 H, OCH_3), 5.95 (s, 1 H, CH), 10.90 (s, 1 H, exch, NH), 11.10 (s, 1 H, exch, NH), 11.76 (s, 1 H, exch, NH).

methyl (7-benzyl-4-oxo-4,5-dihydro-3*H*-pyrrolo[3,2-*d*]pyrimidin-2-yl)carbamate (276)

Compound **276** (synthesized from **259** as described for **277**): yield = 73%; TLC R_f 0.6 (MeOH: $CHCl_3$; 1:15). white solid; mp 287-289 °C; ^{1}H NMR[103] (400 MHz, DMSO-d_6) δ 3.71 (s, 3 H, CH3), 3.88 (s, 2 H, CH2), 7.0−7.3 (m, 6 H, Ar), 11.00 (br, 1 H, exch, NH), 11.23 (br, 1 H, exch, NH), 11.80 (br, 1 H, exch, NH)

2-amino-6-methyl-3*H*-pyrrolo[3,2-*d*]pyrimidin-4(5*H*)-one (279)

A suspension of methyl (6-methyl-4-oxo-4,5-dihydro-3*H*-pyrrolo[3,2-*d*]pyrimidin-2-yl) carbamate (**277**, 1 g, 4.5 mmol) in 1 N NaOH (35 mL) was heated to reflux for 3 h. The resulting solution was cooled in an ice bath and neutralized with acetic acid. The precipitated solid was collected by filtration, washed with brine, and dried in vacuo to afford 0.67 g (92%) of **279** as a white solid: mp[105] 252–254 °C; TLCR_f = 0.15 (CH_3OH /$CHCl_3$, 1:5); ^{1}H NMR (400 MHz, DMSO-d_6) δ ppm 2.22 (s, 3 H, CH_3) 5.66 - 5.69 (m, 1 H, 7-CH) 5.70 (br, 2 H, exch, NH_2) 10.26 (br, 1 H, exch, NH) 11.19 (br, 1 H, exch, NH)

2-amino-7-benzyl-3*H*-pyrrolo[3,2-*d*]pyrimidin-4(5*H*)-one (278)

Compound **278** (synthesized from **276** as described for **279**): yield = 97%; TLC R_f 0.6 (CH_3OH: $CHCl_3$; 1:15). white solid; mp[103] 273-274°C ^{1}H NMR (DMSO-d_6) δ 3.81 (s, 2 H, CH_2), 5.85 (s, 1 H, exch, NH_2), 6.91 (d, J = 2.9 Hz, 2 H, Ar), 7.1−7.3 (m, 5 H, Ar), 10.39 (br, 1 H, exch, NH), 11.25 (br, 1 H, exch, NH)

***N*-(6-methyl-4-oxo-4,5-dihydro-3*H*-pyrrolo[3,2-*d*]pyrimidin-2-yl)pivalamide (281)**

A suspension of 2-amino-6-methyl-3*H*-pyrrolo[3,2-*d*]pyrimidin-4(5*H*)-one (**279**, 1.37 g, 8 mmol in 30 mL of trimethylacetic anhydride was heated at 100 °C for 2 hours. The resulting mixture was cooled, diluted with hexanes and filtered. The solid obtained was resuspended in water and ammonia solution was added to adjust the pH to 8. Ethyl acetate was added and the organic layer was separated, dried over sodium sulphate and the solvent was evaporated to afford 1.33 g (87%) of **281** as a white solid: TLC R_f = 0.47 (CH_3OH /$CHCl_3$, 1:10); mp[105] 156–157 °C; ^{1}H NMR (400 MHz, DMSO-d_6) δ ppm 1.24

(s, 9 H, $C(CH_3)_3$) 2.31 (s, 3 H, CH_3) 6.00 (d, *J* = 0.75 Hz, 1 H, 7-CH) 10.06 - 10.97 (m, 2 H, exch, NH, NH) 11.65 (br, 1 H, exch, NH)

N-(7-benzyl-4-oxo-4,5-dihydro-3H-pyrrolo[3,2-*d*]pyrimidin-2-yl)pivalamide (280)

Compound **280** (synthesized from **278** as described for **281**): yield = 97%; TLC R_f = 0.47 (CH_3OH /$CHCl_3$, 1:10); light brown solid; mp 185-187°C ^{1}H NMR (400 MHz, DMSO-d_6) δ ppm 1.25 (s, 9 H, $(CH_3)_3$) 3.95 (s, 2 H, CH_2) 7.11 (s, 1 H, Ar) 7.13 - 7.19 (m, 1 H, Ar) 7.20 - 7.30 (m, 4 H, Ar) 10.77 (br, 1 H, exch, NH) 11.88 (br, 1 H, exch, NH) 12.09 (br, 1 H, exch, NH) Anal. Calcd. for $C_{18}H_{20}N_4O_2 \cdot H_2O$: C, 63.14; H, 6.48; N, 16.36. Found C, 63.17; H, 6.24; N, 16.30.

***N*-(4-chloro-6-methyl-5*H*-pyrrolo[3,2-*d*]pyrimidin-2-yl)pivalamide (283)**

Phosphorus oxychloride (30 mL) was added to *N*-(6-methyl-4-oxo-4,5-dihydro-3*H*-pyrrolo[3,2-*d*]pyrimidin-2-yl)pivalamide (**281**, 1.16 g, 4.67 mmol). The reaction mixture was heated at reflux with stirring in an anhydrous atmosphere for 3 h. The dark-orange solution was allowed to cool to room temperature and the solvent removed under vacuum to afford a brown gum. Aqueous ammonium hydroxide was added to the residue at 0 °C with vigorous stirring to attain pH 8 to give a precipitate, which was collected by filtration, washed with water, and dried in vacuo. The crude product was purified by silica gel column chromatography with 2% MeOH/$CHCl_3$ to afford 1.07 g (86%) of **283** as a white solid: TLC R_f = 0.35 (CH_3OH /$CHCl_3$, 1:10); mp 162–163 °C; ^{1}H NMR (400 MHz, DMSO-d_6) δ ppm 1.22 (s, 9 H, $C(CH_3)_3$) 3.37(s, 3 H, CH_3) 6.35 (d, *J* = 0.50 Hz, 1 H, 7-CH) 9.88 (s, 1 H, exch, NH) 12.11 (s, 1 H, exch, NH)

N-(7-benzyl-4-chloro-5*H*-pyrrolo[3,2-*d*]pyrimidin-2-yl)pivalamide (282)

Compound **282** (synthesized from **280** as described for **283**): yield = 80%; TLC R_f = 0.55 (CH_3OH /$CHCl_3$, 1:10); white solid; mp 171-173°C ^{1}H NMR (400 MHz, DMSO-d_6) δ ppm 1.37 (s, 9 H, $(CH_3)_3$) 3.98 (s, 2 H, CH_2) 7.15 (s, 1 H, Ar) 7.18 - 7.23 (m, 1 H, Ar) 7.25 - 7.36 (m, 4 H, Ar) 12.01 (br, 1 H, exch, NH) 12.22 (br, 1 H, exch, NH)

***N*-(4-((4-methoxyphenyl)(methyl)amino)-6-methyl-5*H*-pyrrolo[3,2-*d*]pyrimidin-2-yl)pivalamide (286)**

Compound **286** (synthesized from **283** as described for **161**): yield = 80%; TLC R_f 0.6 (CH_3OH: $CHCl_3$; 1:15). pale yellow solid; mp 287-289 °C; ^{1}H NMR (400 MHz, DMSO-d_6) δ ppm 1.31 (s, 9 H, $(CH_3)_3$) 2.29 (s, 3 H, CH_3) 3.66 (s, 3 H, CH_3) 3.84 (s, 3 H, CH_3) 6.42 - 6.45 (m, 1 H, Ar) 7.10 (s, 2 H, Ar) 7.40 (d, J = 8.78 Hz, 2 H, Ar) 9.67 (s, 1 H, exch, NH) 11.03 (s, 1 H, exch, NH) 13.59 (br, 1 H, exch, HCl) Anal. Calcd. for $C_{20}H_{25}N_5O_2$·HCl: C, 59.47; H, 6.49; N, 17.34; Cl, 8.78. Found C, 59.45; H, 6.54; N, 17.10; Cl, 8.49.

***N*-(7-benzyl-4-((4-methoxyphenyl)(methyl)amino)-5*H*-pyrrolo[3,2-*d*]pyrimidin-2-yl)pivalamide (284)**

Compound **284** (synthesized from **282** as described for **285**): yield = 81%; TLC R_f 0.6 (CH_3OH: $CHCl_3$; 1:10). white solid; mp 217-218 °C; ^{1}H NMR (400 MHz, DMSO-d_6)δ ppm 1.31 (s, 9 H, $(CH_3)_3$) 3.38 (s, 3 H, CH_3) 3.80 (s, 3 H, CH_3) 3.81 (s, 2 H, CH_2) 6.71 (d, J = 3.26 Hz, 1 H, Ar) 6.97 - 7.02 (m, 2 H, Ar) 7.13 (m, J = 4.30 Hz, 1 H, Ar) 7.20 - 7.25 (m, 6 H, Ar) 9.62(s, 1 H, exch, NH) 11.00 (s, 1 H, exch, NH) 13.11 (br, 1 H, exch, HCl)

_N_4-(4-methoxyphenyl)-_N_4,6-dimethyl-5_H_-pyrrolo[3,2-_d_]pyrimidine-2,4-diamine (219)

_N_-(4-((4-methoxyphenyl)(methyl)amino)-6-methyl-5_H_-pyrrolo[3,2-_d_]pyrimidin-2-yl)pivalamide (**286**, 50 mg, 0.13 mmol) was suspended in 1 N NaOH (10 mL) and methanol (5 mL). The reaction mixture was heated to reflux for 10 hours. The solution was cooled to room temperature and neutralized with acetic acid. The resulting precipitate was collected by filtration and dried in vacuo. The crude product was purified by silica gel column chromatography, eluting with 5% CH_3OH /$CHCl_3$ to yield 25 mg (73%) of **219** as a white powder: TLC R_f 0.6 (CH_3OH: $CHCl_3$; 1:10) mp 217-219 °C; ^1H NMR (400 MHz, DMSO-d_6) δ ppm 2.13 (s, 3 H, CH_3) 3.39 (s, 3 H, CH_3) 3.79 (s, 3 H, CH_3) 5.32 (s, 2 H, exch, NH_2) 5.69 - 5.73 (m, 1 H, Ar) 6.96 - 7.00 (m, 2 H, Ar) 7.15 - 7.18 (m, 2 H, Ar) 8.17 (s, 1 H, exch, NH) Anal. Calcd. for $C_{17}H_{19}N_5O \cdot 0.7H_2O$: C, 63.42; H, 6.39; N, 21.75. Found C, 63.67; H, 6.08; N, 21.52.

7-benzyl-_N_4-(4-methoxyphenyl)-_N_4-methyl-5H-pyrrolo[3,2-_d_]pyrimidine-2,4-diamine (217)

Compound **217** (synthesized from **284** as described for **219**): yield = 83%; TLC R_f 0.6 (CH_3OH: $CHCl_3$; 1:15). white solid; mp 167-169 °C; ^1H NMR (400 MHz, DMSO-d_6) δ ppm 3.38 (s, 3 H, CH_3) 3.80 (s, 3 H, CH_3) 3.81 (s, 2 H, CH_2) 5.46 (s, 2 H, exch, NH_2) 6.71 (d, J = 3.26 Hz, 1 H, Ar) 6.97 - 7.02 (m, 2 H, Ar) 7.13 (m, J = 4.30 Hz, 1 H, Ar) 7.20 - 7.25 (m, 6 H, Ar) 7.86 (d, J = 2.76 Hz, 1 H, exch, NH) Anal. Calcd. for $C_{21}H_{21}N_5O$: C, 70.17; H, 5.89; N, 19.48. Found C, 70.11; H, 5.96; N, 19.42.

***N*-(4-(6-methoxy-3,4-dihydroquinolin-1(2H)-yl)-6-methyl-5*H*-pyrrolo[3,2-*d*]pyrimidin-2-yl)pivalamide (287)**

Compound **287** (synthesized from **283** and 6-methoxy-1,2,3,4-tetrahydroquinoline as described for **161**): yield = 75%; TLC R_f 0.6 (CH_3OH: $CHCl_3$; 1:15). white solid; mp 287-289 °C; ^{1}H NMR (400 MHz, DMSO-d_6) δ ppm 1.30 (s, 9 H, $C(CH_3)_3$) 1.98 - 2.06 (m, 2 H, CH_2) 2.35 (s, 3 H, CH_3) 2.80 - 2.87 (m, 2 H, CH_2) 3.79 (s, 3 H, CH_3) 4.07 - 4.14 (m, 2 H, CH2) 6.44 - 6.48 (m, 1 H, Ar) 6.74 - 6.79 (m, 1 H, Ar) 6.91 - 6.94 (m, 1 H, Ar) 7.06 - 7.09 (m, 1 H, Ar) 10.87 (s, 1 H, exch, NH) 11.06(s, 1 H, exch, NH) 13.68 (s, 1 H, exch, NH)

***N*-(7-benzyl-4-(6-methoxy-3,4-dihydroquinolin-1(2*H*)-yl)-5*H*-pyrrolo[3,2-*d*]pyrimidin-2-yl)pivalamide (285)**

Compound **285** (synthesized from **282** and 6-methoxy-1,2,3,4-tetrahydroquinoline as described for **161**): yield = 78%; TLC R_f 0.62 (CH_3OH: $CHCl_3$; 1:15). light yellow solid; mp 211-213 °C; ^{1}H NMR (400 MHz, DMSO-d_6) δ ppm 1.30 (s, 9 H, $C(CH_3)_3$)1.85 - 1.94 (m, 2 H, CH_2) 2.71 - 2.81 (m, 2 H, CH_2) 3.73 (s, 3 H, OCH_3) 3.86 (s, 4 H, CH_2) 6.64 - 6.70 (m, 1 H, Ar) 6.75 - 6.81 (m, 2 H, Ar) 6.88 - 6.92 (m, 1 H, Ar) 7.12 - 7.18 (m, 1 H, Ar) 7.26 (s, 4 H, Ar) 10.80 (s, 1 H, exch, NH) 11.15(s, 1 H, exch, NH) 13.11 (s, 1 H, exch, NH)

4-(6-methoxy-3,4-dihydroquinolin-1(2*H*)-yl)-6-methyl-5*H*-pyrrolo[3,2-*d*]pyrimidin-2-amine (220)

Compound **220** (synthesized from **287** as described for **219**): yield = 92%; TLC R_f 0.6

(CH_3OH: $CHCl_3$; 1:10). white solid; mp 268-270 °C; ^1H NMR (400 MHz, DMSO-d_6) δ ppm 1.91 (quin, J = 6.27 Hz, 2 H, CH_2) 2.26 (s, 3 H, CH_3) 2.79 (t, J = 6.40 Hz, 2 H, CH_2) 3.70 - 3.75 (m, 3 H, CH_3) 3.77 - 3.82 (m, 2 H, CH_2) 5.37 (s, 2 H, exch, NH_2) 5.79 (s, 1 H, Ar) 6.61 - 6.66 (m, 1 H, Ar) 6.70 - 6.74 (m, 1 H, Ar) 6.75 (d, J = 2.76 Hz, 1 H, Ar) 9.79 (s, 1 H, exch, NH) Anal. Calcd. for $C_{17}H_{19}N_5O \cdot 0.7H_2O$: C, 63.42; H, 6.39; N, 21.75. Found C, 63.67; H, 6.08; N, 21.52.

7-benzyl-4-(6-methoxy-3,4-dihydroquinolin-1(2*H*)-yl)-5*H*-pyrrolo[3,2-*d*]pyrimidin-2-amine (218)

Compound **218** (synthesized from **285** as described for **219**): yield = 90%; TLC R_f 0.6 (CH_3OH: $CHCl_3$; 1:10). grey solid; mp 239-240 °C; ^1H NMR (400 MHz, DMSO-d_6) δ ppm 1.85 - 1.94 (m, 2 H, CH_2) 2.71 - 2.81 (m, 2 H, CH_2) 3.73 (s, 3 H, OCH_3) 3.86 (s, 4 H, CH_2) 5.55 (br, 2 H, exch, NH_2) 6.64 - 6.70 (m, 1 H, Ar) 6.75 - 6.81 (m, 2 H, Ar) 6.88 - 6.92 (m, 1 H, Ar) 7.12 - 7.18 (m, 1 H, Ar) 7.26 (s, 4 H, Ar) 9.36 (br, 1 H, exch, NH) Anal. Calcd. for $C_{20}H_{18}N_4 \cdot HCl$: C, 68.47; H, 5.46; N, 15.97; Cl, 10.11. Found C, 68.45; H, 5.43; N, 15.89; Cl, 9.99.

2-methyl-7-(3,4,5-trimethoxybenzyl)-3H-pyrrolo[3,2-d]pyrimidin-4(5H)-one (291)

Compound **291** (synthesized from **288** as described for **260**): yield = 35%; TLC R_f 0.6 (CH_3OH: $CHCl_3$; 1:10). white powder; mp 198-200 °C; ^1H NMR (400 MHz, DMSO-d_6) δ ppm 3.60 (s, 3 H, OCH_3) 3.71 (s, 6 H, OCH_3) 3.86 (s, 2 H, CH_2) 6.64 (s, 2 H, CH) 7.13 (s, 1 H, 6-CH) 10.78 (br, 1 H, exch, NH) 11.85 (br, 1 H, exch, 1H)

7-(3,4,5-trimethoxybenzyl)-3H-pyrrolo[3,2-*d*]pyrimidin-4(5*H*)-one (292)

Compound **292** (synthesized from **288** as described for **239**): yield = 31%; TLC R_f 0.5 (CH_3OH: $CHCl_3$; 1:10). brown solid; mp 205-207 °C; ^{1}H NMR (400 MHz, DMSO-d_6) δ ppm 3.60 (s, 3 H, OCH_3) 3.71 (s, 6 H, OCH_3) 3.86 (s, 2 H, CH_2) 6.64 (s, 2 H, CH) 7.13 (s, 1 H, CH) 8.15 (s, 1 H, CH) 10.78 (br, 1 H, exch, NH) 11.85 (br, 1 H, exch, 1H)

N-(4-oxo-7-(3,4,5-trimethoxybenzyl)-4,5-dihydro-3*H*-pyrrolo[3,2-*d*]pyrimidin-2-yl)pivalamide (293)

Compound **293** (synthesized from **288** as described for **281**): yield = 52%; TLC R_f 0.5 (CH_3OH: $CHCl_3$; 1:10). pale yellow solid; mp 193-195 °C; ^{1}H NMR (400 MHz, DMSO-d_6) δ ppm 1.25 (s, 9 H, $(CH_3)_3$) 3.60 (s, 3 H, OCH_3) 3.71 (s, 6 H, OCH_3) 3.86 (s, 2 H, CH_2) 6.64 (s, 2 H, CH) 7.13 (s, 1 H, 6-H) 10.78 (br, 1 H, exch, NH) 11.85 (br, 1 H, exch, NH) 12.05 (br, 1 H, exch, NH) Anal. Calcd. for $C_{21}H_{26}N_4O_5$: C, 60.86; H, 6.32; N, 13.52. Found C, 60.88; H, 6.18; N, 13.40.

4-chloro-2-methyl-7-(3,4,5-trimethoxybenzyl)-5*H*-pyrrolo[3,2-*d*]pyrimidine (294)

Compound **294** (synthesized from **291** as described for **283**): yield = 79%; TLC R_f 0.5 (CH_3OH: $CHCl_3$; 1:10). light brown solid; mp 193-195 °C; ^{1}H NMR (500 MHz, DMSO-d_6) δ ppm 2.66 (s, 3 H, CH_3) 3.60 (s, 3 H, OCH_3) 3.71 (s, 6 H, OCH_3) 4.02 (s, 2 H, CH_2) 6.67 (s, 2 H, CH) 7.82 (s, 1 H, 6-CH) 8.65 (s, 1 H, 2-CH) 12.27 (s, 1 H, exch, NH_2)

4-chloro-7-(3,4,5-trimethoxybenzyl)-5*H*-pyrrolo[3,2-*d*]pyrimidine (295)

Compound **295** (synthesized from **292** as described for **283**): yield = 82%; TLC R_f 0.4

(CH_3OH: $CHCl_3$; 1:10). yellow solid; mp 179-180 °C; ^1H NMR (500 MHz, DMSO-d_6) δ ppm 3.60 (s, 3 H, OCH_3) 3.71 (s, 6 H, OCH_3) 4.02 (s, 2 H, CH_2) 6.67 (s, 2 H, CH) 7.82 (s, 1 H, 6-H) 8.65 (s, 1 H, 2-H) 12.27 (s, 1 H, exch, NH_2) Anal. Calcd. for $C_{16}H_{14}N_3O_3Cl$: C, 57.58; H, 4.83; N, 12.59; Cl, 10.62. Found C, 57.57; H, 4.94; N, 12.55; Cl, 10.46.

_N_-(4-chloro-7-(3,4,5-trimethoxybenzyl)-5_H_-pyrrolo[3,2-_d_]pyrimidin-2-yl)pivalamide (296)

Compound **296** (synthesized from **293** as described for **283**): yield = 87%; TLC R_f 0.6 (CH_3OH: $CHCl_3$; 1:10). light yellow solid; mp 179-180 °C; ^1H NMR (500 MHz, DMSO-d_6) δ ppm 1.24 (s, 9 H, $(CH_3)_3$) 3.59 (s, 3 H, OCH_3) 3.72 (s, 6 H, OCH_3) 3.96 (s, 2 H, CH_2) 6.74 (s, 2 H, CH) 7.73 (s, 1 H, 6-CH) 9.98 (s, 1 H, exch, NH) 12.12 (s, 1 H, exch, NH) Anal. Calcd. for $C_{21}H_{25}N_4O_4Cl$: C, 58.26; H, 5.82; N, 12.94; Cl, 8.19. Found C, 58.06; H, 5.74; N, 12.86; Cl, 8.05.

_N_-(4-methoxyphenyl)-_N_,2-dimethyl-7-(3,4,5-trimethoxybenzyl)-5_H_-pyrrolo[3,2-_d_]pyrimidin-4-amine (222)

Compound **222** (synthesized from **294** as described for **161**): grey solid; mp 98-100 °C; ^1H NMR (500 MHz, DMSO-d_6) δ ppm 2.61 (s, 3 H, CH_3) 3.59 (s, 3 H, CH_3) 3.66 (s, 3 H, OCH_3) 3.73 (s, 6 H, OCH_3) 3.84 (s, 3 H, OCH_3) 4.00 (s, 2 H, CH_2) 6.73 (s, 2 H, Ar) 7.10 (d, J = 9.12 Hz, 2 H, Ar) 7.42 (d, J = 8.80 Hz, 2 H, Ar) 7.81 (s, 1 H, Ar) 8.72 (d, J = 2.76 Hz, 1 H, exch, NH) 14.68 (br, 1 H, exch, HCl)

***N*4-(4-methoxyphenyl)-*N*4-methyl-7-(3,4,5-trimethoxybenzyl)-5*H*-pyrrolo[3,2-*d*]pyrimidine-2,4-diamine (223)**

Compound **222** (synthesized from **296** as described for **161**): Intermediate *N*-(4-((4-methoxyphenyl)(methyl)amino)-7-(3,4,5-trimethoxybenzyl)-5*H*-pyrrolo[3,2-*d*]pyrimidin-2-yl)pivalamide: ^{1}H NMR (500 MHz, DMSO-d_6) δ ppm 3.34 (s, 9 H, $(CH_3)_3$) 3.59 (s, 3 H, CH_3) 3.60 (br, 3 H, CH_3) 3.76 (s, 6 H, OCH_3) 3.85 (s, 3 H, CH_3) 3.92 (s., 2 H, CH2) 6.67 (s, 2 H, Ar) 7.10 (d, *J* = 8.49 Hz, 2 H, Ar) 7.41 (s., 2 H, Ar) 9.03 (br, 1 H, exch, NH) 11.23 (br, 1 H, exch, NH) 13.39 (br, 1 H, exch, HCl) Anal. Calcd. for $C_{29}H_{35}N_5O_5 \cdot HCl \cdot 0.5H_2O$: C, 60.15; H, 6.44; N, 12.09; Cl, 6.12. Found C, 60.26; H, 6.51; N, 11.96; Cl, 5.87. Compound **22** white solid; mp 113-115 °C; ^{1}H NMR (400 MHz, DMSO-d_6) δ ppm 3.38 (s, 3 H, CH_3) 3.59 (s, 3 H, OCH_3) 3.70 (s, 6 H, OCH_3) 3.73 (s, 2 H, CH_2) 3.79 (s, 3 H, OCH_3) 5.48 (s, 2 H, exch, NH_2) 6.66 (s, 2 H) 6.71 (d, *J* = 2.76 Hz, 1 H, exch, NH) 6.99 (d, *J* = 8.78 Hz, 2 H, Ar) 7.21 (d, *J* = 9.03 Hz, 2 H, Ar) 7.81 (s, 1 H, Ar) Anal. Calcd. for $C_{24}H_{27}N_5O_4 \cdot 1.25H_2O$: C, 61.14; H, 6.29; N, 14.85. Found C, 61.15; H, 5.99; N, 14.71.

***N*-(4-methoxyphenyl)-*N*-methyl-7-(3,4,5-trimethoxybenzyl)-5*H*-pyrrolo[3,2-*d*]pyrimidin-4-amine (224)**

Compound **222** (synthesized from **295** as described for **161**): yellow solid; mp 223-225 °C; ^{1}H NMR (500 MHz, DMSO-d_6) δ ppm 3.59 (s, 3 H, CH_3) 3.66 (s, 3 H, OCH_3) 3.73 (s, 6 H, OCH_3) 3.84 (s, 3 H, OCH_3) 4.00 (s, 2 H, CH_2) 6.73 (s, 2 H, Ar) 7.10 (d, *J* = 9.12 Hz, 2 H, Ar) 7.42 (d, *J* = 8.80 Hz, 2 H, Ar) 7.47 (s, 1 H, Ar) 8.71 (s, 1 H, Ar) Anal.

Calcd. for $C_{24}H_{26}N_4O_4 \cdot HCl$: C, 61.21; H, 5.78; N, 11.90; Cl, 7.53. Found C, 61.14; H, 5.87; N, 11.67; Cl, 7.36.

7-benzyl-*N*-(4-bromo-2-fluorophenyl)-2-methyl-5*H*-pyrrolo[3,2-*d*]pyrimidin-4-amine (225)

Compound **225** (synthesized from **261** and 2-fluoro 4-bromo aniline as described for **161**): yield = 76%; TLC R_f 0.6 (CH_3OH: $CHCl_3$; 1:20). white solid; mp 277-279 °C; ^{1}H NMR (400 MHz, DMSO-d_6) δ ppm 2.61 (s, 3 H, CH_3) 4.14 (s, 2 H, CH_2) 7.16 - 7.23 (m, 1 H, Ar) 7.29 (d, J = 4.02 Hz, 4 H, Ar) 7.51 (d, J = 8.53 Hz, 1 H, Ar) 7.72 - 7.82 (m, 3 H, Ar) 11.05 (br, 1 H, exch, NH) 12.56 (br, 1 H, exch, NH) 14.68 (br, 1 H, exch, HCl) Anal. Calcd. for $C_{20}H_{16}N_4BrF \cdot HCl$: C, 53.65; H, 3.83; N, 12.51; Cl, 7.92; Br, 17.85. Found , 53.29; H, 3.82; N, 12.14; Cl, 8.04; Br, 17.52.

7-benzyl-*N*-(4-chloro-2-fluorophenyl)-2-methyl-5*H*-pyrrolo[3,2-*d*]pyrimidin-4-amine (226)

Compound **226** (synthesized from **261** and 2-fluoro 4-chloro aniline as described for **161**): yield = 67%; TLC R_f 0.7 (CH_3OH: $CHCl_3$; 1:20). light brown solid; mp 251-252 °C; ^{1}H NMR (400 MHz, DMSO-d_6) δ ppm 2.61 (s, 3 H, CH_3) 4.15 (s, 2 H, CH_2) 7.16 - 7.22 (m, 1 H, Ar) 7.26 - 7.32 (m, 4 H, Ar) 7.39 (d, J = 8.53 Hz, 1 H, Ar) 7.64 (dd, J = 10.29, 2.26 Hz, 1 H, Ar) 7.76 (d, J = 2.76 Hz, 1 H, Ar) 7.80 (t, J = 8.53 Hz, 1 H, Ar) 11.19 (br, 1 H, exch, NH) 12.71 (br, 1 H, exch, NH) 14.76 (br, 1 H, exch, HCl) Anal. Calcd. for $C_{20}H_{16}N_4ClF \cdot HCl$: C, 59.57; H, 4.25; N, 13.89; Cl, 17.58; F, 4.71. Found C, 59.77; H, 4.15; N, 13.78; Cl, 17.69; F, 4.67.

7-benzyl-*N*-(3-ethynylphenyl)-2-methyl-5*H*-pyrrolo[3,2-*d*]pyrimidin-4-amine (227)

Compound **227** (synthesized from **261** and 3-ethynyl aniline as described for **161**): yield = 78%; TLC R_f 0.7 (CH_3OH: $CHCl_3$; 1:20). off-white solid; mp 275-277 °C; ^1H NMR (400 MHz, DMSO-d_6) δ ppm 2.70 (s, 3 H, CH_3) 4.13 (s, 2 H, CH_2) 7.17 - 7.22 (m, 1 H, Ar) 7.26 - 7.32 (m, 6 H, Ar) 7.45 (t, J = 8.03 Hz, 1 H, Ar) 7.74 (d, J = 3.01 Hz, 1 H, Ar) 8.00 - 8.04 (m, 1 H, Ar) 8.06 (d, J = 1.76 Hz, 1 H, Ar) 11.54 (br, 1 H, exch, NH) 12.84 (br, 1 H, exch, NH) 14.55 (br, 1 H, exch, HCl) Anal. Calcd. for $C_{22}H_{19}N_4 \cdot HCl$: C, 70.49; H, 5.11; N, 14.95; Cl, 9.46. Found C, 70.43; H, 5.06; N, 14.79; Cl, 9.34.

7-benzyl-*N*-(3-bromophenyl)-2-methyl-5*H*-pyrrolo[3,2-*d*]pyrimidin-4-amine (228)

Compound **228** (synthesized from **261** and 3-bromo aniline as described for **161**): yield = 72%; TLC R_f 0.7 (CH_3OH: $CHCl_3$; 1:20). light yellow solid; mp 299-300 °C; ^1H NMR (400 MHz, DMSO-d_6) δ ppm 2.71 (s, 3 H, CH_3) 4.13 (s, 2 H, CH_2) 7.17 - 7.22 (m, 1 H, Ar) 7.26 - 7.32 (m, 4 H, Ar) 7.36 - 7.41 (m, 2 H, Ar) 7.75 (d, J = 2.76 Hz, 1 H, Ar) 7.95 - 7.99 (m, 1 H, Ar) 8.25 (s, 1 H, Ar) 11.62 (br, 1 H, exch, NH) 12.86 (br, 1 H, exch, NH) 14.62 (br, 1 H, exch, HCl) Anal. Calcd. for $C_{20}H_{17}N_4Br \cdot HCl$: C, 55.90; H, 4.22; N, 13.04; Cl, 8.25; Br, 18.59. Found C, 55.97; H, 4.15; N, 12.95; Cl, 8.29; Br, 18.50.

7-benzyl-*N*-(3-chloro-4-fluorophenyl)-2-methyl-5*H*-pyrrolo[3,2-*d*]pyrimidin-4-amine (229)

Compound **229** (synthesized from **261** and 3-chloro 4-floro aniline as described for **161**): yield = 75%; TLC R_f 0.55 (CH_3OH: $CHCl_3$; 1:20). white solid; mp 289-291 °C; ^1H NMR (400 MHz, DMSO-d_6) δ ppm 2.70 (s, 3 H, CH_3) 4.12 (s, 2 H, CH_2) 7.15 - 7.34 (m, 5 H,

Ar) 7.49 (t, *J* = 9.16 Hz, 1 H, Ar) 7.72 (d, *J* = 2.01 Hz, 1 H, Ar) 7.88 - 7.96 (m, 1 H, Ar) 8.22 (dd, *J* = 6.40, 2.13 Hz, Ar) 11.74 (br, 1 H, exch, NH) 12.86 (br, 1 H, exch, NH) 14.63 (br, 1 H, exch, HCl) Anal. Calcd. for $C_{20}H_{16}N_4ClF \cdot HCl \cdot 0.4C_3H_8O$: C, 59.59; H, 4.76; N, 13.11; Cl, 16.59; F, 4.45. Found C, 59.56; H, 4.57; N, 13.05; Cl, 16.61; F, 4.47.

7-benzyl-*N*-(3-chloro-4-methoxyphenyl)-2-methyl-5*H*-pyrrolo[3,2-*d*]pyrimidin-4-amine (230)

Compound **230** (synthesized from **261** and 3-chloro 4-methoxy aniline as described for **161**): yield = 76%; TLC R_f 0.6 (CH_3OH: $CHCl_3$; 1:20). white solid; mp 307-309 °C; ^1H NMR (400 MHz, DMSO-d_6) δ ppm 2.67 (s, 3 H, CH_3) 3.87 (s, 3 H, OCH_3) 4.11 (s, 2 H, CH_2) 7.15 - 7.33 (m, 6 H, Ar) 7.70 (d, *J* = 2.76 Hz, 1 H, Ar) 7.81 (dd, *J* = 9.16, 2.64 Hz, Ar) 8.04 (d, *J* = 2.26 Hz, 1 H, Ar) 11.44 (br, 1 H, exch, NH) 12.67 (br, 1 H, exch, NH) 14.42 (br, 1 H, exch, HCl) Anal. Calcd. for $C_{21}H_{19}N_4ClO \cdot HCl$: C, 60.73; H, 4.85; N, 13.49; Cl, 13.70. Found C, 60.83; H, 4.78; N, 13.36; Cl, 16.90.

7-benzyl-2-methyl-*N*-(3,4,5-trimethoxyphenyl)-5*H*-pyrrolo[3,2-*d*]pyrimidin-4-amine (231)

Compound **231** (synthesized from **261** and 3,4,5 trimethoxy aniline as described for **161**): yield = 71%; TLC R_f 0.5 (CH_3OH: $CHCl_3$; 1:20). light yellow solid; mp 270-271 °C; ^1H NMR (400 MHz, DMSO-d_6) δ ppm 2.70 (s, 3 H, CH_3) 3.66 (s, 3 H, CH_3) 3.80 (s, 6 H, OCH_3) 4.12 (s, 2 H, CH_2) 7.12 - 7.37 (m, 6 H, Ar) 7.70 (d, *J* = 2.01 Hz, Ar) 11.29 (br, 1 H, exch, NH) 12.61 (s, 1 H, exch, NH) 14.45 (br, 1 H, exch, HCl) Anal. Calcd. for $C_{23}H_{24}N_4O_3 \cdot HCl$: C, 62.65; H, 5.71; N, 12.71; Cl, 8.04. Found C, 62.41; H, 5.77; N,

12.67; Cl, 8.02.

7-benzyl-2-methyl-*N*-phenyl-5*H*-pyrrolo[3,2-*d*]pyrimidin-4-amine (232)

Compound **232** (synthesized from **261** and aniline as described for **161**): yield = 75%; TLC R_f 0.6 (CH_3OH: $CHCl_3$; 1:20). white solid; mp 300-302 °C; ^1H NMR (400 MHz, DMSO-d_6) δ ppm 2.70 (s, 3 H, CH_3) 4.13 (s, 2 H, CH_2) 7.19 - 7.26 (m, 2 H, Ar) 7.27 - 7.34 (m, 4 H, Ar) 7.46 (t, J = 7.91 Hz, 2 H, Ar) 7.73 (s, 1 H, Ar) 7.91 (d, J = 7.78 Hz, 2 H, Ar) 11.20 (s, 1 H, exch, NH) 12.56 (s, 1 H, exch, NH) 14.42 (s, 1 H, exch, HCl) Anal. Calcd. for $C_{20}H_{18}N_4 \cdot HCl$: C, 68.47; H, 5.46; N, 15.97; Cl, 10.11. Found C, 68.45; H, 5.43; N, 15.89; Cl, 9.99.

VI. SUMMARY

This dissertation describes the design and synthesis of pyrimidine fused heterocycles as single agents with combination chemotherapy potential. These efforts led to the identification of structural features that are necessary for inhibition of tubulin polymerization. Structural modifications also led to the identification of antiangiogenic agents which inhibit one or more of the receptor tyrosine kinases (RTKs)- vascular endothelial growth factor receptor-2, platelet derived growth factor receptor-β and epidermal growth factor receptor. Single agents with both antiangiogenic activities as well as cytotoxicity would afford single entities that circumvent pharmacokinetic problems of multiple agents, avoid drug-drug interactions, could be used at lower doses to alleviate toxicity, devoid of overlapping toxicities, and delay or prevent tumor cell resistance. The novel target compounds synthesized as part of this study are listed below:

1. *N*-(4-methoxyphenyl)-*N*,2-dimethyl-5*H*-pyrrolo[3,2-*d*]pyrimidin-4-amine (**161**)
2. *N*-(4-methoxyphenyl)-*N*-methyl-5*H*-pyrrolo[3,2-*d*]pyrimidin-4-amine (**162**)
3. *N*,2-dimethyl-*N*-phenyl-5*H*-pyrrolo[3,2-*d*]pyrimidin-4-amine (**126**)
4. *N*-(4-methoxyphenyl)-2-methyl-5*H*-pyrrolo[3,2-*d*]pyrimidin-4-amine (**123**)
5. *N*-(2,4-dimethoxyphenyl)-2-methyl-5*H*-pyrrolo[3,2-*d*]pyrimidin-4-amine (**125**)
6. 4-(5-methoxyindolin-1-yl)-2-methyl-5*H*-pyrrolo[3,2-*d*]pyrimidine (**166**)
7. 6-methoxy-1-(2-methyl-5*H*-pyrrolo[3,2-*d*]pyrimidin-4-yl)-1,2,3,4-tetrahydroquinoline (**167**)
8. *N*-(4-methoxyphenyl)-*N*,2,5-trimethyl-5*H*-pyrrolo[3,2-*d*]pyrimidin-4-amine (**170**)
9. *N*-(4-methoxyphenyl)-2,5-dimethyl-5*H*-pyrrolo[3,2-*d*]pyrimidin-4-amine (**171**)

10. *N*-(2,4-dimethoxyphenyl)-2,5-dimethyl-5*H*-pyrrolo[3,2-*d*]pyrimidin-4-amine (**172**)
11. 1-(2,5-dimethyl-5*H*-pyrrolo[3,2-*d*]pyrimidin-4-yl)-6-methoxy-1,2,3,4-tetrahydroquinoline (**173**)
12. *N*-(4-methoxyphenyl)-*N*,2,6-trimethyl-5H-pyrrolo[3,2-*d*]pyrimidin-4-amine (**174**)
13. 4-(5-methoxyindolin-1-yl)-2,6-dimethyl-5*H*-pyrrolo[3,2-*d*]pyrimidine (**175**)
14. 1-(2,6-dimethyl-5*H*-pyrrolo[3,2-*d*]pyrimidin-4-yl)-6-methoxy-1,2,3,4-tetrahydroquinoline (**176**)
15. *N*-(4-methoxyphenyl)-*N*,2-dimethyl-5*H*-pyrimido[5,4-*b*]indol-4-amine (**178**)
16. 4-(5-methoxyindolin-1-yl)-2-methyl-5*H*-pyrimido[5,4-*b*]indole (**179**)
17. 4-(6-methoxy-3,4-dihydroquinolin-1(2*H*)-yl)-2-methyl-5*H*-pyrimido[5,4-*b*]indole (**180**)
18. *N*-(4-methoxyphenyl)-*N*,2-dimethylfuro[3,2-*d*]pyrimidin-4-amine (**181**)
19. *N*-(4-methoxyphenyl)-2-methylfuro[3,2-*d*]pyrimidin-4-amine (**182**)
20. *N*-(2,4-dimethoxyphenyl)-2-methylfuro[3,2-*d*]pyrimidin-4-amine (**183**)
21. 4-(5-methoxyindolin-1-yl)-2-methylfuro[3,2-*d*]pyrimidine (**184**)
22. 4-(6-methoxy-3,4-dihydroquinolin-1(2*H*)-yl)-2-methylfuro[3,2-*d*]pyrimidine (**185**)
23. 7-benzyl-*N*-(4-methoxyphenyl)-*N*,2-dimethyl-5*H*-pyrrolo[3,2-*d*]pyrimidin-4-amine (**187**)
24. 7-benzyl-*N*,2-dimethyl-*N*-phenyl-5*H*-pyrrolo[3,2-*d*]pyrimidin-4-amine (188)
25. 7-benzyl-*N*-(4-methoxyphenyl)-2-methyl-5*H*-pyrrolo[3,2-*d*]pyrimidin-4-amine (**189**)
26. 7-benzyl-*N*-(2,4-dimethoxyphenyl)-2-methyl-5*H*-pyrrolo[3,2-*d*]pyrimidin-4-amine (**190**)

27. 5-ethyl-*N*-(4-methoxyphenyl)-*N*,2-dimethyl-5*H*-pyrrolo[3,2-*d*]pyrimidin-4-amine (**191**)
28. 5-isopropyl-*N*-(4-methoxyphenyl)-*N*,2-dimethyl-5*H*-pyrrolo[3,2-*d*]pyrimidin-4-amine (**192**)
29. *N*-(4-methoxyphenyl)-*N*,2-dimethyl-5-propyl-5*H*-pyrrolo[3,2-*d*]pyrimidin-4-amine (**193**)
30. 5-isobutyl-*N*-(4-methoxyphenyl)-*N*,2-dimethyl-5*H*-pyrrolo[3,2-*d*]pyrimidin-4-amine (**194**)
31. 5-butyl-*N*-(4-methoxyphenyl)-*N*,2-dimethyl-5*H*-pyrrolo[3,2-*d*]pyrimidin-4-amine (**195**)
32. *N*-(4-methoxyphenyl)-*N*,2-dimethyl-6,7-dihydrofuro[3,2-*d*]pyrimidin-4-amine (**196**)
33. 4-(6-methoxy-3,4-dihydroquinolin-1(2*H*)-yl)-2-methyl-6,7-dihydrofuro[3,2-*d*]pyrimidine (**197**)
34. *N*-ethyl-*N*-(4-methoxyphenyl)-2-methylfuro[3,2-*d*]pyrimidin-4-amine (**198**)
35. *N*-isopropyl-*N*-(4-methoxyphenyl)-2-methylfuro[3,2-*d*]pyrimidin-4-amine (**199**)
36. *N*-(4-methoxyphenyl)-2-methyl-*N*-propylfuro[3,2-*d*]pyrimidin-4-amine (**200**)
37. *N*-(4-methoxyphenyl)-*N*,2-dimethylbenzofuro[3,2-*d*]pyrimidin-4-amine (**202**)
38. 4-(5-methoxyindolin-1-yl)-2-methylbenzofuro[3,2-*d*]pyrimidine (**203**)
39. 4-(6-methoxy-3,4-dihydroquinolin-1(2*H*)-yl)-2-methylbenzofuro[3,2-*d*]pyrimidine (**204**)
40. 7-benzyl-*N*-(4-methoxyphenyl)-*N*,2-dimethylfuro[3,2-*d*]pyrimidin-4-amine (**205**)
41. 7-benzyl-4-(6-methoxy-3,4-dihydroquinolin-1(2*H*)-yl)-2-methylfuro[3,2-*d*]pyrimidine (**206**)

42. *N*,2-dimethyl-*N*-phenylfuro[3,2-*d*]pyrimidin-4-amine (**207**)

43. *N*,2-dimethyl-*N*-(p-tolyl)furo[3,2-*d]*pyrimidin-4-amine (**208**)

44. *N*-(4-chlorophenyl)-*N*,2-dimethylfuro[3,2-*d*]pyrimidin-4-amine (**209**)

45. *N*-(3,4-dichlorophenyl)-*N*,2-dimethylfuro[3,2-*d*]pyrimidin-4-amine (**210**)

46. 7-benzyl-*N*-(4-methoxyphenyl)-2,5-dimethyl-5*H*-pyrrolo[3,2-*d*]pyrimidin-4-amine (**211**)

47. *7*-benzyl-*N*-(4-methoxyphenyl)-*N*,2,5-trimethyl-5*H*-pyrrolo[3,2-*d*]pyrimidin-4-amine (**212**)

48. 1-(7-benzyl-2-methyl-5*H*-pyrrolo[3,2-*d*]pyrimidin-4-yl)-6-methoxy-1,2,3,4-tetrahydroquinoline (**213**)

49. 1-(7-benzyl-2,5-dimethyl-5*H*-pyrrolo[3,2-*d*]pyrimidin-4-yl)-6-methoxy-1,2,3,4-tetrahydroquinoline (**214**)

50. *N*-(4-methoxyphenyl)-*N*,2,5,6-tetramethyl-5*H*-pyrrolo[3,2-*d*]pyrimidin-4-amine (**215**)

51. 6-methoxy-1-(2,5,6-trimethyl-5*H*-pyrrolo[3,2-*d*]pyrimidin-4-yl)-1,2,3,4-tetrahydroquinoline (**216**)

52. 7-benzyl-*N*4-(4-methoxyphenyl)-*N*4-methyl-5H-pyrrolo[3,2-*d*]pyrimidine-2,4-diamine (**217**)

53. 7-benzyl-4-(6-methoxy-3,4-dihydroquinolin-1(2*H*)-yl)-5*H*-pyrrolo[3,2-*d*]pyrimidin-2-amine (**218**)

54. *N*4-(4-methoxyphenyl)-*N*4,6-dimethyl-5*H*-pyrrolo[3,2-*d*]pyrimidine-2,4-diamine (**219**)

55. 4-(6-methoxy-3,4-dihydroquinolin-1(2*H*)-yl)-6-methyl-5*H*-pyrrolo[3,2-*d*]pyrimidin-2-amine (**220**)

56. *N*-(4-methoxyphenyl)-*N*,2-dimethyl-7-(3,4,5-trimethoxybenzyl)-5*H*-pyrrolo[3,2-*d*]pyrimidin-4-amine (**222**)
57. *N*4-(4-methoxyphenyl)-*N*4-methyl-7-(3,4,5-trimethoxybenzyl)-5*H*-pyrrolo[3,2-*d*]pyrimidine-2,4-diamine (**223**)
58. *N*-(4-methoxyphenyl)-*N*-methyl-7-(3,4,5-trimethoxybenzyl)-5*H*-pyrrolo[3,2-*d*]pyrimidin-4-amine (**224**)
59. 7-benzyl-*N*-(4-bromo-2-fluorophenyl)-2-methyl-5*H*-pyrrolo[3,2-*d*]pyrimidin-4-amine (**225**)
60. 7-benzyl-*N*-(4-chloro-2-fluorophenyl)-2-methyl-5*H*-pyrrolo[3,2-*d*]pyrimidin-4-amine (**226**)
61. 7-benzyl-*N*-(3-ethynylphenyl)-2-methyl-5*H*-pyrrolo[3,2-*d*]pyrimidin-4-amine (**227**)
62. 7-benzyl-*N*-(3-bromophenyl)-2-methyl-5*H*-pyrrolo[3,2-*d*]pyrimidin-4-amine (228)
63. 7-benzyl-*N*-(3-chloro-4-fluorophenyl)-2-methyl-5*H*-pyrrolo[3,2-*d*]pyrimidin-4-amine (**229**)
64. 7-benzyl-*N*-(3-chloro-4-methoxyphenyl)-2-methyl-5*H*-pyrrolo[3,2-*d*]pyrimidin-4-amine (**230**)
65. 7-benzyl-2-methyl-*N*-(3,4,5-trimethoxyphenyl)-5*H*-pyrrolo[3,2-*d*]pyrimidin-4-amine (**231**)
66. 7-benzyl-2-methyl-*N*-phenyl-5*H*-pyrrolo[3,2-*d*]pyrimidin-4-amine (**232**)

VII. BIBLIOGRAPHY

1. Folkman, J. Tumor angiogenesis: Therapeutic implications. *N. Engl. .J Med.* **1971**, *285*, 1182-1186.
2. Ferrara, N.; Kerbel, R. S. Angiogenesis as a therapeutic target. *Nature* **2005**, *438*, 967-974.
3. Carmeliet, P.; Jain, R. K. Angiogenesis in cancer and other diseases. *Nature* **2000**, *407* , 249-257.
4. Bouck, N.; Stellmach, V.; Hsu, S. C. How tumors become angiogenic. *Adv. Cancer Res.* **1996**, *69*, 135-174.
5. Gao, D.; Nolan, D. J.; Mellick, A. S.; Bambino, K.; McDonnell, K.; Mittal, V. Endothelial progenitor cells control the angiogenic switch in mouse lung metastasis. *Science* **2008**, *319*, 195-198.
6. Joyce, J. A.; Pollard, J. W. Microenvironmental regulation of metastasis. *Nat. Rev. Cancer* **2009**, *9*, 239-252.
7. Zhang, C.; Tan, C.; Ding, H.; Xin, T.; Jiang, Y. Selective VEGFR inhibitors for anticancer therapeutics in clinical use and clinical trials. *Curr. Pharm. Des.* **2012**, *18*, 2921-2935.
8. Sun, W. Angiogenesis in metastatic colorectal cancer and the benefits of targeted therapy. *J. Hematol. Oncol.* **2012**, *5*, 1-9.
9. Carmeliet, P.; Jain, R. K. Principles and mechanisms of vessel normalization for cancer and other angiogenic diseases. *Nat. Rev. Drug Discov.* **2011**, *10*, 417-427.
10. Zwick, E.; Bange, J.; Ullrich, A. Receptor tyrosine kinases as targets for anticancer drugs. *Trends Mol. Med.* **2002**, *8*, 17-23.

11. Floor, S. L.; Dumont, J. E.; Maenhaut, C.; Raspe, E., Hallmarks of cancer: of all cancer cells, all the time? *Trends Mol. Med.* **2012**, *18*, 509-515.
12. Levitzki, A., Tyrosine kinase inhibitors: Views of selectivity, sensitivity, and clinical performance. *Annu. Rev. Pharmacol. Toxicol.* **2013**, *53*, 161-185.
13. Arnold, D.; Tabernero, J. Antiangiogenic yyrosine kinase inhibition: How do we optimize treatment for metastatic colorectal cancer? *J. OncoPathol.* **2013**, *1*, 11-20.
14. Shibuya, M. Vascular endothelial growth factor and its receptor system: physiological functions in angiogenesis and pathological roles in various diseases. *J. Biochem.* **2013**, *153*, 13-19.
15. Holmes, K.; Roberts, O. L.; Thomas, A. M.; Cross, M. J. Vascular endothelial growth factor receptor-2: Structure, function, intracellular signalling and therapeutic inhibition. *Cell. Signal.* **2007**, *19*, 2003-2012.
16. Musumeci, F.; Radi, M.; Brullo, C.; Schenone, S. Vascular endothelial growth factor (VEGF) receptors: Drugs and new inhibitors. *J. Med. Chem.* **2012**, *55*, 10797-10822.
17. Zhang, J.; Shan, Y.; Pan, X.; He, L. Recent advances in antiangiogenic agents with VEGFR as target. *Mini Rev. Med. Chem.* **2011**, *11*, 920-946.
18. Cook, K. M.; Figg, W. D. Angiogenesis inhibitors: current strategies and future prospects. *CA Cancer J. Clin.* **2010**, *60*, 222-243.
19. Scagliotti, G.; Govindan, R. Targeting angiogenesis with multitargeted tyrosine kinase inhibitors in the treatment of non-small cell lung cancer. *Oncologist* **2010**, *15*, 436-446.
20. Patel, R.; Y. Leung, H. Targeting the EGFR-family for therapy: Biological challenges and clinical perspective. *Curr. Pharm.Des.* **2012**, *18*, 2672-2679.

21. Seshacharyulu, P.; Ponnusamy, M. P.; Haridas, D.; Jain, M.; Ganti, A. K.; Batra, S. K. Targeting the EGFR signaling pathway in cancer therapy. *Expert Opin. Ther. Targets* **2012**, *16*, 15-31.
22. Mendrola, J. M.; Shi, F.; Park, J. H.; Lemmon, M. A. Receptor tyrosine kinases with intracellular pseudokinase domains. *Biochem. Soc. Trans.* **2013**, *41*, 1029-1036.
23. Liao, J. J.; Andrews, R. C. Targeting protein multiple conformations: a structure-based strategy for kinase drug design. *Curr. Top. Med. Chem.* **2007**, *7*, 1394-1407.
24. Morphy, R. Selectively nonselective kinase inhibition: Striking the right balance. *J. Med. Chem.* **2009**, *53*, 1413-1437.
25. Liu, Y.; Gray, N. S. Rational design of inhibitors that bind to inactive kinase conformations. *Nat. Chem. Biol.* **2006**, *2*, 358-364.
26. Dumontet, C.; Jordan, M. A. Microtubule-binding agents: A dynamic field of cancer therapeutics. *Nat. Rev. Drug Discov.* **2010**, *9*, 790-803.
27. Katsetos, C. D.; Draber, P. Tubulins as therapeutic targets in cancer: From bench to bedside. *Curr. Pharm. Des.* **2012**, *18*, 2778-2792.
28. Jordan, M. A.; Wilson, L. Microtubules as a target for anticancer drugs. *Nat. Rev. Cancer* **2004**, *4*, 253-265.
29. Bowne-Anderson, H.; Zanic, M.; Kauer, M.; Howard, J. Microtubule dynamic instability: a new model with coupled GTP hydrolysis and multistep catastrophe. *BioEssays* **2013**, *35*, 452-461.
30. Etienne-Manneville, S. From signaling pathways to microtubule dynamics: The key players. *Curr. Opin. Cell Biol.* **2010**, *22*, 104-111.

31. Quiniou, E.; Guichard, P.; Perahia, D.; Marco, S.; Mouawad, L. An atomistic view of microtubule stabilization by GTP. *Structure* **2013**, *21*, 833-843.
32. Howard, J.; Hyman, A. A. Growth, fluctuation and switching at microtubule plus ends. *Nat. Rev. Mol. Cell Biol.* **2009,** *10*, 569-574.
33. Gardner, M. K.; Zanic, M.; Howard, J. Microtubule catastrophe and rescue. *Curr. Opin. Cell Biol.* **2013**, *25*, 14-22.
34. Wilson, L.; Panda, D.; Ann Jordan, M. Modulation of Microtubule Dynamics by Drugs : A Paradigm for the Actions of Cellular Regulators. *Cell Struct.Funct.* **1999**, *24*, 329-335.
35. Kavallaris, M., Microtubules and resistance to tubulin-binding agents. *at. Rev. Cancer* **2010**, *10*, 194-204.
36. Jordan, M. A.; Wilson, L., Microtubules as a target for anticancer drugs. *Nat. Rev. Cancer* **2004**, *4*, 253-265.
37. Amos, L. A. What tubulin drugs tell us about microtubule structure and dynamics. *Semin. Cell Dev. Biol.* **2011**, *22*, 916-926.
38. McGrogan, B. T.; Gilmartin, B.; Carney, D. N.; McCann, A. Taxanes, microtubules and chemoresistant breast cancer. *Biochim. Biophys. Acta.* **2008**, *1785*, 96-132.
39. Field, Jessica J.; Díaz, José F.; Miller, John H., The binding sites of microtubule-stabilizing agents. *Chem. Biol.* **2013**, *20*, 301-315.
40. Lu, Y.; Chen, J.; Xiao, M.; Li, W.; Miller, D., An overview of tubulin inhibitors that interact with the colchicine binding site. *Pharm. Res.* **2012**, *29*, 2943-2971.
41. Mita, M. M.; Sargsyan, L.; Mita, A. C.; Spear, M. Vascular-disrupting agents in oncology. *Expert Opin. Investig. Drugs* **2013**, *22*, 317-328.

42. Hollebecque, A.; Massard, C.; Soria, J. C., Vascular disrupting agents: A delicate balance between efficacy and side effects. *Curr. Opin. Oncol.* **2012**, *24*, 305-315.

43. Tozer, G. M.; Prise, V. E.; Wilson, J.; Cemazar, M.; Shan, S.; Dewhirst, M. W.; Barber, P. R.; Vojnovic, B.; Chaplin, D. J. Mechanisms associated with tumor vascular shut-down induced by combretastatin A-4 phosphate: Intravital microscopy and measurement of vascular permeability. *Cancer Res.* **2001**, *61*, 6413-6422.

44. Griggs, J.; Metcalfe, J. C.; Hesketh, R. Targeting tumour vasculature: The development of combretastatin A4. *Lancet Oncol.* **2001**, *2*, 82-87.

45. Tozer, G. M.; Kanthou, C.; Parkins, C. S.; Hill, S. A. The biology of the combretastatins as tumour vascular targeting agents. *Int. J. Exp. Pathol.* **2002**, *83*, 21-38.

46. Prise, V. E.; Honess, D. J.; Stratford, M. R.; Wilson, J.; Tozer, G. M. The vascular response of tumor and normal tissues in the rat to the vascular targeting agent, combretastatin A-4-phosphate, at clinically relevant doses. *Int. J. Oncol.* **2002**, *21*, 717-726.

47. Davis, P. D.; Dougherty, G. J.; Blakey, D. C.; Galbraith, S. M.; Tozer, G. M.; Holder, A. L.; Naylor, M. A.; Nolan, J.; Stratford, M. R.; Chaplin, D. J.; Hill, S. A. ZD6126: A novel vascular-targeting agent that causes selective destruction of tumor vasculature. *Cancer Res.* **2002**, *62*, 7247-7253.

48. Jordan, A.; Hadfield, J. A.; Lawrence, N. J.; McGown, A. T. Tubulin as a target for anticancer drugs: agents which interact with the mitotic spindle. *Med. Res. Rev* **1998**, *18*, 259-296.

49. Ballatore, C.; Brunden, K. R.; Huryn, D. M.; Trojanowski, J. Q.; Lee, V. M. Y.; Smith, A. B. Microtubule stabilizing agents as potential treatment for alzheimer's disease and related neurodegenerative tauopathies. *J. Med. Chem.* **2012**, *55*, 8979-8996.

50. Kavallaris, M. Microtubules and resistance to tubulin-binding agents. *Nat. Rev. Cancer* **2010**, *10*, 194-204.

51. Ganguly, A.; Cabral, F. New insights into mechanisms of resistance to microtubule inhibitors. *Biochim. Biophys. Acta.* **2011**, *1816*, 164-171.

52. Fojo, A. T.; Menefee, M. Microtubule targeting agents: Basic mechanisms of multidrug resistance (MDR). *Semin. Oncol.* **2005**, *32*, S3-8.

53. Gangjee, A.; Zhao, Y.; Lin, L.; Raghavan, S.; Roberts, E. G.; Risinger, A. L.; Hamel, E.; Mooberry, S. L. Synthesis and discovery of water-soluble microtubule targeting agents that bind to the colchicine site on tubulin and circumvent Pgp mediated resistance. *J. Med. Chem.* **2010**, *53*, 8116-8128.

54. Lhomme, C.; Joly, F.; Walker, J. L.; Lissoni, A. A.; Nicoletto, M. O.; Manikhas, G. M.; Baekelandt, M. M.; Gordon, A. N.; Fracasso, P. M.; Mietlowski, W. L.; Jones, G. J.; Dugan, M. H. Phase III study of valspodar (PSC 833) combined with paclitaxel and carboplatin compared with paclitaxel and carboplatin alone in patients with stage IV or suboptimally debulked stage III epithelial ovarian cancer or primary peritoneal cancer. *J. Clin. Oncol.* **2008**, *26*, 2674-2682.

55. Kuttesch, J. F.; Parham, D. M.; Luo, X.; Meyer, W. H.; Bowman, L.; Shapiro, D. N.; Pappo, A. S.; Crist, W. M.; Beck, W. T.; Houghton, P. J. P-glycoprotein expression

at diagnosis may not be a primary mechanism of therapeutic failure in childhood rhabdomyosarcoma. *J Clin Oncol.* **1996**, *14*, 886-900.

56. Zhang, C. C.; Yang, J. M.; Bash-Babula, J.; White, E.; Murphy, M.; Levine, A. J.; Hait, W. N. DNA damage increases sensitivity to vinca alkaloids and decreases sensitivity to taxanes through p53-dependent repression of microtubule-associated protein 4. *Cancer Res.* **1999**, *59*, 3663-3670.
57. Kavallaris, M.; Tait, A. S.; Walsh, B. J.; He, L.; Horwitz, S. B.; Norris, M. D.; Haber, M. Multiple microtubule alterations are associated with Vinca alkaloid resistance in human leukemia cells. *Cancer Res.* **2001**, *61*, 5803-5809.
58. Don, S.; Verrills, N. M.; Liaw, T. Y.; Liu, M. L.; Norris, M. D.; Haber, M.; Kavallaris, M. Neuronal-associated microtubule proteins class III beta-tubulin and MAP2c in neuroblastoma: Role in resistance to microtubule-targeted drugs. *Mol. Cancer Ther.* **2004**, *3*, 1137-1146.
59. Seve, P.; Dumontet, C. Is class III beta-tubulin a predictive factor in patients receiving tubulin-binding agents? *Lancet Oncol.* **2008**, *9*, 168-175.
60. Gangjee, A.; Zhao, Y.; Hamel, E.; Westbrook, C.; Mooberry, S. L. Synthesis and biological activities of (*R*)- and (*S*)-*N*-(4-methoxyphenyl)-*N*,2,6-trimethyl-6,7-dihydro-5*H*-cyclopenta[*d*]pyrimidin-4-a minium chloride as potent cytotoxic antitubulin agents. *J. Med. Chem.* **2011**, *54*, 6151-6155.
61. Freedman, H.; Huzil, J. T.; Luchko, T.; Luduena, R. F.; Tuszynski, J. A. Identification and characterization of an intermediate taxol binding site within microtubule nanopores and a mechanism for tubulin isotype binding selectivity. *J. Chem. Inf. Model* **2009**, *49*, 424-436.

62. Gan, P. P.; Pasquier, E.; Kavallaris, M. Class III beta-tubulin mediates sensitivity to chemotherapeutic drugs in non small cell lung cancer. *Cancer Res.* **2007**, *67*, 9356-9363.

63. Cicchillitti, L.; Penci, R.; Di Michele, M.; Filippetti, F.; Rotilio, D.; Donati, M. B.; Scambia, G.; Ferlini, C. Proteomic characterization of cytoskeletal and mitochondrial class III beta-tubulin. *Mol. Cancer Ther.* **2008**, *7*, 2070-2079.

64. Raspaglio, G.; Filippetti, F.; Prislei, S.; Penci, R.; De Maria, I.; Cicchillitti, L.; Mozzetti, S.; Scambia, G.; Ferlini, C. Hypoxia induces class III beta-tubulin gene expression by HIF-1alpha binding to its 3' flanking region. *Gene* **2008**, *409*, 100-108.

65. Katsetos, C. D.; Draberova, E.; Legido, A.; Dumontet, C.; Draber, P. Tubulin targets in the pathobiology and therapy of glioblastoma multiforme. I. Class III beta-tubulin. *J. Cell Physiol.* **2009**, *221*, 505-513.

66. Markman, M. Combination cytotoxic and antiangiogenic therapy in the management of epithelial ovarian cancer. *Comb. Prod. Ther.* **2012**, *1*, 1-7.

67. Bar, J.; Onn, A. Combined anti-proliferative and anti-angiogenic strategies for cancer. *Expert Opin. Pharmacother.* **2008**, *9*, 701-715.

68. Bocci, G.; Loupakis, F. The possible role of chemotherapy in antiangiogenic drug resistance. *Med. Hypotheses* **2012**, *78*, 646-648.

69. Murray, A.; Little, S. J.; Stanley, P.; Maraveyas, A.; Cawkwell, L. Sorafenib enhances the in vitro anti-endothelial effects of low dose (metronomic) chemotherapy. *Oncol. Rep.* **2010**, *24*, 1049-1058.

70. Blansfield, J. A.; Caragacianu, D.; Alexander, H. R., 3rd; Tangrea, M. A.; Morita, S. Y.; Lorang, D.; Schafer, P.; Muller, G.; Stirling, D.; Royal, R. E.; Libutti, S. K.

Combining agents that target the tumor microenvironment improves the efficacy of anticancer therapy. *Clin. Cancer Res.* **2008**, *14*, 270-280.

71. Naganuma, Y.; Choijamts, B.; Shirota, K.; Nakajima, K.; Ogata, S.; Miyamoto, S.; Kawarabayashi, T.; Emoto, M. Metronomic doxifluridine chemotherapy combined with the anti-angiogenic agent TNP-470 inhibits the growth of human uterine carcinosarcoma xenografts. *Cancer Sci.* **2011**, *102*, 1545-1552.
72. Zhou, F.; Hu, J.; Shao, J. H.; Zou, S. B.; Shen, S. L.; Luo, Z. Q. Metronomic chemotherapy in combination with antiangiogenic treatment induces mosaic vascular reduction and tumor growth inhibition in hepatocellular carcinoma xenografts. *J. Cancer Res. Clin. Oncol.* **2012**, *138*, 1879-1890.
73. Jain, R. K. Normalization of tumor vasculature: An emerging concept in antiangiogenic therapy. *Science* **2005**, *307*, 58-62.
74. Goel, S.; Duda, D. G.; Xu, L.; Munn, L. L.; Boucher, Y.; Fukumura, D.; Jain, R. K. Normalization of the vasculature for treatment of cancer and other diseases. *Physiol. Rev.* **2011**, *91*, 1071-1121.
75. Fukumura, D.; Jain, R. K. Tumor microvasculature and microenvironment: targets for anti-angiogenesis and normalization. *Microvasc. Res.* **2007**, *74*, 72-84.
76. Fukumura, D.; Jain, R. K. Tumor microenvironment abnormalities: causes, consequences, and strategies to normalize. *J. Cell. Biochem.* **2007**, *101*, 937-949.
77. Batchelor, T. T.; Sorensen, A. G.; di Tomaso, E.; Zhang, W. T.; Duda, D. G.; Cohen, K. S.; Kozak, K. R.; Cahill, D. P.; Chen, P. J.; Zhu, M.; Ancukiewicz, M.; Mrugala, M. M.; Plotkin, S.; Drappatz, J.; Louis, D. N.; Ivy, P.; Scadden, D. T.; Benner, T.; Loeffler, J. S.; Wen, P. Y.; Jain, R. K. AZD2171, a pan-VEGF receptor tyrosine

kinase inhibitor, normalizes tumor vasculature and alleviates edema in glioblastoma patients. *Cancer Cell.* **2007**, *11*, 83-95.

78. Tong, R. T.; Boucher, Y.; Kozin, S. V.; Winkler, F.; Hicklin, D. J.; Jain, R. K. Vascular normalization by vascular endothelial growth factor receptor 2 blockade induces a pressure gradient across the vasculature and improves drug penetration in tumors. *Cancer Res.* **2004**, *64*, 3731-3736.
79. Yoshizawa, Y.; Ogawara, K.-i.; Fushimi, A.; Abe, S.; Ishikawa, K.; Araki, T.; Molema, G.; Kimura, T.; Higaki, K. Deeper penetration into tumor tissues and enhanced in vivo antitumor activity of liposomal paclitaxel by pretreatment with angiogenesis inhibitor SU5416. *Mol. Pharm.* **2012**, *9*, 3486-3494.
80. Huber, P. E.; Bischof, M.; Jenne, J.; Heiland, S.; Peschke, P.; Saffrich, R.; Grone, H. J.; Debus, J.; Lipson, K. E.; Abdollahi, A. Trimodal cancer treatment: beneficial effects of combined antiangiogenesis, radiation, and chemotherapy. *Cancer Res.* **2005**, *65*, 3643-55.
81. Costantino, L.; Barlocco, D. Designed multiple ligands: Basic research vs clinical outcomes. *Curr. Med. Chem.* **2012**, *19*, 3353-3387.
82. Melisi, D.; Piro, G.; Tamburrino, A.; Carbone, C.; Tortora, G. Rationale and clinical use of multitargeting anticancer agents. *Curr. Opin. Pharmacol.* **2013**, *13*, 536-542.
83. Arooj, M.; Sakkiah, S.; Cao, G. p.; Lee, K. W. An innovative strategy for dual inhibitor design and its application in dual inhibition of human thymidylate synthase and dihydrofolate reductase enzymes. *PLoS ONE* **2013**, *8*, e60470.
84. Azmi, A. S. Network pharmacology for cancer drug discovery: Are we there yet? *Future Med. Chem.* **2012**, *4*, 939-941.

85. Bischof, M.; Abdollahi, A.; Gong, P.; Stoffregen, C.; Lipson, K. E.; Debus, J. U.; Weber, K. J.; Huber, P. E. Triple combination of irradiation, chemotherapy (pemetrexed), and VEGFR inhibition (SU5416) in human endothelial and tumor cells. *Int. J. Radiat. Oncol. Biol. Phys.* **2004**, *60*, 1220-1232.

86. Liu, J.; Guo, W.; Xu, B.; Ran, F.; Chu, M.; Fu, H.; Cui, J. Angiogenesis inhibition and cell cycle arrest induced by treatment with Pseudolarix acid B alone or combined with 5-fluorouracil. *Acta Biochim. Biophys. Sin.* **2012**, *44*, 490-502.

87. Bello, E.; Taraboletti, G.; Colella, G.; Zucchetti, M.; Forestieri, D.; Licandro, S. A.; Berndt, A.; Richter, P.; D'Incalci, M.; Cavalletti, E.; Giavazzi, R.; Camboni, G.; Damia, G. The tyrosine kinase inhibitor E-3810 combined with paclitaxel inhibits the growth of advanced-stage triple-negative breast cancer xenografts. *Mol. Cancer Ther.* **2013**, *12*, 131-140.

88. Boere, I. A.; Hamberg, P.; Sleijfer, S. It takes two to tango: Combinations of conventional cytotoxics with compounds targeting the vascular endothelial growth factor-vascular endothelial growth factor receptor pathway in patients with solid malignancies. *Cancer Sci.* **2010**, *101*, 7-15.

89. Jo, M. Y.; Kim, Y. G.; Kim, Y.; Lee, S. J.; Kim, M. H.; Joo, K. M.; Kim, H. H.; Nam, D. H. Combined therapy of temozolomide and ZD6474 (vandetanib) effectively reduces glioblastoma tumor volume through anti-angiogenic and anti-proliferative mechanisms. *Mol. Med. Rep.* **2012**, *6*, 88-92.

90. Moschetta, M.; Cesca, M.; Pretto, F.; Giavazzi, R. Angiogenesis inhibitors: Implications for combination with conventional therapies. *Curr. Pharm. Des.* **2010**, *16*, 3921-3931.

91. Gangjee, A.; Zeng, Y.; Ihnat, M.; Warnke, L. A.; Green, D. W.; Kisliuk, R. L.; Lin, F.-T. Novel 5-substituted, 2,4-diaminofuro[2,3-*d*]pyrimidines as multireceptor tyrosine kinase and dihydrofolate reductase inhibitors with antiangiogenic and antitumor activity. *Bioorg. Med. Chem.* **2005**, *13*, 5475-5491.

92. Gangjee, A.; Li, W.; Lin, L.; Zeng, Y.; Ihnat, M.; Warnke, L. A.; Green, D. W.; Cody, V.; Pace, J.; Queener, S. F. Design, synthesis, and X-ray crystal structures of 2,4-diaminofuro[2,3-*d*]pyrimidines as multireceptor tyrosine kinase and dihydrofolate reductase inhibitors. *Bioorg. Med. Chem.* **2009**, *17*, 7324-7336.

93. Gangjee, A.; Zaware, N.; Raghavan, S.; Ihnat, M.; Shenoy, S.; Kisliuk, R. L. Single agents with designed combination chemotherapy potential: Synthesis and evaluation of substituted pyrimido[4,5-*b*]indoles as receptor tyrosine kinase and thymidylate synthase inhibitors and as antitumor agents. *J. Med. Chem.* **2010**, *53*, 1563-1578.

94. Gangjee, A.; Zhao, Y.; Ihnat, M. A.; Thorpe, J. E.; Bailey-Downs, L. C.; Kisliuk, R. L. Novel tricyclic indeno[2,1-*d*]pyrimidines with dual antiangiogenic and cytotoxic activities as potent antitumor agents. *Bioorg. Med. Chem.* **2012**, *20*, 4217-4225.

95. Montgomery, J. A.; Laseter, A. G. The use of enamines in the synthesis of heterocycles. *J. Het. Chem.* **1972**, *9*, 1077-1079.

96. Xu, L.; Lewis, I. R.; Davidsen, S. K.; Summers, J. B. Transition metal catalyzed synthesis of 5-azaindoles. *Tetrahedron Lett.* **1998**, *39*, 5159-5162.

97. Zhao, L.; Tao, K.; Li, H.; Zhang, J., Practical one-pot protocol for the syntheses of 2-chloro-pyrrolo[3,2-*d*]pyrimidines. *Tetrahedron* **2011**, *67*, 2803-2806.

98. Furneaux, R. H.; Tyler, P. C. Improved syntheses of 3*H*,5*H*-pyrrolo[3,2-*d*]pyrimidines. *J. Org. Chem.* **1999**, *64*, 8411-8412.

99. Taylor, E. C.; Young, W. B. Pyrrolo[3,2-*d*]pyrimidine folate analogs: "Inverted" analogs of the cytotoxic agent LY231514. *J. Org. Chem.* **1995**, *60*, 7947-7952.

100. Sokolova, V. N.; Modnikova, G. A.; Novitskii, K. Y.; Shcherbakova, L. I.; Pershchin, G. N.; Zykova, T. N. Study of a pyrrole [3,2-*d*]pyrimidine series. II. *Pharm. Chem. J.* **1974**, *8*, 13-16.

101. Murray, R. E.; Zweifel, G. Preparation of phenyl cyanate and its utilization for the synthesis of α,β-unsaturated nitriles. *Synthesis* **1980**, *1980*, 150-151.

102. Chen, N.; Lu, Y.; Gadamasetti, K.; Hurt, C. R.; Norman, M. H.; Fotsch, C. A short, facile synthesis of 5-substituted 3-amino-1*H*-pyrrole-2-carboxylates. *J. Org. Chem.* **2000**, *65*, 2603-2605.

103. Elliott, A. J.; Morris, P. E.; Petty, S. L.; Williams, C. H. An improved synthesis of 7-substituted pyrrolo[3,2-*d*]pyrimidines. *J. Org. Chem.* **1997**, *62*, 8071-8075.

104. Norman, M. H.; Chen, N.; Chen, Z.; Fotsch, C.; Hale, C.; Han, N.; Hurt, R.; Jenkins, T.; Kincaid, J.; Liu, L.; Lu, Y.; Moreno, O.; Santora, V. J.; Sonnenberg, J. D.; Karbon, W. Structure−activity relationships of a series of pyrrolo[3,2-*d*]pyrimidine derivatives and related compounds as neuropeptide Y5 receptor antagonists. *J. Med. Chem.* **2000**, *43*, 4288-4312.

105. Gangjee, A.; Li, W.; Yang, J.; Kisliuk, R. L. Design, synthesis, and biological evaluation of classical and nonclassical 2-amino-4-oxo-5-substituted-6-methylpyrrolo[3,2-*d*]pyrimidines as dual thymidylate synthase and dihydrofolate reductase inhibitors. *J. Med. Chem.* **2007**, *51*, 68-76.

106. Modnikova, G. A.; Titkova, R. M.; Glushkov, R. G.; Sokolova, A. S.; Silin, V. A.; Chernov, V. A. Synthesis and biological activity of aminopyrrolo[3,2-*d*]pyrimidines. *Pharm. Chem. J.* **1988**, *22*, 135-141.

107. Venugopalan, B.; Desai, P. D.; De Souza, N. J., Synthesis of 6,7-dimethoxypyrimido[4,5-*b*]-indoles as potential antihypertensive agents. *J. Het. Chem.* **1988**, *25*, 1633-1639.

108. Semeraro, T.; Mugnaini, C.; Corelli, F. Preparation of a set of 4,5-dihydro-3*H*-pyrrolo[3,2-*d*]pyrimidin-4-ones as potential Hsp90 ligands. *Tetrahedron Lett.* **2008**, *49*, 5965-5967.

109. Sun, C. L.; Li, X.; Zhu, Y. Preparation of aminopteridinone derivatives and analogs for use as HSP90 inhibitors. WO2009139834A1, **2009**.

110. Kostlan, C. R.; Sircar, J. C. Preparation and testing of aralkyldeazaguanines as immunosuppressants. EP260491A1, **1988**.

111. Elliott, A. J.; Kotian, P. L.; Montgomery, J. A.; Walsh, D. A. Synthesis of pyrrolo[3,2-*d*]pyrimidines (9-deazaguanines) by reductive cyclodeamination reactions. *Tetrahedron Lett.* **1996**, *37*, 5829-5830.

112. Shih, H.; Cottam, H. B.; Carson, D. A. Facile synthesis of 9-substituted 9-deazapurines as potential purine nucleoside phosphorylase inhibitors. *Chem. Pharm. Bull.* **2002**, *50*, 364-367.

113. Unangst, P. C., Pyrido[1′,2′:1,2]pyrimido[5,4-*d*]indoles. A new heterocyclic ring system. *J. Het. Chem.* **1983**, *20*, 495-499.

114. Shestakov, A. S.; Shikhaliev, K. S.; Sidorenko, O. E.; Kartsev, V. G.; Simakov, S. V. Methyl 3-amino-1*H*-indole-2-carboxylates in the synthesis of 5*H*-pyrimido[5,4-*b*]indole derivatives. *Russ. J. Org. Chem.* **2009**, *45*, 777-782.

115. Showalter, H. D. H.; Bridges, A. J.; Zhou, H.; Sercel, A. D.; McMichael, A.; Fry, D. W. Tyrosine kinase inhibitors. 16. 6,5,6-tricyclic benzothieno[3,2-*d*]pyrimidines and pyrimido[5,4-*b*]- and -[4,5-*b*]indoles as potent inhibitors of the epidermal growth factor receptor tyrosine kinase. *J. Med. Chem.* **1999**, *42* , 5464-5474.

116. Biswas, S.; Batra, S. One-step synthesis of 2-amino-5*H*-pyrimido[5,4-*b*]indoles, substituted 2-(1,3,5-triazin-2-yl)-1*H*-indoles, and 1,3,5-triazines from aldehydes. *Eur. J. Org. Chem.* **2012**, 18, 3492-3499.

117. Kumar, A. S.; Amulya Rao, P. V.; Nagarajan, R., Synthesis of pyrido[2,3-*b*]indoles and pyrimidoindoles *via* Pd-catalyzed amidation and cyclization. *Org. Biomol. Chem.* **2012**, *10*, 5084-5093.

118. Matasi, J. J.; Caldwell, J. P.; Hao, J.; Neustadt, B.; Arik, L.; Foster, C. J.; Lachowicz, J.; Tulshian, D. B. The discovery and synthesis of novel adenosine receptor (A2A) antagonists. *Bioorg. Med. Chem. Lett.* **2005**, *15*, 1333-1336.

119. Morris, P. E.; Elliott, A. J.; Montgomery, J. A. New syntheses of 7-substituted-2-aminothieno- and furo[3,2-*d*]pyrimidines. *J. Het. Chem.* **1999**, *36*, 423-427.

120. Heffron, T. P.; Wei, B. Q.; Olivero, A.; Staben, S. T.; Tsui, V.; Do, S.; Dotson, J.; Folkes, A. J.; Goldsmith, P.; Goldsmith, R.; Gunzner, J.; Lesnick, J.; Lewis, C.; Mathieu, S.; Nonomiya, J.; Shuttleworth, S.; Sutherlin, D. P.; Wan, N. C.; Wang, S.; Wiesmann, C.; Zhu, B.-Y. Rational design of phosphoinositide 3-kinase α inhibitors

that exhibit selectivity over the phosphoinositide 3-kinase β isoform. *J. Med. Chem.* **2011**, *54*, 7815-7833.

121. Blagg, J. 2-Amino-6-oxopurine derivatives as GTP cyclohydrolase 1 inhibitors and their preparation, pharmaceutical compositions and use in the treatment of pain. WO2011035009A1, **2011**.

122. Babu, Y. S.; Chand, P.; Kotian, P. L.; Kumar, V. S. Preparation of piperidine derivatives as immunosuppressant for the treatment of diseases associated with pathologic JAK3 activation. WO2010014930A2, **2010**.

123. Carceller, G. E.; Medina, F. E. M.; Virgili, B. M.; Marti, V. J. Preparation of furo[3,2-*d*]pyrimidine derivatives as H4 receptor antagonists. WO2009115496A1, 2009.

124. Lisowski, V.; Vu, D. N.; Feng, X.; Rault, S. Synthesis of new ethyl 3-amino-4-arylfuran-2-carboxylates. *Synthesis* **2002**, 0753-0756.

125. Tumey, L. N.; Bom, D.; Huck, B.; Gleason, E.; Wang, J.; Silver, D.; Brunden, K.; Boozer, S.; Rundlett, S.; Sherf, B.; Murphy, S.; Dent, T.; Leventhal, C.; Bailey, A.; Harrington, J.; Bennani, Y. L., The identification and optimization of a N-hydroxy urea series of flap endonuclease 1 inhibitors. *Bioorg. Med. Chem. Lett.* **2005**, *15*, 277-281.

126. Tumey, L. N.; Bennani, Y.; Huck, B.; Bom, D. C. Preparation of fused 3-hydroxypyrimidine-2,4-diones as inhibitors of flap endonuclease. WO2006014647A2, 2006.

127. Hertzog, D. L.; Al-Barazanji, K. A.; Bigham, E. C.; Bishop, M. J.; Britt, C. S.; Carlton, D. L.; Cooper, J. P.; Daniels, A. J.; Garrido, D. M.; Goetz, A. S.; Grizzle, M.

K.; Guo, Y. C.; Handlon, A. L.; Ignar, D. M.; Morgan, R. O.; Peat, A. J.; Tavares, F. X.; Zhou, H. The discovery and optimization of pyrimidinone-containing MCH R1 antagonists. *Bioorg. Med. Chem. Lett.* **2006**, *16*, 4723-4727.

128. Theoclitou, M.-E.; Aquila, B.; Block, M. H.; Brassil, P. J.; Castriotta, L.; Code, E.; Collins, M. P.; Davies, A. M.; Deegan, T.; Ezhuthachan, J.; Filla, S.; Freed, E.; Hu, H.; Huszar, D.; Jayaraman, M.; Lawson, D.; Lewis, P. M.; Nadella, M. V. P.; Oza, V.; Padmanilayam, M.; Pontz, T.; Ronco, L.; Russell, D.; Whitston, D.; Zheng, X. Discovery of (+)-*N*-(3-aminopropyl)-*N*-[1-(5-benzyl-3-methyl-4-oxo-[1,2]thiazolo[5,4-*d*]pyrimidin-6-yl)-2-methylpropyl]-4-methylbenzamide (AZD4877), a kinesin spindle protein inhibitor and potential anticancer agent. *J. Med. Chem.* **2011**, *54*, 6734-6750.

129. Chao, B.; Lin, S.; Ma, Q.; Lu, D.; Hu, Y. Copper(I)-mediated cascade reactions: An efficient approach to the synthesis of functionalized benzofuro[3,2-*d*]pyrimidines. *Org. Lett.* **2012**, *14* , 2398-2401.

130. Liu, J.; Fitzgerald, A. E.; Mani, N. S.Facile Assembly of Fused Benzo[4,5]furo Heterocycles. *J. Org. Chem.* **2008**, *73*, 2951-2954.

131. Cramp, S.; Dyke, H. J.; Higgs, C.; Clark, D. E.; Gill, M.; Savy, P.; Jennings, N.; Price, S.; Lockey, P. M.; Norman, D.; Porres, S.; Wilson, F.; Jones, A.; Ramsden, N.; Mangano, R.; Leggate, D.; Andersson, M.; Hale, R. Identification and hit-to-lead exploration of a novel series of histamine H4 receptor inverse agonists. *Bioorg. Med. Chem. Lett.* **2010**, *20*, 2516-2519.

132. Samarghandian, S.; Shibuya, M. Vascular endothelial growth factor receptor family in ascidians, *Halocynthia roretzi* (Sea Squirt). Its high expression in circulatory system-containing tissues. *Int. J. Mol. Sci.* **2013**, *14*, 4841-4853.

133. Wu, J. M.; Staton, C. A. Anti-angiogenic drug discovery: Lessons from the past and thoughts for the future. *Expert Opin. Drug Discov.* **2012**, *7*, 723-743.

134. Tejpar, S.; Prenen, H.; Mazzone, M. Overcoming resistance to antiangiogenic therapies. *Oncologist* **2012**, *17* , 1039-1050.

135. Goel, S.; Wong, A. H.; Jain, R. K. Vascular normalization as a therapeutic strategy for malignant and nonmalignant disease. *Cold Spring Harb. Perspect Med.* **2012**, *2*, a006486.

136. Ma, J.; Chen, C. S.; Blute, T.; Waxman, D. J. Antiangiogenesis enhances intratumoral drug retention. *Cancer Res.* **2011**, *71*, 2675-2685.

137. Winkler, F.; Kozin, S. V.; Tong, R. T.; Chae, S. S.; Booth, M. F.; Garkavtsev, I.; Xu, L.; Hicklin, D. J.; Fukumura, D.; di Tomaso, E.; Munn, L. L.; Jain, R. K., Kinetics of vascular normalization by VEGFR2 blockade governs brain tumor response to radiation: role of oxygenation, angiopoietin-1, and matrix metalloproteinases. *Cancer Cell.* **2004**, *6*, 553-563.

138. Narang, A. S.; Varia, S. Role of tumor vascular architecture in drug delivery. *Adv. Drug Deliv. Rev.* **2011**, *63*, 640-658.

139. Van der Veldt, A. A.; Lubberink, M.; Bahce, I.; Walraven, M.; de Boer, M. P.; Greuter, H. N.; Hendrikse, N. H.; Eriksson, J.; Windhorst, A. D.; Postmus, P. E.; Verheul, H. M.; Serne, E. H.; Lammertsma, A. A.; Smit, E. F. Rapid decrease in

delivery of chemotherapy to tumors after anti-VEGF therapy: Implications for scheduling of anti-angiogenic drugs. *Cancer Cell.* **2012**, *21*, 82-91.

140. Shang, B.; Cao, Z.; Zhou, Q. Progress in tumor vascular normalization for anticancer therapy: challenges and perspectives. *Front. Med.* **2012**, *6*, 67-78.
141. Jain, R. K. Normalizing tumor microenvironment to treat cancer: bench to bedside to biomarkers. *J. Clin. Oncol.* **2013**, *31*, 2205-2218.
142. Ulahannan, S. V.; Brahmer, J. R. Antiangiogenic agents in combination with chemotherapy in patients with advanced non-small cell lung cancer. *Cancer Invest.* **2011**, *29*, 325-337.
143. Bar, J.; Onn, A. Combined anti-proliferative and anti-angiogenic strategies for cancer. *Expert Opin. Pharmacother.* **2008**, *9*, 701-715.
144. O'Connor, P. M.; Jackman, J.; Bae, I.; Myers, T. G.; Fan, S.; Mutoh, M.; Scudiero, D. A.; Monks, A.; Sausville, E. A.; Weinstein, J. N.; Friend, S.; Fornace, A. J.; Kohn, K. W. Characterization of the p53 tumor suppressor pathway in cell lines of the National Cancer Institute anticancer drug screen and correlations with the growth-inhibitory potency of 123 anticancer agents. *Cancer Res.* **1997**, *57*, 4285-4300.
145. Wang, Z.; Sun, Y., Targeting p53 for novel anticancer therapy. *Transl. Oncol.* **2010**, *3*, 1-12.
146. www.clinicalrials.gov.
147. Honore, S.; Kamath, K.; Braguer, D.; Horwitz, S. B.; Wilson, L.; Briand, C.; Jordan, M. A., Synergistic suppression of microtubule dynamics by discodermolide and paclitaxel in non-small cell lung carcinoma cells. *Cancer Res.* **2004**, *64*, 4957-4964.

148. D'Agostino, G.; del Campo, J.; Mellado, B.; Izquierdo, M. A.; Minarik, T.; Cirri, L.; Marini, L.; Perez-Gracia, J. L.; Scambia, G. A multicenter phase II study of the cryptophycin analog LY355703 in patients with platinum-resistant ovarian cancer. *Int. J. Gynecol. Cancer* **2006**, *16*, 71-67.

149. Argyriou, A. A.; Koltzenburg, M.; Polychronopoulos, P.; Papapetropoulos, S.; Kalofonos, H. P. Peripheral nerve damage associated with administration of taxanes in patients with cancer. *Crit. Rev. Oncol. Hematol.* **2008**, *66*, 218-228.

150. Gidding, C. E.; Kellie, S. J.; Kamps, W. A.; de Graaf, S. S. Vincristine revisited. *Crit. Rev. Oncol. Hematol.* **1999,** *29*, 267-287.

151. Markman, M. Managing taxane toxicities. *Support. Care Cancer* **2003**, *11*, 144-147.

152. Cunningham, C.; Appleman, L. J.; Kirvan-Visovatti, M.; Ryan, D. P.; Regan, E.; Vukelja, S.; Bonate, P. L.; Ruvuna, F.; Fram, R. J.; Jekunen, A.; Weitman, S.; Hammond, L. A.; Eder, J. P. Jr. Phase I and pharmacokinetic study of the dolastatin-15 analogue tasidotin (ILX651) administered intravenously on days 1, 3, and 5 every 3 weeks in patients with advanced solid tumors. *Clin.Cancer Res.* **2005**, *11*, 7825-7833.

153. Aghajanian, C.; Burris, H. A., 3rd; Jones, S.; Spriggs, D. R.; Cohen, M. B.; Peck, R.; Sabbatini, P.; Hensley, M. L.; Greco, F. A.; Dupont, J.; O'Connor, O. A., Phase I study of the novel epothilone analog ixabepilone (BMS-247550) in patients with advanced solid tumors and lymphomas. *J. Clin. Oncol.* **2007**, *25*, 1082-1088.

154. Zatloukal, P.; Gervais, R.; Vansteenkiste, J.; Bosquee, L.; Sessa, C.; Brain, E.; Dansin, E.; Urban, T.; Dohollou, N.; Besenval, M.; Quoix, E. Randomized multicenter phase II study of larotaxel (XRP9881) in combination with cisplatin or

gemcitabine as first-line chemotherapy in nonirradiable stage IIIB or stage IV non-small cell lung cancer. *J. Thorac. Oncol.* **2008**, *3*, 894-901.

155. Gangjee, A.; Zhao, Y.; Raghavan, S.; Ihnat, M. A.; Disch, B. C. Design, synthesis and evaluation of 2-amino-4-m-bromoanilino-6-arylmethyl-7*H*-pyrrolo[2,3-*d*]pyrimidines as tyrosine kinase inhibitors and antiangiogenic agents. *Bioorg. Med. Chem.* **2010**, *18*, 5261-5273.

156. Gangjee, A.; Zhao, Y.; Lin, L.; Raghavan, S.; Roberts, E. G.; Risinger, A. L.; Hamel, E.; Mooberry, S. L., Synthesis and discovery of water-soluble microtubule targeting agents that bind to the colchicine site on tubulin and circumvent Pgp mediated resistance. *J. Med. Chem.* **2010**, *53*, 8116-8128.

157. Gangjee, A.; Zhao, Y.; Lin, L.; Raghavan, S.; Roberts, E. G.; Risinger, A. L.; Hamel, E.; Mooberry, S. L., Corrections to synthesis and discovery of water-soluble microtubule targeting agents that bind to the colchicine site on tubulin and circumvent Pgp mediated resistance. *J. Med. Chem.* **2011**, *54*, 913-913.

158. Leonard, G. D.; Fojo, T.; Bates, S. E. The role of ABC transporters in clinical practice. *Oncologist* **2003**, *8* , 411-424.

159. Ling, V. Multidrug resistance. Molecular mechanisms and clinical relevance. *Cancer Chemother. Pharmacol.* **1997**, *40* , S3-S8.

160. Ferrandina, G.; Zannoni, G. F.; Martinelli, E.; Paglia, A.; Gallotta, V.; Mozzetti, S.; Scambia, G.; Ferlini, C. Class III β-tubulin overexpression is a marker of poor clinical outcome in advanced ovarian cancer patients. *Clin. Cancer Res.* **2006**, *12* , 2774-2779.

161. Mozzetti, S.; Ferlini, C.; Concolino, P.; Filippetti, F.; Raspaglio, G.; Prislei, S.; Gallo, D.; Martinelli, E.; Ranelletti, F. O.; Ferrandina, G.; Scambia, G. Class III β-tubulin overexpression is a prominent mechanism of paclitaxel resistance in ovarian cancer patients. *Clin. Cancer Res.* **2005**, *11* , 298-305.

162. Rosell, R.; Scagliotti, G.; Danenberg, K. D.; Lord, R. V. N.; Bepler, G.; Novello, S.; Cooc, J.; Crino, L.; Sanchez, J. J.; Taron, M.; Boni, C.; De, M. F.; Tonato, M.; Marangolo, M.; Gozzelino, F.; Di, C. F.; Rinaldi, M.; Salonga, D.; Stephens, C. Transcripts in pretreatment biopsies from a three-arm randomized trial in metastatic non-small-cell lung cancer. *Oncogene* **2003**, *22* , 3548-3553.

163. Seve, P.; Isaac, S.; Tredan, O.; Souquet, P.-J.; Pacheco, Y.; Perol, M.; Lafanechere, L.; Penet, A.; Peiller, E.-L.; Dumontet, C. Expression of Cclass III β-tubulin is predictive of patient outcome in patients with non-small cell lung cancer receiving vinorelbine-based chemotherapy. *Clin. Cancer Res.* **2005**, *11*, 5481-5486.

164. Tommasi, S.; Mangia, A.; Lacalamita, R.; Bellizzi, A.; Fedele, V.; Chiriatti, A.; Thomssen, C.; Kendzierski, N.; Latorre, A.; Lorusso, V.; Schittulli, F.; Zito, F.; Kavallaris, M.; Paradiso, A. Cytoskeleton and paclitaxel sensitivity in breast cancer: The role of β-tubulins. *Int. J. Cancer* **2007**, *120* , 2078-2085.

165. Oguro, Y.; Miyamoto, N.; Takagi, T.; Okada, K.; Awazu, Y.; Miki, H.; Hori, A.; Kamiyama, K.; Imamura, S. N-Phenyl-N′-[4-(5*H*-pyrrolo[3,2-*d*]pyrimidin-4-yloxy)phenyl]ureas as novel inhibitors of VEGFR and FGFR kinases. *Bioorg. Med. Chem.* **2010**, *18*, 7150-7163.

166. Oguro, Y.; Miyamoto, N.; Okada, K.; Takagi, T.; Iwata, H.; Awazu, Y.; Miki, H.; Hori, A.; Kamiyama, K.; Imamura, S., Design, synthesis, and evaluation of 5-

methyl-4-phenoxy-5*H*-pyrrolo[3,2-*d*]pyrimidine derivatives: Novel VEGFR2 kinase inhibitors binding to inactive kinase conformation. *Bioorg. Med. Chem.* **2010**, *18*, 7260-7273.

167. Awazu, Y.; Mizutani, A.; Nagase, Y.; Iwata, H.; Oguro, Y.; Miki, H.; Imamura, S.; Hori, A., A novel pyrrolo[3, 2-*d*]pyrimidine derivative, as a vascular endothelial growth factor receptor and platelet-derived growth factor receptor tyrosine kinase inhibitor, shows potent antitumor activity by suppression of tumor angiogenesis. *Cancer Sci.* **2012**, *103*, 939-944.
168. Kawakita, Y.; Miwa, K.; Seto, M.; Banno, H.; Ohta, Y.; Tamura, T.; Yusa, T.; Miki, H.; Kamiguchi, H.; Ikeda, Y.; Tanaka, T.; Kamiyama, K.; Ishikawa, T., Design and synthesis of pyrrolo[3,2-*d*]pyrimidine HER2/EGFR dual inhibitors: Improvement of the physicochemical and pharmacokinetic profiles for potent in vivo anti-tumor efficacy. *Bioorg. Med. Chem.* **2012**, *20*, 6171-6180.
169. Gangjee, A.; Zaware, N.; Raghavan, S.; Disch, B. C.; Thorpe, J. E.; Bastian, A.; Ihnat, M. A. Synthesis and biological activity of 5-chloro-*N*4-substituted phenyl-9*H*-pyrimido[4,5-*b*]indole-2,4-diamines as vascular endothelial growth factor receptor-2 inhibitors and antiangiogenic agents. *Bioorg. Med. Chem.* **2013**, *21*, 1857-1864.
170. Gangjee, A.; Zaware, N.; Raghavan, S.; Yang, J.; Thorpe, J. E.; Ihnat, M. A. *N*(4)-(3-Bromophenyl)-7-(substituted benzyl) pyrrolo[2,3-*d*]pyrimidines as potent multiple receptor tyrosine kinase inhibitors: Design, synthesis, and in vivo evaluation. *Bioorg. Med. Chem.* **2012**, *20*, 2444-2454.

171. Huang, D.; Zhou, T.; Lafleur, K.; Nevado, C.; Caflisch, A. Kinase selectivity potential for inhibitors targeting the ATP binding site: A network analysis. *Bioinformatics* **2010**, *26*, 198-204.

172. Miyazaki, Y.; Matsunaga, S.; Tang, J.; Maeda, Y.; Nakano, M.; Philippe, R. J.; Shibahara, M.; Liu, W.; Sato, H.; Wang, L.; Nolte, R. T. Novel 4-amino-furo[2,3-*d*]pyrimidines as Tie-2 and VEGFR2 dual inhibitors. *Bioorg. Med. Chem. Lett.* **2005**, *15*, 2203-2207.

173. Tabernero, J. The role of VEGF and EGFR inhibition: Implications for combining anti–VEGF and anti–EGFR agents. *Mol. Cancer Res.* **2007**, *5*, 203-220.

174. Burger, R. A. Overview of anti-angiogenic agents in development for ovarian cancer. *Gynecol. Oncol.* **2011**, *121*, 230-238.

175. Socinski, M. A. Multitargeted receptor tyrosine kinase inhibition: an antiangiogenic strategy in non-small cell lung cancer. *Cancer Treat. Rev.* **2011**, *37*, 611-617.

176. Ellis, P. M.; Al-Saleh, K. Multitargeted anti-angiogenic agents and NSCLC: Clinical update and future directions. *Crit. Rev. Oncol. Hematol.* **2012**, *84*, 47-58.

177. Denison, T. A.; Bae, Y. H. Tumor heterogeneity and its implication for drug delivery. *J. Control. Release* **2012**, *164*, 187-191.

178. Fisher, R.; Pusztai, L.; Swanton, C. Cancer heterogeneity: implications for targeted therapeutics. *Br. J. Cancer* **2013**, *108*, 479-485.

179. Marusyk, A.; Almendro, V.; Polyak, K. Intra-tumour heterogeneity: A looking glass for cancer? *Nat. rev. Cancer* **2012**, *12*, 323-34.

180. Turner, N. C.; Reis-Filho, J. S. Genetic heterogeneity and cancer drug resistance. *Lancet Oncol.* **2012**, *13*, e178-e185.

181. Antonello, A.; Tarozzi, A.; Morroni, F.; Cavalli, A.; Rosini, M.; Hrelia, P.; Bolognesi, M. L.; Melchiorre, C. Multitarget-directed drug design strategy: A novel molecule designed to block epidermal growth factor receptor (EGFR) and to exert proapoptotic effects. *J. Med. Chem.* **2006**, *49*, 6642-6645.
182. Karpel-Massler, G.; R. Wirtz, C.; Halatsch, M.-E. Drug combinations enhancing the antineoplastic effects of erlotinib in high-grade glioma. *Recent Pat. Anticancer Drug Discov.* **2011**, *6*, 384-394.
183. Zhang, C.; Zhou, S. S.; Li, X. R.; Wang, B. M.; Lin, N. M.; Feng, L. Y.; Zhang, D. Y.; Zhang, L. H.; Wang, J. B.; Pan, J. P. Enhanced antitumor activity by the combination of dasatinib and combretastatin A-4 in vitro and in vivo. *Oncol. Rep.* **2013**, *29*, 2275-2282.
184. Chen, P.; Wang, L.; Liu, B.; Zhang, H.-Z.; Liu, H.-C.; Zou, Z. EGFR-targeted therapies combined with chemotherapy for treating advanced non-small-cell lung cancer: a meta-analysis. *Eur. J. Clin. Pharmacol.* **2011**, *67*, 235-243.
185. Mok, T. S.; Wu, Y.-L.; Thongprasert, S.; Yang, C.-H.; Chu, D.-T.; Saijo, N.; Sunpaweravong, P.; Han, B.; Margono, B.; Ichinose, Y.; Nishiwaki, Y.; Ohe, Y.; Yang, J.-J.; Chewaskulyong, B.; Jiang, H.; Duffield, E. L.; Watkins, C. L.; Armour, A. A.; Fukuoka, M., Gefitinib or carboplatin–paclitaxel in pulmonary adenocarcinoma. *N. Engl. J. Med.* **2009**, *361*, 947-957.
186. Topliss, J. G. A manual method for applying the Hansch approach to drug design. *J. Med. Chem.* **1977**, *20*, 463-469.
187. Gangjee, A.; Namjoshi, O. A.; Ihnat, M. A.; Buchanan, A. The contribution of a 2-amino group on receptor tyrosine kinase inhibition and antiangiogenic activity in 4-

anilinosubstituted pyrrolo[2,3-*d*]pyrimidines. *Bioorg. Med. Chem. Lett.* **2010**, *20*, 3177-3181.

188. Gangjee, A.; Zaware, N.; Raghavan, S.; Yang, J.; Thorpe, J. E.; Ihnat, M. A., *N*4-(3-Bromophenyl)-7-(substituted benzyl) pyrrolo[2,3-*d*]pyrimidines as potent multiple receptor tyrosine kinase inhibitors: Design, synthesis, and in vivo evaluation. *Bioorg. Med. Chem.* **2012**, *20*, 2444-2454.
189. Zhang, J.; Yang, P. L.; Gray, N. S. Targeting cancer with small molecule kinase inhibitors. *Nat. Rev. Cancer* **2009**, *9*, 28-39.
190. Shaw, L. M. The insulin receptor substrate (IRS) proteins: At the intersection of metabolism and cancer. *Cell Cycle* **2011**, *10*, 1750-1756.
191. Hardie, D. G. AMP-activated protein kinase—an energy sensor that regulates all aspects of cell function. *Genes Dev.* **2011**, *25*, 1895-1908.
192. Lemmon, M. A.; Schlessinger, J. Cell signaling by receptor tyrosine kinases. *Cell* **2010**, *141*, 1117-1134.
193. Boyer, S. J. Small molecule inhibitors of KDR (VEGFR2) kinase: An overview of structure activity relationships. *Curr. Top. Med. Chem.* **2002**, *2*, 973-1000.
194. Gangjee, A.; Pavana, R. K.; Ihnat, M. A. Design and synthesis of 7-(3,4,5-trimethoxybenzyl)-*N*4-substituted phenyl-5*H*-pyrrolo[3,2-*d*]pyrimidine-2,4-diamines as receptor tyrosine kinase inhibitors. *American Chemical Society:* **2009**, pp MEDI-366.
195. Gangjee, A.; Zeng, Y.; McGuire, J. J.; Kisliuk, R. L., Synthesis of classical and nonclassical, partially restricted, linear, tricyclic 5-deaza antifolates1. *J. Med. Chem.* **2002**, *45*, 5173-5181.

196. Gangjee, A., *et al.* Unpublished results.

197. Gangjee, A.; Zaware, N.; Devambatla, R. K. V.; Raghavan, S.; Westbrook, C. D.; Dybdal-Hargreaves, N. F.; Hamel, E.; Mooberry, S. L. Synthesis of *N*4-(substituted phenyl)-*N*4-alkyl/desalkyl-9H-pyrimido[4,5-*b*]indole-2,4-diamines and identification of new microtubule disrupting compounds that are effective against multidrug resistant cells. *Bioorg. Med. Chem.* **2013**, *21*, 891-902.

198. Sizova, O. S.; Modnikova, G. A.; Glushkov, R. G.; Solov'eva, N. P.; Ryabokon, N. A.; Chernov, V. A.; Okinshevich, O. V.; Pershin, G. N. Synthesis and biological activity of 4,7-substituted pyrrolo[3,2-*d*]pyrimidines. *Pharm. Chem. J.* **1984**, *18*, 567-571.

199. Haraguchi, K.; Horii, C.; Yoshimura, Y.; Ariga, F.; Tadokoro, A.; Tanaka, H. An access to the β-anomer of 4′-thio-C-ribonucleosides: Hydroboration of 1-C-aryl- or 1-C-heteroaryl-4-thiofuranoid glycals and its regiochemical outcome. *J. Org. Chem.* **2011**, *76*, 8658-8669.

APPENDIX

The biological evaluations of were performed by Dr. Michael Ihnat (Department of Pharmaceutical Sciences, University of Oklahoma College of Pharmacy, Oklahoma City, OK 73117), Dr. Ernest Hamel (Screening Technologies Branch, Developmental Therapeutics Program, Division of Cancer Treatment and Diagnosis, Frederick National Laboratory for Cancer Research, National Cancer Institute, Frederick, MD 21702), Dr. Susan Mooberry (Department of Pharmacology, University of Texas Health Science Center at San Antonio, San Antonio, TX 78229), National Cancer Institute (Developmental Therapeutics Program) and Luceome Biotechnologies (1775 S. Pantano Rd, Suite 100, Tucson, AZ 85710).

Biological evaluations

The EC_{50} (concentration required to cause 50% loss of cellular microtubules) was determined in A-10 cells(1). The effects of the compounds on interphase and mitotic microtubules were evaluated using indirect immunofluorescence techniques, and the EC_{50} values were calculated from a minimum of three experiments.

Antiproliferative effects were evaluated against the drug sensitive MDA-MB-435 melanoma cells using sulforhodamine B assay and the IC_{50} values (concentration required to cause 50% inhibition of proliferation) were calculated.

In experiments with purified tubulin, the control compound was combretastatin A-4 (CSA4), a potent colchicine site agent generously supplied by Dr. G. R. Pettit, Arizona State University, Tempe AZ. Tubulin polymerization was measured by turbidimetry at 350 nm in Beckman DU7400 and DU7500 recording spectrophotometers equipped with

temperature controllers. In brief, 10 μM bovine brain tubulin, purified as described previously (20), was preincubated for 15 min in a 0.24 mL volume at 30°C containing 0.75 M monosodium glutamate (adjusted to pH 6.6 with HCl in a 2 M stock solution), varying compound concentrations, and 4% (v/v) dimethyl sulfoxide (compound solvent). Following the preincubation, which permits detection of activity in slow binding compounds such as colchicinoids (19), samples were chilled on ice, and 10 μL of 10 mM GTP was added (0.4 mM). The addition of GTP is an absolute requirement for assembly under these reaction conditions. All concentrations refer to the final 0.25 mL reaction volume. Samples were transferred to cuvettes held at 0°C in the recording spectrophotometers, and the temperature was jumped to 30°C, which takes less than a minute. Assembly at 30°C was followed for 30 min, and the compound concentration to inhibit extent of assembly after 30 min was determined by interpolation of data obtained with individual compound concentrations. After determining the likely range for the IC_{50} value, 2-4 individual determinations were made, and the average from these determinations are presented in Table 1.

The binding of [^{3}H]colchicine to tubulin was performed by the DEAE-cellulose filter technique (21) with a stack of two filters, as described in detail previously (22). In brief, reaction mixtures contained, in a 0.10 mL volume, 1.0 μM purified tubulin, 5.0 μM [^{3}H]colchicine, potential inhibitor at 5.0 μM, 5% (v/v) dimethyl sulfoxide (the compound solvent), and other components previously found to stabilize the colchicine binding activity of tubulin for prolonged periods at 37°C (23). Incubation was at 37°C for 10 min, at which time samples were diluted with 2 mL of ice-cold water and poured over the DEAE-filters under mild suction, with several rinses of the reaction vessel and of the

filtration chamber. The amount of radiolabel bound to the filters was determined by liquid scintillation counting, and samples containing test compounds were compared to reaction mixtures without compound. The percent inhibition relative to the control was determined for each compound in 2-4 independent experiments.

Table 1. Effects in cellular assays and on purified tubulin

	EC_{50} Microtubule Depolymerization (μM)	MDA-MB-435 IC_{50}±SD (nM)	Inhibition of	
			Tubulin Assembly IC_{50}±SD (μM)	% Colchicine Binding inhibited at 5μM compound concentration
161	1.2	96.6 ± 5.3	10 ± 0.6	
162	1.4	193 ± 5.3		
163	Not Active Up To 10 μM	ND		
164	Not Active Up To 10 μM	ND		
165	Not Active Up To 10 μM	ND		
174	0.22	30.3 ± 2.7	3.1 ± 0.3	65 ± 1
219	8.4	298 ± 19.7		
166	0.23	42.7 ±3.2	3.1 ± 0.08	62 ± 2
CSA4	0.0131	3.47 ± 0.6	1.2 ± 0.01	98 ± 0.3

Table 2. Tumor cell growth inhibition GI_{50} (10^{-8} M) of NCI 60 cell line panel by **161**

Panel/Cell line	GI_{50}	Panel/Cell line	GI_{50}	Panel/Cell line	GI_{50}	Panel/Cell line	GI_{50}
Leukemia	**161**	**Colon Cancer**	**161**	**Melanoma**	**161**	**Renal Cancer**	**161**
CCRF-CEM	33.9	COLO 205	13.4	LOX IMVI	51.2	786-0	44.6
HL-60(TB)	21.7	HCC-2998	12.9	MALME-3M	13.6	A498	4.45
K-562	8.69	HCT-116	29.2	M14	16.7	ACHN	71.2
MOLT-4	40.2	HCT-15	36.3	MDA-MB-435	2.79	CAKI-1	37.2
RPMI-8226	30.1	HT29	18.9	SK-MEL-2	18.5	RXF 393	9.65
SR	4.47	KM12	7.56	SK-MEL-28	405	SN12C	86.3
NSCLC		SW-620	16.5	SK-MEL-5	17.1	TK10	56.6
A549/ATCC	27.1	**CNS Cancer**		UACC-257	37.0	UO-31	43.5
EKVX	35.2	SF-268	58.6	UACC-62	47.4	**Prostate Cancer**	
HOP-62	33.7	SF-295	13.0	**Ovarian cancer**		PC-3	25.9
HOP-92	295	SF-539	25.3	IGROVI	29.5	DU-145	21.2
NCI-H226	55.9	SNB-19	48.9	OVCAR-3	16.0	**Breast Cancer**	
NCI-H23	32.8	SNB-75	24.1	OVCAR-4	252	MCF7	8.67
NCI-H322M	37.2	U251	26.0	OVCAR-5	45.4	MDA-MB-231/ATCC	46.6
NCI-H460	19.1			OVCAR-8	39.2	HS 578T	17.9
NCI-H522	4.56			NCI/ADR-RES	66.9	BT-549	24.7
				SK-OV-3	23.3	MDA-MB-468	11.6

For the vinblastine and GTP binding experiments, ttubulin was freed of unbound nucleotide by preparative gel filtration chromatography on Sephadex G-50 (superfine). Control compounds were CA, a potent inhibitor of colchicine binding to tubulin, and dolastatin 10, a potent inhibitor of both vinblastine binding and nucleotide exchange. Both agents were generously provided by Dr. George R. Pettit, Arizona State University. The 0.3 mL reaction mixtures contained 10 μM (1.0 mg/mL) tubulin, 0.1 M 4-morpholineethane sulfonate (pH 6.9 in a 1.0 M stock solution with NaOH), 0.5 mM $MgCl_2$, 6% DMSO, either 10 μM [^{3}H]vinblastine (from GE Healthcare) or 50 μM [8-^{14}C]GTP (from Moravek Biochemicals, repurified to > 99% purity by triethylammonium bicarbonate gradient chromatography on DEAE-Sephacel), and the indicated potential inhibitor at 50 μM. Samples were incubated for 30 min at room temperature for vinblastine and at 4 °C for GTP. Duplicate aliquots (0.15 ml) were placed on microcolumns of Sephadex G50 (superfine) and were processed by centrifugal gel filtration at room temperature or 4 °C. Aliquots of the filtrates were processed for protein concentration by the Lowry assay and counted in a liquid scintillation counter.

Table 2. Effects of **187** on [^{3}H]Vinblastine and Colchicine Binding to Tubulin and on Nucleotide Exchange, as Measured by [8-^{14}C]GTP Binding to Tubulin.

	% of control ± SD		Inhibition of colchicine binding % Inhibition ± SD	
	Vinblastine binding	GTP binding	5 µM inhibitor	50 µM inhibitor
187	100 ± 10	100 ± 10	17 ± 4	55 ± 2
Dolastatin 10	9 ± 1	4 ± 0		
CA			99 ± 1	

Antibodies

The PY-HRP antibody was from BD Transduction Laboratories (Franklin Lakes, NJ). Antibodies against VEGFR-2 were purchased from Cell Signaling Technology (Danvers, MA).

Phosphotyrosine ELISA

Cells used were tumor cell lines naturally expressing high levels of VEGFR-2 (U251). Expression levels at the RNA level were derived from the NCI Developmental Therapeutics Program (NCI-DTP) web site public molecular target information. Briefly, cells at 60–75% confluence are placed in serum-free medium for 18 h to reduce the background phosphorylation. Cells were always >98% viable by trypan blue exclusion.

Cells were then pretreated for 60 min with a dose-response relation of 100-1.4 μM compound followed in ⅓ Log increments by 100 ng/mL VEGF for 10 min. The reaction was stopped and cells permeabilized by quickly removing the media from the cells and adding ice-cold Tris-buffered saline (TBS) containing 0.05% Triton X-100, protease inhibitor cocktail and tyrosine phosphatase inhibitor cocktail. The TBS solution was then removed and cells fixed to the plate for 30 min at 60 °C with a further incubation in 70% ethanol for an additional 30 min. Cells were exposed to a blocking solution (TBS with 1% BSA) for 1 h, washed, and then a horseradish peroxidase (HRP)-conjugated phosphotyrosine (PY) antibody was added overnight. The antibody was removed, and the cells were washed again in TBS, exposed to an enhanced luminol ELISA substrate (Pierce Chemical EMD, Rockford, IL) and light emission was measured using a UV Products (Upland, CA) BioChemi digital darkroom. Data were graphed as a percent of cells receiving growth factor alone, and IC_{50} values were calculated from two to three separate experiments (n = 8–24) using non-linear regression dose-response relation analysis.

OVCAR-8, NCI/ADR-RES and HeLa cells

The OVCAR-8 and the Pgp overexpressing NCI/ADR-RES cell lines were generously provided by the Drug Screening group of the Developmental Therapeutics Program, NCI. The wild-type and β-III overexpressing HeLa cells were generous gifts, respectively, of Dr. Richard F. Ludueña and Dr. Susan L. Mooberry. The OVCAR-8 and NCI/ADR-RES cells were grown in RPMI 1640 medium with 5% fetal bovine serum at 37 °C in a 5% CO_2 atmosphere for 96 h in the presence of varying compound concentrations. The HeLa

cells were grown in MEM supplemented with Earle's salts, nonessential amino acids, 2 mM L-glutamine, and 10% fetal bovine serum at 37 °C in a 5% CO_2 atmosphere for 96 h in the presence of varying compound concentrations. In all cultures, the DMSO concentration was 0.5%. Protein was the parameter measured by the sulforhodamine B technique,[8] and the IC_{50} was defined as the compound concentration causing a 50% reduction in the increase in cell protein as compared with cultures without compound addition.

Chorioallantoic membrane assay of angiogenesis

The CAM assay is a standard assay for testing antiangiogenic agents. The CAM assay used in these studies was modified from a procedure by Sheu and Brooks and as published previously. Briefly, fertile leghorn chicken eggs (CBT Farms, Chestertown, MD) were allowed to grow until 10 days of incubation. The proangiogenic factors human VEGF-165 and bFGF (100 ng each) were then added at saturation to a 6 mm microbial testing disk (BBL, Cockeysville, MD) and placed onto the CAM by breaking a small hole in the superior surface of the egg. Antiangiogenic compounds were added 8 h after the VEGF/bFGF at saturation to the same microbial testing disk and embryos allowed to incubate for an additional 40 h. After 48 h, the CAMs were perfused with 2% paraformaldehyde/3% glutaraldehyde containing 0.025% Triton X-100 for 20 sec, excised around the area of treatment, fixed again in 2% paraformaldehyde/3% glutaraldehyde for 30 min, placed on Petri dishes, and a digitized image taken using a dissecting microscope (Wild M400; Bannockburn, IL) at 7.5X and a SPOT enhanced digital imaging system (Diagnostic Instruments, Sterling Heights, MI). A grid was then

added to the digital CAM images and the average number of vessels within 5–7 grids counted as a measure of vascularity. Sunitinib and semaxanib were used as a positive control for antiangiogenic activity. Data were graphed as a percent of CAMs receiving bFGF/VEGF only and IC_{50} values calculated from two to three separate experiments (n = 5–11) using non-linear regression dose-response relation analysis.

Table 3: Inhibition of tubulin assembly and cellular VEGFR2 receptor tyrosine kinase and the growth of β-III and P-gp overexpressing cells.

COMPOUND	Inhibition of tubulin assembly IC_{50} (nM)	VEGFR2 inhibition IC_{50} (nM)	WT HeLa IC_{50} (nM)	β-III overexpressing HeLa IC_{50} (nM)	Parental OVCAR-8 IC_{50} (nM)	P-gp overexpressing NCI/ADR-RES IC_{50} (nM)
187	21 ± 1	21.3 ± 3.2	280 ± 40	280 ± 40	1000 ± 300	700 ± 200
188	> 20 (no act)	50.1 ± 8.8	> 10,000	> 10,000		
189	> 20 (no act)	40.6 ± 7.8	> 10,000	> 10,000		
190	> 40 (no act)	30.1 ± 5.1			> 5,000	> 5,000
CA	1.2 ± 0.01		1.8 ± 0.4	2.5 ± 0.7		
paclitaxel			5.3 ± 2	16 ± 1	10 ± 0	5,000 ± 0
semaxinib		12.9				
sunitinib		18.9 ± 2.7				

Tubulin immunofluorescence assay

MDA-MB-435 cells were plated in chamber slides at ~30% confluency and allowed to attach overnight. Cells were then treated with drug at the IC_{50} concentration for 2 h in serum free media. After 2 h, drug was removed, cells were washed and then fixed in 3.7%

buffered formalin for 10 min. Fixed cells were then washed 3x with PBS, permeabilized with 0.5% Triton 100-X in PBS for 10 min at RT then blocked in 10% goat serum for 30 min at RT. Slides were washed again with PBS 3x and then incubated with anti-alpha-tubulin Alexa Fluor® 488 (Invitrogen, Carlsbad CA) in PBS containing 10% goat serum at a concentration of 2.5 µg/mL for 1 h at RT in the dark. After incubation, cells were washed, chambers removed, SlowFade Gold (Molecular Probes/Invitrogen, Carlsbad CA) added and a cover slip applied. Slides were imaged using a fluorescent microscope, Leica DM4000 B (Wetzlar, Germany) at EX488 nm/EM519 nm.

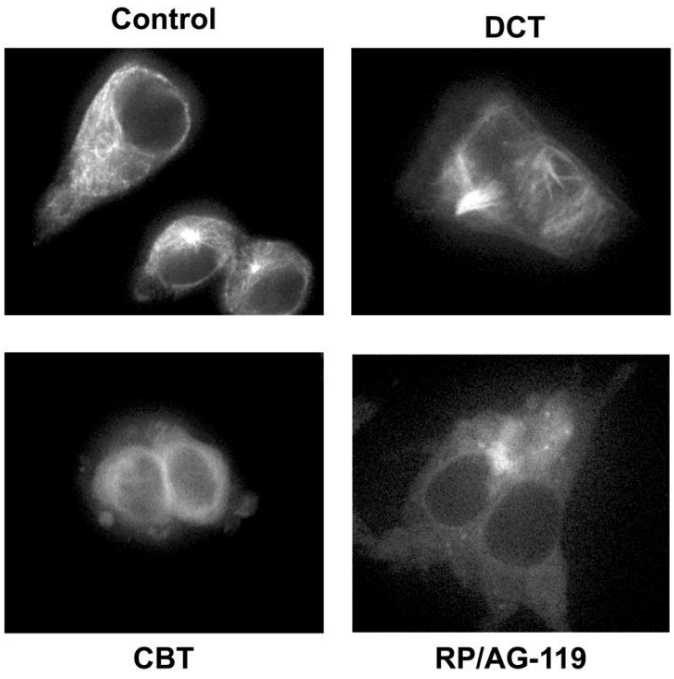

Figure 1. Microtubule Staining by Docetaxel (DCT, COmbretastatin (CBT) and 187 (RP/AG-119)

Cell cycle analysis and apoptosis

MDA-MB-435 cells were plated at 30% confluence into 6 well plates (Costar, Cambridge, MA) and allowed to attach overnight. Drugs were added at their IC_{50} concentrations for 2 h in serum free media and then 10% Cosmic Calf Serum was added. Cells were incubated for 24-48 h at 37 °C with 5% CO_2 and then fixed in 50% ethyl alcohol solution and stored at 4 °C for up to a week. After fixation, pelleted cells were re-suspended and labeled in PBS containing 0.1% Triton X-100, 100 µg/mL RNase A, and 25 µg/mL propidium iodide and then incubated for 30 min at 37 °C. Cells were subjected to flow cytometry using a side scatter plot versus fluorescence (EX535 nm/EM617 nm) on a FACSCalibur flow cytometer (Becton-Dickenson, San Jose, CA). Analysis of DNA content was performed using MODFIT Lt software (Verity Software, Topsham, ME) to generate percent G_1/G_0 phase, S, and G_2/M phase. Data were graphed as mean ± standard deviation.

Western blot. Cells were treated with drug for 24 and 48 hours. Whole cell lysates were made from each sample in M-PER lysis reagent (Pierce-Thermo, Rockland, IL) containing phosphate and protease inhibitors (Sigma-Aldrich cocktail II, St Louis, MO), and 300mM final concentration of NaCl to lyse the nuclear membrane. Protein concentrations were quantified using the bicinchonic acid (BCA) protein assay kit (Pierce-Thermo, Rockland, IL) as compared to a standard BSA concentration curve. Equal amounts (30µg or 50µg) of cellular protein was loaded onto the SDS-PAGE gels, subjected to electrophoresis at 120V, transferred to a nitrocellulose membrane using iBlot apparatus (InVitrogen) for 20V for 7 min, blocked in Superblock (Pierce-Thermo,

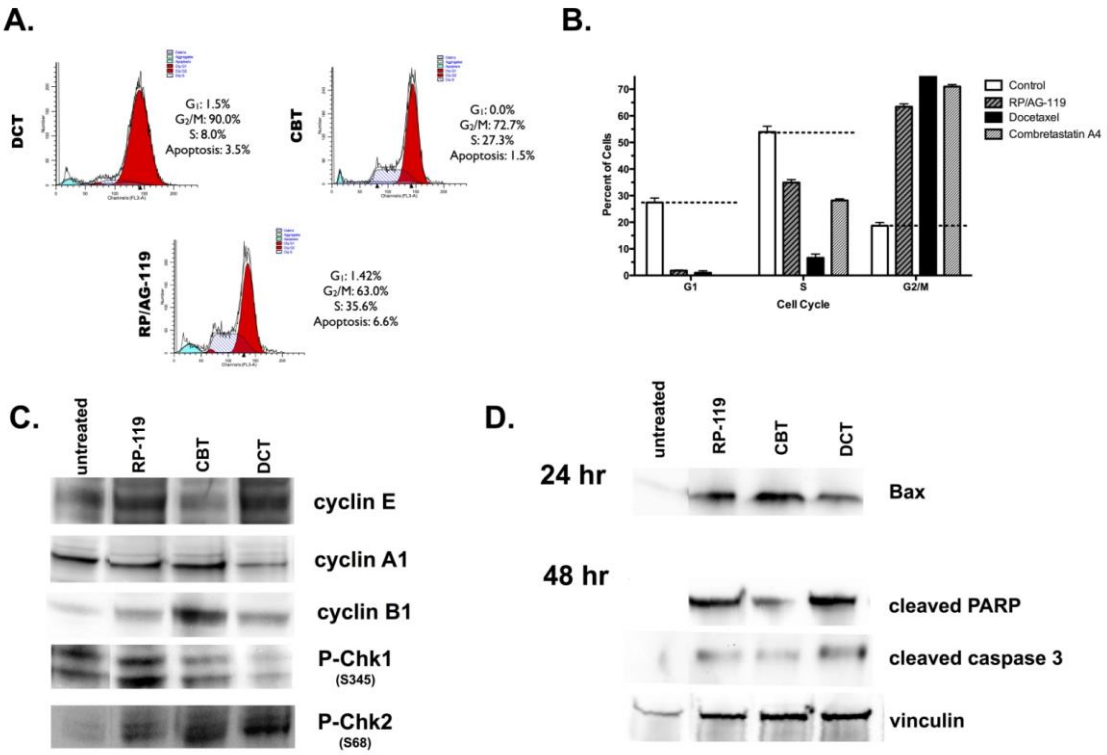

Figure 2. Effect of **187** [RP/AG-119] on cell cycle (panels A and B), cell cycle protein expression (panel C) and apoptotic protein expression (panel D)

Rockland, IL) and incubated with primary antibody overnight at 4°C in Superblock according to manufacturer's instructions. Membranes were then washed three times in TBS containing 0.25% Tween-20, incubated with the secondary antibody (Cell Signaling Technology, Beverly, MA), washed again three times and ECL (Western Dura Substrate, Pierce-Thermo, Rockford, IL) added. Membranes were imaged using a digital charge-coupled device (CCD) camera digital darkroom (FluorChem HD, Cell Biosciences, Santa Clara, CA). Loading controls used were either anti-vinculin antibody (Sigma Chemical; product V9131; 1:4000 dilution) or anti ß-actin antibody (Cell Signaling cat#4970, Beverly, MA; 1:1000 dilution). Primary antibodies used were Bax (Cell Signaling

cat#9661), cleaved caspase-3 (Cell Signaling #9664), cleaved PARP (Cell Signaling #5625, P-Chk1 (Cell Signaling #2341), P-Chk2 (Cell Signaling #2661); cyclin A1 (Cell Signaling #); cyclin B1 (Cell Signaling #4138), cyclin E1 (Cell Signaling #4129); and were all diluted 1:1000 per manufacturer's recommendations.

Maximum tolerated dose in mice

To determine the maximum tolerated dose (MTD) of compounds and drugs, a dose finding study was performed using BALBc/J mice (Jackson Laboratories, Bar Harbor, ME). Drugs were first dissolved at 50 mg/mL in DMSO and frozen in aliquots at -80 °C. Solutol-15 (BASF, Ludwigshafen, Germany) was melted at 60 °C for 5-10 min, then mixed in a ratio of 1 part DMSO/drug to 1.8 parts solutol-15 to 7.2 parts sterile dextrose 5% in water (D_5W). This solvent mixture was used for all drugs. Starting at 10 mg/kg and 15 mg/kg body weight (n = 2 mice per treatment), mice were weighed and doses increased in 10 mg/kg increments every other day until weight loss was observed. At this point the MTD was estimated to be the approximate dose of first weight loss. The MTD of docetaxel was found to be 35 mg/kg, sunitinib 30 mg/kg and **187** [RP/AG-119] 25 mg/kg, temozolomide 30 mg/kg.

MDA-MB-435 flank tumor model

Human MDA-MB-435 BLBCs (500,000) in media were implanted into the lateral flank of 8 wk old female NCr athymic nu/nu nude mice (Charles River, Wilmington, DE). Tumor sizes (length, width, depth) were measured twice weekly. When volumes reached 75-100 mm^3, (day 7 after implantation) treatment with drugs at their MTD (above) was

begun and animal weights and tumor volumes measured twice weekly. At the end of the experiment, animals were humanely euthanized using the AALAC approved method of carbon dioxide asphyxiation. Tumors were removed, fixed in neutral buffered formalin, paraffin embedded, sectioned and sections stained against CD31/PECAM-1 using an antibody from Abcam (ab28364) and staining done using a Vectastain ABC kit (Vector Laboratories, Burlingame, CA). Vessel density was assessed by counting the number of CD31-positive vessels in a 200x microscope field in a blinded fashion and graphed as a percent vessel density of carrier treated animals.

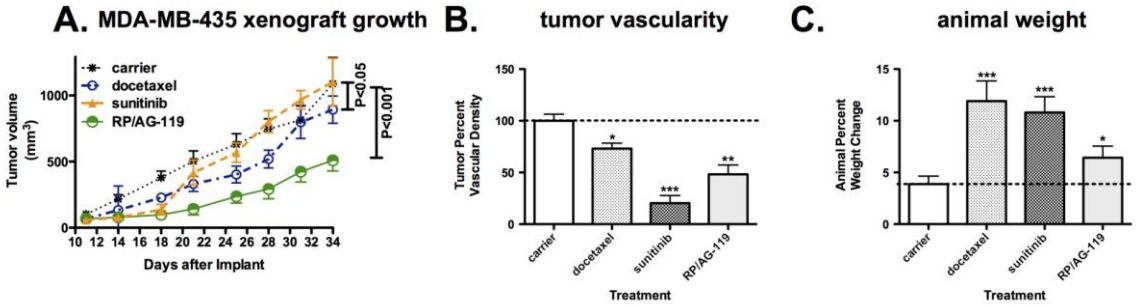

Figure 3: *Treatment with* **187** [RP/AG-119] *decreased primary tumor growth and tumor vascular density in MDA-MB-435 flank xenograft model.* * P<0.05, ** P<0.01, *** P<0.001 by one way ANOVA with Neuman-Keuls post test. Human BLBCs, MDA-MB-435, were implanted into the lateral flank of NCr athymic nu/nu nude mice at 500,000 cells, and the mice were treated with carrier, docetaxel, sunitinib, or **3**·HCl twice weekly at their MTD's until the end of the experiment. Data is representative of 6-8 animals. (A) Tumor size was assessed by measuring tumor length, width, and depth twice weekly using Vernier calipers. Tumor volume was calculated with the ellipsoid formula: volume = 0.52 (length x width x depth) and graphically represented as days after

implantation. Statistics on this graphs were two way ANOVA with repeated measures post test. (B) Tumor vascular density was examined at the end of the experiment by staining tumor sections with CD31/PECAM-1 antibodies and a Vectastain ABC kit. Vascular density was determined by counting CD31-positive vessels and graphed as percent vessel density as compared with carrier treated animals. (C) Graphical representation of percent change in animal weight as determined by measuring animal weight at the beginning and end of the experiment.

U251 flank xenograftraft model

Human U251 glioblastoma cells (500,000) in media were implanted into the lateral flank of 8 wk old male NCr athymic nu/nu nude mice (Charles River, Wilmington, DE). Tumor sizes (length, width, depth) were measured twice weekly. When volumes reached 75-100 mm^3 (day 8 after implantation), treatment with drugs at their MTD (above) was begun and animal weights and tumor volumes measured twice weekly. At the end of the experiment, animals were humanely euthanized using the AALAC approved method of carbon dioxide asphyxiation. Tumors were removed, fixed in neutral buffered formalin, paraffin embedded, sectioned and sections stained against CD31/PECAM-1 using an antibody from Abcam (ab28364) and staining done using a Vectastain ABC kit (Vector Laboratories, Burlingame, CA Vessel density was assessed by counting the number of CD31-positive vessels in a 200x microscope field in a blinded fashion and graphed as a percent vessel density of carrier treated animals.

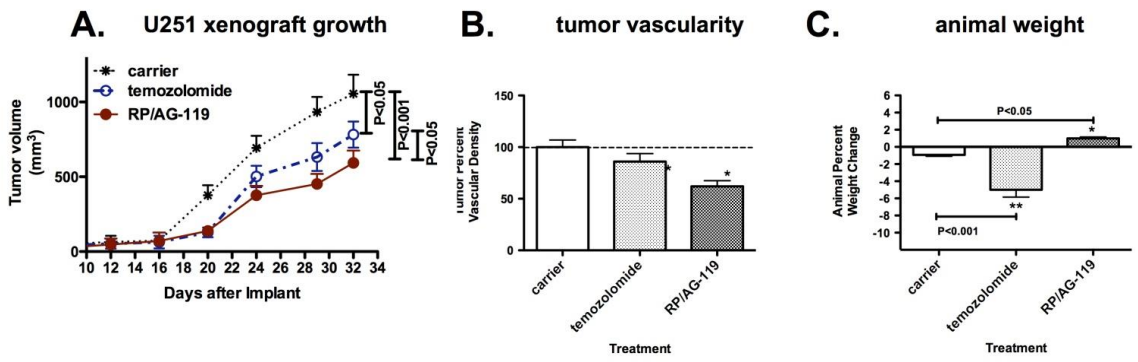

Figure 4: *Treatment with* **187** [RP/AG-119] *decreased primary tumor growth and tumor vascular density in U251 flank xenograft mouse model.* * P<0.05, ** P<0.01, *** P<0.001 by one way ANOVA with Neuman-Keuls post test. U251 human glioma cells were implanted into the lateral flank of NCr athymic nu/nu nude mice at 500,000 cells, and the mice were treated with carrier temozolomide or **187** [RP/AG-119] twice weekly at their MTD's until the end of the experiment. Data is representative of 6-8 animals. (A) Tumor size was determined as described in the legend of Figure 3. Statistics on this graph were two way ANOVA with repeated measures post test. (B) Tumor vascular density was examined at the end of the experiment as described in the legend of Figure 3.(C) Graphical representation of percent change in animal weight as determined by measuring animal weight at the beginning and end of experiment.

4T1 triple negative breast orthotopic allograft model

4T1-Luc2GFP dual luciferase/GFP tagged cells were purchased from Caliper Life Sciences (Hopkinton, MA) and maintained in Dulbecco's modification of minimal essential media (DMEM) containing 10% Cosmic Calf Serum (Hyclone, Logan, UT). 750 cells (verified by fluorescence imaging to be >98% GFP positive and counted three times on a TC10 automated cell counter (BioRad, Hercules, CA)) in 100 µL PBS with 1

mM EDTA were implanted subcutaneously into the left fat pad #4 of 8 wk old female BALBc/J mice using a tuberculin syringe. The MTD of drugs were delivered to animals twice weekly on Tuesday and Friday starting three days after implantation beginning when tumors had reached 75-100 mm^3 (day 7 after implantation). Tumor sizes (length, width, depth) were measured three times weekly. Animal weights were also taken twice weekly. At day 33 post implantation, the experiment was ended due to moribund animals in the untreated group. At the end of the experiment, animals were humanely euthanized using the AALAC approved method of carbon dioxide asphyxiation. Tumors and lungs were removed and fresh lungs imaged using a LumaScope fluorescent imaging system (Bulldog Bio, Portsmouth, NH) at 25x magnification with the number of metastases per lung counted by hand from captured images.

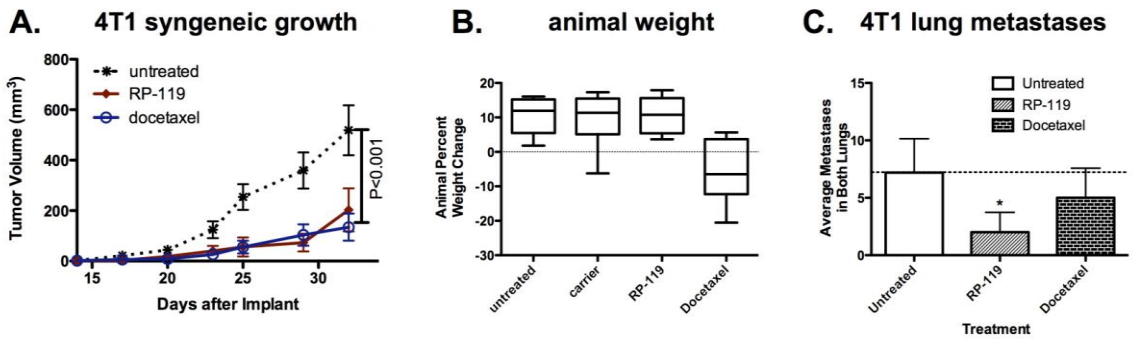

Figure 5: Treatment with **187** [RP/AG-119] decreased primary tumor growth and lung metastases in the 4T1 orthotopic breast model. 4T1-Lucerase/GFP tagged cells were implanted orthotopically into BALB/c mice at 7,500 cells, and the mice were treated with carrier, docetaxel or **187** [RP/AG-119] at their MTD's twice weekly until the end of the experiment. (A) Tumor volume was as described in the legend of Figure 3. (B) Animal weights were recorded before each treatment and graphed as percent weight change. (C)

After 32 days, animals were euthanized and lungs were excised and immediately imaged at 25x using the LumaScope fluorescent imaging system. The number of metastases in both lungs was counted visually and represented graphically.

Table 4. Tumor cell inhibitory activity (NCI) GI_{50} (nM) of **187**

Panel/ Cell line	**GI_{50} (nM)**	**Panel/ Cell line**	**GI_{50} (nM)**	**Panel/ Cell line**	**GI_{50} (nM)**	**Panel/ Cell line**	**GI_{50} (nM)**
Leukemia	**187**	**Colon Cancer**	**187**	**Melanoma**	**187**	**Renal Cancer**	**187**
CCRF-CEM	306	COLO 205	252	LOX IMVI	485	786 - 0	547
HL-60(TB)	222	HCC-2998	896	M14	297	A498	136
K-562	258	HCT-116	459	MDA-MB-435	117	ACHN	741
MOLT-4	398	HCT-15	385	SK-MEL-2	352	CAKI-1	316
RPMI-8226	480	HT29	309	SK-MEL-28	917	RXF 393	362
SR	277	KM12	435	SK-MEL-5	357	SN12C	543
NSCLC		SW-620	331	UACC-62	318	TK10	644
A549/ATCC	713	**CNS Cancer**		**Ovarian cancer**		UO-31	488
EKVX	310	SF-268	791	IGROVI	432	**Prostate Cancer**	
HOP-62	396	SF-295	249	OVCAR-3	236	PC-3	642
HOP-92	1320	SF-539	257	OVCAR-4	1260	DU-145	347
NCI-H226	776	SNB-19	531	OVCAR-5	1190	**Breast Cancer**	
NCI-H23	441	SNB-75	164	OVCAR-8	676	MCF7	347
NCI-H322M	381	U251	371	NCI/ADR-RES	268	MDA-MB-231/ATCC	699
NCI-H460	331			SK-OV-3	371	HS 578T	291
NCI-H522	181					MDA-MB-468	197